

**MODELLING AND ANALYSIS OF MICROGRID CONTROL
TECHNIQUES FOR GRID STABILISATION**

by

ANGES AKIM AMINOU MOUSSAVOU

Thesis submitted in fulfilment of the requirements for the degree

Master of Technology: Electrical Engineering

in the Faculty of Engineering

at the

Cape Peninsula University of Technology

Supervisor: Dr. M Adonis

Co-supervisor: Dr. AK Raji

Bellville

December 2014

CPUT copyright information

The thesis may not be published either in part (in scholarly, scientific or technical journals), or as a whole (as a monograph), unless permission has been obtained from the University

ABSTRACT

In recent times, renewable energy-based distributed generation (DG) has captivated the industrial sector and on a global scale this has become a leading research area. Distributed generation using wind, solar energy or biomass as a source of energy can produce electricity on a small scale. Therefore, there is a strong focus on using renewable energy as a safe alternative source of energy, especially because it can in future play a dominant role in the world's energy production and help to tackle the increase of global warming caused by fossil energy. However, a major problem facing renewable energies is that they are highly dependent on weather conditions. Since the power generated by DG, as well as consumption, depends on the weather conditions, irregularity of production and consumption leads to frequency and voltage fluctuations, and it can become difficult to determine and monitor consumer usage at any given time. Distributed generation can then be subjected to discrepancies in consumer usage and this can lead to severe overloading. As a result, microgrids powered by DG, operating in a single, stand-alone controllable system mode, face new challenges in terms of balancing a cluster of loads. Balancing a cluster of loads by making sure at all times that the entire system operates without overloading, is an essential requirement for the proper operation of a power system. The microgrid load considered in this project is the sum of sensitive and non-sensitive loads, respectively 5 kW and 100 kW, which constitute load requirement of one village; this total load required by a number of villages is called a cluster load. Depending on the input power generated by a DG-based photovoltaic (PV) system, these loads can be controlled using a logic control switch (LCS). When the power produced is less than the minimum load required by a component of a cluster, overloading occurs. The purpose of using an LCS is to ensure that a stable system is maintained under various loads and resource conditions. An LCS is used to continuously monitor and adjust load through circuit breakers. It is a good alternative to load balancing for a cluster of villages in rural area where a microgrid is operating in stand-alone mode.

The focus of this research is to design a photovoltaic system with a maximum capacity of 1 MW providing power to a cluster of rural villages, and operating in stand-alone mode, and then to apply different control techniques (droop control, dq0 reference frame + proportional integral (PI) controller, and PI controller alone) at the inverter terminal of the PV system, in order to evaluate the stability of the output voltage. Another goal of the research is to develop an energy management system (EMS) algorithm to support the PV system in reducing loads. Therefore, a

stable system under various load and resource conditions, as well as suitable control mechanisms are required to model a PV system.

There is a need for the modelling of a PV array using a physical modelling block in MATLAB (SIMULINK) software. The state flow provided by SIMULINK is used in this project to develop an algorithm for load balancing. The state flow gives possibilities of modelling complex algorithms by combining graphical and tabular representations to create sequential decision logic, derived from state transition diagrams and tables, flow charts and truth tables.

Furthermore, the design of a microgrid using photovoltaic DG and an energy management system, has been developed. The present work mainly consists of a stand-alone microgrid operation, where the power generated must be equal to the load power. In addition, different control methods, consisting of a dq0 reference frame + PI controller, are analysed at the inverter terminal. Subsequently an LCS algorithm is developed; this is required to maintain the system within certain limits and prevents overloading. LCS algorithms are based on a flowchart and allow switching automatically selected loads, depending on the power (solar radiation) available. In addition, a flow chart provides an easy way of using a graphical transition state and state chart to establish a set of rules for the system.

The simulation results show that both droop control and a dq0 reference frame + PI controller are much better than a PI controller alone; these results also compared well with similar studies found in the literature. Also, these results are further improved with an EMS in order to maintain the output voltage of the microgrid, by switching on and off certain loads depending on the input power.

The modelling of the microgrid using DG, based on photovoltaic systems with a maximum capacity of 1 MW, supports and improves the PV system by reducing loads. Moreover, droop control, and dq0 transformation + PI control present a better result than PI controller alone.

Keywords:

PV array design, boost converter, inverter control, droop control, EMS

ACKNOWLEDGEMENTS

My sincere gratitude goes to the Almighty God for giving me the opportunity to complete my research work successfully.

Most important of all, I would like to express my gratitude to my mother. It would have been impossible for me to finish my studies without her constant encouragement, assistance, endless love, and noble dedication to my education.

I will like to thank my supervisors (Dr. Adonis and Dr. Raji) for their supervision and immeasurable support throughout the course of this research work. Their encouragement and guidance helped me to stay focused and consistent during this research period. Your constant supervision has made this thesis a success.

I am taking this opportunity to express my sincere gratitude to all members of Faculty of Engineering, Dr. Neils Wieffering, Charles Adewole, Berenice Alinde, Ayokunle Ayeleso, Ndjawel Clement, John Shamu, olawale Ibrahim, Pamela M'vouezolo, John Retonda and Yohan Mfoumboulou for their constructive criticism and invaluable suggestion throughout this work. I am also thankful to all those who have contributed, directly or indirectly, to achieve this work.

AMINOU MOUSSAVOU Anges Akim

Contents

ABSTRACT	ii
ACKNOWLEDGEMENTS	iv
LIST OF ACRONYMS.....	xviii
LIST OF SYMBOLS	xxii
GLOSSARY OF TERMS.....	xxiii
Chapter 1 : INTRODUCTION.....	1
1.1 Background.....	1
1.2 Statement of the research problem	3
1.3 The challenge facing inverter control	3
1.4 Motivation for research	5
1.5 Research objectives.....	5
1.6 Thesis organisation.....	5
Chapter 2 : LITERATURE REVIEW	7
2.1 Introduction.....	7
2.2 Concept of microgrid and distributed network	7
2.2.1 A comparison between a conventional power grid and a microgrid.....	8
2.2.2 Fundamentals of a microgrid	8
2.2.3 Microgrid benefits	9
2.3 Rearrangement of the structures and components of a microgrid	10
2.3.1 Microgrid structure	10
2.3.2 Microgrid types: AC and DC	11
2.3.2.1 The DC microgrid system	11
2.3.2.2 AC microgrid system.....	12
2.3.2.3 Hybrid microgrid	13

2.4	Distributed energy resources	14
2.5	Non-traditional energy sources	15
2.5.1	Combined heat and power systems.....	15
2.5.2	Photovoltaic system description.....	15
2.5.2.1	Solar radiation on a photovoltaic cell	16
2.5.2.2	Photovoltaic module	17
2.5.2.3	Photovoltaic array.....	17
2.5.2.4	Photovoltaic system configurations.....	18
2.5.2.5	Control algorithm of photovoltaic system	19
2.5.2.6	Algorithms for maximum power point tracking.....	19
2.5.2.7	Perturbation and observation algorithm	19
2.5.2.8	Incremental conductance algorithm	21
2.5.3	Wind energy system	22
2.5.3.1	Configuration of a wind system.....	22
2.5.4	Microturbine.....	23
2.5.5	Energy storage systems	23
2.5.6	Storage system configuration	24
2.5.7	Microgrid loads	24
2.6	Microgrid control layer.....	25
2.6.1	Microgrid control.....	26
2.6.1.1	Control involving communication	26
2.6.1.2	Control with no communication inverter	27
2.6.2	Control structures of distributed generation units in a microgrid.....	28
2.6.2.1	Local control of distributed generation structure in the microgrid	28
2.6.2.2	Central control of distributed generation in a microgrid	33
2.6.2.3	Other control methods used for power management: decentralised control..	37

2.6.3	Existing Control Methods within the inverter	38
2.6.3.1	Single Voltage Loop Control Method	39
2.6.3.2	Multi-Loop Control Method.....	40
2.6.3.3	Predictive Control Method	40
2.6.3.4	Deadbeat Control Method.....	41
2.6.3.5	Sliding mode control method	41
2.6.3.6	Hysteresis control	41
2.6.4	Control methods based on pulse width modulation within inverters	42
2.6.4.1	Inverter-based DG Interface	42
2.6.4.2	Current control methods for controlling PWM inverter.....	43
2.6.4.3	Proportional integral control.....	44
2.6.4.4	Proportional resonant control.....	45
2.6.4.5	Fuzzy logic control.....	47
2.7	Microgrid smart metering	47
2.8	Frequency control in power systems.....	49
2.9	Conclusion.....	49
Chapter 3 : POWER ELECTRONICS CONVERSION.....		50
3.1	Introduction.....	50
3.2	Power semiconductor devices	51
3.3	Power converters.....	52
3.3.1	The AC voltage sourced inverter or DC-AC converter.....	53
3.3.2	Half-bridge voltage source inverter	54
3.3.3	Single-phase bridge voltage source inverter	55
3.3.3.1	Switching power devices rules.....	56
3.3.3.2	Operation principles of inverter switching circuits.....	57
3.3.4	Voltage control in a single-phase inverter	57

3.3.4.1	Pulse-width modulation control	58
3.3.4.2	Sinusoidal-pulse-width modulation.....	59
3.3.4.3	Sinusoidal-pulse-width modulation with bipolar switching	59
3.3.4.4	Sinusoidal-pulse-width modulation with unipolar switching	60
3.3.5	Three-phase voltage source inverter	60
3.4	Transformation and control	63
3.4.1	Transformation reference frames: three- to two-dimensional frames	63
3.4.1.1	Frame transformation: $abc \rightarrow \alpha\beta$	63
3.4.1.2	Frame transformation: $abc \rightarrow dq$	65
3.4.2	Notch filter	65
3.4.3	Fast Fourier transform	66
3.4.4	Phase-locked loop	66
3.5	Filter topology	67
3.5.1	L-filter	68
3.5.2	LC- and LCL-filter	68
3.6	Digital platforms for inverter control.....	70
3.6.1	Some examples of algorithms used in implementing digital control for inverters ..	72
3.6.2	Harmonics	74
3.6.3	Total harmonic distortion	75
3.7	Conclusion.....	75
Chapter 4 : SYSTEM MODELLING AND CONTROL		77
4.1	Introduction.....	77
4.2	Photovoltaic system model	77
4.2.1	Photovoltaic module model.....	77
4.2.2	Load profile determination in Africa.....	81
4.2.3	Photovoltaic system design	82

4.3	Boost converter design	83
4.3.1	Inductor voltage and capacitor current at first interval	85
4.3.2	Inductor voltage and capacitor current at second interval	85
4.3.3	Inductor volt-second balance	86
4.3.3.1	Conversion ratio $M(D)$ of the boost converter	86
4.3.4	Determination of current DC component of the inductor current	87
4.3.5	Determination of inductor value based on its ripple current.....	88
4.3.6	Determination of capacitor ripple voltage	90
4.3.7	Inverter LC- filter design	91
4.4	Control algorithms for an inverter output voltage.....	92
4.4.1	Inverter and linear model	92
4.4.2	Inverter control using a PI controller	94
4.4.3	Inverter control using the dq0 transformation + PI controller	95
4.4.4	Inverter controls using droop methods.....	96
4.4.4.1	Active and reactive power calculations	97
4.4.4.2	Voltage control.....	98
4.4.4.3	Reactive power versus voltage droop	99
4.4.4.4	Real power versus frequency droop	100
4.5	Energy management system control algorithm	100
4.6	Conclusion.....	103
Chapter 5 : SIMULATION RESULTS AND DISCUSSION.....		104
5.1	Introduction.....	104
5.2	Simulation of PV array model.....	104
5.2.1	Simulation results	106
5.3	Simulation result of the inverter output voltage, without a controller	113
5.4	Simulation result of inverter controls using a PI controller	115

5.4.1	Inverter output voltage control using a PI controller under load power changes	115
5.4.2	Inverter voltage control during an input voltage change, using a PI controller	118
5.5	Simulation result of an inverter voltage control using the dq0 transformation + PI controller simulation	121
5.5.1	Inverter control using dq0 transformation + PI controller under constant parameters	121
5.5.2	Inverter control using dq0 transformation + PI controller under load power changes	123
5.5.3	Inverter controls under input voltage battery change	125
5.6	Droop control simulation	128
5.6.1	Inverter control using droop control subject to constant parameters	128
5.6.2	Inverter control using droop control under load power changes	130
5.6.3	Inverter control using droop control when the battery voltage changes	132
5.7	Simulation result of the system incorporating the energy management system (EMS) algorithm	134
5.7.1	Inverter control operating with sensitive load power, but without activating the EMS of the system	135
5.7.2	Inverter control operating with sensitive and non-sensitive loads, but without activating the EMS of the simulated microgrid	137
5.7.3	Inverter control operating with sensitive and non-sensitive loads and the EMS of the system activated	139
5.8	Conclusion	142
Chapter 6 : CONCLUSION AND FUTURE WORK		144
6.1	Conclusion	144
6.2	Future work	145
REFERENCES		146
APPENDICES		164
Appendix 1 inverter without a controller under load power changes		164

Appendix 2 Inverter control under load power changes	164
Appendix 3 Inverter control using under input voltage changes.....	165
Appendix 4 Inverter control operating with sensitive load power without activating the EMS to the system	165
Appendix 5 Inverter control operating with load power without activating EMS to the system over the minimum input voltage	166
Appendix 6 Inverter control operating with sensitive and non-sensitive loads without activating the EMS to the system.....	166

LIST OF FIGURES

Figure 2.1: General architecture of a centralised electricity power system showing losses	8
Figure 2.2: Typical microgrid configuration.....	10
Figure 2.3: Classification of the microgrid based power type (AC or DC)	11
Figure 2.4: Concept of a DC microgrid system with DG units and mixed load types.....	12
Figure 2.5: AC microgrid structure with DG units and mixed types of loads	13
Figure 2.6: DG types and technologies	14
Figure 2.7: Photovoltaic operation.....	16
Figure 2.8: PV module anatomy.....	17
Figure 2.9: Solar cell	18
Figure 2.10: Flowchart of the perturbation and observation algorithm	20
Figure 2.11: Main components of a wind generation system.....	22
Figure 2.12: Microgrid communication: local and centralised controller.....	25
Figure 2.13: Control schemes of power converters	39
Figure 2.14: Single feedback loop block diagram.....	39
Figure 2.15: Multiple-loop controller	40
Figure 2.16: Predictive current control block diagram.....	41
Figure 2.17: Classification of current control methods.....	44
Figure 3.1: Switching device chronology	51
Figure 3.2: General block diagram of inverter	54
Figure 3.3: Single half-bridge VSI	54
Figure 3.4: Single-bridge VSI	55
Figure 3.5: The values of V_{ab} in single bridge.....	57
Figure 3.6: Three-phase voltage source.....	60
Figure 3.7: Basic structure of a PLL	67
Figure 3.8: L- filter.....	68

Figure 3.9: LC-filter configuration	70
Figure 3.10: LCL-filter configuration	70
Figure 4.1: Equivalent circuit model of PV cell	77
Figure 4.2: Equivalent of N circuit model of solar array	78
Figure 4.3: Ideal boost converter circuit	83
Figure 4.4: Switch in position 1	83
Figure 4.5: Switch in position 2	83
Figure 4.6: Boost converter circuit using power MOSFET and diode	84
Figure 4.7: Inductor voltage waveform	86
Figure 4.8: Conversion ratio $M(D)$ of the boost converter	87
Figure 4.9: Capacitor current waveform	88
Figure 4.10: Inductor current ripple	88
Figure 4.11: Capacitor voltage ripple	90
Figure 4.12: A single-phase full- bridge voltage source diagram	92
Figure 4.13: Open loop PWM inverter plus output filter and linear load model	93
Figure 4.14: Closed- loop PWM inverter current voltage controller.....	93
Figure 4.15: V_{rms} + PI controller method.....	95
Figure 4.16: Generation of virtual grid voltages.....	95
Figure 4.17: dq0 transformation + PI controller	96
Figure 4.18: Control technique.....	97
Figure 4.19: P and Q calculation.....	97
Figure 4.20: Voltage control.....	98
Figure 4.21: Q-voltage droop	99
Figure 4.22: Block diagram of the active power droop.....	100
Figure 4.23: EMS transition state.....	101
Figure 4.24: EMS flow chart.....	102

Figure 5.1: Representation of a diode characteristic in SIMULINK	105
Figure 5.2: Equivalent circuit of a solar cell	105
Figure 5.3: Autonomous microgrid system	106
Figure 5.4: The output voltage of the 10-array PV system.....	107
Figure 5.5: The variation of the duty cycle for the second PV system (multi-array).....	107
Figure 5.6: Output voltage of boost converter for the second PV system (multi-array)	108
Figure 5.7: Second PV system (multi-array) input power delivery	109
Figure 5.8: The output voltage of second PV system inverter before the filter	109
Figure 5.9: Switching of the second PV system voltage phase a.....	110
Figure 5.10: Filtered output voltage of three-phase inverter of the second PV system(multi-array).....	111
Figure 5.11: The output current after the LC filter of the second PV system(multi-array).....	111
Figure 5.12: Instantaneous power delivered to the load of the second PV system(multi-array) .	112
Figure 5.13: For the load: the output power, line-to-ground output voltage, and line-to-ground output current of the second PV system(multi-array).....	112
Figure 5.14: V_{abc} (V_{rms}) under load change	113
Figure 5.15: V_{abc} under load change	114
Figure 5.16: I_{abc} under load change.....	114
Figure 5.17: Phase-to-phase V_{rms} under load change	115
Figure 5.18: Modulation index under load change.....	117
Figure 5.19: Output peak voltage under load change.....	117
Figure 5.20: Current waveform under load change	118
Figure 5.21: Input battery voltage.....	119
Figure 5.22: Phase-to-phase V_{rms} under input voltage change	119
Figure 5.23: Modulation index subjected to input voltage change	120
Figure 5.24: Output peak voltage and current under input voltage change.....	120
Figure 5.25: Modulation index under constant voltage and loads.....	121
Figure 5.26: Phase-to-phase V_{rms} under constant voltage and loads.....	122

Figure 5.27: Load voltage under constant input voltage and loads.....	122
Figure 5.28: Current under constant input voltage and load power	123
Figure 5.29: Phase-to-phase V_{rms} under load power change.....	123
Figure 5.30: Modulation index under load power change	124
Figure 5.31: Peak voltage under load power change	125
Figure 5.32: Current under load power change.....	125
Figure 5.33: V_{rms} under input voltage change.....	126
Figure 5.34: Modulation index under an input voltage change	127
Figure 5.35: Output voltage waveform under an input voltage change.....	127
Figure 5.36: Output current waveform under an input voltage change	128
Figure 5.37: Phase-to-phase V_{rms} from droop control.....	129
Figure 5.38: line-to-line peak voltage under constant parameters	129
Figure 5.39: Peak current under constant parameters	130
Figure 5.40: V_{rms} under load power change.....	130
Figure 5.41: line-to-line peak output voltage under load power change.....	131
Figure 5.42: Current waveform under load power change.....	132
Figure 5.43: V_{rms} under input voltage change.....	133
Figure 5.44: Output voltage waveform under droop control.....	133
Figure 5.45: Output current waveform under droop control	134
Figure 5.46: EMS integrated with a dq0 transformation + PI controller.....	134
Figure 5.47: input voltage, logic activating switch and phase-to-ground V_{rms} without activating the EMS of the simulated microgrid.....	135
Figure 5.48: The V_d component of the sensitive load without activating the EMS of the simulated microgrid.....	136
Figure 5.49: Peak output voltage and current waveforms without activating the EMS of the simulated microgrid	136

Figure 5.50: input voltage, logic control switch and phase to ground V_{rms} of the total load without active EMS of the simulated microgrid..... 137

Figure 5.51: The V_d component in the total load without activating the EMS of the simulated microgrid 138

Figure 5.52: Peak output voltage and current of the loads without an active EMS of the simulated microgrid..... 139

Figure 5.53: Input voltage, logic control switch and phase to ground V_{rms} of the total load with activation of the EMS of the simulated microgrid 140

Figure 5.54: The V_d component of the dq0 transformation in the total load with activation of the EMS of the simulated microgrid..... 141

Figure 5.55: Peak output volatge and current in the total load with activation of the EMS of the simulated microgrid 142

LIST OF TABLES

Table 3.1: Power device comparison (Little, 2005).....	52
Table 3.2: Leg voltage of a three-phase VSI during six step mode operation.....	62
Table 3.3: Phase-to-neutral voltages for the six-step operation.....	62
Table 3.4: Line voltages for six-step mode of operation	63
Table 4.1: PV cell parameters.....	80
Table 4.2: Module specification under standard test conditions (STC)	81
Table 4.3: Module parameters for one module.....	81
Table 4.4: Appliances used in one household (adapted from anon, 2014)	81
Table 4.5: State transition matrix	102
Table 5.1: System paramters	115

LIST OF ACRONYMS

AC	alternating current
AMI	advanced metering infrastructure
BESS	battery energy storage systems
CAES	compressed air energy storage
CC	central control
CHP	combined heat and power
CPUT	Cape Peninsula University of Technology
CSI	current source inverter
CFPIC	conventional fuzzy PI control
DER	distributed energy resource
DC	direct current
DNO	distribution network operator
DG	distributed generation
DSP	digital signal processor
dq0	direct–quadrature–zero
ESR	equivalent series resistance
EMS	energy management system

EPLL	enhanced phase-locked loop
FFT	fast Fourier transform
FPGA	field-programmable gate arrays
FMPPT	filed maximum power point tracking
GTO	gate-turn-off thyristor
ICT	information and communications technology
IEA	international energy association
IEC	international electro-technical commission
IEEE 519	Institute of Electrical and Electronics Engineers 519
INC	incremental conductance
IGBT	insulated-gate bipolar transistor
HAN	home automation network
HVDC	high-voltage, direct current
LCS	logic control switch
MAS	multi-agent system
MC	micro-source controller
MGCC	microgrid central control
MMO	multi-master operation

MPPT	maximum power point tracker
MCT	mos-controlled thyristor
NO _x	nitrogen oxide
PCC	point of common coupling
PD	proportional derivative
PET	power electronic transformer
PLD	programmable logic devices
PLL	phase-locked loop
P	real power
P&O	perturbation and observation
PI	proportional integral
PMSG	permanent-magnet synchronous generator
PLD	programmable logic device
PR	proportional resonant
QP	active and reactive power
PV	photovoltaic
PWM	pulse width modulation
RES	renewable energy sources

R/X	line resistance to reactance ratio
SPWM	sinusoidal-pulse-width modulation
SMC	sliding mode control
SMES	superconducting magnetic energy storage
SMO	single master operation
SVPWM	space vector pulse width modulation
TCP	transmission control protocol
THD	total harmonic distortion
VCO	voltage-controlled oscillator
VSI	voltage source inverter
WECS	wind energy conversion systems
3C	circular chain control

LIST OF SYMBOLS

V_{rms}	root mean square voltage
Z	Impedance
Z_L	load impedance
Z_O	output impedance
Z_{Line}	line impedance

GLOSSARY OF TERMS

Anode	An electrode, or electrical conductor, through which electric current flows into a polarized electrical device
Bus	Communication system connection between IED with communication facilities
Cogeneration	Simultaneous production of heat and electricity at the point of use, also referred to as combined heat and power generation
Distributed energy resources	Sources of electric power that are not directly connected with a bulk power transmission system; these include both generation and energy storage technologies
Distributed generation	The process of generating electricity using renewable energy resources – these resources generating the electricity are usually distributed over an area, like a photovoltaic farm. Electricity obtained by distributed generation is usually fed into a microgrid
Distribution network	A system of cables that deliver power to consumers at usage voltage levels
Electric power system	An assemblage of equipment and circuits for generating, transmitting and distributing electrical energy
Electrode	An electrical conductor used to make contact with a non-metallic part of a circuit, such as an electrolyte in an electrochemical device
Electrolyte	A substance containing free ions that make the substance electrically conductive

Fossil fuel	Fuel produced by remains of living organisms that built up underground over geological periods; it mainly consists of carbon and hydrogen
Function	Task performed by the substation automation system such as application function. Generally, function exchanges data with other functions. Details are dependent on the functions involved. function is performed by IED (physical device) A function may be split into parts residing in different IEDs but communicating with each other (distributed function) and with parts of other functions. These communicating parts are called logical nodes.
Generator	An electric machine that converts mechanical energy to electrical energy
Greenhouse emissions	Gas emitted into the atmosphere that absorbs infrared radiation, thus contributing to the greenhouse effect
Hydronic heating	Use of hot water as the heat-transfer medium in a heating system
IEC 61850	An international standard for communication in substations, also extensible to the rest of the power system
Inverter	An electrical device that converts direct current to alternating current
Load	A device that consumes electrical power
MATLAB/SIMULINK	A numerical computing and simulation environment belonging to the MathWorks suite
Microgrid	A micro power system that includes a cluster of loads, storage and multiple DG sources. A microgrid can usually operate in autonomous mode, or it can be connected to the national

	electricity grid
Model	Representation of some aspects of reality, created to aid understanding, description and/or prediction of real-world phenomena
Natural gas	A naturally occurring hydrocarbon gas, composed primarily of methane, and fewer percentages of other hydrocarbons as well as impurities
Object	A useful item that has an identity, a structure and certain behaviour
Real-time digital simulator	A modular, fully digital power system simulator that performs detailed hard real-time electromagnetic transient simulations of the power system's behaviour and response
Renewable energy resource	Natural sources of energy such as sunlight, wind, rain, tides and geothermal heat, which are naturally replenished
Smartgrid	The term given to the modernized electric grid that employs ICT and computational intelligence to improve the efficiency, reliability, economics and sustainability of electricity supply
Voltage profile	A plot of voltage variations of a given supply network over a period of time

Chapter 1 : INTRODUCTION

1.1 Background

Centralised generation, mostly known as conventional power generation, uses energy from fossil fuels (oil, gas, coal) or nuclear material to produce electricity via some form of rotating machine. The system is established such that a power generator is linked to several consumers, just as in a paradigm tree. In that model, the high voltage transmission lines from the central power station act as the trunk of the tree, transporting electricity through a long distance to the distribution network. The distribution network can be assimilated to the branches that deliver power to the consumers (industrial, commercial and residential) (Sporn, 1946).

One of important characteristics of the modern world is the rapid increase its population and the associated increase in the demand for electrical energy; this leads to increasing primary energy consumption (non-renewable energy) and consequently to depletion of fossil fuel reserves which are finite (Bose, 2010; Steimer, 2010). As a result, end-users suffered severe blackouts and ongoing electricity price hikes. The power blackout faced in South Africa in 2007 was the consequence of electricity demand temporarily exceeding the available resources for the supply by the power utility ESKOM (Grover & Pretorius, 2007).

Other challenges faced by the power generation industry are losses, as well as the ageing of infrastructure; the energy produced by a power plant is considerably reduced before reaching the end-users, due to losses that occur in long transmissions lines during the transport of energy from the power plants to distribution points. Also, it is complex to incorporate new automated systems into existing centralized control schemes that were installed 30 to 50 years ago (Shipley & Elliott, 2006; Martin, 2009).

However, the most important challenges actually faced by the generation industry are the issues of global warming, pollution, and climate change. According to several authors (Nagaraj, 2012; Bose, 2010; Harley & Paine, 2009; Alley et al., 2003) the use of the fossil energy, which conventional power plants depend on, results in greenhouse gas emissions and has a significant negative impact on the atmosphere. Also, a study by McConnach (2006) shows that 25% of the CO₂ emissions are from the electricity sector, due to the burning of coal, gas, and oil. As such, many countries have engaged in the Kyoto Protocol to considerably reduce greenhouse gas emission by at least 34% by 2020 and 80% by 2050. Governments are now supporting the use of renewable energy sources (RES), in order to produce eco-friendly, clean power, having a

minor impact on the environment (Maheswaran et al., 2012; Zhaoguang et al., 2010; Pereira et al., 2006).

The problems of ageing and underdevelopment of distribution grid infrastructure make electricity penetration into the African continent more difficult. The continent presents the highest non-electrified rural areas compared to the rest of the world and this, despite the immense potential in resources available (Belward et al., 2011). Rural areas are sparsely populated with very low electricity in consumption. In Uganda for instance, only about 1% of households have access to electricity in rural areas, and more than 40000 people do not have access to national utility grid (Applewhite, 2002).

For more than 50 years, stand-alone diesel generator systems and grid extensions have been used to cover electricity needs in some rural areas in Africa. However, these methods are not desirable, not only due to their high production costs high costs (about 1 US Dollar per kWh in Uganda against 5 cents per kWh in the USA), but also because of their environmental impact (Applewhite, 2002).

Considering all the above-mentioned problems, it is obvious that traditional power plants can no longer guarantee safe, reliable, and sustainable electricity supply. DG appears as the solution of choice for this matter; it is the key to improving electrical supply (Buritica-Arboleda & Alvarez-Bel, 2011). The concept of a DG was introduced in the late 1990s to overcome the multiple challenges faced by the centralised generation and has since gain popularity. DG generates electrical power from small energy sources (normally less than 50 MW) using non-traditional RES such as wind power, solar power, biomass. With this form of generation, transmission line losses are considerably reduced since the power plants are usually very close to the consumer (Anwar & Pota, 2011; Martin, 2009). Furthermore, the distributed power unit can be directly connected to the customer load or to the supporting distribution network (Isle et al., 2014; Bhadoria et al., 2014). Besides providing cheaper electricity, DG has the advantage that the power is clean because no fossil fuels are used. One of the most popular renewable energy sources is solar energy because it is abundant, accessible and easily converted into electricity (MN Ambia, 2010). The demand for solar energy has increased by 20% to 25% per annum over the last two decades (Selvaraj & Rahim, 2009). More importantly the PV system is one of the most efficient renewable energy technologies, especially in remote areas where electricity from the central grid is not available and alternative sources of electricity are expensive (Ahmad et al., 2003; Chel et al., 2009). The South African government is planning to provide power to 200000 homes, 100000 small businesses, 2000 clinics and 16800 schools, using PV or solar home systems, as a part of their off-grid electrification program (IEP, 2013).

A microgrid is a group of DG units, controllable loads, and interconnected and communicated storage devices, all operating together as a single system by using power electronic interfaces and controls for flexibility. Microgrids supply electricity to small communities such as small towns, universities, and industrial areas; they can operate in two ways, either connected to a grid or in stand-alone mode. It is essential to adopt a flexible control to a microgrid in order to be seen by a primer grid as a single controllable unit (Katiraei & Iravani, 2006; Dimeas & Hatziargyriou, 2005). A connected microgrid is defined as a grid that is connected to a utility grid at a static switch called the point of common coupling (PCC), and cooperates with the utility grid by adjusting the power balance of the utility grid in terms of facilitating the import/export of power. On the other hand, a stand-alone microgrid is referred to as a utility grid which is disconnected from the utility grid at the PCC, and operates autonomously.

Nevertheless, implementing intelligent control as part of the energy management system of a microgrid presents a challenge. In order to monitor the entire microgrid system, the use of intelligent devices integrated into the DG system, increases the amount of information available in individual microgrids; this applies whether connected to the main grid or not. This information can be used by the energy management system for making intelligent decisions with regard to the best use of the generators for producing electric power and it can do so without human intervention.

1.2 Statement of the research problem

The increase in the demand for power is one of the challenges faced by the conventional power system. The introduction of the decentralized system paradigm provides some solutions to the current problems for customers connected to an existing grid. Importantly, the research aims to determine the best implementation and design of smart control for microgrids utilising solar PV, with the microgrid operating in isolation from the main electrical utility grid. A further aim is to determine how information can be efficiently used and intelligently exchanged between the different components of a microgrid as well as analysing how the sensors can increase the information on load demand. This research will also look at how smart microgrid controllers can incorporate sensing and control algorithms to effectively stabilize the grid.

1.3 The challenge facing inverter control

DG has the characteristic that energy generated available at given time are uncertain; fluctuations are unavoidable. To stabilize voltage received by the inverter, which is interfacing between the DG system and the rest of the microgrid, requires a systematic control.

When DG is connected to the main grid, the following disturbances can occur:

- The inverter is sensitive to temperature variation which influences the interface impedance. It affects the stability of the inner controls of the DG system. The grid impedance associated with the AC filter of the inverter in a DG installation system may be subject to high frequency resonance dynamics. A DG system injects a distorted current which leads to the presence of harmonics in the voltage and current of the drivers (Liserre et al., 2006; Bindner & Lundsager, 2002).
- Current control using a pulse width modulation (PWM) inverter in DG is a common method implemented to ensure better quality power injection (Blaabjerg et al., 2004). This method of design requires an inner current control loop at high bandwidth to keep tracking the current. The current control reduces maximum transient period possible and the voltage source inverter (VSI) should react as an amplifier source for the inner current loop bandwidth. This instability is associated with oscillations in the injected current due to the saturation effect of the PWM.
- The inverter controller is likely to be affected by instability in the impedance at the PCC, as well as by fluctuations in the frequency. The grid voltage at the PCC can be distorted by multiple types of nonlinear loads, especially in a weak grid. This leads to an imbalance in, and distortion of the exporting power (Asbafkan et al., 2013).
- The inverter control can regulate the voltage disturbances caused by time variant loads, grid faults, as well as by the transition voltage resulting from capacitor switching.

The autonomous microgrid system is composed of a group of DG installations providing assistance to the main grid. Also, such a system operates independently, should a grid fault occur in the main electrical grid:

- Unlike most conventional power systems, inverters of the DG systems do not have a physical inertia: as a consequence system disturbances occur which sometimes cause oscillation of the microgrid. A number of disturbances have been recorded due to the variation in load over time, and also power share between parallel inverter.
- Proper load sharing control strategies for a microgrid present a challenge. The communication-based, centralized, control mechanism adopted in microgrids, performs well. In remote areas however, the distance between inverters can be unreasonably large, making centralised control vulnerable to malfunction because communication is characterised by (unreliable) high bandwidth signals. Also, decentralised control of microgrid DG installations presents some problems.

1.4 Motivation for research

There is on-going research focused on microgrids and a lot of investigation has been conducted by many research groups to determine the feasibility and benefits attached to the microgrid. Even though the fundamental principles of microgrids are well known, implementation of the system is not always well mastered. The effect of distributed generation on microgrid behaviour is unpredictable as soon as the system is subjected to several interconnections from different sources, or load variance and voltage disturbances. Applying the basic control of a conventional distribution system is not efficient anymore with the microgrid development. The development of an inverter interface-based control is needed for the core of microgrid research. The effectiveness of a robust control for a microgrid connected inverter to interface with distributed generation systems, will be the main focus of this research.

1.5 Research objectives

To overcome the challenges outlines in Section 1.3 above the inverter control to be developed should comply with the following objectives:

- Modelling and development of an inverter controller for carrying out the investigation and analysis of the experimental results.
- Modelling of a distributed generator, based a PV array sufficient for a cluster villages
- Modelling and analysis of an autonomous microgrid
- Development tools to be used for the simulation and analysis work, will be a MATLAB/SIMULINK environment
- An inverter voltage control to withstand disturbances
- Analysis of control using a digital platform
- Autonomous microgrid simulations will be carried out to investigate the integration of a distributed inverter base control for an energy management system.

1.6 Thesis organisation

- Chapter one presents the research problem and statement. It also highlights the methodology, significance and contribution of the research work carries out in this thesis.
- Chapter Two sets out the literature review, and covers discussions on the performance of different control methods as applied in a microgrid which contains Distributed Generation interfacing with voltage source inverter (VSI).
- Chapter Three covers a further discussion of the literature review, power electronic devices and inverter control using different digital control platforms.

- Chapter Four discusses the modelling and control carried out in the project.
- Chapter Five discusses the results and the research outcomes. It presents all the simulation results which found using the MATLAB / SIMULINK platform
- Chapter SIX concludes the research. A summary of the research is (presented / given) and also recommendations for future work are suggested.

Chapter 2 : LITERATURE REVIEW

2.1 Introduction

The chapter focuses on the literature, which relates to the proposed research topic. An overview of the benefits of a microgrid system using DG based on photovoltaic systems, wind, and micro-turbines are discussed. Furthermore, the major problems associated with a microgrid system, frequency deviation and voltage drop, are also discussed; these problems are controlled by mechanisms such as droop control and master-slave methods. The control mechanisms used to maintain the output voltage waveform and power sharing in a microgrid is through the VSI. Furthermore, several other control methods for improving the power quality and load sharing of a microgrid connected to the main grid or operating in autonomous mode. The stability of microgrid performance is analysed under unbalanced and nonlinear-loads.

Most of the distributed energy sources interface with the utility grid and to the customer loads through a DC-to-AC VSI. The inverter is an important component of the microgrid forming the main interface component which integrates the DC voltage of the renewable energy source with the AC voltage requirements of the demand load and the grid utility. It is used for the stabilization of the grid by controlling the voltage, frequency, the active power and reactive power (Yang et al., 2003; Kolmakov & Bakhovtsev, 2013).

The remainder of this chapter is organized as follows. In Section 2.2 the benefits of the microgrid concept and distributed network are presented. In Section 2.3 a detailed explanation of microgrid structures and components is given. In Sections 2.4 and 2.5 distributed generation types and technologies, especially non-traditional generators, are presented. In Section 2.6 the microgrid control layer and distributed generation control structure are discussed. In Section 2.7 the smart meter in a microgrid is discussed. In Section 2.8 frequency control in a power system is presented. A conclusion is drawn in Section 2.9.

2.2 Concept of microgrid and distributed network

Basically a microgrid involves the integration of multiple distributed energy collection sources; the electricity from these sources is gathered, processed and distributed to meet the demand loads. When power electronics interfaces with micro energy forming a single entity, its operation requires a control system. Such a control system is needed, not only to provide flexibility, but also to preserve the specific energy output and the power quality.

2.2.1 A comparison between a conventional power grid and a microgrid

The deviations between conventional power grid and microgrid are the following (Chowdhury et al., 2009):

- The output capabilities of producing electricity by microsources are much smaller when compared to a conventional power plant that can produce.
- Microgrid installations are usually closer to the customer load which leads to low loss in transmission lines. Microgrids are therefore highly efficient in terms of voltage supply and frequency profile as opposed to centralised power plant with transmission and distribution network see Figure 2.1 below.
- It is more practical in microgrid to supply power to remote areas where it is almost not suitable for the national grid
- The process of traditional power system restoration is awkward. It requires a fast intervention, usually manually and in real time, whereas with a microgrid procedure the entire restoration process is very easy because of the limited number of controllable variables.

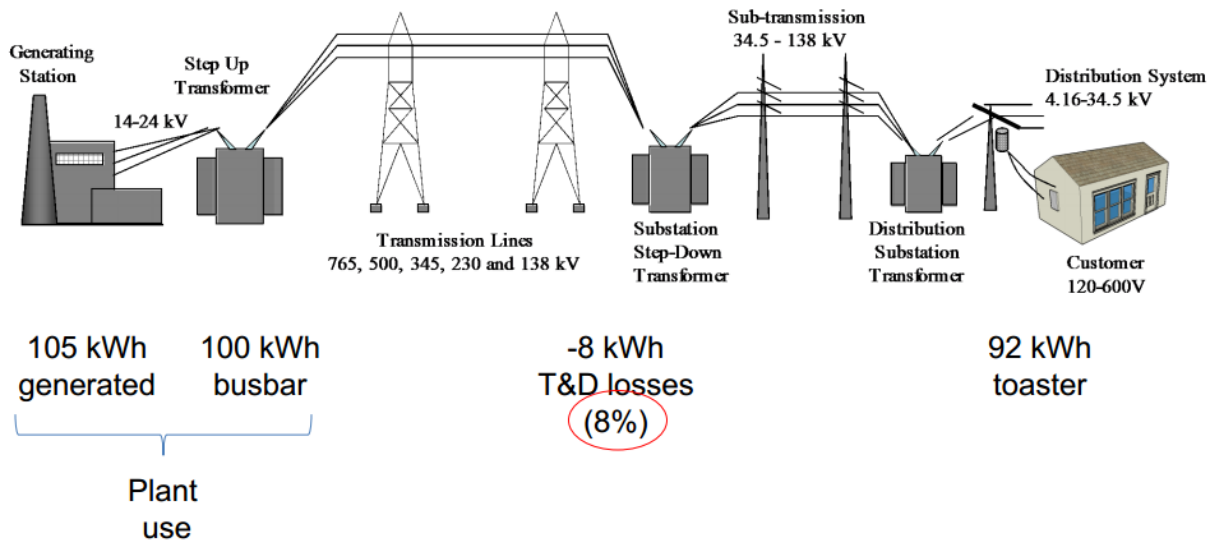


Figure 2.1: General architecture of a centralised electricity power system showing losses (Firouz, 2010)

2.2.2 Fundamentals of a microgrid

Low and medium DG infrastructure is in rapid development around the globe. They are powered by renewable, non-conventional generators which include; fuel cells, wind turbines, and photovoltaic system (Li et al., 2004; Chowdhury et al., 2009). Normally, they are used to

augment the utility grid during peak hour load, where that time corresponds to a shortage of power. They can also provide support to power in cases the main system grid fails.

In recent years, the concept has gotten more interesting where the grouping of an arrangement of loads forming a cluster, together with parallel DG units, constitute what is known as a microgrid. Small generators can be incorporated into the power system, like in the traditional method where a small generator unit was aimed to reduce the impact of grid operation in each interconnected microsource. For an outage in the grid network due to an error detected in the utility grid, it will systematically affect and shut down the generator units, compared to a microgrid when the grid network is off, the power shuts down, the microgrid will systematically disconnect from the grid network and operates independently in providing power to its local load when the utility is back to normal.

2.2.3 Microgrid benefits

The development of microgrid serves as a way of gaining an advantage compared to other systems, this is summarized below (Chowdhury et al., 2009):

- With regard to environmental concerns, a microgrid helps to cut down pollution because it uses microsource that produce low or zero emissions.
- Microgrids work in parallel to the utility grid; by taking care of certain loads they support the utility grid. The extra capacity provided by microgrids can assist in preventing overload situations and blackouts of the national grid.
- Economically, there is reduction in long transmission line installation and the corresponding transmission. The low-cost installation of the microgrid systems locally considerably saves infrastructure costs and transmission losses. Microgrids also help in reducing the consumption of fossil energy.
- By operating in both grid-connected and autonomous mode, it ensures uninterrupted loads. This makes it more reliable and delivers high quality power to the critical loads.
- The microgrid takes advantage of thermal energy saving when using combined heat and power. This is an easy process to achieve with the microsource in a microgrid. The microsource can be deployed closer to thermal and electrical loads for maximizing energy efficiency.
- The microgrid takes advantage of thermal energy saving when using combined heat and power. This is an easy process to achieve with the microsource of a microgrid. For maximizing energy efficiency, the microsource can be deployed closer to the thermal and electrical loads.

2.3 Rearrangement of the structures and components of a microgrid

2.3.1 Microgrid structure

The structure of microgrid consists of five major components. These are microsources (power sources), loads, storage devices, control systems and the point of common coupling. These five components are connected to a low voltage distribution network. The low voltage distribution incorporates a variety of microsources and different types of load that are supported by the power electronic interface. In order to provide synchronization and control the operation during the grid connected mode or autonomous mode, the mode of operation can be determined by the PCC. This is the point where the microgrid is coupled with the main medium voltage utility grid; it is indicated by CB4 in Figure 2.2. The function of CB4 is either to connect or disconnect the operation of the microgrid from, or to the main grid. The operation and management of a microgrid are supported and coordinated through different levels of control to ensure the overall stability of the system, using the following controllers: microsource controller, central controller (Katiraei et al., 2008; Ilić & Zaborszky, 2000).

A description of each component is provided in Figure 2.2 below:

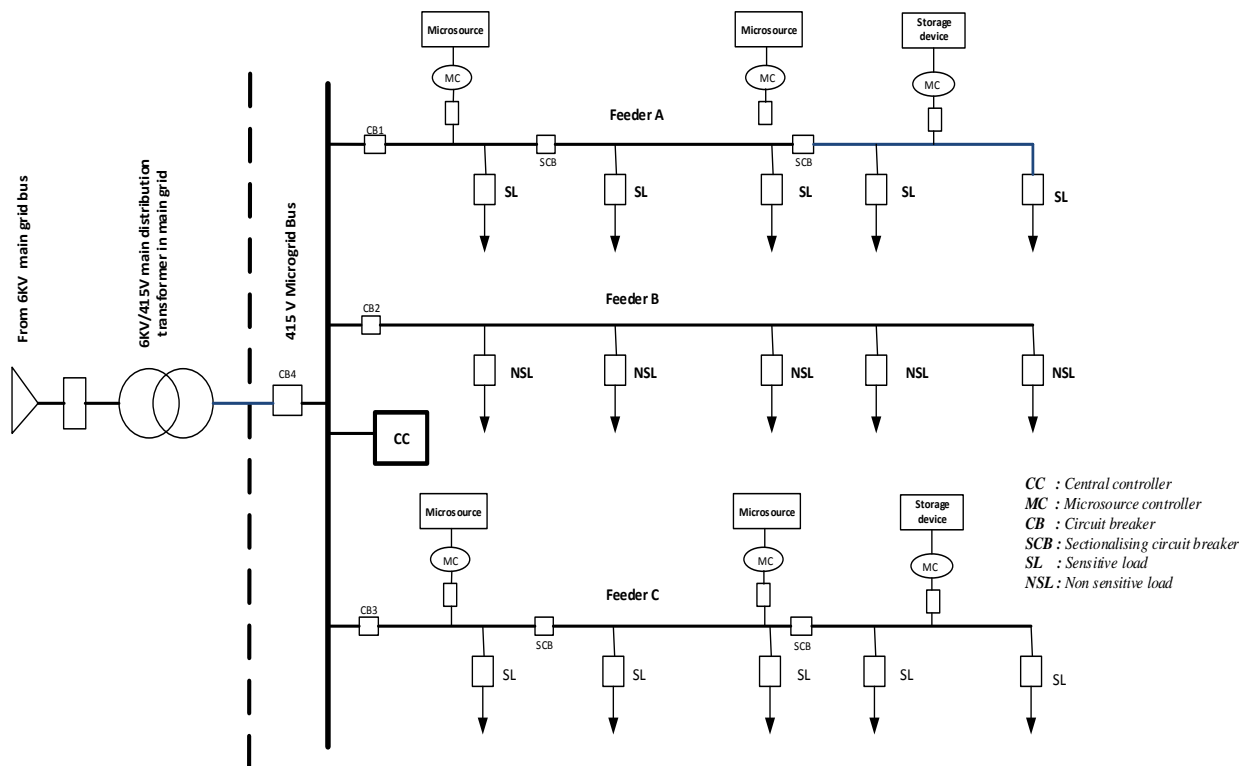


Figure 2.2: Typical microgrid configuration
(Chowdhury et al., 2009)

2.3.2 Microgrid types: AC and DC

The microgrid is similar to a small power system which encompasses various components such as DG units, loads and storage devices that are interconnected. In terms of power, the microgrid can be classified as an AC power system, a DC power system, or a hybrid system. When used, each microgrid type presents advantages and disadvantages. Figure 2.3 below depicts some the microgrid types.

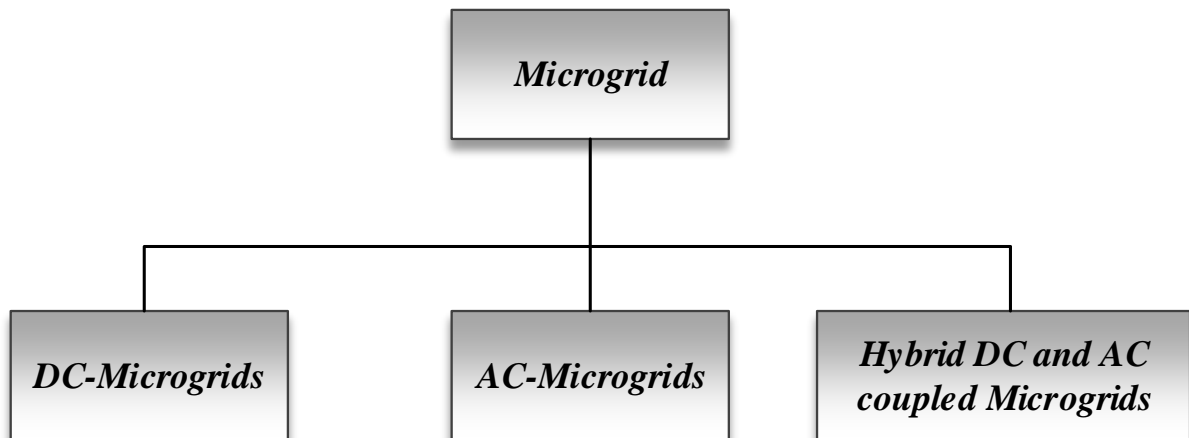


Figure 2.3: Classification of the microgrid based power type (AC or DC)

2.3.2.1 The DC microgrid system

The DC microgrid can be used in grid-connected mode, or in autonomous mode. It presents several operational advantages (Ilić & Zaborszky, 2000).

- Most of the DG systems employed in the microgrids, are such as PV units and fuel cells DC supply. Storage devices have a DC output voltage, so connecting them to the DC microgrid will only require a voltage regulator, as compared to an AC microgrid which additionally needs to synchronise the system by matching the voltage magnitude, the phase and the frequency to the grid.
- Most of the loads that are connected to a DC microgrid in are conventional loads, typically electronic devices, TVs, computers, fluorescent lights, variable speed drives, households, businesses, and industrial appliances. So being connected to a DC type microgrid there is no for need for multiple conversions of the power system stages such as AC-to-DC, DC-to-AC or AC-to-DC-to-DC, as would be required for an AC microgrid.
- The DC microgrid does not use transformers; this makes it more efficient, smaller in size, and reliable in a DC power system. In addition a DC microgrid operates with twin wire cable, whilst an AC microgrid operate with three or four wires

- Reactive power flow does not exist in DC microgrids, so the voltage control is concerned with the active power flow, while in AC microgrid the voltage control is related to the reactive power flow at the same time injecting the active power mostly to delimit the local power angle of the interfacing VSI.

However, a DC microgrid still has several challenges which have to be overcome. It is not well developed to handle fault conditions and lacks basic protection equipment like circuit breakers, fuses, and protection relays, as seen in AC microgrids (Salomonsson et al., 2009; Lago & Heldwein, 2011). It is very expensive to implement the current protection system of an AC microgrid and make it to be compatible with a DC microgrid. The DC network faces an imbalance problem. The acceleration of the system losses is due to the problem of unbalanced loads or generation between the positive and the negative line of the bipolar DC microgrid. This produces a current that flows in a third reference of the DC cable (Lago & Heldwein, 2011; Jamian et al., 2011). Figure 2.4 shows a typical structure of a DC microgrid interconnected with a medium-voltage AC network of conventional power plants.

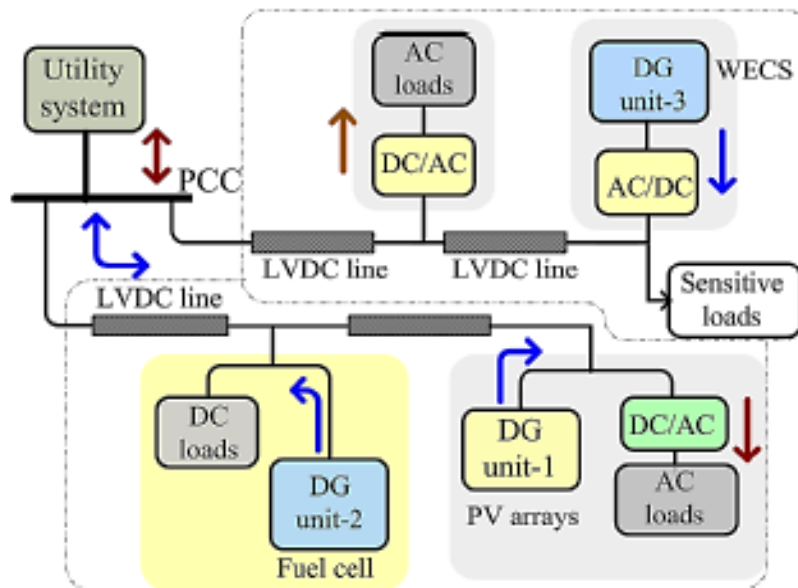


Figure 2.4: Concept of a DC microgrid system with DG units and mixed load types
(Justo et al., 2013)

2.3.2.2 AC microgrid system

All the distributed generation units that are producing an AC output power, such as wind turbines, and biogas, can be directly linked to an AC-bus line of the microgrid or via an AC/DC/AC power converter (Baran & Mahajan, 2003).

An AC microgrid has a facility to use existing infrastructure from the utility grid, due to the nature of its power system and its compatibility with the utility grid. When using an AC microgrid, there is no requirement to reconfigure loads or the building power system of the supply. This implies that the AC loads are connected directly to the AC microgrid without any power conversion through an AC-DC converter interface (Justo et al., 2013). Also, it contributes to the utility grid stability by offering reactive power support for balancing and ancillary services. With a view to power sharing, there are many controllers that have been developed with the purpose of maintaining stability in an AC microgrid. The power sharing loop results in the stability of the AC microgrid. For instance, power sharing for parallel inverters has been investigated by many authors. Figure 2.5 below shows the typical structure of DC microgrid interconnected medium voltage AC network of conventional power plants.

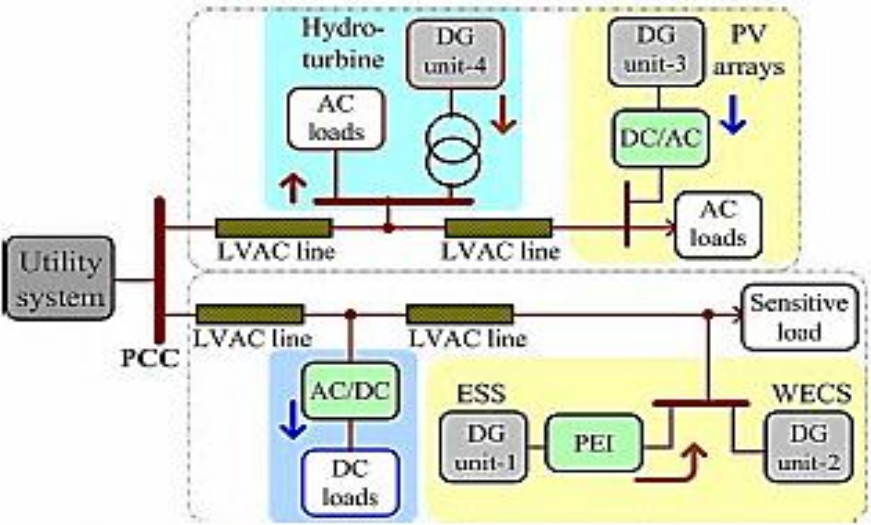


Figure 2.5: AC microgrid structure with DG units and mixed types of loads
(Justo et al., 2013)

2.3.2.3 Hybrid microgrid

The hybrid microgrid consists of the combination of both the AC and DC microgrid. The bidirectional power electronics is used to achieve the hybrid microgrid system. The system presents some advantages from both AC and DC microgrid. AC or DC loads can be supplied without need of an additional converter interface, which increases the efficiency and reliability of the system. However, the disadvantage is that the system may require a coordinated control algorithm to accomplish a stable performance.

2.4 Distributed energy resources

distributed energy resources (DER) technologies are defined as smaller power sources, and storage resources usually located at customer loads side and provide power necessary to supply the entire or a portion of the end-user electric load demand. Also, they have the ability to function in parallel with the utility distribution system. they can work separately from the utility as a stand-alone system in an isolated area (Laaksonen, 2010; Kanellos & Hatziaargyriou, 2009).

The microgrid is fed by renewable energy to generate electricity; renewable energy is also known as DERs (Justo et al., 2013). They are microsource units integrated into a microgrid. They can either be renewable energy units or conventional generators such as synchronous and induction generators see in Figure 2.6. From the source side the output of a micro generator requires power electronics to convert the power to its different forms; it can produce a fixed or variable frequency AC or DC. The conversion may require an inverter, or both rectifiers and an inverter to ensure that the output frequency and voltage are similar to that of the grid.

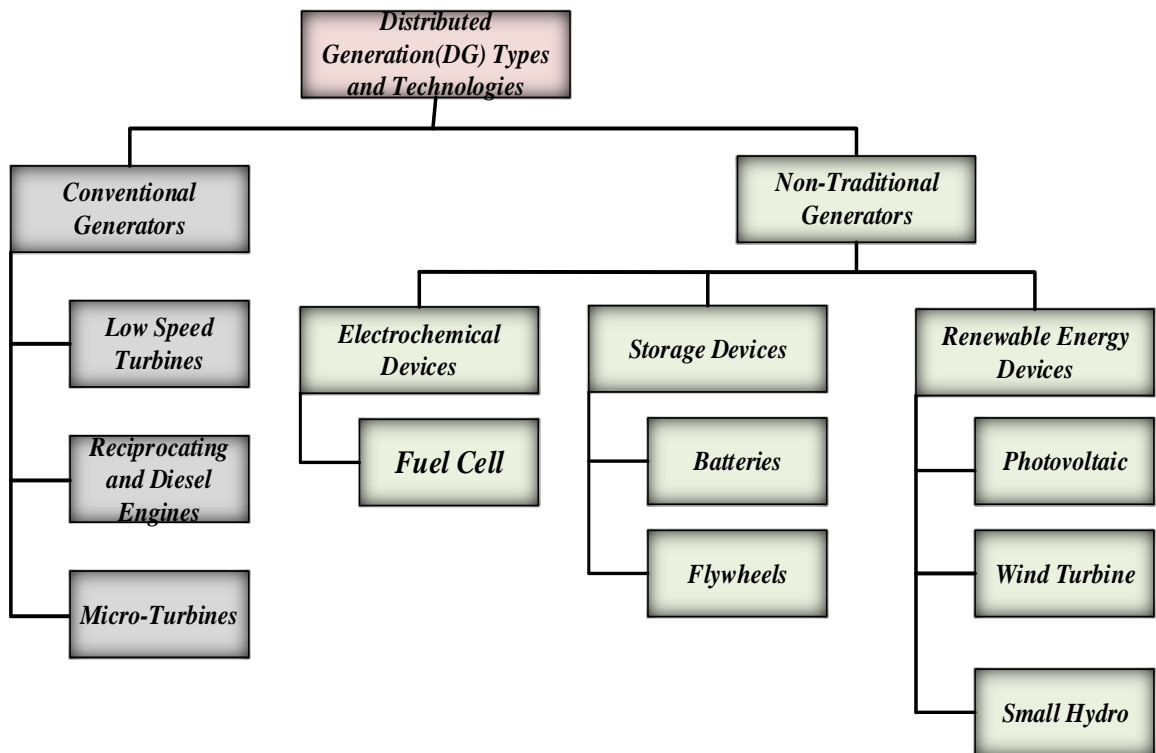


Figure 2.6: DG types and technologies

In terms of power flow control, a microsource can be considered as either dispatchable or non-dispatchable. The supervisory control system defines the set point of the output operation of the dispatchable units. Thus, synchronous generators are conventional units that can be regulated

and controlled externally. DG units using renewable energy sources are often non-dispatchable units; their output power can only be regulated, based on the optimal output power of the primary energy source – for example, the maximum power point tracker control in a photovoltaic system.

There are a number of DG technologies, such as: combined heat and power (CHP) systems, wind energy conversion systems (WECS), solar photovoltaic systems, small-scale hydroelectric generation and other renewable energy sources storage devices are examples of technologies developed from DERs. The climate and the topology of a region are important elements to consider before installing DER (Abdullah et al., 2011; Li & Chen, 2008; Parida et al., 2011; Erdinc & Uzunoglu, 2012).

2.5 Non-traditional energy sources

2.5.1 Combined heat and power systems

A combined heat and power or cogeneration system produces useful electricity and heat simultaneously. The electrical energy generated in this type of system ranges from 10–100 kW; this capacity is used locally and excess electricity can be dispatched to the grid. Due to the high cost and huge losses of transporting heat, it is rather used locally for domestic and industrial processes. The CHP system reaches an efficiency of more than 80% when compared to a conventional power plant which is about 35% efficient; this due to the CHP system being much closer to the user. The incorporation of a CHP system can contribute to a reduction of up to 35% in primary energy use, as well as reducing CO₂ emissions by 30% when compared to a large coal-fired power station (Gu et al., 2010; Tsourapas et al., 2005; Dolman & Peters, 2003).

2.5.2 Photovoltaic system description

A large quantity of electricity is produced when PV modules are connected into an array configuration. A PV panel produces a constant DC voltage depending on the solar radiation. Generally, power electronics is required at the interface with a microgrid connection, where an inverter changes the DC voltage generated, into a suitable 50 Hz AC voltage.

Variations in weather conditions make it necessary to control the output voltage in order to achieve optimum output voltage. Maximum power point tracking (MPPT) is a special control technique developed to constantly extract the maximum possible power from the various available power variations produced by one PV panel or a PV array, under varying conditions

(Blaabjerg et al., 2004). This preserves the operation of a PV array at the highest possible efficiency by maximizing the energy captured.

2.5.2.1 Solar radiation on a photovoltaic cell

PV cells constituted of semiconductor materials which have the capacity to absorb solar energy and change it into usable electrical energy (the p-n junction directly converts light energy into electricity, directly proportional to the incident radiation) (Blaabjerg et al., 2004; Md Kafiul Islam, 2011).

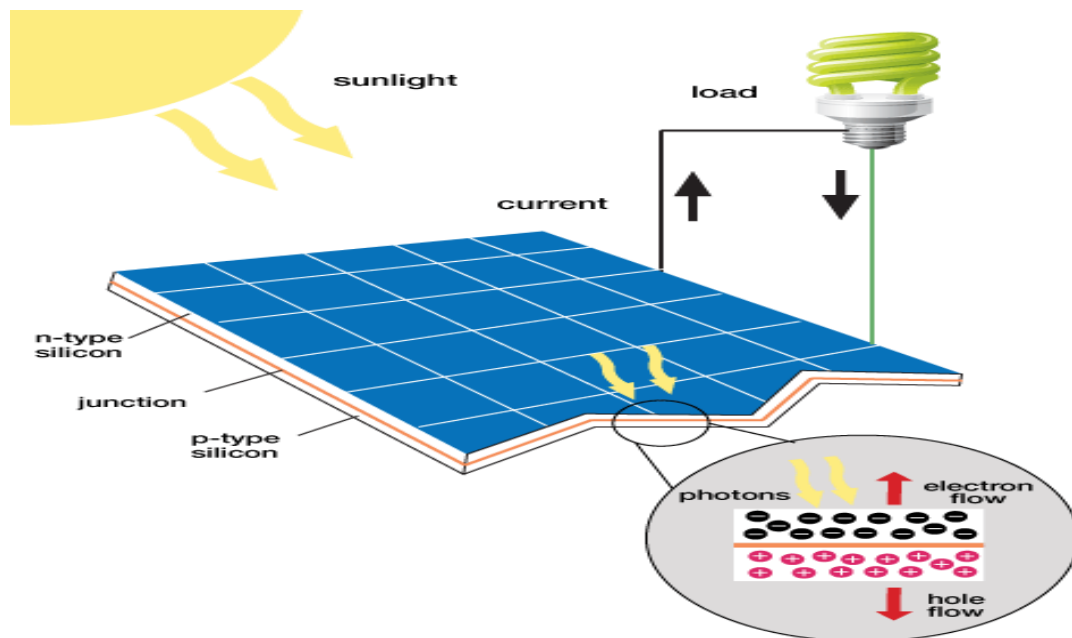


Figure 2.7: Photovoltaic operation
(www.sumberkhatulistiwa.com)

The mode of operation is as follows: Two silicon layers forming the solar cell; one of the layers is positive and the other is negative. So when the silicon semiconductor is irradiated by direct sunlight, and provided that the energy absorbed from the sunlight is more than the band gap energy of the semiconductor, then this provokes electrons to detach themselves from the atoms of the silicon material. In other words, the electrons move from a valence band to a conductor band. Consequently, the hole-electron pairs are formed in the illuminated region of the silicon semiconductor. The electrons move freely in the conduction band and a specific direction is imposed by the PV cell. Hence, the electron flow produces an electrical current. The electricity can be used to power a load if an electrical circuit is established by connecting to the top and bottom silicon layers of the solar cell; this is shown in Figure 2.7 above.

2.5.2.2 Photovoltaic module

PV cells are assembled into modules to provide the desired output; they are connected in series to obtain a high voltage and in parallel to obtain high current. The physical PV modules are comprised of a number of connected PV cells, encapsulated by a transparent front panel and back panel. The front panel is usually a low-iron, tempered glass material. The number of cells in a PV module can vary depending on the manufacturer, but mostly a set of 36 or 72 PV cells is used. A cut-away, isometric view of a typical module is shown in Figure 2.8 below.

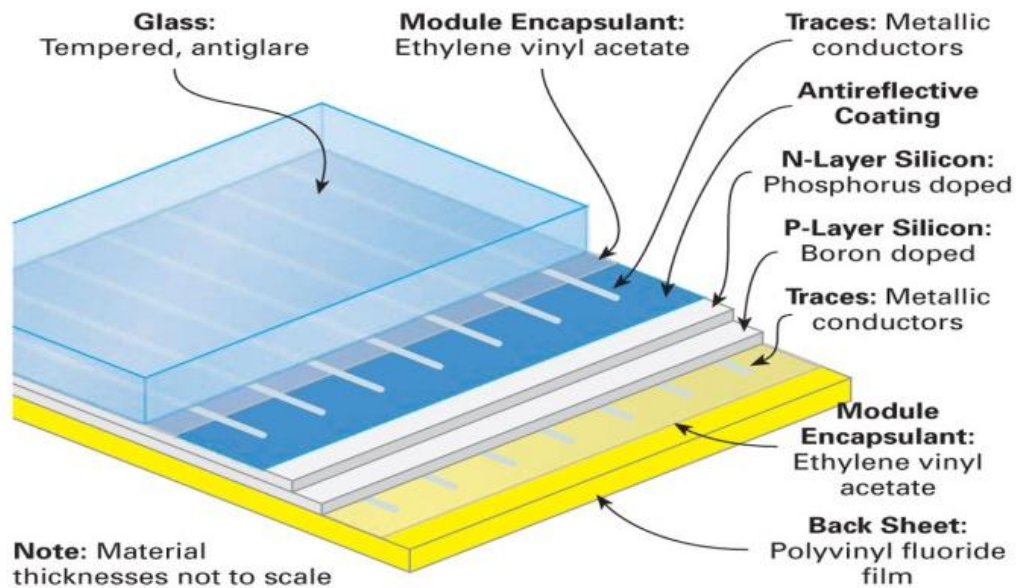


Figure 2.8: PV module anatomy
(<http://www.homepower.com>)

2.5.2.3 Photovoltaic array

A single PV module usually cannot produce enough power to meet the load requirements. Several adjoining PV modules are electrically connected to form a photovoltaic array. Several PV modules are assembled and connected to form an array; the inter-connection between the modules and the number of modules would be determined by the array requirements. The progression from a single PV cell to a PV array is depicted in Figure 2.9 below. The requirements above alludes to both the amount of power required (bigger array- more modules) and whether a high voltage or a high current is required (series or parallel connection). The PV modules in an array are connected in a similar way to which the cells in a module are connected (Mohan et al., 2002; Rahim et al., 2010).

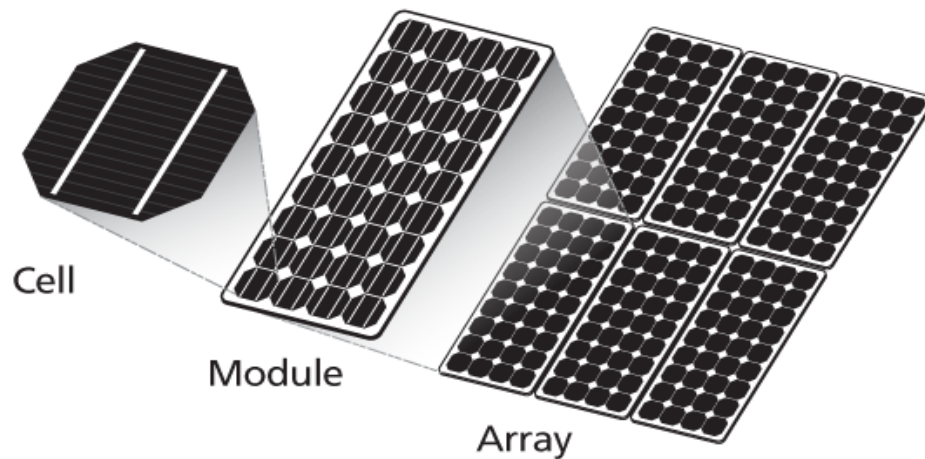


Figure 2.9: Solar cell
(www.wifinotes.com)

2.5.2.4 Photovoltaic system configurations

PV systems are operated using different types of configuration structures. Each configuration is attached to a power electronics device to interface with a microgrid or the national utility grid. The most common configuration structure used, is the centralised inverter installation. Multiple PV arrays are tied together either in series or parallel connection to a centralised inverter, which in turn converts the DC generated, to AC. The main convenience of this design is that, it uses only one inverter; this reduces the installation cost of a PV system. However, this configuration presents a high power loss due to the mismatch between the PV arrays and also, it is not reliable because it has a single point of failure at the inverter.

By contrast, the configuration of the PV string array system has PV panels connected in series to form a single string. Individual strings with their own inverter can be connected to the microgrid, or multiple strings can be interfaced to their own DC-DC converter, converging through a common inverter which is connected to the microgrid (Kjaer et al., 2005). Practically, this configuration does not have losses and MPPT can be applied to each string. It is however expensive to run several inverters.

Finally, the so called AC module configuration is made such that each PV panel has its own inverter. The primary advantage of this configuration is that it is simpler to increase the array size in the microgrid because the existing PV panels already have an DC-AC inverter. Furthermore, this configuration is more reliable because it does not have a single point of failure, and it is flexible (Blaabjerg et al., 2004; Kjaer et al., 2005; Saiful Islam, 2006). Also, it this configuration reduces the power loss to a minimum level, unlike the string array configuration

which causes a mismatch between PV panels. On the downside is, high costs are required to realize such a system configuration due to the number of inverters which need to be used.

2.5.2.5 Control algorithm of photovoltaic system

In addition to the non-linear characteristics of PV arrays, unpredictable environmental conditions have a negative effect on the output of a PV panel. Applying maximum power point tracking to PV arrays is a way of extracting the maximum power that PV modules are capable of generating and that this power is available for application to loads. So MPPT is required to be implemented to the PV where it varies the module's operating point with the intention that the modules will be able to deliver the maximum power available. The maximum energy from the radiation of the sun occurs when the derivative of power is equal to zero. There exists a peak power corresponding to a particular voltage and current.

2.5.2.6 Algorithms for maximum power point tracking

Different algorithms have been developed to spontaneously track the peak power point of a solar PV module. The common method is maximum power point (MPP) tracking of a PV system, so that the maximum power possible can be extracted. Popular controllers for PV systems developed using MPPT methods are:

- The perturbation and observation (P&O) algorithm
- Incremental conductance (INC)
- Parasitic capacitance
- Voltage-based peak power tracking
- Current-based peak power tracking

2.5.2.7 Perturbation and observation algorithm

Three different, popular and simple P&O algorithm techniques for controlling a PV system were established in subject literature (Alonso et al., 2009; Femia et al., 2009). One of these algorithms relates to reference voltage perturbation as displays in Figure 2.10. A P&O algorithm represents a permanent perturbation at the peak power point due to its oscillation at the steady state. It has a faster response to irradiance and temperature transients, but cannot operate at a high perturbation rate due to its loss of stability. Also, when the system use a low pass filter for rejecting noise, the reference current perturbation (Tan et al., 2008; Tan et al., 2007). This is highly susceptible to noise and presents a slow response to irradiance transient changes, the PI controller oscillation, and direct duty ratio perturbation (Pandey et al., 2008; Femia et al., 2005;

Koutroulis et al., 2001). At a slower transient response, direct duty ratio control presents a better stability characteristics and high-efficiency energy utilization. However, the performance of P&O algorithm is when there is a rapid change in irradiance, is worse. System stability is not affected by using low-pass feedback filters and it allows the use of high perturbation rates. A reference consulted, examined performances of the voltage perturbation and direct duty ratio perturbation on the system stability, characteristics, and energy utilization for autonomous PV pumping systems (B. Wu, 2007).

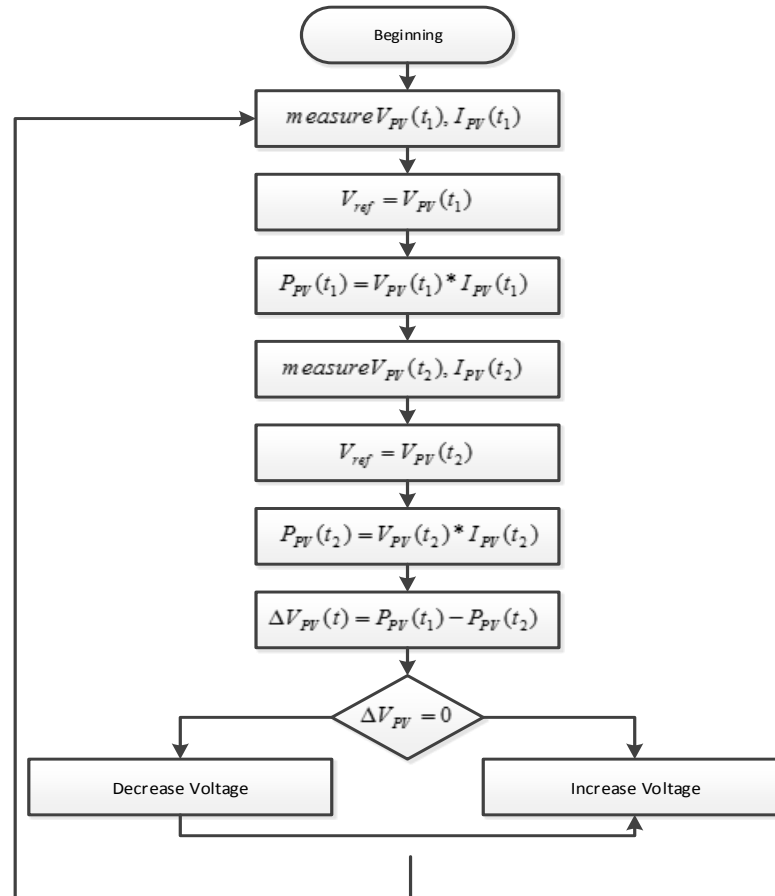


Figure 2.10: Flowchart of the perturbation and observation algorithm
(B. Wu, 2007)

In general, perturbation leads to some power loss; also it is vulnerable to tracking the power under fast-varying atmospheric conditions.

Hence, the perturbation and observation algorithm is subject to problems such as:

- sustained oscillation around the maximum power point
- fast-tracking versus oscillation trade-offs
- using predefined constants.

Optimization of the perturbation and observation algorithm is based on the following parameters: the amplitude of duty cycle perturbation and the sampling time required for the MPPT of the PV system. So, decreasing the duty cycle perturbation lessens the oscillation around the maximum power point, which therefore; this reduces steady-state losses. However, P&O algorithm is vulnerable at a rapid variation in atmospheric conditions. The selected sampling time should be more than the threshold to escape the instability of MPPT and should be selected to reduce oscillations around the steady state of the maximum power point. In this algorithm, the system should be at a steady state before the next measurement. The P&O algorithm becomes give an incorrect result when the time interval is very high (Femia et al., 2005).

Filed maximum power point tracking (FMPPT) is not a popular or usual method for tracking the maximum power point in PV systems. This method is not is not recommended for large PV system due to different orientations of PV arrays belonging to the same PV field.

2.5.2.8 Incremental conductance algorithm

The Incremental conductance is used mostly to focus directly on power variation in order to overcome the shortcomings of the perturbation & observation algorithm applied to MPPT under atmospheric conditions. Fundamentally, the incremental conductance algorithm is used to find and compare the conductance and the incremental conductance. Both are derived by calculation using the voltage and the current. Then, from the outcome it can decided whether to increase or decrease the PV voltage in order to be at the maximum power point as follows:

$$P = V \cdot I$$

$$\frac{dP}{dV} = 0, \quad \text{at maximum power point}$$

$$\frac{dP}{dV} \geq 0, \quad \text{shift left of maximum power point}$$

$$\frac{dP}{dV} \leq 0, \quad \text{shift right of maximum power point}$$

$$\frac{dP}{dV} = \frac{d(IV)}{dV} = I + V \frac{d(I)}{dV} = 0$$

$$\frac{d(I)}{dV} + \frac{I}{V} = 0, \quad \text{at MPP}$$

$$\frac{d(I)}{dV} + \frac{I}{V} > 0, \quad \text{at shift left of MPP}$$

$\frac{d(I)}{dV} + \frac{I}{V} < 0$, at right shift of maximum power point the value of the incremental conductance indicates that the MPPT has reached the state of the maximum power point.

2.5.3 Wind energy system

The wind energy system converts kinetic energy into mechanical rotation, from which electricity is generated. The mechanical rotation is effected by the blowing of wind onto the blades connected to the rotor of a generator; electrical power is generated either by a generator which requires a power electronics interface to be connected to a microgrid, or an induction generator as shown in Figure 2.11 below. The wind system is capable of a power output ranging between 10 W and 2.5 MW (Farret & Simoes, 2006).

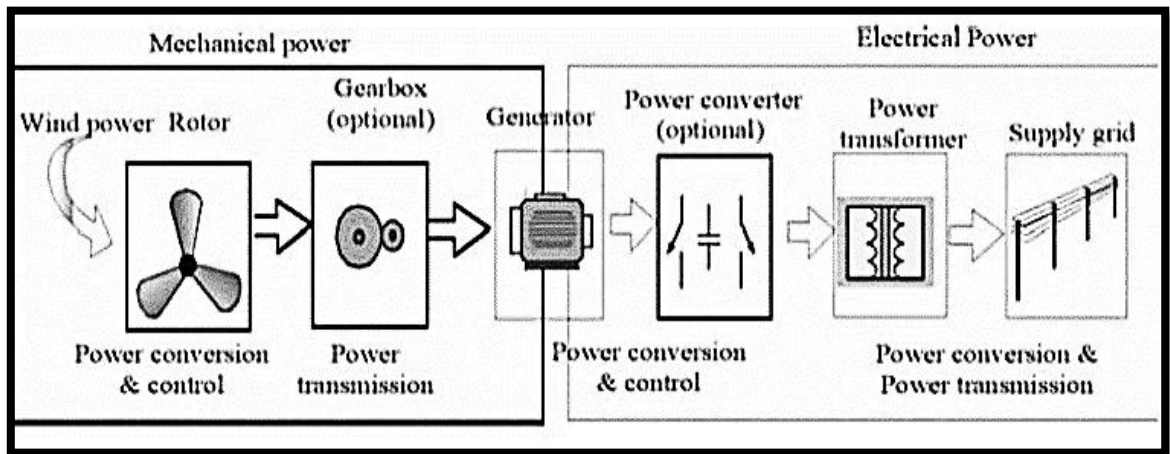


Figure 2.11: Main components of a wind generation system (Chen & Blaabjerg, 2006)

In addition, a wind farm can harvest a large amount of wind energy from many individual wind turbines which is normally grouped in the same locality, covering an area several square kilometres.

2.5.3.1 Configuration of a wind system

The induction generator does not need an inverter, so it can be directly connected to microgrid networks. However, the turbine must have a steady speed which requires a constant adjustment of the rotor speed control by adjusting the pitch of the blades.

There are some wind systems that incorporate wound rotor inductor generators in their turbines and these generators are associated partially with power electronics to interface with microgrid connections. Power electronics and an inverter are simultaneously converting the power from the wind system to suitable frequency and voltage, compatible with the AC power of the

microgrid or the national utility grid (Blaabjerg et al., 2004); alternatively an additional resistor is added in the rotor controlled by the inverter. Additionally it requires a reactive power compensator and starter. An improvement to the system has been the development of a doubly-fed induction generator (DFIG), which incorporates an AC-DC-AC IGBT-based PWM converter (Carrasco et al., 2006). This last configuration creates the flexibility by which the wind turbine can handle variations in wind speed. The grid provides electrical power to the rotor when the generator is working in sub-synchronous mode. Moreover, it increases the energy capture and provides reactive power compensation (Chen & Blaabjerg, 2006).

The configuration uses a rectifier and an inverter acting as an interface, which matches the frequency and the voltage of the wind turbine, to that of the national utility grid or microgrid. This brings about more power loss during the conversion. This topology does however, increase the technical performance and the power gain (Chen & Blaabjerg, 2006).

In addition, the entire wind system configuration uses a control design based on power electronics named back-to-back. This enhances the power flow control and it increases the efficiency of interconnection. The back-to-back PWM converter offers various benefits, such as: unity power factor with no harmonic current injection; wind generator output current that is sinusoidal; a fuzzy-logic-based vector control which is part of intelligent control.

2.5.4 Microturbine

Microturbines are relatively small combustion turbines operating as simple gas cycle turbines. They are a common energy resource used around the world. They can be included in a microgrid system and their output power capability can range from 25 to 300 kW. The turbine shaft spins at up to 120,000 rpm and drives a high-speed generator. It requires an AC-DC-AC converter to transform the high frequency output of the generator to AC.

2.5.5 Energy storage systems

Energy storage systems are used to support the distribution network at peak load time, when the use of electricity by consumers is high. This energy storage helps microgrid in balancing the power between the loads and generation units, by providing energy whenever the microsource units have insufficient energy to power the load. For instance, when the loads increase, a point is reached when the distributed resources cannot cover the demand for electricity; it is at that stage that the incorporation of the storage system batteries boosts the system by supplying the power needed. Normally, during the time that the energy demand is lowest, the excess generation of power will be used to charge the energy storage device. This means that at

periods of high demand, caused by the heavy usage of electricity, the energy stored, can be used to feed additional electricity into the network. Various types of battery technologies have been developed and are available to store energy. However, the most commonly used storage methods which are integrated into distribution system, are flywheels and electrochemical capacitors. Others energy storage technologies are compressed air energy storage (CAES), and superconducting magnetic energy storage (SMES) batteries

2.5.6 Storage system configuration

Storage systems produce DC voltage, but to be compatible with the utility grid, this has to be converted to AC voltage. In order to achieve the required current output or voltage, storage systems is available in different configurations; each single battery cell can be connected the other cells in either series or parallel. The purpose of the different storage system configurations is to provide power for consumer load demand in the microgrid, or to transfer the electricity to the main grid. Storage system requires a battery energy storage system (BESS) that includes an inverter and DC-DC converter. Energy storage is bidirectional in the sense that both are getting power during the charging time. And also it provides power during the discharge from or to grid (Ponnaluri et al., 2005).

An energy storage system, which consists of a battery bank and a DC-AC converter, is the simplest configuration that can be coupled with the main grid. Coupling with a microgrid involves the integration of a transformer into the utility grid system. The primary drawback of system is the fact that the low-frequency transformer placed at the output of the inverter, makes the system bulky and costly (Ponnaluri et al., 2005).

Sometimes, the DC-DC converter, which is bidirectional, is placed between the battery energy storage systems (BESS) and the inverter, this allows the converter to deliver enough voltage at the input of the inverter, enabling the inverter to produce an AC voltage compatible to the utility grid. Some BESS are hybrid systems which include renewable resources; they can facilitate autonomous operations or transients, and also offset the daily intermittency of the energy.

2.5.7 Microgrid loads

Microgrid loads can be either sensitive or non-sensitive loads, and furthermore, each type of load can be either an electrical or a thermal load. Power is supplied to the loads concurrently by the utility grid and the microgrid when the microgrid is in the grid connected mode. The loads only receive power from the microgrid when the microgrid operates in autonomous mode, which involves load-shedding so that the microgrid can maintain the power balance.

The point of common coupling is the static switch that plays a major interfacing role between the utility grid and a microgrid. It is the point in the electric circuit where a microgrid is connected to a main grid. It allows the microgrid to connect and disconnect from the main grid when disturbances occur in the utility grid; disturbances such as faults, IEEE 1547 events, or power quality events. It guarantees the protection of microgrid-sensitive loads in the event of the following:

- voltage sags in the utility grid due to the nearly asymmetrical loads
- the frequency of the utility falls out of the range limit
- high current injection from the main grid in the system, resulting from a fault
- poor voltage quality that lasts longer than local-sensitive loads.

2.6 Microgrid control layer

The microgrid control system makes sure that the ensemble of control tasks is achieved. The entire control operation is located at three control layers in the microgrid as can be seen in Figure 2.12. These control levels are the following (Vandoorn et al., 2013):

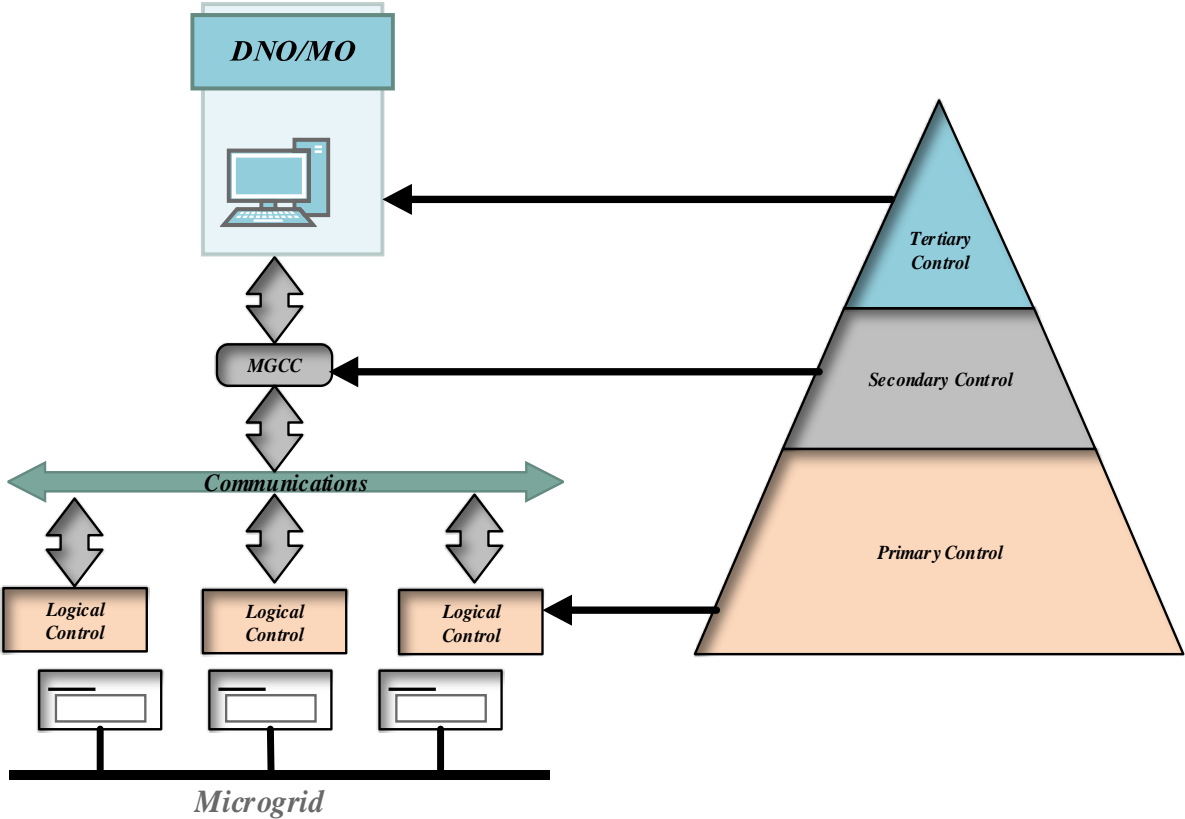


Figure 2.12: Microgrid communication: local and centralised controller
(Vandoorn et al., 2013)

- The primary level is the lower level containing the local control which is responsible for the control of DERs, some local load, and the balance of the active and reactive power. At this level some decisions can be made locally when a microgrid is operating in decentralised control, while when operating in centralised control, it will receive set point from MGCC.
- The second level refers to the microgrid central control (MGCC); it is the area where DER clusters are integrated into the microgrid. The MGCC is in charge of stabilizing the voltage and frequency within a specific, limited range, at the PCC. Also, it is responsible for the active and reactive powers dispatched from an individual DER.
- The third level is the distribution network operator (DNO) control incorporating a market operator (MO), which is situated in the main grid. This presents the upper management area and it facilitates the buying and selling of energy between consumers.

2.6.1 Microgrid control

Microgrid operation relies on the control scheme of the generators. Inverter control is used to ensure the accuracy of the power sharing while controlling or regulating the microgrid frequency and the voltage magnitude of the microgrid. The control method used in inverters can either be communication based or without communication (Lasseter, 2001; Lasseter & Paigi, 2004; Katiraei & Iravani, 2006). In addition, the single master operation (SMO) and the multi-master operation (MMO) are the two main control strategies employed for a microgrid in stand-alone mode. They use the reference from the VSI to control the voltage and frequency. SMO primarily operates as follows: among the inverters there is one that operates as a master while others are performing as slaves. During a power supply interruption the slaves operate in autonomous mode by taking over the voltage reference from the master. In MMO many inverters act as a master, where some inverters can be connected to the DERs or to storage device systems and others are affiliated to the QP control. The MGCC can change the generation profile by redefining a new set point (Moreira et al., 2007; Peas Lopes et al., 2006; Madureira et al., 2005).

2.6.1.1 Control involving communication

The active load-sharing method is used in parallel connected, microgrid converters. Inverter control is based on communication that relies on sharing information among different microgrid generators. In addition, differing information from inverters at different load conditions converge to a centralised microgrid controller (Lasseter & Paigi, 2004). The microgrid controller in turn gives specific control commands to each individual inverter unit. Communication between the microgrid controller and the inverters can involve the following control techniques:

- Master-slave control
- Current limitation control
- Circular chain control (3C)
- Average load sharing control

This approach of control, based on communication represents a critical need for the intercommunication lines. However, the active load-sharing method decreases system reliability and expandability.

Some drawbacks are listed below:

1. The communication infrastructure needs a high bandwidth to be able to share dynamic information among inverters. This is costly and the distance of connections between inverters is considerable in rural areas, which makes it an impractical solution.
2. Single failure is eminent due to the centre controller acting as a master control.
3. The design of the dispatch algorithm for the load profile of the microgrid system is complex because it is unpredictable when compared to the conventional power system.
4. The distribution control signal reduces the consistency of the microgrid which causes problems where the control of information is critical.

2.6.1.2 Control with no communication inverter

Inverter control without communication is mainly based on droop control. This scheme adjusts the output voltage and frequency in response to the active power (P) and reactive power (Q) delivered by the inverter. Each DG inverter has the ability to regulate the output voltage and frequency, while at the same time sharing the active and reactive power command. This method identifies power sharing in (a parallel inverter parallel inverters) and provides signal injection as occurs in a decentralization system. However, this signal produces some variation in the output power. It can be noted that frequency and voltage droop techniques are used for power sharing in non-communication based systems. Drooping the frequency allows each microgrid generator to deliver real output power and share the reactive power (Lasseter & Piagi, 2006; Chandorkar et al., 1993; Guerrero et al., 2008; Guerrero et al., 2007).

The droop method does not require communication signals between units in parallel. Therefore, it enhances the reliability of the system and the cost is reduced. Nowadays, the droop method is considered to be a standard control method in microgrid systems. However, this method is inadequate for the detection of voltage measurement errors. The errors which infiltrate during

current/voltage measurement of feedback signal will destabilize the operation of power sharing in the system (Katiraei & Iravani, 2006).

(Katiraei et al., 2008; Chandorkar et al., 1993) proposed a static droop controller to be used for power sharing. Guerrero et al. (2004) proposed an improvement of the droop control feature. Others authors proposed an enhancement of droop control by incorporating virtual output impedance in order to improve the operation of active and reactive decoupling (Guerrero et al., 2004; Chiang et al., 2001). In the conventional generation a tiny variation in power angle is admissible, but in a microgrid inverter a large power angle can be tolerated. A microgrid is subjected to several load conditions due to the lack of a base load concept. The change in power demand of each inverter leads to low frequency modes of the power sharing.

2.6.2 Control structures of distributed generation units in a microgrid

2.6.2.1 Local control of distributed generation structure in the microgrid

The distributed generation sources are normally connected to the main grid or to the load through the interface of power electronics, which manage the power and the output voltage. Therefore, the implementation of droop control within the context of controlling distributed generation, concentrates on the concept that inverters will be connected to the energy source in the electrical system. Moreover, power electronic systems will interact with microsources and local controllers, and in the process carry out the following functions: active and reactive power control; data storage for fast load tracking; and load sharing through power-frequency control, being mainly with droop control. Multiple control strategies have been introduced to eliminate or lower the current flow among parallel distributed generation source. Among the adapted controls is the master-slave control method which is: the master–slave control method which tends to equalize the load current shared between the inverters (Holtz & Werner, 1990). Additionally, a modular control method has been proposed to meet the objective with no signal communication between the inverters connected in parallel (Chandorkar et al., 1993). Although this control method produces a high reactive power, it is insufficient for the requirements of the capacitors. Moreover, Hanaoka et al. (2003) have analysed the behaviour of inverters in parallel operation, using a power protection technique or the power deviation in the system. As a result the power protection performs better unless the line resistance increases and influences the phase and amplitude difference. Other authors (Yao et al., 2007) presented a frequency voltage droop method for a parallel inverter. This method is derived from the conventional droop method by adding four compensation loops to it; the result shows improved execution of individual inverters. Finally, the response and power sharing accuracy have been improved.

However, the traditional droop control is inadequate for the elimination of the circulation of current. This is due to the low efficiency of power sharing in a complex situation, where the system is characterised by the coupled, active and reactive power (De Brabandere et al., 2007).

Moreover, some authors (Sao & Lehn, 2008) proposed that the voltage power droop/frequency reactive power, be designed to control several voltage source converters (VSCs). The voltage power droop/frequency reactive power performs in a parallel microgrid in both autonomous and grid-connected modes. Energy management is improved using the droop controller.

At a low voltage, traditional droop control, using frequency and voltage magnitude droop, introduces instability in a microgrid; this instability is detected in the inductive line impedance. The stability of the system is compromised by many factors, for example, a high R/X ratio (line resistance to reactance ratio) makes the autonomous system more vulnerable to voltage collapse (Chakravorty & Das, 2001; Li et al., 2004). However, another method called the virtual ω -E frame droop method, overcomes the difficulties caused by the traditional droop and improves the stability. Like the traditional droop method, the ω -E frame droop method controls the power sharing between DG units in autonomous mode by decoupling real and reactive power control.

Several authors (Guerrero et al., 2009) proposed a method for controlling the parallel connection of an uninterruptable power supply (UPS) by implementing the droop control scheme. The droop method utilises the phase and amplitude adjustment of the inverter to control active and reactive power flow. The droop method was readily adapted for parallel connection to UPS systems in both autonomous and grid-connected modes. The droop control strategy resulted in good steady-state regulation and good transience in sharing linear and non-linear loads.

Other authors (Majumder et al., 2010) offered a relevant control system that deals with the demands in distributed generation (DG) units of a micro-grid by simulation. These others used PSIM simulation software for controlling the demands of DG, and applied droop characteristics to active and reactive power (PQ) control, as adopted for parallel DG. This was done in order to establish a reference power when the microgrid is connected to the main grid. In addition, the frequency and voltage control are adopted to act on each DG output by adjusting them to share the load power once the microgrid is disconnected from the main grid. QP control is used in renewable energy such as PV and wind generation systems, and VF control is used for fuel cells and gas turbines. The simulation result showed that the control strategy is effective and leads to better performance in satisfying the demand.

Some authors (Majumder et al., 2010) discussed the advantage of angle droop control over frequency droop control to avoid the limitation of a frequency. Hence, it is beneficial and convenient to use angle droop over frequency droop for load sharing. Moreover, Majumder et al. (2010) investigated the load sharing with the microgrid in autonomous mode. For a weak system, a high gain angle droop control performs well in load sharing. However, it has a side-effect on the system stability. Nevertheless, an additional loop is suggested for the traditional droop control of each individual DG unit, in order to stabilise it while the system is still implementing the high angle droop gains.

Renewable energy sources (RESs) in microgrids are faced with a problem of active power balancing. which has an impact on the frequency in autonomous operation (Serban & Marinescu, 2011). Frequency control participates on the RES of microgrids, mostly at the energy storage units in which it compensates for the difference between parallel DG production and the load power demand. However, it is difficult to track an instantaneous frequency measurement like that of active power. Therefore, the phase-locked loop is used to measure the instantaneous frequency of the the national electricity grid.

The parallel inverters of microgrids supply power to the load by exploring active power versus voltage frequency and reactive power versus voltage magnitude of droop controls. The variance in frequency, phase angle, and voltage magnitude affect the multi-inverters of a microgrid by enabling unwanted currents to circulate (Lyer et al., 2011). Even a small change in voltage magnitude will drive the circulation of current in the parallel AC system.

Several authors (Trujillo Rodriguez et al., 2013) emphasised reconfiguration of the inverters, to be achieved by adding some functionality to allow a micro-inverters to operate in both modes: autonomous and grid-connected. It used in PQ control strategies in the inverters, to share the power delivered to the loads. These inverters keep the same control algorithm throughout the transition. The retained control algorithm the inverters from overload when when changing from a grid-connected to an autonomous mode.

The operation of the wind and PV generators must be kept at the maximum power set point by using the PQ control method. Due to the shortcomings of the master-slave control method, the peer-to-peer control method is limited in the demand to the better control inverters (Wei et al., 2012). However, based on the simulation result using MATLAB/SIMULINK, the combination photovoltaics, PQ and droop control substantially solve the problem of parallel inverters.

Problem and solution of microgrid control objective:

Some authors (Serban & Serban, 2010; Moreira et al., 2007) pointed out the problem related to in-line frequency deviation when batteries are overcharged. This problem causes an unbalanced supply and frequency regulation; also it has an effect on the accuracy of the load sharing and the accuracy of the voltage regulation. This trouble is resolved by manipulating the direction of the real power (P) with respect to battery voltage regulation.

Other authors (Piagi & Lasseter, 2006; Lasseter, 2011; Lasseter & Piagi, 2006) focused on the problem of the reactive current circulation that occurs with any change that takes place in load impedance (Z_L), output impedance (Z_O) or line impedance (Z_{Line}). This causes a low Z_L among the DERs in the microgrid system and affects the voltage regulation. One possible solution is to change the local set point in a way that increases the set point at the inductive reactive power (Q_L) and decreases the capacitive reactive power (Q_C) (Wang et al., 2012; Azmi et al., 2013; Kim et al., 2008).

A possible imbalance of reactive power can arise when there is a change in Z_{Line} . It may disturb the accuracy of load sharing and the accuracy of voltage regulation. As a solution, Mihalache (2013) suggested the injection of a high frequency signal through the power line, but the implementation of this method comes with the disadvantage of the limiting the power rating of the DERs.

The imbalance in reactive power when there is a change in Z_{Line} leads to a disturbance in the accuracy of load sharing, as well as in the accuracy of voltage regulation. As a potential solution some authors (Chandorkar et al., 1994) suggested adding external data communication signals, but the disadvantage of doing so, is low reliability and low expandability.

The different in distances between the various DERs and the MGCC, results in an imbalance in the line impedances. The imbalance in Z_{Line} affects the control accuracy objective of load sharing of linear and non-linear loads. As part of the solution Guerrero et al. (2005; 2009) insisted that Z_O should be properly designed.

Several authors (Wang et al., 2012; Peas Lopes et al., 2006; Ito & Lyama, 1997; Wang et al., 2012) have attempted to improve the problem of imbalanced Z_{Line} by modifying the distances between the various DERs and the MGCC. These change had an immediate negative impact on Z_{Line} . As a consequence, modifying the distances induces some irregularity on the accuracy of the load sharing for linear and non-linear loads. The implementation of an adaptive, virtual Z_O is

proposed as a solution to the problem. The outcome of this proposed solution results in good reactive power sharing, regardless of Z_L (Guerrero et al., 2009; Hatziargyriou et al., 2005).

Other authors (Kamel et al., 2011; Peas Lopes et al., 2006; Mihalache, 2003) claimed that the droop method is not efficient when applied to the load sharing, including the sum of Z_O and Z_L when they are not balanced. It is caused by an imbalance in Z_O because Z_L is always affecting the active and reactive power. An solution to the problem is the use of the adaptive virtual Z_O method, with emulating resistive, and reactive loads with less loss (Z. Zhang et al., 2010; Guerrero et al., 2009; Barklund et al., 2008; Dimeas & Hatziargyriou, 2005).

Unequal, instantaneous supply and demand can cause a problem of frequency deviation. This badly affects the frequency regulation of the system. The method used to solve the problem of frequency deviation, is to change the no-load generator speed or the power dispatch (Guerrero et al., 2011; Yubing et al., 2008; Blaabjerg et al., 2004).

The other control objectives of load sharing include balancing the sum of Z_O and Z_{Line} , which always affects the balance by influencing Z on PQ. Chandorkar et al. (1993) proposed a solution to eradicate the problem by using an interface inductor between the inverter and the load; the drawback however, is that it is heavy and bulky.

A deviating frequency and voltage occur when unintentional autonomous occurs due to the loss of the load or imported power. This causes disturbances in the on-going frequency regulation of the system. One suggestion to solve the problem, was to incorporate a load shedding controller module. This technique systematically disconnects a number of the important load feeders (Delghavi & Yazdani, 2012; De & Ramanarayanan, 2010).

The control of voltage regulation and load sharing are difficult to implement due to the resistive nature of the distribution network. Thus, the control objective of voltage regulation and load sharing are becoming a priority. The proposed solution to the problem is to use the voltage power droop technique; this involves the direct relation between power and voltage (Delghavi & Yazdani, 2012; Sao & Lehn, 2006; Katiraei et al., 2005).

Failure of any functions associated with a microgrid will result in failure of the microgrid itself. So the potential solution could be in the triple-layer control structure comprising DNO, MGCC and local control (LC) which are respectively the primary, secondary and tertiary control layers (Delghavi & Yazdani, 2012; Colet-Subirachs et al., 2012; Katiraei et al., 2008; Meiqin et al., 2008; Piagi & Lasseter, 2006).

The problem connected to any failure related to load sharing criteria, is produced by the load and the changeable energy demand. This is due to the change in load which affects the active and reactive power. The change in active and reactive power has a severely detrimental effect on instantaneous equal load sharing, as well as on voltage regulation. Some solutions to the problem have been suggested by different authors, such as (Sun et al., 2003; Martins et al., 1995) who used the centralised load technique, and Chen et al. (2001) and Chiang et al. (2004) who implemented the average load sharing technique. Several authors (Li et al., 2004: 3; Tsai-Fu Wu, 2000) proposed current limitation control as a solution. Other authors (Guerrero et al., 2008; Tsai-Fu Wu, 2000) suggested the use of circular chain control (3C). Zhao et al. (2012) and Holtz & Werner (1990) solved the problem by using the master-slave method. These methods were used with communication interconnections which are based on active load sharing techniques. Others like Zhao et al. (2012), Ustun et al. (2011), Guerrero et al. (2011), Serban & Serban (2010), Katiraei et al. (2008), Peas Lopes et al. (2006), and Chandorkar et al. (1994), used the droop method without communication interconnections, which provides high reliability and flexibility.

The accuracy of the load sharing is affected by the harmonics. Unbalanced power is poorly compensated for, due to non-linear and unbalanced loads when there is a low ratio of distribution Z_{Line} . Some scholars (El Khateb et al., 2013; Rahim et al., 2010; Cheng et al., 2009; Guerrero et al., 2005; Mihalache, 2003; Ito & Iyama, 1997) suggested the use of frequency components, active power, reactive power and distortion power as a solution to the unbalanced power. Another solution to the problem is the implementation of an adaptive virtual Z_o . Thus, the virtual impedance has no power losses and can provide plug & play operation (Silva et al., 2012; Kamel et al., 2011; Peas Lopes et al., 2006; Mihalache, 2003; Ito & Iyama, 1997).

The frequency deviation problem occurs when there is intentional autonomous with no synchronous machine to balance the demand and supply during the unbalanced demand and supply. For the solution to the problem some authors preferred a single master and multi-master operation (Kamel et al., 2011; Georgakis et al., 2004; Guerrero et al., 2007).

2.6.2.2 Central control of distributed generation in a microgrid

An energy management system makes decisions by providing the active power and voltage set points for the micro-source controller (MC), while the basic micro-source control executes the order from the central control (CC).

Several authors (Katiraei & Iravani, 2006) acknowledged that they used real and reactive power droop control for management strategy in electronically interfaced DG units. This is implemented

in the context of multiple DG units by examining the parameter gains of real and reactive power control. This control method is based on investigating the dynamic behaviour of a microgrid, and also selecting the control parameters utilizing eigen value analysis. The study showed that electronically interfaced DG unit controls have an important effect on the behaviour of a microgrid in autonomous mode.

Several authors (Khan & Iravani, 2007) worked on hybrid control techniques which involve an extension of the finite state machine. This has brought some improvement to different modes of operation of a microgrid. The structure of hybrid control as a supervisory controller is situated at the top level of the hierarchy and interacts with both the unit level regulators and the regulated plant. The simulation showed that the concept of hybrid control has been run to analyse the supervisory scheme.

Smart grid development is the new research focus area in many countries. This focus has resulted in better security features, higher efficiency and improved environmentally friendly operation of renewable energy sources, surmounting the difficulties normally encountered with distributed generation in power systems. Several research angles, from the architecture to the control side, have been undertaken and tested in the laboratory.

Some authors (Kim et al., 2011) examined the management of the power flow among microgrid inverters in flexible-phase. In order to improve the power loop dynamics, this approach involves implementing the interaction of droop control and proportional derivative (PD) control in autonomous mode. The power factor is controlled at the PCC by the combined operation a droop controller and a PI controller with the microgrid in grid-connected mode. Hence, the system can operate smoothly in both grid-connected mode and autonomous mode.

Alternatively, several authors (Azevedo et al., 2011) suggested the master-slave configuration as alternative, suitable option to droop control. In the master-slave configuration a master could be seen as a single inverter that alternates between two modes. Therefore, this master inverter will be controlling the voltage in grid-connected mode, and the current in autonomous mode, while other inverters are slaves and control the current. In order to synchronize with the system, the master inverter has the ability to connect smoothly in either mode by using a frequency-locked loop as opposed to a phase-locked loop. This system also responds as a voltage reference oscillator in accordance with an input selector. In addition, Cheng et al. (2012) stated that a master-slave control strategy can perform a seamless, smooth transient between grid-connected and autonomous operations. This means that when the microgrid is connected to the

utility grid, the PQ control is applied to both master unit and slave units. While in disconnected mode, VF control is applied to the master unit and, PQ control is applied to the slave unit.

Another control method used for power management is: decentralised control

Agent-based framework control is used in a decentralised system for microgrid system. Where each agent technology takes full control of its sector without knowing what is happening in the rest of the system. They are acting in the sense of organizing and making decisions without any intervention, even from the central controller. It runs on software environmental platform. Similarly, a multi-agent system (MAS) is used to control a set of small power producing units and to take action in case of autonomous mode on power quality, demand and supply, and also communicate between microgrids (Dou et al., 2009).

Furthermore, several authors (Yunusov et al., 2011) stated that the multi-agent in energy management system controls the distributed generation and also the demand side. For them, it is the ultimate solution to overcome loss in a transmission line, which is forcing the system to be at low efficiency. Therefore, decentralization controls are used to improve the efficiency by applying suitable control strategies and methods like agent base on DG. Instead, they presented an overall view of a multi-agent based model in the hierarchical and distributed energy control of microgrid. The multi-agent is designed under C++ development for client and server. This concept of agent based applied to Energy management system of microgrid (EMS-MG) is explained in detail with multiple functions applicable to the micro grid at three different levels of control (Meiqin et al., 2011).

Several authors (Shah et al., 2011) mentioned how to enhance the power management achieved on smart micro-grid by acting on a power electronic transformer (PET) at the point of common coupling (PCC) using software simulation MATLAB/SIMULINK. This strategy has been employed within the decentralised controller on the microgrid. It utilizes the change in the grid frequency as a parameter in the presence of the active power control, without the necessity of implementing grid synchronization. Hence, the power management system of the microgrid is improved, while the grid is connected because of the bidirectional active power flow control at PCC.

However, renewable energy integrates an AC and DC in the microgrids, so (Guerrero et al., 2011) developed a hierarchical control derived from ISA-95 and the electrical dispatching standards. The droop control is used to prevent current to flow among converters in the absence of commutation when the prime mover and the microgrid are interfacing. Most of the time, the power electronic converters behave like a voltage source. The hierarchical control has three-

level control, which can be applied on AC and DC on microgrids. It is enabling the MGs to operate in both autonomous and grid-connected modes, as well as, in transient between the two modes. Firstly, the control of AC microgrid emulates a large-scale power system AC grid, showing the concordance between both systems. Secondly, the hierarchical control in DC microgrid exhibits novel characteristics, which may be helpful applications in distributed power systems, such as telecommunication DC-voltage networks and more.

In contrast, (Vargas-Serrano et al., 2012) presented the master-slave control strategy to regulate the main energy storage VSI (Voltage Source Inverter) developed in the microgrid on account of reducing the communication between VSI and microgrid controller. In addition, this control strategy seems to achieve a seamless transfer between grid connected and autonomous modes with minimum communication. The microsource controller (MC) of the battery energy storage system (BESS) uses droop curves to follow the set points with a linear droop function and It has three levels of control, namely; high level, medium level and low level. The high level controller acts according to the droop function parameters from the central control (CC) and also depending on micro-grid operating conditions. The mid-level controller generates simultaneous voltage amplitude and phase references for the VSI output. The low-level controller is based on hysteresis, SPWM or SVPWM.

Moreover, some authors (Wang et al., 2012) insisted on a design of an intelligent multilayer supervisor control and smart grid communications based on MATLAB simulation. The structure of the supervisory control brings more organization in the control balance to participate in optimizing energy cost and to exchange information with the smart grid by dealing with the end users demand.

However, (Piacentini, 2012) developed a program in LABVIEW with a set of instrument, which is proposed to be used in the smart grid enabling an easy monitoring and supervising the system by making decisions. The LABVIEW software is used to facilitate an easy management data. This comes to erase the use of FPGA or MATLAB. Besides, it uses multiple communication protocols to operate the entire system, which can be an advantage over other platform, because, one protocol cannot usually meet with the entire requirement of communication of the system.

A technique of double layer control is designed in microgrid energy management operation in the stand-alone and connected grid mode. This controller consists of two layers which are the schedule layer for an economic operation scheme based on forecasting data, and the dispatch layer which provides power for controllable units based on real-time data. Therefore, it improves microgrid to operate economically, safely and stably (Jiang et al., 2013).

2.6.2.3 Other control methods used for power management: decentralised control

Agent-based framework control is used in a decentralised system for microgrid system. Each sector of the system is controlled by an agent, in full control of that sector, but oblivious to what is going on in the rest of the system. These agents act in the sense of organizing and making decisions without any intervention, even from the central controller. The framework runs on software environmental platform. Similarly, a multi-agent system (MAS) is used to control a set of small power producing units. The MAS can take action on power quality in case of autonomous mode, control demand and supply, and also communicate between microgrids (Dou et al., 2009).

Furthermore, several authors (Yunusov et al., 2011) stated that in an energy management system, a MAS controls distributed generation, as well as the demand side. For these authors, a MAS is the ultimate solution to overcoming transmission line losses; these losses cause the system to run at a low efficiency. Therefore, decentralization controls are used to improve the efficiency by applying suitable control strategies and methods like agent-based DG. The authors presented an overall view of a multi-agent-based model in the hierarchy of distributed energy control in a microgrid. A MAS is designed using C++ development for both client and server. This concept of MAS applied to an energy management system in a microgrid (EMS-MG) is explained in detail, outlining the multiple functions applicable to a microgrid at the three different levels of control (Meiqin et al., 2011).

Several authors (Shah et al., 2011) mentioned how to enhance the power management achieved on smart micro-grid, using power electronic transformer (PET) at the point of common coupling (PCC). This strategy has been employed within the decentralised controller on a microgrid. It utilizes the change in the grid frequency as a parameter in the presence of the active power control, without the necessity of implementing grid synchronization. Hence, the power management system of the microgrid is improved while the grid is connected, because of the bidirectional active power flow control at PCC.

However, in the microgrids renewable energy integrates an AC and a DC. Accordingly Guerrero et al. (2011) developed a hierarchical control derived from the electrical dispatching standards. When the microsource and the microgrid are interfacing, droop control is used to prevent commutation between converters. Most of the time, power electronic converters behave like a voltage source. Hierarchical control has three levels, which can be applied to AC and DC in microgrids. Hierarchical control enables a MG to operate in both autonomous and grid-connected modes, as well as, in the transient period between the two modes. There are two

advantages in using hierarchal control. Firstly, the control of AC In a microgrid emulates a large-scale power system AC grid, showing the concordance between the two systems. Secondly, the hierarchical control in a DC microgrid exhibits novel characteristics, which may provide helpful applications in distributed power systems, such as telecommunication DC-voltage networks.

Vargas-Serrano et al. (2012) presented a master-slave control as a strategy to regulate the voltage source inverter developed in the microgrid, to reduce the communication between VSI and microgrid controller. In addition, this control strategy seems to achieve a seamless transfer between grid-connected and autonomous modes with minimum communication. The micro-source controller (MC) of the battery energy storage system uses droop curves to follow the set points with a linear droop function. It has three levels of control, namely; high level, medium level and low level. The high level controller acts in response to the droop function parameters from the central control (CC), and also depends on the micro-grid operating conditions. The mid-level controller generates simultaneous voltage amplitude and phase references for the VSI output. The low-level controller is based on hysteresis, SPWM, or SVPWM.

Piacentini (2012) developed a set of instruments using a system design platform called LABVIEW. He suggested that these instruments, used in a smart grid, would enable easy monitoring and supervising of the system, as well as decision-making. The LABVIEW software was used because it facilitated the easy management of data. The development of this set of instruments on the LABVIEW platform, could decrease the popularity of FPGA and MATLAB for this kind of application. Additionally, the instruments make use of multiple communication protocols to operate the entire system, which can be an advantage over other platforms, because, a single protocol cannot usually meet the communication requirements of the entire system.

2.6.3 Existing Control Methods within the inverter

For many years competitive control methods have been developed to control the instantaneous output voltage of the inverter, including the elimination of the steady state error.

Figure 2.13 below presents different types of control schemes for a power converter, inverter, and generalized predictive control.

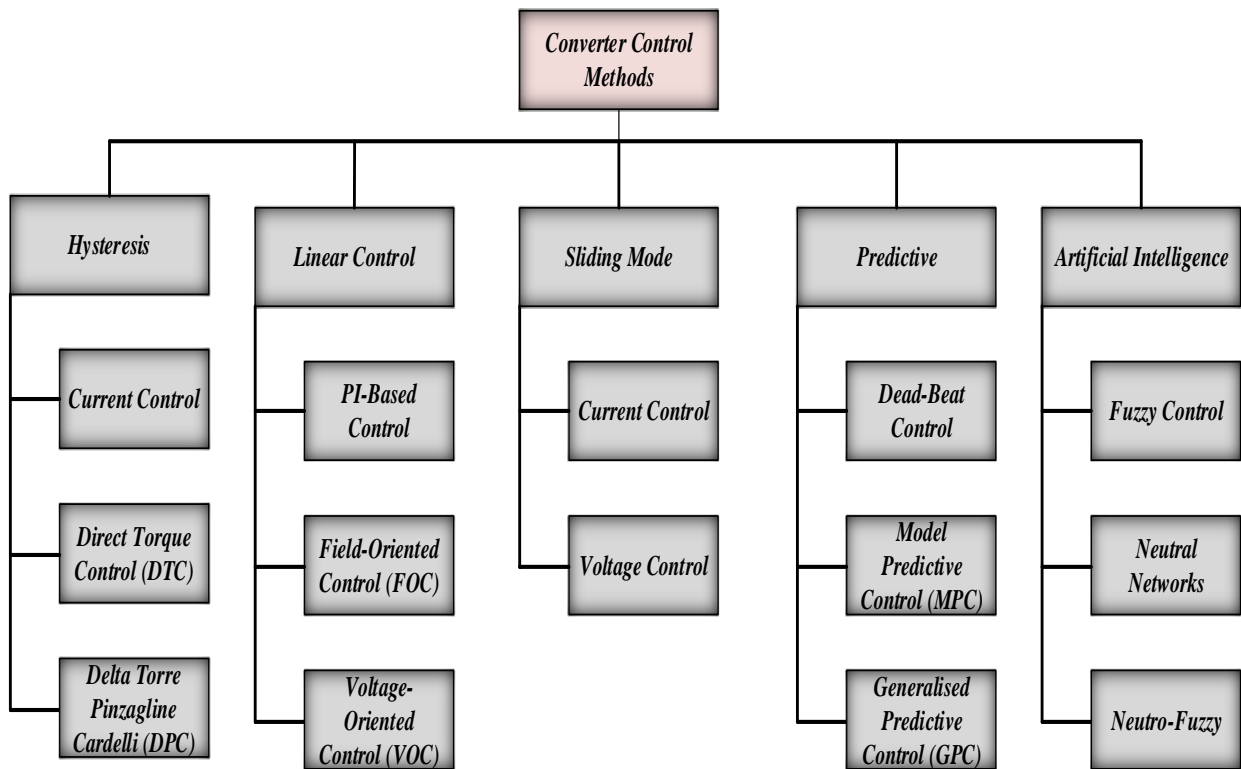


Figure 2.13: Control schemes of power converters

2.6.3.1 Single Voltage Loop Control Method

This is a feedback loop designed to regulate the inverter voltage output and detect errors, by comparing the output of the inverter to the sinusoidal reference – this loop can be seen in Figure 2.14. It is simple, and easy to design and implement, but it does not take into account the time-varying nature of the inverter. The controller compensates for errors by producing a sinusoidal reference duty cycle with low THD for the module. However, this method experiences a problem regulating non-linear loads. Also, at the fundamental frequency of the converter, the presence of a steady state error because of the finite loop gain of the controller, has been observed (Bekiarov & Emadi, 2002; Chen & Chu, 1995).

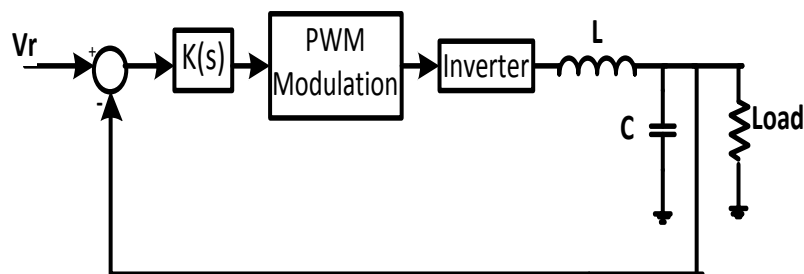


Figure 2.14: Single feedback loop block diagram

2.6.3.2 Multi-Loop Control Method

The multi-loop control technique contains two control loops, namely the inner and the outer. The inner control loop handles the inductor current, while the outer control loop handles the output voltage. The outer voltage loop in the control design uses the output voltage as a feedback signal, comparing it to the reference signal. The error from the comparison is then compensated for by the PI controller: this stabilizes the output voltage during the steady state. The error detected by the voltage loop is considered to be the reference to the current loop. This allows the system to have a fast and dynamic response when it is used in the inverter. This control technique is however, not efficient because of a problem resulting from the time-varying nature of the inverter (Bekiarov & Emadi, 2002; Chen & Chu, 1995). Figure 2.15 presents a block diagram of a typical control system with multiple feedback loops.

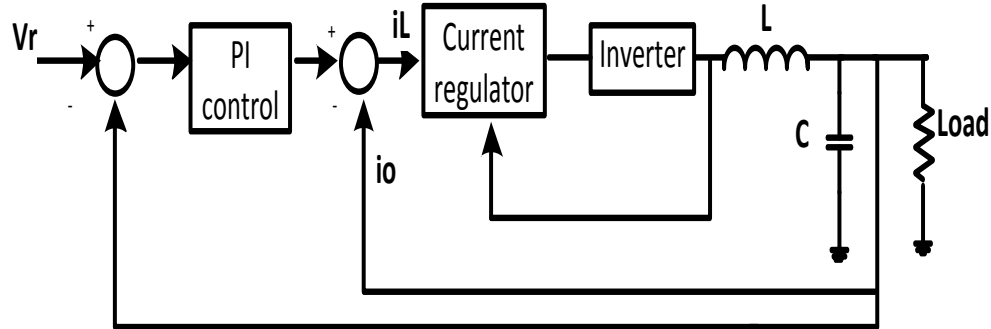


Figure 2.15: Multiple-loop controller

2.6.3.3 Predictive Control Method

Predictive control predicts the future behaviour of the dependent variable to minimize the error in the output voltage of the inverter. This control method gives a much better performance than the multi-loop control method. Considering every possible switching condition at the end of each sample, it can predict and define the optimum switching combination for the desired state. This control technique gives better stability than the conventional control technique, but for the overall system under non-linear load and transient load operation, it does require a lot of complex computations (Kawamura et al., 1988).

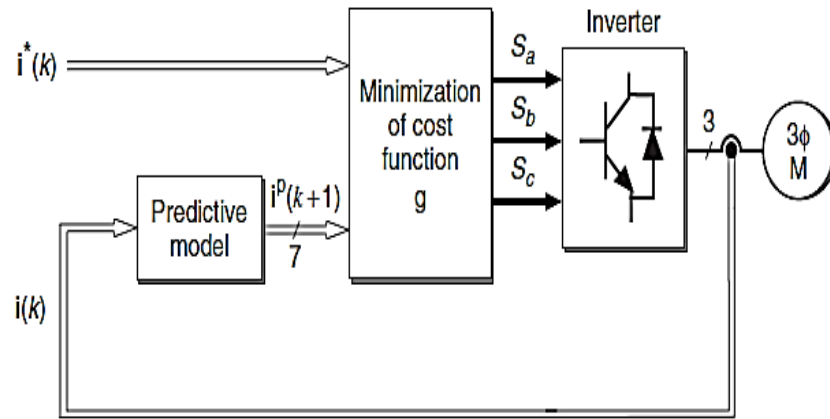


Figure 2.16: Predictive current control block diagram
(Rodriguez et al.,2007)

2.6.3.4 Deadbeat Control Method

The deadbeat method is an old control method with many variations. It presents a fast, dynamic response on a digital platform. When operating at high gain, it is however, very sensitive to noise, and relies on a parameter converter. The deadbeat control method can be used for the compensation of the digital delay by implementing the state error; it can be used both for the output voltage and the inductor current. This includes the disturbance observation used for estimation of the load current. Accurate disturbance monitoring and the feed-forward decoupling method allows the deadbeat control method to perform as an excellent disturbance rejection selector, having a fast dynamic response (Mattavelli, 2002; Kawamura & Yokoyama, 1990).

2.6.3.5 Sliding mode control method

The sliding mode control SMC is a robust control method, designed for non-linear systems. It is a variable-structure control system that can effectively perform in non-linear plants. The SMC method exhibits a very good dynamic response to microgrid system. It applies a discontinuous control signal to force the system to slide, and the state-feedback control law is not a continuous function of time. However, the problem with this control technique however, is the chattering phenomenon, which is provoked by the existence of parasitic.

2.6.3.6 Hysteresis control

Hysteresis control exhibits a good dynamic response and it is insensitive to the system parameters. It is based on an **on/off** control which considers the state of the inverter. When an error goes over the designated tolerance, a signal is sent to the control switch

2.6.4 Control methods based on pulse width modulation within inverters

A voltage-source inverter serves to convert the DC voltage from the source to AC; in addition it facilitates the interaction between DG sources and the utility grid. DG encompasses different energy sources, which are grouped as follows:

- Wind: variable generation dependent on changes in weather as well as seasonal variations
- Micro turbine generator: a typical high frequency source
- Fuel cells and photovoltaics: these resources operate by direct conversion of other forms of energy, into electricity.

In general, an inverter is composed of two legs for a single-phase system, or three legs for a 3-phase system; additionally an inverter is usually associated with an AC filter. The power circuit of an inverter is driven by a designed control circuit, that should allow flexible operation of the inverter. When the power quality is needed with the microgrid in autonomous mode, voltage regulation is critical. Regulating voltage fluctuations and maintaining a stable voltage is done via power management. In addition, power management takes care of load sharing in accordance with the contribution from each inverter connected to the load of the microgrid.

In addition, applying the method of PWM technology at the gate of the inverter will result in the negative side-effect of low harmonic distortion; this harmonic distortion must still be attenuated with an AC filter to ensure compliance with IEEE 519, the regulation standard of the for connecting the inverter to the grid (Anon, 2003).

The inverter should perform under an appropriate control loop to ease the negative impact of the DG unit operation on the system or *visa versa*.

2.6.4.1 Inverter-based DG Interface

Current control based on PWM within an inverter, is a widely used scheme in AC drivers (example: AC motor or AC power supply) in recent years, especially because it provides a durable advantage over other techniques such as removing the stator.

2.6.4.2 Current control methods for controlling PWM inverter

This method has several advantages such as the following (Kazmierkowski & Malesani, 1998):

- It ensures accurate current tracking, monitoring the instantaneous current with a high accuracy.
- It guarantees overcurrent protection (peak current projection) and overload protection.
- It reduces the transient period.
- It can provide compensation because of the load parameter changes (resistance and or inductance).
- It provides compensation at the DC link and AC side voltage.

However, the current control operation might influence internal grid problems such as: grid voltage harmonics, unbalanced grid voltage, as well as transients and grid parameters. These problems affect the balance of the inverter and the power quality itself (Liserre et al., 2006). A small increase in distortion of the grid voltage is significant for total harmonic distortion. Instability of the inverter can be due to a small distortion of the grid voltage which, as mentioned above, significantly increases the THD of the injected current.

There is a list of various control methods used for regulating the output current of a current controlled by VSI. These control techniques can be categorised into two groups. There are some techniques that are affiliated with linear control while others are affiliated with non-linear control (refer to the Figure 2.17 above). Examples of linear controllers are deadbeat control schemes, resonant controls, and synchronous and stationary used in frame proportional integral. Examples of non-linear controllers are: hysteresis band control scheme, artificial intelligence, and online optimization.

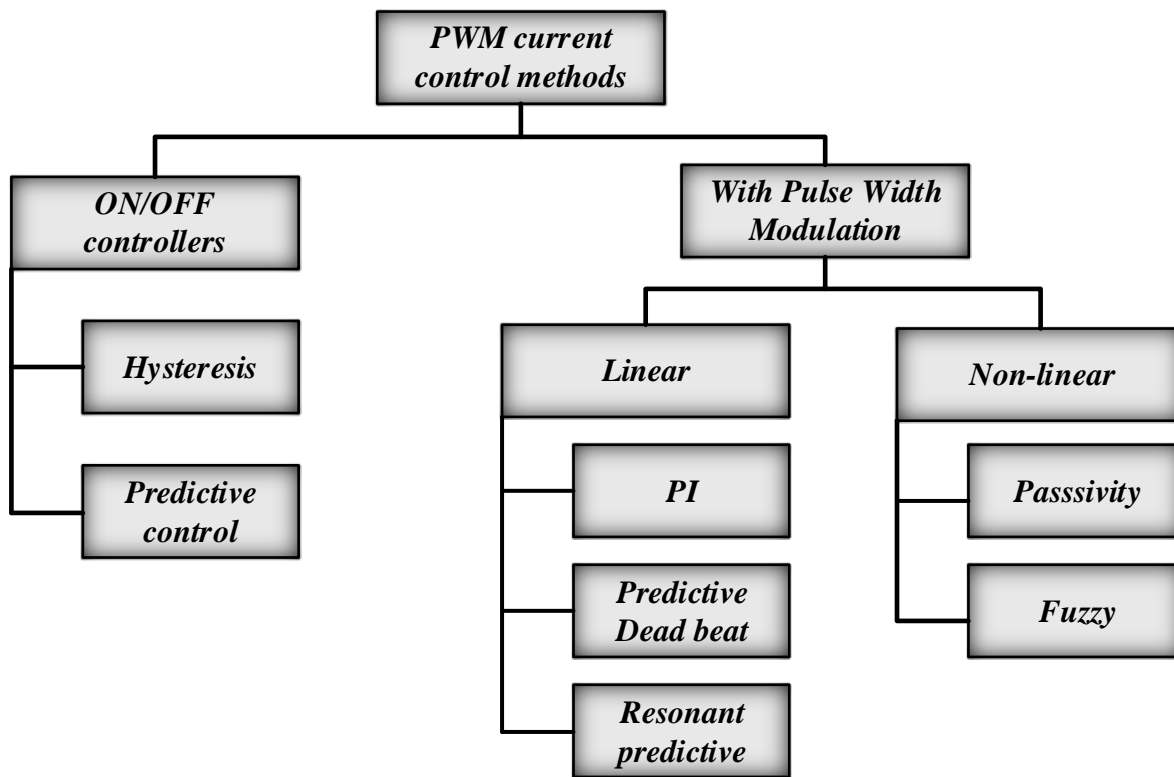


Figure 2.17: Classification of current control methods

A hysteresis control scheme is widely used in applications due to its simplicity in implementation (Brod & Novotny, 1985). It offers a fast response current loop and does not need knowledge of the load parameters switching frequencies when compared to more fundamental systems. In the hysteresis control scheme, hysteresis has been enhanced by the various band switching techniques. However, it has a number of problems such as: inter-phase distortion, and also has a low steady state error, with up to two times the hysteresis band. The harmonic ripple is unpredictable due to the unpredictable average switching frequency which varies with the load parameter.

2.6.4.3 Proportional integral control

The linear PI regulator was often used in the past to regulate the DC value with zero steady state error, but it is not an appropriate controller for tracking disturbances and sinusoidal waveforms, since it cannot eliminate the steady state error (Asbafkan et al., 2013). Nowadays the PI controller is implemented along with a stationary frame. The stationary controller uses the PI error compensator to regulate the voltage commands of a sinusoidal PWM. Thus, it is a solution for regulating sinusoidal current in balanced three-phase systems. However, this scheme is not effective in correcting unbalanced disturbance currents in distribution systems, because the stationary reference frame PI cannot track the sinusoidal variation reference (Brod

& Novotny, 1985). It presents an amplitude and steady state phase error between the desired and the actual output current. PI controller compensation is poor for the low-order harmonics. Also, it needs exact tuning to adjust to the load parameters (Holmes & Martin, 1996). Nevertheless, the resonance stationary frame controller was developed to eliminate the phase error. However, the process is difficult, since the PI controller in a synchronous frame is more intricate than compared to a PR controller in a stationary frame. Rowan and Kerkman (1986) proposed a synchronous frame PI with dq control, which uses a DC quantity rather than a variable component to regulate current. The method makes use of a transformation module to change a, b, c of the the AC current into a DC direct-quadrature (the control variable is transformed into a DC component value) rotating frame; this makes achieving control easy. The synchronous rotation frame is described by using dual, PI-error compensators of the current. The PI regulator associated with a synchronous rotational frame can be used independently. Nevertheless, it is weak and has a slow transient response.

2.6.4.4 Proportional resonant control

In compensating for lower order harmonics, the action of controllers (stationary and synchronous frame) is against grid disturbances. However, taking into consideration the large drawback that occurs in grid or stand-alone mode, the result is not satisfactory. Proportional resonant (PR) controllers are widely used for utility-connected converters, due to their ability to get rid of a steady state error, as well as for individual harmonic attenuation (Hwang et al., 2010; Teodorescu et al., 2006; Shen et al., 2010; Blaabjerg et al., 2006). PR control has become the target of the new adopted strategy to overcome the difficulties of the PI control face to the sinusoidal signal. It theoretically introduces an infinite gain (it has an infinite gain) at a selected resonance frequency. This is seen as an AC regulator/integrator in the sense that it is much more comparable to an integrator integrator having an infinite DC gain because the error was forcibly made zero (Teodorescu et al., 2006). Employing the resonant controller to improve and overcome the difficulties encountered using selective harmonics removal by tuning, the PR operates to remove the steady state error for a selected resonant frequency; it is used as a harmonic compensator in order to minimize the THD current (Timbus et al., 2006; Blaabjerg et al., 2006; Sera et al., 2005). However, PR controller cannot eliminate a large band of harmonics (Twining & Holmes, 2003). Also, the resonance controllers have a drawback regarding the variation of the grid impedance and the AC filter parameter.

An alternative method is to use a high band width current control from the PWM-VSI which, in inverter controls, might be more robust than the resonance controller. Grid disturbance causes lower order harmonics, which requires a high disturbance rejection to eliminate it. At high

bandwidths, the operation of current control allows facilitates tracking to regulate current in nature and a stationary reference frame. This can attenuate the effect of an unbalanced grid voltage on the injected current. Also the internal current is represented as ideal for the control of the power sharing, which is a significant factor employed in the microgrid. Nevertheless, the uncertainty and the system delay will not make higher bandwidth control vulnerable.

Deadbeat control:

Deadbeat control belongs to the family of predictive controls. It has been widely used for voltage-source PWM converters. It is based on the prediction of the current error at the start of each sample. Then the developed controller is used to decrease the estimated error in such a way that the reference reference current is error-free. This method has a fast transient response and zero steady state error, giving accurate current control and can be synchronized to a digital control platform (Timbus et al., 2009; Mohamed & El-Saadany, 2008; Kim & Youn, 2001; Svensson & Lindgren, 1999; Habetler, 1993). This control method improves the power quality of the injected current of the system, which implies that it only allows the very low harmonic distortion; it is however sensitive to uncertainty such as zero pole order of the PWM, voltage calculation, and deadbeat gain, all of which reduce the delay in the system.

Dealing with the delay issue, it cannot be implemented over long period because it has to accommodate different features, such as voltage calculation. For precision and high bandwidth purposes however, a short time period is required during discrete control. The longer the control period, the lower the bandwidth and control precision of the deadbeat control. The field programmable gate array (FPGA) has been added to partly ease computation, which then reduces the voltage calculation time that the deadbeat controls. Sometimes, to save control period time and resources, it is structured in such a way that there are two processes (FPGA and deadbeat processors) that are working in parallel; this however, this requires high-level programming and the cost of operation is high.

The use of a short control period in deadbeat with a delay compensation technique is implemented. Kennel and Linder (2000) suggested a negative feedback controller for delay compensation. However, this method amplified the transient period and the overshoot response. They proposed a predictive control strategy based on predicting the future behaviour of the plant relative to its input and output. They present an algorithm of predictive current control, also known as a digital dead-beat controller, to reduce or minimize the distortion and unwanted harmonic noise. However, it is complex to implement, suffers from long computation time delay

problems and it has poor stability (Nussbaumer et al., 2008; Cortes et al., 2008; Odavic et al., 2006).

2.6.4.5 Fuzzy logic control

To solve the persistent problem of parameter sensitivity, some authors (Li & Gatland, 1995) proposed a fuzzy logic control, tuned to a deadbeat controller. However, the control algorithm is based on the assumption of a back-EMF voltage that makes it difficult to implement in real-time. To enhance the robustness by implementing an estimated feed forward control, some authors (Lu et al., 2012) estimated the voltage disturbance based on the uncertainty estimation. The estimation used, is the disturbance theory and the time control delay, but the method is based on the inverse current dynamics theory which leads to noise. The phase delay caused by the actual and real voltage disturbances, limits the performance and therefore makes the compensation method weak; this is improved by assuming the load inductance.

2.7 Microgrid smart metering

AC microgrids may be associated with smart meters, communications and remote controls; these elements will form the basis of future smart grids. The collection of data is an integral process in the operation of a smart meter within the microgrid. Smart meters can also be applied in the energy market of a smart grid.

The following examples illustrate development in the field:

Luan et al. (2009) developed and implemented the design of a smart meter using Microchip dsPIC30F4011, embedded into the advance metering infrastructure. The purpose of the smart meter they developed, was to monitor the consumption of the end-user and also to detect the the occurrence of outage events. By adopting the star topology, data is transferred wirelessly using ZigBee communication; this allows the ZigBee coordinator to initiate and maintain the ZigBee devices. The smart meter developed shows how much of the smart meter can significantly integrate the advanced metering infrastructure (AMI).

The concept of a smart meter controller is an important component in the smart grid. It fulfils multi-functions between the utility control unit and the network interfacing with the information flow. Moreover, this smart meter can be involved in the marketing of energy, communicating with the smart appliances in the process, and regulate the frequency balance. The communication between a smart meter, a smart server, and a smart regional

server, is based on a TCP protocol that deals with the congestion control and is secure from data losses (Jamian et al., 2011).

Several authors (Chen & Klemm, 2011) developed statistical approaches for the malfunctioning of meter detection; data collected from different meters in real-time operation are statistically analysed. The smart meter can optimize the decision-making process in order to manage those floods of data in an efficient way. The smart meter can also detect anomalies and assist with forecasting load demand.

Furthermore, some authors (Percec et al., 1995) have designed the smart meter to overcome the incapability of a traditional meter which is unable to satisfy the demands of new generation of electricity supply devices. Smart meters display improved speeds of information collection in order to manage the electrical energy. These meters have the ability to make certain decisions and communicate with the central controller via wireless links. The core of the controller is a TMS320C6474 DSP from Texas Instruments, which has multi-task capabilities.

Similarly, other authors (Kulatunga et al., 2012) have developed a smart meter with ZigBee wireless communication that works in conjunction with the micro controller TMS320C6474 in the HAN connected to the main grid. The design is built in an intelligent way so as to measure the instantaneous and accumulative consumption of the electricity value. The demand side of the energy is managed by monitoring the daily energy demand as per the actual forecast, and availability of resources. This approach improves the security of the AMI and integration of key management schemes.

However, other researchers (Sofla & King, 2012) proposed the optimization of the operation and guarantee the stability of a microgrid by using the hierarchical control strategy. This strategy incorporates advanced metering infrastructure and communication, supporting the higher decision-making which enables interconnection with a multi-microgrid (MMG). Therefore, hierarchical control is an intelligent control scheme, composed of multi-microgrid features, and one that contributes a system which has commendable advantages.

Additionally, other authors (Singh et al., 2013) proposed a smart meter architecture which, in case of power failure, sends data directly to the control centre. The more efficient way of achieving this is to use two radios that permit the smart meter to cater for the needs of the smart grid on a large scale. The communication is established between the consumers

and the production through the HAN/NAN concentrator, WAN aggregator and the control centre.

2.8 Frequency control in power systems

The balance between the power generated and the demand for power can be related to the frequency in the power system. However, this frequency may be subjected to some variation due to the load variation. More frequency deviation occurs from the imbalance of the power, due to several factors such as power plant outages, and line-tripping registration. Therefore, frequency regulation is necessary for the stabilisation of the power system.

2.9 Conclusion

In this chapter, the literature guiding this research has been discussed. The overall configuration of a hybrid microgrid system, along with the importance of renewable energy has been reviewed. The control strategies of the microgrid structure have also been discussed. In addition, local load power sharing methods were reviewed in microgrids with DG sources. The control efficacy of microgrid stability under unbalanced and non-linear loads, are compared. The next chapter discusses the power electronics interface and inverter control using digital control platforms.

Chapter 3 : POWER ELECTRONICS CONVERSION

3.1 Introduction

The interface of power electronics devices serves as a micro source when a microgrid is connected. Power electronics technology is solid-state electronics which uses electric power for conversion and control purposes and the devices which achieve this are known as inverters. The fundamental operation of an inverter using different pulse width modulation techniques for digital control platforms are developed and analysed.

The discovery of power semi-conductor devices in 1950, led to their application in converter circuits and controls. This discovery initiated the modern use of power semi-conductors with high efficiency power conversion at low cost and small size, when compared to the conventional method used, i.e. the transformer. Power converter circuit elements consist of resistors, capacitors, inductors and switches. Some of these components may be used for high or low power systems, depending on the application. For good efficiency, power converter circuits are restricted to capacitors, inductors and transistors. In addition, these components must be used in switch mode. Components such as resistors in linear switch mode power supplies, are not relevant because they decrease the efficiency of power circuits. There are also significant losses in power caused by power dissipation (thermal problems) of these components.

In power electronics, the power converter is built from power semi-conductor switching devices which can be grouped into two parts:

- The first part of the circuitry converts the input power to a suitable output power for a particular an application.
- The second part, which is electronics, controls the functioning of the converter by monitoring the input and output voltages and currents.

The power semi-conductor converters can be used in the design for several areas such as power processing, computation, control system and automobile industries. They can also be used in electronic circuitry to control current and voltage magnitude, as well as the frequency delivered by a power converter.

The remainder of this chapter is organised as follows. Power semiconductor devices used in power electronics are presented in Section 3.2. Power converters related to inverter fundamental operation are presented in Section 3.3. The transformations and control are described in Section 3.4. Section 3.5 presents the filter topology required to filter out the presence of the higher-order harmonic components. Section 3.6 presents a comparison of digital control platform to the voltage and frequency through inverter. A conclusion is drawn in Section 3.7.

3.2 Power semiconductor devices

Power semi-conductor devices are used as a switch in power electronics, because they dissipate a very small amount of power during switching; this makes the system efficient. For instance, in the switch-mode power supply, the power device switches **on** and **off** at a determined frequency. There are varieties of power devices such as: Gate-turn-off thyristor (GTO), Insulated-gate bipolar transistor (IGBT) and MOS-controlled thyristor (MCT).

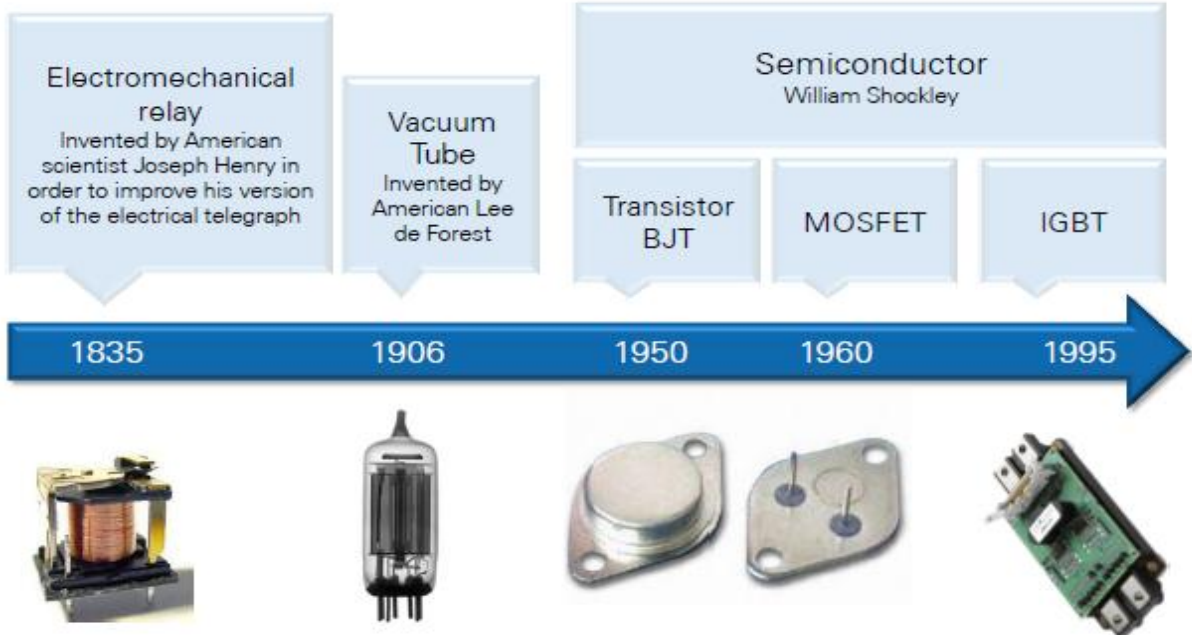


Figure 3.1: Switching device chronology

Figure 3.1 above shows the chronological order of the development of the various power devices. Those devices vary in switching speed, as well as in their power handling capacity. There are drawbacks resulting from a device with a slow switching speed: power is lost during the switching transition, and radiation and electromagnetic interference is created (Mohan, 2012).

However, power devices can be selected according to the type of application and there are some trade-offs between voltage, current and frequency ratings. In addition, the design takes into consideration power handling and power dissipation. In table 3.1 the various power semiconductor devices have been grouped into different categories, according to how they compare in terms of capacity and efficiency (Little, 2005).

Table 3.1: Power device comparison (Little, 2005)

DEVICE:	GTO	IGCT	IGBT	IEGT
Device Type	Thyristor Based Devices		Transistor Based Devices	
Efficiency	Low	Medium-High	High	High
Gate Control Signal	Current	Current	Voltage	Voltage
Gate Current	400-1000A	4000A	< 1A	< 1.5 A
Voltage Rating	High	6000V	4500V	4500V
AC Voltage Limit (2/3 Voltage Rating)	High	4000 V	3000 V	3000 V
Current Rating	1000A	4500A	1200A	4000A
Switching Losses	High	Medium	Low	Low
Snubber Parts	Many	None	None	Low
Switching Speed	Low	Medium	High	High

Inverter applications comprise power switches and the control of the power devices, which can be complex at high frequency. The controller needs to be capable of high speed processing in order to satisfy the output requirements. Moreover, the application of a digital signal processing controller significantly improves the real-time control capability of the switching mode power converters.

3.3 Power converters

Power electronics can accomplish a multitude of conversion types. It can take any input signal and convert it to any desired output signal suitable for a particular load requirement. For example, the output of a DC power supply may need to be regulated and the output of a DC motor drive may need to be adjusted. Another example is the output of an AC power supply, which may need to be constant while the AC input of a motor drive may need to adjust both frequency and the voltage magnitudes.

For each of the following power conversion systems (a typical application is given to the input and desired output power) (Mohan, 2012):

- AC-DC Converter: This is used mostly with electronic devices such as TVs, computers
- DC-AC Converter (inverter): It is widely used in renewable energy systems or UPSs.
- DC-DC Converter (chopper): This is used to maintain the level of the voltage in an integrated microchip in a mobile phone.
- AC-AC Converter (matrix converter or cyclo-converter): This is used to exchange power.

3.3.1 The AC voltage sourced inverter or DC-AC converter

The inverter is also known as a DC-AC converter which converts the DC power to AC power at a desired output voltage and frequency, by controlling the semi-conductor power switching devices. This represents an adjustable frequency and the voltage source as shown in Figure 3.2 below. The DC power input can be from a fuel cell, battery or photovoltaic array and is fed to the inverter. The capacitor across the input terminals of the inverter serves as a filter to provide a constant DC link voltage.

Inverters can be classified into two groups: the voltage source inverter which controls the output voltage waveform, and the current source inverter (CSI) which controls the current waveform.

There are three different types of inverter typologies that can be configured; these are the single-phase half-bridge inverter, the single-phase full-bridge inverter, and the three-phase voltage source inverter structure. Furthermore, the inverter can also consist of multi-phase typologies.

Today, diverse applications rely on inverters and some of the areas where they are employed are listed below:

- Traction
- Uninterruptible power supply (UPS)
- Adjustable speed drives (ASD) for AC motors
- Electronic frequency changer circuits used in induction heating, welding
- HVDC transmission at lower power levels
- Renewable energy such as solar, fuel cell-to-AC conversion
- Electronic ballasts and compact fluorescent lamps
- Active filters for power quality improvement

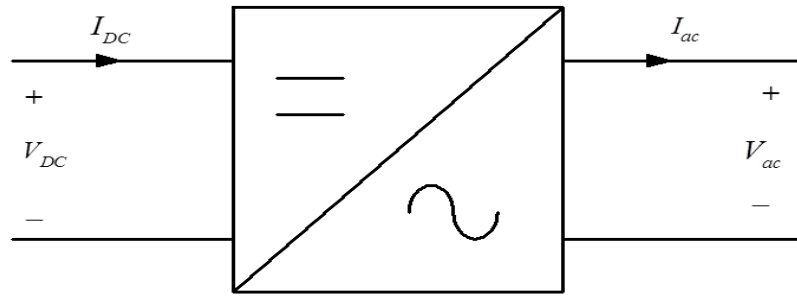


Figure 3.2: General block diagram of inverter

3.3.2 Half-bridge voltage source inverter

The single-phase half bridge rectifier is used for low voltage applications. It consists of a set of semiconductor devices or controllable switches. The purpose of the switching processes of the power switch devices is to modify the DC voltage source into an AC output voltage.

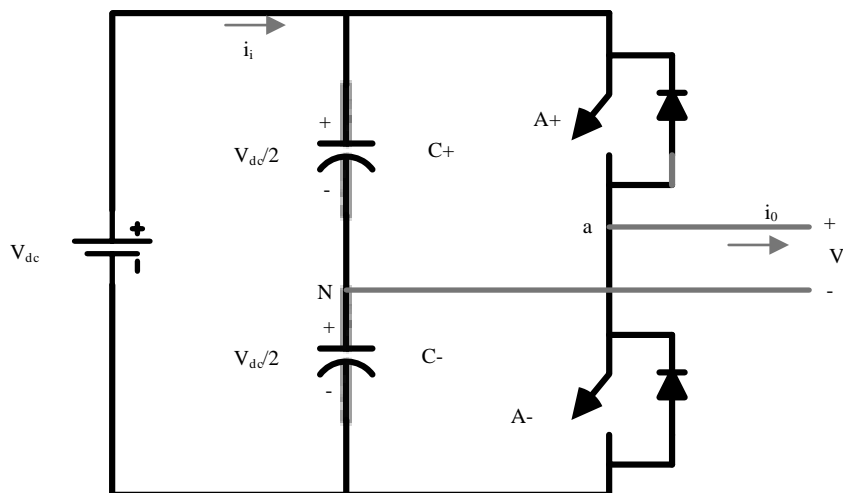


Figure 3.3: Single half-bridge VSI

This is achieved by applying modulation techniques to control the state of the switches. A diode in a reverse direction to the current is placed over each IGBT switch. This allows a freewheeling path for inductive loads during the switching transition as seen in Figure 3.3.

Two large capacitors of the same value are connected in series across the DC voltage source side. The N junction between the two capacitors represents the allocation at the mid potential point. The rule states that the upper and lower or both switches of each leg cannot be **on** at the same time. The condition where the switches of the same leg are **on** simultaneously would cause a short circuit that will destroy the switches. Nevertheless, in reality, during the transition

of the switches from **on** to **off**, there is still both voltage drop and current flow across the switches (Ming & Zhong, 2014; Ghosh & Narayanan, 2007; Lin & Yang, 2004).

3.3.3 Single-phase bridge voltage source inverter

The half bridge generates only one pulse per half-cycle and the variation in width of the pulse changes the V_{rms} voltage. However, a single-phase inverter topology is comprised of two legs, each of them having two switching devices as seen in Figure 3.4.

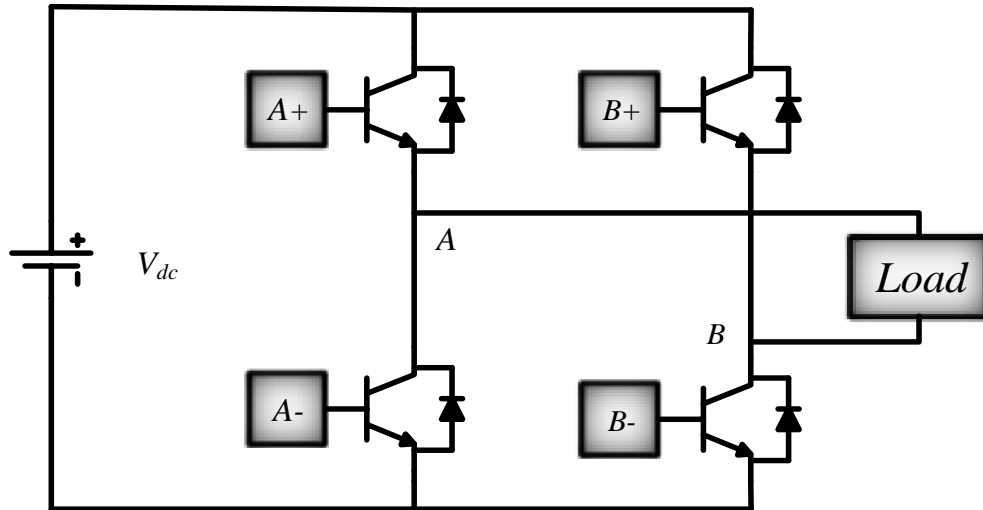


Figure 3.4: Single-bridge VSI

The output power produced by a full-bridge inverter is twice as much as the output power of a half-bridge inverter having the same input voltage. However, different techniques of PWM switching are reviewed to enhance the characteristic inverter operation. The main objective is to insert a zero voltage sequence in the transition change between the positive and negative voltage sequences. This is done in order to improve the output voltage of the inverter as well as to reduce the THD and increase the load factor.

The power circuit of a single-phase bridge inverter is made up of four semiconductor switches which are used to generate sinusoidal waves at the output (Ming & Zhong, 2014; Ghosh & Narayanan, 2007; Lin & Yang, 2004).

3.3.3.1 Switching power devices rules

Using Figure 3.3 above as a reference to illustrate the rules that are applied to a functioning inverter, it can be said that:

On no occasion should two switches of a leg A be closed at the same time. It is normally either A+ or A-, otherwise it would cause a short circuit from V_{dc} to ground (shoot-through).

On no occasion should two switches of a leg B be closed at the same time, it is normally either B+ or B-, otherwise it would cause a short circuit from V_{dc} to ground (shoot-through).

There are some delays during switching **on** and switching **off**, this is to avoid shoot-through. When using real-time switches, a dead time or blanking time is implemented

The corresponding values of V_a and V_b in single bridge are as follows:

$$\text{A+ closed, } V_a = \frac{V_{dc}}{2}$$

$$\text{A- closed, } V_a = -\frac{V_{dc}}{2}$$

$$\text{B+ closed, } V_b = \frac{V_{dc}}{2}$$

$$\text{B- closed, } V_b = -V_{dc}/2$$

Figure 3.5 below displays corresponding values of V_{ab} in single bridge:

$$\text{A+ closed and B- closed, } V_{ab} = V_{dc}$$

$$\text{A+ closed and B+ closed, } V_{ab} = 0$$

$$\text{B+ closed and A- closed, } V_{ab} = -V_{dc}$$

$$\text{B- closed and A- closed, } V_{ab} = 0$$

$$V_{load} = V_A - V_B = V_{AB}$$

The freewheeling diodes allow current to flow even if all switches are open; these diodes also permit lagging currents to flow during inductive loads.

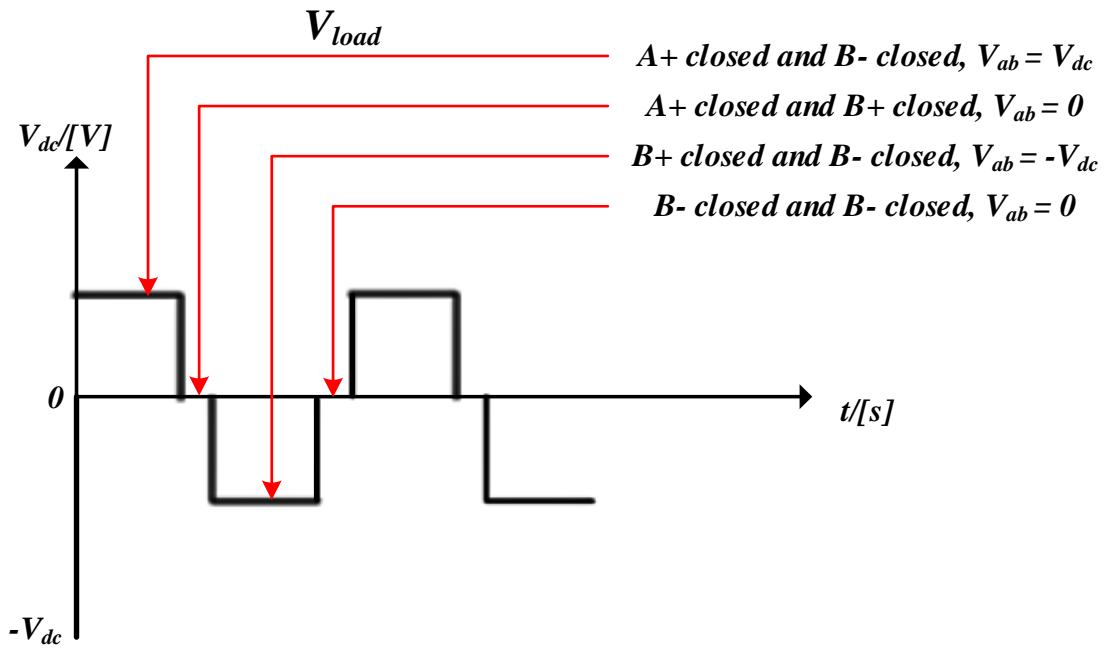


Figure 3.5: The values of V_{ab} in single bridge

3.3.3.2 Operation principles of inverter switching circuits

The inverter topology regarding the switching of its gate, is based on comparing the fundamental frequency to a high carrier frequency signal. This carrier frequency is a triangular waveform for most of the inverters.

The voltage magnitude and frequency are controlled by the PWM. This PWM is created by the combination of a sign control frequency, which is the sinusoidal waveform, and the carrier frequency in triangular waveform. Therefore, the carrier signal is at a higher frequency compared to the signal control frequency.

3.3.4 Voltage control in a single-phase inverter

The loads may require a constant or an adjustable voltage at their input terminals. The DC voltage source input of the inverter can be from a simple battery bank, a solar photovoltaic cell stack or a rectifier from an AC supply. These are applied to the inverter with the goal of controlling the AC output voltage magnitude and frequency of the AC load requirement (Nousiainen & Suntio, 2012).

The output of the inverter voltage is controlled to meet the input load requirement for the purpose of input connection. The output of the inverter is ideally a sinusoidal waveform.

However, in practice the sine waveform is not really a sinusoidal waveform and contains harmonics.

There are two ways to obtain the required voltage variation in inverters; either by varying the input voltage source and keeping the inverter gain constant, or by implementing pulse-width modulation within the inverter. The width of the square pulse is positive and the negative halves of PWM can be adjusted according to the V_{rms} output required. When employing a PWM method, the V_{rms} output voltage remains fixed when the input voltage of the source is fixed.

The commonly used PWM techniques are listed below (Yu et al., 1997):

- Single-pulse-width modulation
- Sinusoidal-pulse-width modulation
- Space-vector-pulse-width modulation
- Multiple-pulse-width modulation
- Modified-sinusoidal-pulse-width modulation
- Phase-displacement control

3.3.4.1 Pulse-width modulation control

PWM is employed to control the output voltage of an inverter. This allows a steady output by constantly employing a PWM control method in the inverter, without an additional external circuitry. The inverter is fed with a constant input voltage and reproduces a controlled AC voltage due to the adjustment of the duty cycle PWM of the inverter components (IGBT) (Loh et al., 2005; Loh et al., 2004).

The advantages of this type of control are that it:

- does not require the support of external circuitry to obtain the required output voltage.
- can minimize low-order harmonics.

The disadvantages are that:

- it requires a fast switching device to be used in the inverter; this is expensive.
- the PWM is characterised by a constant amplitude pulse, with different duty cycles for each period.
- the harmonic content for a particular output voltage can vary for a variety of PWM schemes. A particular PWM scheme is usually referred to a permissible harmonic content in the application.

3.3.4.2 Sinusoidal-pulse-width modulation

Sinusoidal-pulse-width modulation (SPWM) is a method known as a sub-oscillation technique, which is popular in industrial applications. It generates multiple pulses per half-cycle and the width of each pulse is varied with respect to the sine wave magnitude. SPWM consists of a mixture of signals, namely a comparison between a high triangular frequency waveform known as a carrier wave (V_c), and a sinusoidal wave (V_r) of the required frequency. The point of intersection between the V_c and V_r waves, control and define the switching instant for generating the modulated pulses. The V_c carrier frequency wave associated with the modulating signal V_r . Both signal waves are fed into a comparator and the switching time is controlled by the result of a comparison between the reference signal and the carrier wave. The comparison is formulated as follows: when the magnitude of the sinusoidal wave is higher than the triangular wave, it results in a high output of the comparator, otherwise it will be low.

$V_r > V_c$: S11 is **on**, and S12 is **off**, $V_{out} = V_{dc}/2$

$V_r < V_c$: S12 is **on**, and S11 is **off**, $V_{out} = -V_{dc}/2$

As noted, the magnitude of the ratio of V_r/V_c is called modulation index m_a and it is proportionally equal to the magnitude of the fundamental component of the output voltage. Also, it is relatively influenced by the harmonic content in the output voltage waveform. The amplitude of V_r is generally kept constant.

The general condition is that the switches in the same leg of the inverter cannot be turned on at the same time. The output voltage of the half-bridge changes between $v_{dc}/2$ and $-v_{dc}/2$.

3.3.4.3 Sinusoidal-pulse-width modulation with bipolar switching

Diagonally opposite switches of the inverter turn **on** or **off** at the same time. The comparator output voltage, is based on the comparison of V_r and the triangular signal and defined by the

state of the switches. The method is named bipolar PWM because the output voltage of switches alternates between two poles $-v_{dc}$ and v_{dc} (Cai & Qian, 2008).

$V_r > V_c$ S11 is **on** $\implies V_{ao} = v_{dc}/2$, and S22 is **on** $\implies V_{bo} = -v_{dc}/2$;

$V_r < V_c$ S12 is **on** $\implies V_{ao} = -v_{dc}/2$, and S21 is **on** $\implies V_{bo} = -v_{dc}/2$;

$V_{ab} = m_a V_d$ is the peak output voltage of the fundamental frequency component where $m_a < 1.0$.

3.3.4.4 Sinusoidal-pulse-width modulation with unipolar switching

Compared the bipolar, unipolar switching has the effect of doubling the switching frequency. The output voltage level changes between either 0 to $-V$, or from 0 to $+V$, when applying the unipolar switching method. In this method, the switches of one leg are turned **on** and **off** based on the comparison of the signal wave V_r , while the switching of the second leg is turned **on** and **off**, based on comparison between the inverse of V_r and a high carrier frequency (Srisawang, 2010).

3.3.5 Three-phase voltage source inverter

The three-phase voltage source inverter is depicted in Figure 3.6. The structure of the model is composed of two switches in series for each phase, with the three phases connected in parallel.

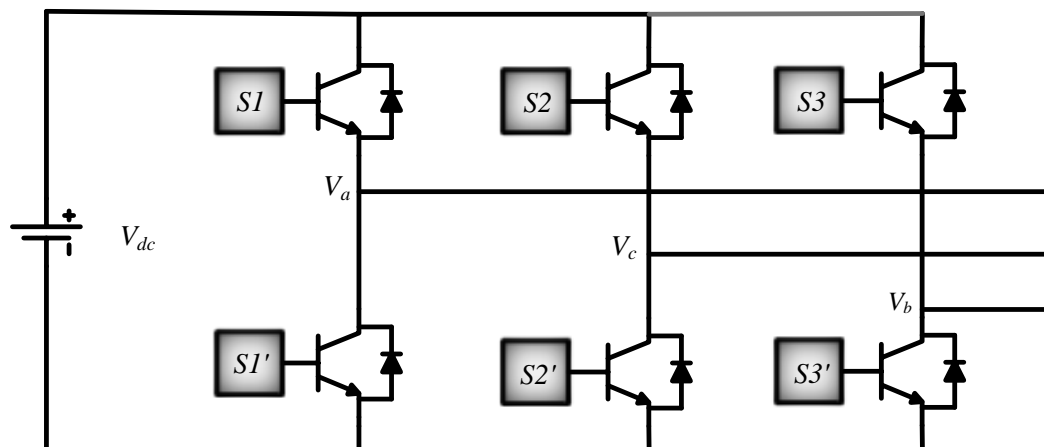


Figure 3.6: Three-phase voltage source

The control of the pair of power switches with anti-parallel diodes, in each parallel leg, plays a significant role. Each of the three legs operate at 120 degrees out of phase to the other two, to produce the three-phase voltage balance (Abu-Rub et al., 2012).

The star-and-delta connection to loads can be represented in by a space vector. The sum of the phase voltages is assumed to be zero when loads are star-connected are in balance:

$$V_a + V_b + V_c = 0$$

The phase voltages at load are defined as follows:

$$V_a = V_A - V_{nN}$$

$$V_b = V_B - V_{nN}$$

$$V_c = V_C - V_{nN}$$

where n represents the neutral point at the load, and
N is the negative rail of the DC bus in the inverter

So that: $V_a + V_b + V_c = V_A - V_{nN} + V_B - V_{nN} + V_C - V_{nN}$

$$V_{nN} = \frac{1}{3}(V_A + V_B + V_C) \quad (1)$$

In summary :

$$V_a = \frac{2}{3}V_A + \left(-\frac{1V_B}{3} - \frac{1V_C}{3}\right) \quad (2)$$

$$V_b = \frac{2}{3}V_B + \left(-\frac{1V_a}{3} - \frac{1V_c}{3}\right) \quad (3)$$

$$V_c = \frac{2}{3}V_C + \left(-\frac{1V_a}{3} - \frac{1V_b}{3}\right) \quad (4)$$

$$V_{nN} = \frac{V_{dc}}{3}(a^* + b^* + c^*) \quad (5)$$

this represents the state of switch of V_{nN}

The mathematical expression relating the variable switching vectors and the neutral output voltage vector is:

$$\begin{bmatrix} V_a \\ V_b \\ V_c \end{bmatrix} = \frac{V_{dc}}{3} \begin{bmatrix} 2 & -1 & -1 \\ -1 & 2 & -1 \\ -1 & -1 & 2 \end{bmatrix} \begin{bmatrix} a \\ b \\ c \end{bmatrix} \quad (6)$$

The magnitude of the phase voltage is estimated to be $\sqrt{3}V_{ph}$, and it is 30 degrees out of phase.

The mathematical expression relating the variable switching vectors and the phase-to-phase voltage vector is:

$$\begin{bmatrix} V_{ab} \\ V_{bc} \\ V_{ca} \end{bmatrix} = V_{dc} \begin{bmatrix} 1 & -1 & 0 \\ 0 & 1 & -1 \\ -1 & 0 & 0 \end{bmatrix} \begin{bmatrix} a \\ b \\ c \end{bmatrix} \quad (7)$$

Table 3.2, Table 3.3, Table 3.4, show the state of the switching of each phase during the six step operation.

Table 3.2: Leg voltage of a three-phase VSI during six step mode operation
(Abu-Rub et al., 2012)

Switching Mode	Switches 'on'	Leg voltage V_A	Leg voltage V_B	Leg voltage V_C
1	S_1, S'_2, S_3	$0.5V_{dc}$	$-0.5V_{dc}$	$0.5V_{dc}$
2	S_1, S'_2, S'_3	$0.5V_{dc}$	$-0.5V_{dc}$	$-0.5V_{dc}$
3	S_1, S_2, S'_3	$0.5V_{dc}$	$0.5V_{dc}$	$-0.5V_{dc}$
4	S'_1, S_2, S'_3	$-0.5V_{dc}$	$0.5V_{dc}$	$-0.5V_{dc}$
5	S'_1, S_2, S_3	$-0.5V_{dc}$	$0.5V_{dc}$	$0.5V_{dc}$
6	S'_1, S'_2, S_3	$-0.5V_{dc}$	$-0.5V_{dc}$	$0.5V_{dc}$

Table 3.3: Phase-to-neutral voltages for the six-step operation
(Abu-Rub et al., 2012)

Switching mode	Switches 'on'	Phase Voltage v_{an}	Phase voltage v_{bn}	Phase voltage v_{cn}
1	S_1, S'_2, S_3	$1/3 V_{dc}$	$-2/3 V_{dc}$	$1/3 V_{dc}$
2	S_1, S'_2, S'_3	$2/3 V_{dc}$	$-1/3 V_{dc}$	$-1/3 V_{dc}$
3	S_1, S_2, S'_3	$1/3 V_{dc}$	$1/3 V_{dc}$	$-2/3 V_{dc}$
4	S'_1, S_2, S'_3	$-1/3 V_{dc}$	$2/3 V_{dc}$	$-1/3 V_{dc}$
5	S'_1, S_2, S_3	$-2/3 V_{dc}$	$1/3 V_{dc}$	$1/3 V_{dc}$
6	S'_1, S'_2, S_3	$-1/3 V_{dc}$	$-1/3 V_{dc}$	$2/3 V_{dc}$

Table 3.4: Line voltages for six-step mode of operation
(Abu-Rub et al., 2012)

Switching mode	Switches 'on'	Line Voltage v_{ab}	Phase voltage v_{bc}	Phase voltage v_{ca}
1	S_1, S'_2, S_3	V_{dc}	$-V_{dc}$	0
2	S_1, S'_2, S'_3	V_{dc}	0	$-V_{dc}$
3	S_1, S_2, S'_3	0	V_{dc}	$-V_{dc}$
4	S'_1, S_2, S'_3	$-V_{dc}$	V_{dc}	0
5	S'_1, S_2, S_3	$-V_{dc}$	0	V_{dc}
6	S'_1, S'_2, S_3	0	$-V_{dc}$	V_{dc}

The modulation index, m_a is a control variable responsible for the V_{rms} output voltage of the inverter. This is the ratio of the amplitude of the control signals to the amplitude of the triangular wave signal.

3.4 Transformation and control

3.4.1 Transformation reference frames: three- to two-dimensional frames

The control of three-phase inverters is very difficult to achieve due to the sinusoidal nature of the output, alongside a host of other problems. In order to minimize the control problem, the concept of transformations has been introduced to change three-phase AC (three-dimensional frames) into equivalent two-phase DC quantities (two-dimensional frames). The voltages and currents are described in different reference frames or coordinate systems. The $\alpha\beta$ frame and the dq frame are the two-dimensional frames used for the transformation; these frames allow control design to be implemented in different coordinates. Implementing current control of a three-phase VSI will require three simultaneous controllers, one for each phase (Bose, 2009).

3.4.1.1 Frame transformation: $abc \rightarrow \alpha\beta$

This transformation is known as the Clarke's Transformation, named after Edith Clarke who developed it. It minimizes the three control loops of a three-phase VSI by transforming them to an equivalent of two control loops. The $\alpha\beta$ (alpha-beta) frame represents transformed, balanced three-phase, sinusoidal quantities in their equivalent two-phase stationary reference frame counterparts (Teodorescu et al., 2006).

Equations 9 and 10 below outline how the $abc \rightarrow \alpha\beta$ transformation and its inverse transformation are performed:

$$\begin{bmatrix} x_\alpha \\ x_\beta \end{bmatrix} = \frac{2}{3} \begin{bmatrix} 1 & -\frac{1}{2} & -\frac{1}{2} \\ 0 & \frac{\sqrt{3}}{2} & -\frac{\sqrt{3}}{2} \end{bmatrix} \bullet \begin{bmatrix} x_a \\ x_b \\ x_c \end{bmatrix} \quad (8)$$

where, $\begin{bmatrix} 1 & -\frac{1}{2} & -\frac{1}{2} \\ 0 & \frac{\sqrt{3}}{2} & -\frac{\sqrt{3}}{2} \end{bmatrix}$ is called the transformation matrix

and $\begin{bmatrix} x_a \\ x_b \\ x_c \end{bmatrix}$ are the balanced three phase quantities.

Also: $\begin{bmatrix} x_\alpha \\ x_\beta \end{bmatrix}$ are the resulting two-dimensional quantities.

On the other hand, the inverse transformation is given by:

$$\begin{bmatrix} x_a \\ x_b \\ x_c \end{bmatrix} = \frac{2}{3} \begin{bmatrix} 1 & 0 \\ -\frac{1}{2} & \frac{\sqrt{3}}{2} \\ -\frac{1}{2} & -\frac{\sqrt{3}}{2} \end{bmatrix} \bullet \begin{bmatrix} x_\alpha \\ x_\beta \end{bmatrix} \quad (9)$$

where: $\begin{bmatrix} 1 & 0 \\ -\frac{1}{2} & \frac{\sqrt{3}}{2} \\ -\frac{1}{2} & -\frac{\sqrt{3}}{2} \end{bmatrix}$ is known as the inverse transformation matrix.

Thus, a problem of having three control loops has been transformed into an equivalent problem with two control loops. In other words, control can be performed with ease in $\alpha\beta$ frame and the results of the control process are transformed back to three-phase.

3.4.1.2 Frame transformation: $abc \rightarrow dq$

Normally the dq transformation is introduced for a system that has more than two variable states. For example, it is used in a three-phase system to project the system from stationary frame to synchronous frame. Thus, the variables of the three phases are transformed into a two-phase stationary coordinate known as an $\alpha\beta$ frame. The DQ transformation is then applied to all variables that are on the rotating frame. The rotation frame has the same angular frequency as that of the fundamental frequency of the converter. It is much simpler to perform an analysis and design controllers in a three-phase system, in a dq rotating frame because all time varying state variables of the controller become DC time-invariant. Only one operation point needs to be defined and considered in the analysis. In order to establish a rotation frame, at least two independent variables are required. Thus, the concept is mostly applied to three-phase; not to a single phase converter due to the limitation of only one phase available in the system (Teodorescu et al., 2006).

$$\begin{bmatrix} x_d \\ x_q \end{bmatrix} = \frac{2}{3} \begin{bmatrix} \cos \theta & \cos(\theta - 2\pi/3) & \cos(\theta + 2\pi/3) \\ \sin \theta & \sin(\theta - 2\pi/3) & \sin(\theta + 2\pi/3) \end{bmatrix} \bullet \begin{bmatrix} x_a \\ x_b \\ x_c \end{bmatrix} \quad (10)$$

where: θ - is the phase angle

Equation 8 is obtained by combining the $abc \rightarrow \alpha\beta$ frame transformation and the $\alpha\beta \rightarrow dq$ frame transformation. The PLL control system is used to obtain the phase angle, θ of the grid voltage, which is used for the $abc \rightarrow dq$ transformation and this is shown in Equation 10. On the other hand, the 3Φ variables, $x_{a,b,c}$ can be calculated by formulating the inverse transformation equation (Teodorescu et al., 2011).

3.4.2 Notch filter

The notch filter is used for reducing noise and other disturbances in the load current, by leaving the harmonic component and omitting the fundamental frequency. This method reduces the THD at the output by a fast recovery at the step-change transient. However, when used in three-phase loads for determining the current compensation, it causes disturbances (Quinn et al., 1993; Basic et al., 2001).

3.4.3 Fast Fourier transform

Fast Fourier transform (FFT) is a technique mostly used to determine and analyse the THD; it is done by taking the sampled load current for one period and calculating the magnitude and phase of the frequency components. Re-setting the frequency component from 50 Hz to zero and then applying the inverse of the FFT, will remove the fundamental frequency from the input current. Most instruments adopt the FFT algorithm to detect harmonics, because this algorithm can achieve steady harmonic detection, directly and correctly. However, in a power distribution system using the FFT, it is difficult to adhere to an exact measurement under random, non-linear conditions.

3.4.4 Phase-locked loop

A phase-locked loop (PLL) is a system that extracts the phase angle of the grid voltage. It compares the phase difference between the input signal and the output signal of a voltage-controlled oscillator (VCO), using a closed-loop frequency-control. The negative feedback loop of the system forces the PLL to keep the input and output phase in lock step. This is illustrated by the three blocks in Figure 3.7 below. The phase detector block produces an output proportional to the phase difference between the input signals and the signal generated by internal oscillation. The loop filter contains the first order low pass filter or a PI in the block. This represents the low-pass filter used for the purpose of lessening the high frequency AC component in the phase detector. The output is then generated by the voltage-controlled oscillation with a shifted AC frequency in accordance with the cut-off frequency.

The PLL system is employed to detect the frequency and phase of the grid harmonics in order to select a proper speed for the synchronous frame. The reliability of harmonic detection is dependent on the behaviour of the PLL. The grid-connected power converter uses the PLL to synchronize with the grid. It considers the grid voltage frequency and phase as the reference and at the same time it harmonizes the fundamental frequency of the VSI to that of the utility grid.

The PLL is widely employed in power systems and power electronics to facilitate grid synchronization of distributed generation, in order to estimate the following (Karimi-Ghartemani et al., 2004):

- Phases
- Frequencies
- Harmonics
- Inter-harmonics
- Active and reactive powers
- Sequence components
- Disturbances
- Transients

For proper synchronization with utility voltages, special attention needs to be given to the control of grid-connected power converters.

Some authors (Cortes et al., 2008) proposed detection of unbalanced and distorted utility voltage conditions in the fundamental frequency of the positive-sequence component, using a decoupled, double-synchronous reference frame phase-locked loop. They presented an enhanced phase-locked loop (EPLL) which yields the fastest, most accurate estimation using limited computation.

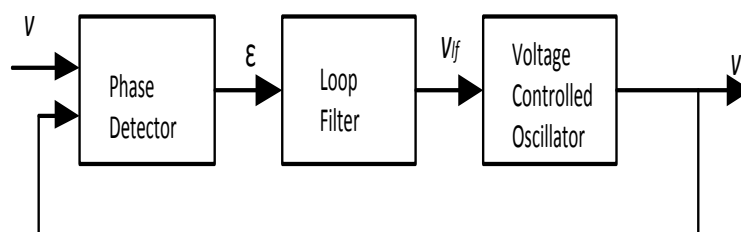


Figure 3.7: Basic structure of a PLL

3.5 Filter topology

Harmonic problems are expected in inverter systems due to the fact that the power delivered to the load from the PV system, passes through a voltage source inverter. Thus, there is a compromise between using a high-speed switching frequency with considerable loss of power and less harmonics, or using a low-speed switching frequency with a high THD and low power loss. The presence of harmonics at the output voltage of the inverter is usually attenuated by

connecting a filter between the voltage source of the inverter system and the load, in order to meet the power quality requirements. However, the size of the filter depends on the switching frequency chosen for the inverter. At a high-speed switching frequency the size of the inverter is small and at a low-speed frequency the size of the inverter is bulky (Wong et al., 2008; Nassif et al., 2010; Ji et al., 2012).

3.5.1 L-filter

An L-filter is shown in Figure 3.8 below. It is defined as a first-order filter, used mostly to attenuate the harmonic content of the output of the inverter. The main objective is to attenuate the current ripples that result from inverter switching (Hurng-Liahng et al., 2008; Hobraiche et al., 2009). It is composed of an inductor only and it is connected in series with the output of the inverter. The L-filter is frequently used in inverter and other applications due to its simplicity of manufacture. In addition, it does not have the resonance problems usually seen in higher-order filters. When it is used with high switching modulation in the inverter, it is capable of an attenuation of -20 dB per decade over the entire frequency range, which is the highly efficient. However, the size of the inductor required to realize a reasonable attenuation of the current harmonics, is very large (Yao et al., 2013; Liu et al., 2009; El-Habrouk et al., 2000).

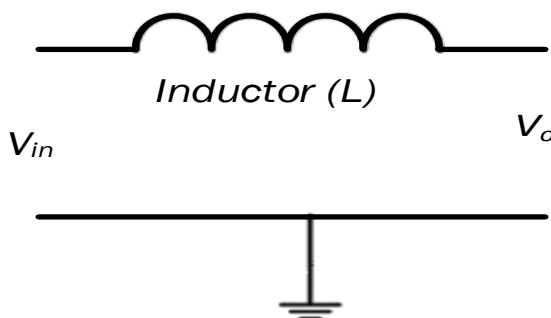


Figure 3.8: L- filter

3.5.2 LC- and LCL-filter

The LC-filter and LCL-filter are represented respectively in Figure 3.9 and Figure 3.10 below. An LC-filter is defined as a second-order filter, while an LCL-filter is defined as a third-order filter. These filter types are connected at the output of the inverter and parallel to the loads. The LC-filter is mostly used in a microgrid operating in stand-alone mode; they are used on the AC terminals of PWM inverters when control of the output voltages is the main objective (Kim et al., 2008; Kim & Sul, 2005). In microgrids that are grid-connected, the LC filter is rarely used

because the resonance frequency of the filter vary with the inductance value of the grid. The resonant frequency of the LC-filter is calculated from the Equation 11.

$$f_o = \frac{1}{2\pi\sqrt{LC}} \quad (11)$$

Looking at the cost and the reactive power consumption, they are both relatively higher in an LC-filter than in an L-filter; this due to the accumulation of a shunt element in the L-filter).

However, in general the LCL-filter has a better attenuation of inverter switching harmonics compared to the L- and LC-filters of similar size. The LCL-filter reduces the problem experienced by the LC-filter in grid-connected microgrid mode, due to the fact that the resonance frequency depends mainly on the filter components. Advantages of an LCL-filter are: attenuation of -60 dB/decade for frequencies exceeding the resonance frequency, an option of low-switching frequency, it can be dedicated to a given harmonic attenuation. These are the advantages of the LCL-filter. The LCL-filter has two more poles and two more zeroes than the LC-filter; this makes dynamic control of the inverter more difficult when using an LCL-filter (Ahmed et al., 2007; Zhang et al., 2013), because additional poles and zeroes can make the system unstable if proper damping is not introduced. The resonant frequency of the LCL filter is calculated from the equation:

$$f_0 = \frac{1}{2\pi} \sqrt{\frac{L_1 + L_2}{L_1 L_2 C}} \quad (12)$$

Furthermore, the gate of an inverter can be driven by digital controller platforms; these digital controller platforms can be programmed to perform a selected electronic function. In the switch-mode of a power electronics converter, digital control platforms are used as switches to turn the inverter gate **on** or **off** with respect to the adopted control algorithm. Within a switching cycle, the duration of the **on** and **off** states is controlled to allow an average-value voltage or current to be created from an input signal. From this simple physical behaviour, an array of switches in differing **on** and **off** patterns, together with the corresponding algorithms, make it possible to create the desired signals.

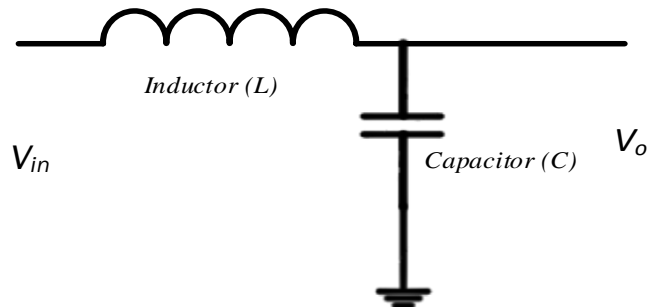


Figure 3.9: LC-filter configuration

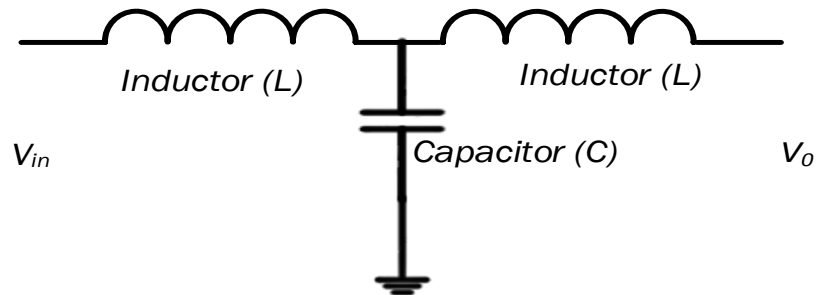


Figure 3.10: LCL-filter configuration

3.6 Digital platforms for inverter control

Analogue controllers and hardware have been mainly employed in the past to control a power electronics system. However, these controllers have many shortcomings such as: increased noise levels; waveform distortion; limitations in response time, and capacity. Analogue controllers cannot be implemented in a complex control algorithm. However, the rise of the digital control created a lot of interest in power electronics. Intensified research in power electronics has led to the development of modern digital control and its various platforms are more flexible than analogue controllers, and are capable of running complex control algorithms. This not only improves individual control, but also improves the entire system. For example, in a distributed power system control strategy, the digital control system can drive a much more complicated controller; something which cannot be achieved by traditional analogue control.

In comparison to analogue control, digital control is more flexible: it is easier to change or to accommodate additional variables. There is a large variety of digital control platforms, the difference between them being their capacity to handle instructions within a set time frame. Some of the commercial platforms available are: TMS320F2812 and, TMS320C6713 DSP from MATLAB/SIMULINK; DS1104 and DS1103 from dSPACE; and, XC3S400 FPGA from Xilinx.

The control strategy associated with a digital microprocessor can be modified or changed by simply reprogramming the controller of a system, without having to change any hardware. For instance, the DSP of an erasable programmable device is flexible because the board can develop a number of different operations, which may only necessitate software reprogramming (Shan et al., 2009; Shan et al., 2008). However, the main drawback is the delay issue in digital control due to the computation period.

Different types of processors such as microprocessors, microcontrollers and programmable logic devices (PLDs), and field-programmable gate arrays (FPGAs) are used to build PWM-controlled inverters (Selvaraj & Rahim, 2009; Shan et al., 2008; El-Hefnawi, 1997; Kawamura & Yokoyama, 1990).

The shortcomings of analogue controllers are the following (Alatise et al., 2009):

- Lack of flexibility
- Low reliability
- Cannot be reprogrammed; has to be replaced

The potential advantages of the digital control are listed below (Prodic & Maksimovic, 2000; Kocybik & Bateson, 1995; Martin & Ang, 1995; Martins et al., 1995; Itoh & Kawauchi, 1991; Query & Tescher, 1990; Oshikata et al., 2003; Query & Tescher, 1990).

- Enhanced flexibility, time saving on design and eminent error, more reliability, and easy integration into the system.
- Unlike the analogue, it allows the implementation of non-linear controllers such as predictability, hysteresis and adaptive control.
- Digital control is less susceptible to noise.
- Less sensitive to environmental variation.

Some disadvantages of digital signal processors related to the fact that DSP uses words of finite length to represent each and every value; causes memory problems and logic gates this causes memory and logic gate problems (Wu & Lin, 2006; Descampe et al., 2006; Iwahashi & Kiya, 2009):

- Problem of signal resolution in sampling data systems due to finite word length of the DSP.
- Operational rounding off errors of variables within the DSP can result because of the finite word lengths.
- The analogue-to-digital or digital-to-analogue converter can limit the cycles because of the finite word length of the DSP.

- The computation of long algorithms in the DSP is influenced amongst others, by the time delay in the control loop, and the time delay of maintaining the phase margin.

3.6.1 Some examples of algorithms used in implementing digital control for inverters

An inverter converts DC voltage and current into AC voltage and current, through power electronics and microprocessors. In the course of the literature survey, various articles on the digital implementation of control algorithms for an inverter system discussed the efficiency, the protective functions, and the automatic synchronization of voltage and frequency by the inverter.

PWM designed for an inverter using Xilinx FPGA PWM generators is an improvement on the limited analogue PWM control. It has been confirmed that it is effective for regulating three-phase inverter output waveform. This is considered to have advantages such as concurrent operation and fast prototyping. The control inverter based on FPGA gives a remarkable output waveform with low THD as a result (Mekhilef & Rahim, 2002).

The PI controller has been used to regulate inverters for years (Sanchis et al., 2005). This involves an explicit mathematical model of the system to be controlled. However, this cannot really be implemented in non-linear systems and the performance of the controller degrades when subjected to disturbances.

The inverter using a 50 Hz isolation transformer is compared to a HF-link inverter in terms of efficiency. Salem et al. (2006) proposed a high-frequency link inverter based on deadbeat control; this was to increase the system efficiency of the converter by reducing the number of power switchings and the size, when compared to analogue inverter. To implement the control algorithm, they selected a ds1104 inverter manufactured by dSPACE.

Several authors (Xuezhi & HongXia, 2009; Shan et al., 2009) worked on a method for regulating the three-phase alternative current into a variable frequency, using sinusoidal pulse width modulation (SPWM). The control algorithm of SPWM technology was implemented in the digital controller TMS320F2812 manufactured by Texas Instruments. Judging from the experimental results obtained, the output showed a good result in transforming 50Hz, 340V AC into 220V at an adjustable frequency ranging from 100-400Hz AC. Furthermore, to improve the output waveform of the inverter with the view of reducing the THD, Selvaraj and Rahim (2009) presented a novel control scheme based on the PWM signal for a single-phase multilevel inverter. This PWM is created from two offset reference signals and a carrier frequency voltage, and was used in the digital controller. The PI control algorithm is used in DSP TMS320F2812 to

control the current injected into the grid with a dynamic response. The results of a simulation experiment indicated that the inverter produces less THD and a high power quality.

The conventional fuzzy PI control (CFPIC) was a fusion of both fuzzy and PI control to create a more robust control system with a high performance regulator control for the inverter. This control algorithm was derived from a large logic table and has a rapid response countering large signal disturbances. However, it is required to be implemented a very fast processor board for the control action. In addition, it needs a long computation time due to the large set of instructions (Ayob et al., 2009).

Generally, the inverter experiences some self-consumption losses due to the switch devices, which can affect the efficiency (Eltawil & Zhao, 2010). However You-jie et al. (2010) recommended a TMS320F2812 DSP (by Texas Instruments) to design multi-cascade inverter topology because it represents an improved approach to control five levels of frequency variables. The control algorithm adopted incorporated into the DSP has a high precision output.

The low cost and low THD of the common SPWM inverter, using a digital PID control strategy, has been proposed for a single-phase inverter. It is structured to control the multi-loop of the instantaneous current and voltage values, by combining the cross-feedback decoupling control, load current feed-forward control, and the closed-loop control of the output voltage V_{rms} . It has been implemented in the TMS320F2812 DSP which has a fast and dynamic response as a result (Gong et al., 2011). It is a novel and practical multi-loop control strategy for photovoltaic Inverters based on digital signal processing.

A control algorithm for fast prototyping for fast prototyping of segment SVPWM was proposed and implemented, based on a TMS320F2812 associated with Simulink including the real-time workshop (RTW). This was done to overcome the limitation of the conventional method of designing a complex control system algorithm with C-code which is prone to errors. SVPWM saves time and promotes cost effectiveness by automatic code generation. However, a small design error might still occur during the process (W. Zhang et al., 2010; Zha & Chen, 2011).

Another platform has been introduced and it is mostly used in the automation industry and in inverter control. To enhance the control performance of these inverter systems under, for instance, the influence of unbalanced load, or high harmonics level, Ghani et al. (2011) proposed fuzzy logic control to regulate 50 Hz three-phase AC current and voltage in a high frequency inverter. This control algorithm is implemented in dSPACE DS1104 platform, allied with the MATLAB/Simulink environment. This was submitted to various load changes to ensure the effectiveness of the control system. Fuzzy logic control implemented in dSPACE DS1104

platform presents an excellent result of 2.48% of THD. In addition, they presented the PI control algorithm based on SPWM developed to be implemented in dSPACE DS1104 platform associated with the MATLAB/Simulink environment. In order to regulate the 50 Hz AC output voltage of the inverter to eventual disturbance, the results are more than satisfactory with 4.6% THD at the output of the inverter (Hannan et al., 2011). Therefore, when comparing the two methods employed to control the output of the inverter for more or less the same objective, both control strategies performed well, although it appears that the fuzzy logic control is more robust than the PI controls.

(Munoz et al., 2012) proposed a control strategy to compensate the reactive power and the fundamental frequency using the multilevel control strategy. This is implemented with a TMS320C6713 DSP for frequency domain and discrete time to produce a low power prototype.

The Fuzzy logic control is structured to handle a non-linear complex control algorithm without a precise mathematical model of the system. This is robust in inverter application against disturbance as reported (Li & Gatland, 1995; Kandlawala & Nguyen, 2009; Lu et al., 2012). This Fuzzy logic control has been implemented by means of a TMS320C6713 for the general purpose of the PID controller. The goal is to overcome the limit of classical control used in the inverter. It can be reprogrammed for different modes of operation without reconfiguring and changing the hardware (Maji et al., 2012). Besides, the Fuzzy control algorithm is used to produce a PWM signal for inverter. This is implemented on the ds1104 board to generate a frequency of 50 Hz AC with 3.5% of THD (Subiyanto et al., 2013).

3.6.2 Harmonics

Rotation machinery and transformers operate with magnetic materials, which cause distortion in the primary source of the current waveform, especially when they are closer to the load. However, the switched power semiconductor device has played a major role in reducing harmonics in power systems. There are a large number of non-linear loads in small rating such as SMPS (switch mode power supply), TVs, PCs and other IT equipment. These are made up of a single-phase, bridge rectifier and power supply. However, load voltages are controlled via static power converters such as rectifiers, inverters, single-phase, and three-phase. These are commonly non-linear and impose a non-sinusoidal waveform onto the power (Chan et al., 2000; Jiang et al., 2010).

Therefore, due to the wide-spread use of non-linear loads in power systems, harmonic problems continually increase which results in reduced power quality. The total harmonic distortion is the sum of distortion in the line current waveform which is measured by means of an index. It is the

amount of the fundamental frequency current of the harmonic components, expressed as a percentage of the fundamental component. Nevertheless, there is a tolerance for the amount of harmonics in the power system. This standard limit for current harmonics is defined by ANSI/IEEE Standard 519-1992 (Mohan et al., 2002). Different techniques have been developed to determine the harmonics in the current waveforms. These methods are: discrete Fourier transform (DFT), phase-locked loop (PLL), notch filtering and theory of instantaneous reactive power.

3.6.3 Total harmonic distortion

The distortion factor is a common method used to measure the total harmonic distortion (THD). This is applied to both voltage and current. When DC is excluded, the THD for a current waveform is defined as:

$$THD_1 = \frac{\sqrt{\sum_{k=2}^{\infty} \left(\frac{I_k}{\sqrt{2}}\right)^2}}{\frac{I_1}{\sqrt{2}}} = \frac{\sqrt{\frac{1}{2} \sum_{k=2}^{\infty} (I_k)^2}}{\frac{I_1}{\sqrt{2}}} \quad (13)$$

THD and RMS values are related by:

$$I_{rms} = \sqrt{I_{rms}^2 + THDI^2} \quad (14)$$

Line losses are proportional to the square of the RMS current, hence line losses are related to the increased harmonics. Sometimes they increase more rapidly due to the resistive skin effect. The voltage distortion is normally less than 5%, while current distortion in loads varies from a few percent to more than 100%. According to IEEE 519, voltage THDs below 5% are considered acceptable, and those greater than 10% are definitely unacceptable and will cause problems for sensitive equipment and loads (da Fonseca et al., 2014; Leelajindakraierk & Chompoo-Inwai, 2012).

3.7 Conclusion

Power electronics are designed using several types of semi-conductor power devices. This design can be used in different operating and inverter control modes. In addition, a review on innovation in digital control platforms was discussed. The advantages of inverters and the control of DG, using a power electronics interface in the microgrid, have been discussed.

Conversions using power electronics is at the heart of numerous electrical applications, and its use is increasing. The next chapter discusses the modelling and control strategies of the microgrid.

Chapter 4 : SYSTEM MODELLING AND CONTROL

4.1 Introduction

This chapter presents the modelling of an autonomous microgrid. The model is composed of a PV array designed for a cluster of villages, a DC-DC converter, an IGBT- based inverter and a LC filter connected to the load power. The development of an inverter control and energy management system control algorithms for the microgrid are also presented.

The remaining part of this chapter is organised as follows. Modelling of PV system using MALATB/SIMULINK is presented in Section 4.2. A boost converter designed for the PV model is presented in Section 3.4. In Section 4.4 the inverter output voltage controls are presented. Section 4.5 presents the Energy Management System Control algorithm of a microgrid system. A conclusion is drawn in Section 4.6.

4.2 Photovoltaic system model

The goal of the modelling is to get inside the performance of the PV system in response to two parameters, namely the radiation and the ambient temperature. The literature search revealed that for advanced systems, the PV models can vary in complexity. The model used is a simple one which will be referred to as preview works model.

4.2.1 Photovoltaic module model

The output characteristic of PV array depends on the cell temperature, solar radiation, and output voltage of the array.

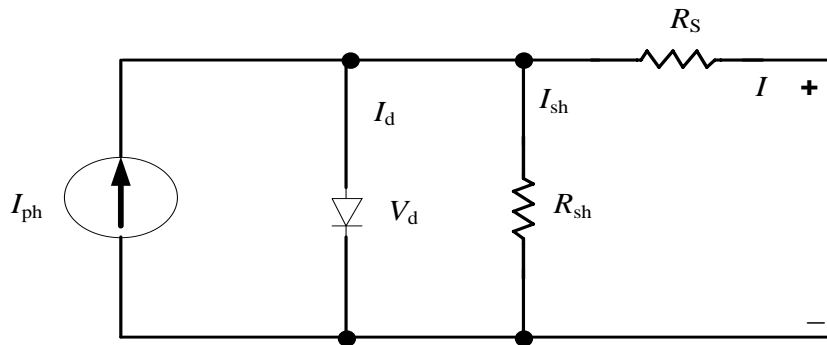


Figure 4.1: Equivalent circuit model of PV cell
(Tarak Salmi, 2012)

The cell temperature and ambient temperature influence the cell characteristics, both are important parameters that are considered in the modelling of a PV system. For instance, intense radiation increases the open circuit voltage, while the short circuit current is linearly a function of the ambient radiation.

An increase in the cell temperature decreases the open circuit voltage, while the short circuit current increases slightly with cell temperature. Therefore, the cell is less efficient when the temperature is high. The equivalent electrical model circuit of a solar cell can be represented with a photocurrent described by a constant current source I_{ph} in parallel to a diode V_d and to a resistor R_{sh} , representing a leakage current and connected to a series resistance R_s , which represents an internal resistance to the current flow; this is shown in Figure 4.1 above.

The equivalent circuit of the PV solar array arranged in N_p parallel and N_s series cells is represented in the Figure 4.2 below (Tarak Salmi, 2012).

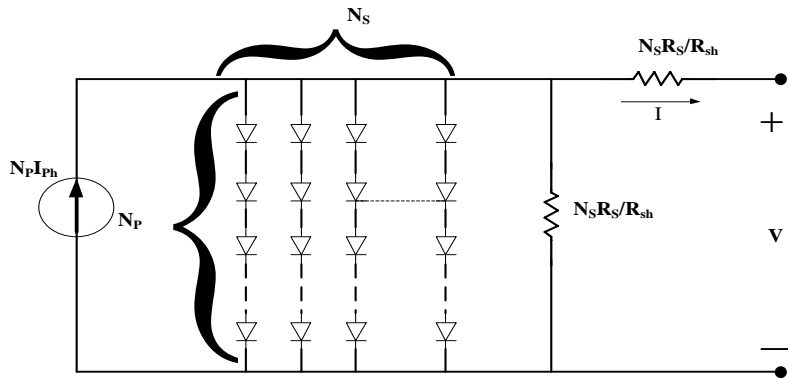


Figure 4.2: Equivalent of N circuit model of solar array
(Tarak Salmi, 2012)

The mathematical model of the voltage-current characteristic equation of a solar cell from Figure 4.1 above (Jung & Ahmed, 2010; Chowdhury et al., 2008; Tarak Salmi, 2012) is expressed in Equation 15:

$$I = I_{ph} - I_s \left(\exp \frac{e(V + IR_s)}{mKT_c} - 1 \right) - \frac{(V + IR_s)}{R_{sh}} \quad (15)$$

The photocurrent I_{ph} relatively depends on the operating temperature of the cells and solar radiation as expressed in Equation 16.

$$I_{ph} = \frac{(I_{SC} + Ki(T_c - T_{Ref})) \lambda}{1000} \quad (16)$$

The saturation current of the cell varies with the cell temperature which is represented as;

$$I_s = I_{RS} \left(\frac{T_c}{T_{Ref}} \right)^3 \exp \left(\frac{qE \left(\frac{1}{T_{Ref}} - \frac{1}{T_c} \right)}{KA} \right) \quad (17)$$

$$I = I_{ph} - ID \quad (18)$$

The components of the PV system as shown in Figure 4.1 are the resistance R_{sh} parallel to the diode, which is inversely proportional to the shunt leakage current to the ground. The variation of this resistance does not have an impact on the PV array and its leakage resistance is assumed to reach infinity without the leakage current to the ground. However, a small variation in series resistance R_{sh} will significantly affect output power of a PV array.

The appropriate model of a PV solar cell with suitable complexity is shown in.

$$I = I_{ph} - I_o \left(\exp \frac{q(V + IR_s)}{mKT_c} - 1 \right) \quad (19)$$

The PV array circuit model is represented in Figure 4.2 where Equation 20 can be used to determine the array current, where the array has N_p parallel (N_p) and N_s series (N_s) cells;

$$I_{PV} = N_p I_{ph} - N_p I_s \left(\exp \frac{q \left(\frac{V_{PV}}{N_s} + \frac{I_{RS}}{N_p} \right)}{KT_c m} - 1 \right) - \frac{(N_p V_{PV} + I_{RS})}{R_p} \quad (20)$$

- where:
- m : ideality zing factor
 - T_c : absolute temperature of the cell in Kelvin
 - q : electric charge ($1.602 \times 10^{-19} C$)
 - v : imposed voltage across the cell
 - I_o : diode dark saturation current

The solar cell is characterised by the following parameters:

- Short circuit current: It represents the highest current value generated by a cell during the condition where the $V=0$.
- Open circuit voltage: This is due to the voltage drop across the diode while it is passed through a photocurrent, I_{ph} , where $I_D=I_{ph}$ and the generated current is zero.
- The mathematical expression of the cell voltage with no light is:

$$V_{oc} = \frac{mkT_c}{e} \ln\left(\frac{I_{ph}}{I_o}\right) = V_t \ln\left(\frac{I_{ph}}{I_o}\right) \quad (21)$$

where: T_c : absolute cell temperature
 $V_t = \frac{mkT_c}{e}$: thermal voltage

- Irradiance and weather: refers to the radiation and weather condition in the PV system. Modelling will face a variety of uncertainties with regard to the radiation.
- Maximum power point: refers to the point at which the power dissipation in resistive load is at the maximum range of operation.
- Maximum efficiency: corresponds to the ratio of maximum power divided by the incident light power.

$$n = \frac{P_{max}}{P_{in}} = \frac{I_{max}V_{max}}{AG_a} \quad (22)$$

where: G_a : refers to the ambient radiation
 A : cell area

- The fill factor corresponds to the ratio of the maximum power that can be delivered to the load as per Equation 23.

$$FF = \frac{P_{max}}{V_{oc}I_{sc}} = \frac{V_{max} \cdot I_{maz}}{V_{oc}I_{sc}} \quad (23)$$

Table 4.1: PV cell parameters

Module type	SunPower SPR-305-WHT
Number of cells per module	96
Number of series connected module per string	9
Number of parallel strings	40

Table 4.2: Module specification under standard test conditions (STC)

V_{oc}	64.2
I_{sc}	5.96
V_{mp}	54.7
I_{mp}	5.58

Table 4.3: Module parameters for one module

R_s	0.037998
R_p	993.51
I_{sat}	1.1753e-08
I_{ph}	5.9602
Q_d	1.3

4.2.2 Load profile determination in Africa

The load profile has been selected from a publication by the US Department of Energy (Engery, 2014) and contains average items that can possibly be found in rural villages in African homes. As can be seen in Table 4.4 below the load consumption is relatively low in rural areas. However, in the simulation, it is assumed that all the households have the same power demand and power factor of one.

Table 4.4: Appliances used in one household (adapted from anon, 2014)

Appliances	Power (W)	Units	Time per day per unit (hours)
Lamp	30	6	8
Radio	70	1	5
Microwave	750	1	1
Cellphone charger	10	2	6
Television	133	1	6
Refrigerator	725	1	24
Ironing clothes	1000	1	1
Water heater (150 litres)	4500	1	4

Each house in the village needs 7368 W peak power and the number of houses are considered to be approximately 136. Thus, at peak time the total power supplied to the cluster of villages is 1 MW, neglecting losses in the energy and delivery system.

The design requirement is thus for a 1 MW_p PV system delivering 398 V_{AC} (V_{rms}) three-phase.

The minimum DC voltage to be supplied to the inverter is $750 V_{dc}$ with a modulation index, m_a of 0.866.

The fundamental voltage, V_{ab} of the inverter output is determined by:

$$m * V_{dc}(\text{Volts peak}) * \frac{\sqrt{3}}{2}$$

$$= 0.866 * \frac{\sqrt{3}}{2} * 750 = 563 V(\text{peak})$$

At the PV system, the output voltage chosen is $450 V_{dc}$ at $1 MW_p$.

4.2.3 Photovoltaic system design

Ten PV systems, each of 100 kW are designed and connected in parallel to make up the $1 MW_p$, by firstly designing 100 kW PV and then multiply it by 10 times to get the desired $1 MW_p$.

The calculation of the number of modules needs to meet the requirement.

The number of panels required in series is $\frac{450}{54.7} = 8.22$

It is not possible to have a fractional panel 0.22, thus the number of the panels to be used is rounded up to 9.

The actual output voltage from the PV system is therefore: $9 * 54.7 = 492.3 V_{dc}$.

The output current from the PV system is calculated as follows:

$$P = VI$$

$$I_{total} = 100000/450 = 222.22 A$$

The number of panels in parallel = $\frac{222.22}{5.58} = 39.82$

It is not possible to have a fractional panel of 0.82, therefore the number of panels in parallel is rounded up to 40.

The actual power is calculated as follows:

$$\text{Actual power} = (40 * 5.58 * 9 * 54.7) = 109.88 kW$$

By interconnecting 10 PV systems of 109.88 kW each in parallel, the total PV system power is:

$$= 10 * 109.88 kW = 1.988 MW_p$$

4.3 Boost converter design

To increase an input voltage, a boost converter is usually used to step-up the voltage by means of switching some components; this produces an output voltage greater than the source. The basic components of a boost converter are a power semi-conductor switch, a diode, an inductor, a condenser and a pulse width modulator.

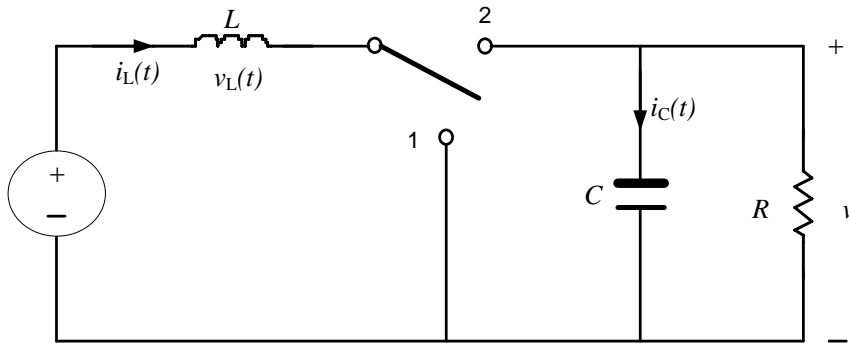


Figure 4.3: Ideal boost converter circuit
(Robert & Maksimovic, 2001)

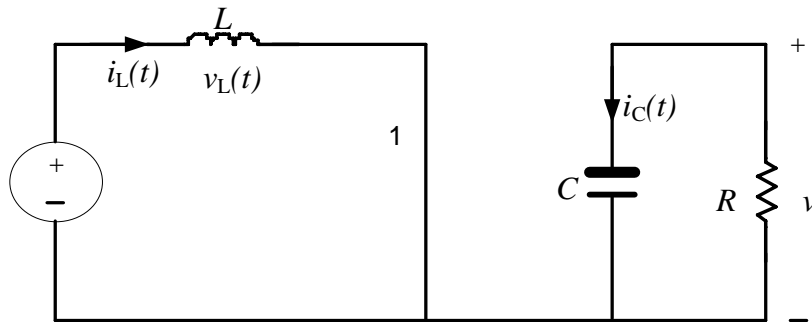


Figure 4.4: Switch in position 1
Robert & Maksimovic, 2001

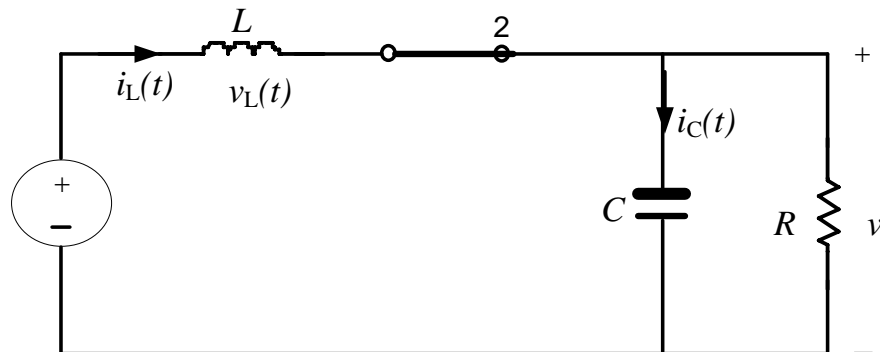


Figure 4.5: Switch in position 2
Robert & Maksimovic, 2001

A boost converter was designed for the PV system by using the volt-second balance technique and the capacitor charge balance technique, with a small ripple approximation to determine the

voltage and current of the boost converter. The techniques are also used to set the values of the components cited above. For the modelling of the boost converter, certain assumptions were made.

The ideal boost converter is shown in Figure 4.3 above which is split into two sub-figures to illustrate the effect of switching – these sub-figures are. In the **on** time of the duty cycle (DT) the switch is in position '1' as in Figure 4.4 below and in the **off** time of the duty cycle D'T the switch is in position '2' as shown in Figure 4.5 below.

In practice, the switch is represented by a power transistor and a diode, and the gate drive circuit (PWM controller) will determine position '1' or position '2' by respectively sensing a high or a low voltage. When the gate circuit voltage is high, it will turn **on** a MOSFET power transistor which the simulates the switch in position '1'. When it senses a low voltage, the MOSFET, it turns **off**, simulating the switch in position '2'.

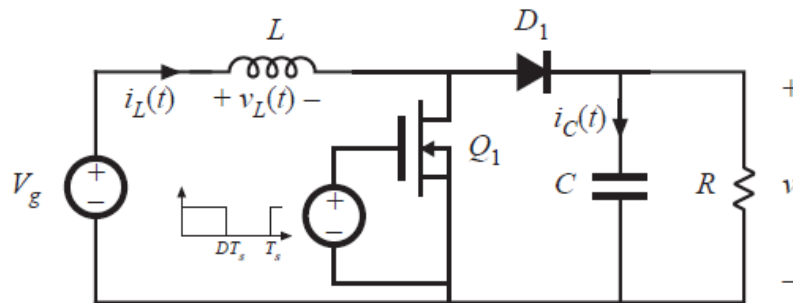


Figure 4.6: Boost converter circuit using power MOSFET and diode
(Robert & Maksimovic, 2001)

When the MOSFET is **off**, the inductor current will forward bias the diode, turn it **on** and effectively putting the switch in position '2'.

The reason for putting a diode in the circuit instead of a mechanical switch, is to enable it to automatically come **on**. One way of looking at the presence of the diode in the circuit is illustrated in Figure 4.6; the formula for the voltage drop over the inductor is given by:

$$v_L = L di/dt \tag{24}$$

Equation 24 represents the potential drop across the inductor when the MOSFET is subject to a high voltage; builds up a positive current that runs through the inductor and to the MOSFET. When the MOSFET is suddenly turned **off**, it is effectively trying to interrupt the inductor current. Thus, the inductor current that was positive, is now compelled, by the MOSFET that is turned **off**, to proceed immediately to zero. Whereas, the value of $L di/dt$ is big and negative if the MOSFET was to be shut off. The voltage will however, tend to infinity, so when $L di/dt$ is hugely

negative ($-\infty$), it will make v_L big and negative. v_L changes from negative to positive in the reference direction so its value is a negative number. Effectively it means that the negative value that is connected, will go change to a large positive voltage to and then to $(+\infty)$, but before it gets there, it forward biases the diode. The inductor is discharging its energy and the polarity of inductor voltage is such that its terminal connected to the diode, is positive with respect to its other terminal, which is connected to the source. It can be seen that the capacitor voltage has to be higher than the source voltage and hence this converter is known as a boost converter.

When the switch is closed, the diode does not conduct and the capacitor sustains the output voltage. As long as the resistor-capacitor (RC) time constant is much larger than the '1' period of the switch, the output voltage will stay more or less invariant.

4.3.1 Inductor voltage and capacitor current at first interval

When the switch is closed, as shown in the equivalent circuit in Figure 4.4 , the inductor voltage is equal to the source voltage that is applied across it:

$$v_L = V_{in}$$

$$i_C = -\frac{v}{R}$$

allowing for a small ripple approximation:

$$v_L = V_{in}$$

$$i_C = -V_{out} / R$$

4.3.2 Inductor voltage and capacitor current at second interval

When the switch is open, the voltage across the inductor is shown in Figure 4.5. Provided that the output voltage is larger than the source voltage, the voltage across the inductor is negative:

$$v_L = V_{in} - v$$

$$v_L = i_L - v / R$$

allowing for a small ripple approximation:

$$v_L = V_{in} - V_{out}$$

$$i_C = I - V_{out} / R$$

4.3.3 Inductor volt-second balance

The voltage drop over and inductor, v_L over time period, T_s is given by:

$$\int_0^{T_s} v_L(t)dt = (V_{in})DT_s + (V_{in} - V_{out}) D'T_s$$

Equate to zero and collect terms:

Net volt-seconds is applied to the inductor over one switching period as seen in Figure 4.7 below. Since the net change in inductor current over a cycle period is zero when the response is $i_L(t)$, the sum of the net changes in inductor current expressed by Equations 5 and 7 should be zero (Robert & Maksimovic, 2001).

$$(V_{in})DT_s + (V_{in} - V_{out})D'T_s = 0$$

$$V_{in} (D + D') - V_{out} D' = 0$$

Solve for V:

$$V_{out} = V_{in} / D'$$

The value of D can be comprised between $0 < D < 1$ as seen in Equation 25 which makes the output voltage to be greater than the source voltage. Hence, this circuit is called the boost converter.

The voltage conversion ratio is therefore:

$$M(D) = \frac{V_{out}}{V_{in}} = \frac{1}{D'} = \frac{1}{1 - D} \quad (25)$$

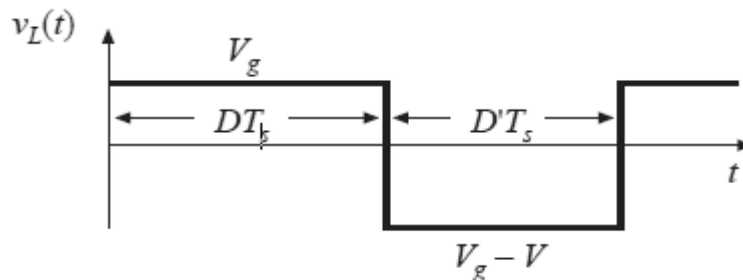


Figure 4.7: Inductor voltage waveform

(Robert & Maksimovic, 2001)

4.3.3.1 Conversion ratio $M(D)$ of the boost converter

Figure 4.8 below represents a plot of the conversion ratio, $M(D)$ of the boost converter; this ratio is:

$$\frac{V_{out}}{V_{in}} = \frac{1}{D'}$$

From the Equation 25: $D' = 1 - D$.

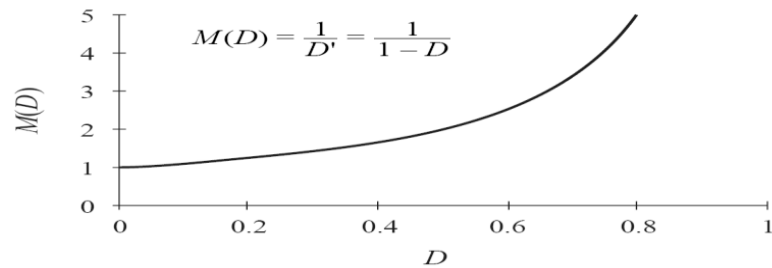


Figure 4.8: Conversion ratio $M(D)$ of the boost converter
(Robert & Maksimovic, 2001)

At $D=0$, the conversion, D' will be equal to 1, which means that the output voltage is equal to the input voltage. As the duty cycle time increases, the function gets larger. In fact, when D approaches unity, and $D'=0$, the output voltage tends to infinity in the ideal converter. However, in a real converter the output voltage will not tend to infinity, but be limited to a maximum output voltage because of losses; these losses will not be considered in the model.

Using the boost converter conversion ratio $M(D)$, the duty cycle is determined using Equation 26.

$$M(D) = \frac{V_{out}}{V_{in}} = \frac{1}{D'} = \frac{1}{1-D} \quad (26)$$

Using Equation 27 :

$$D = 1 - \frac{V_{in}}{V_{out}} \quad (27)$$

the duty cycle values specified in the design are:

$$D = 1 - \frac{492}{750} = 0.344 ; D = 1 - \frac{493}{750} = 0.342 ; D = 1 - \frac{495}{750} = 0.344 ; D = 1 - \frac{492}{750} = 0.344;$$

$$D = 1 - \frac{497}{750} = 0.337$$

4.3.4 Determination of current DC component of the inductor current

To determine the DC component of the inductor current, a balance charge was applied to the capacitor. From the capacitor waveform and the average capacitor current, the DC component can be found. As part of the balance charge, the average capacitor current must be in steady state (Robert & Maksimovic, 2001).

From Figure 4.9 below, the capacitor balance charge is:

$$\int_0^{T_s} i_C(t) dt = (-V_{out}R) DT_s + (I - VR) D'T_s \quad (28)$$

Collecting like terms and equalling to zero:

$$-V_{out}/R (D + D') + I D' = 0 \quad (29)$$

Solve for I :

$$I = V_{out}/(D'R) \quad (30)$$

Expressing V in terms of V_{in} ; where V is variable equivalent to V_{in}/D' :

$$I = \frac{V_{in}}{D'^2 R} \quad (31)$$

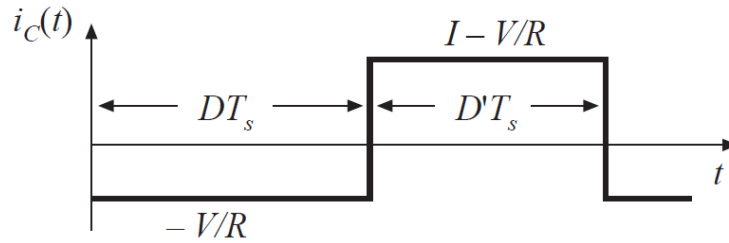


Figure 4.9: Capacitor current waveform

(Robert & Maksimovic, 2001)

4.3.5 Determination of inductor value based on its ripple current

The ripple current relates to the inductor current waveform and its the slope is shown in Figure 4.10. So Δi_L can be found by taking the slope during the first interval and multiplying it by the DT , which will give the peak-to-peak ripple.

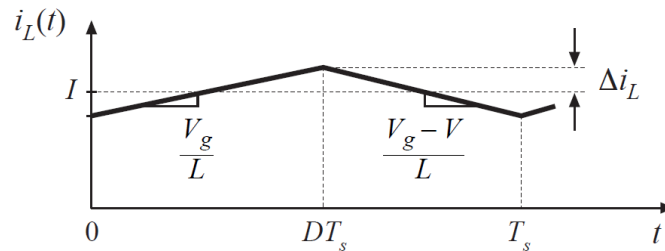


Figure 4.10: Inductor current ripple

(Robert & Maksimovic, 2001)

Inductor current slope during subinterval 1:

The source voltage is applied across the inductor and the rate of rise of inductor current is dependent on the source voltage V_{in} and inductance L as seen in Figure 4.10, If the source voltage remains constant, the rate of rise of inductor current is positive and remains fixed as long as the inductor remains unsaturated. This is indicated in Equation 32.

$$\frac{di_L(t)}{dt} = \frac{v_L(t)}{L} = \frac{V_{in}}{L} \quad (32)$$

Inductor current slope during subinterval 2:

The voltage across the inductor when the switch is open, is depicted in Figure 4.4: when the switch is kept **off** for a time interval equal to $(1 - D)T = D'T_s$, then:

$$\frac{di_L(t)}{dt} = \frac{v_L(t)}{L} = V_{in} - \frac{V_{out}}{L} \quad (33)$$

Change in inductor current during subinterval 1 is (slope) (length of subinterval):

$$2\Delta i_L = \frac{V_{in}}{L} * DT_s$$

Solve for peak ripple:

$$\Delta i_L = \frac{V_{in}}{2L} * DT_s \quad (34)$$

This Equation 34 can be used to select the inductor to any given ripple, as well as the peak current of the inductor

- The inductance L is chosen such that the desired ripple magnitude is obtained using Equation 35

$$L = \frac{V_{in}}{2\Delta i_L} * DT_s \quad (35)$$

Δi_L is set to be equal to 1% of i_L ;

$$\Delta i_L = 1 * \frac{222.2}{100} = 2.2A$$

The time sample is chosen to be $T_s = \frac{1}{5000}$ s

$$L = \frac{492 * 0.34 * \frac{1}{5000}}{2 * 2.2} = 0.0076 H$$

4.3.6 Determination of capacitor ripple voltage

For the capacitor, the net change in capacitor voltage over a cycle is zero when it is periodic. When the switch is closed, the output voltage is sustained by the capacitor. During this period, the capacitor discharges part of its stored energy and it re-acquires this energy when the switch is open. When the switch is open, part of the inductor current charges the capacitor since the inductor current usually remains larger than the current through the load resistor.

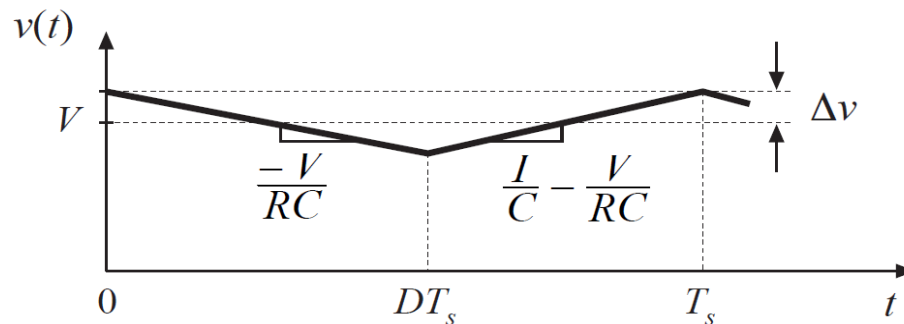


Figure 4.11: Capacitor voltage ripple

(Robert & Maksimovic, 2001)

The slope of the capacitor current from the waveform is shown in Figure 4.11 from which the voltage ripple can be determined. Considering the first interval of the capacitor current in Figure 4.11, the load current will discharge the capacitor and the capacitor voltage will decrease with a slope of $-V/RC$. Thus, knowing the slope and the interval, ΔV one can solve and find the value that will make the output of the ripple voltage sufficiently small to comply with the specifications.

Capacitor voltage slope during subinterval 1:

$$\frac{dv_C(t)}{dt} = \frac{i_C(t)}{C} = -\frac{V}{RC} \quad (36)$$

Capacitor voltage slope during subinterval 2:

$$\frac{dv_C(t)}{dt} = \frac{i_C(t)}{C} = IC - \frac{V}{RC} \quad (37)$$

Change in capacitor voltage during subinterval 1 is: (slope) x (length of subinterval):

$$- 2\Delta v = -\frac{V}{RC} * DT_s$$

Solve for peak ripple:

$$\Delta v = \frac{V}{2RC} * DT_s \quad (38)$$

The capacitance C is chosen such that the desired voltage ripple magnitude is obtained using Equation 38.

$$\Delta v \text{ is set to equal to 1\% of } V, \quad \text{so } \Delta v = 1 * \frac{750}{100} = 7.5V$$

$$\text{The time sample is chosen to be } T_s = \frac{1}{5000} \text{ s}$$

therefore:

$$C = \frac{750 * 0.34 * \frac{1}{5000}}{2 * 7.5 * 5.12} = 0.00066402F$$

4.3.7 Inverter LC- filter design

The design of the output LC-filter is necessary to reduce the inverter output harmonics. This delivers clean power to the load. The inductor ripple current is influenced by the size of the inductor and switching frequency. The value of the inductance of the output filter inductor is given by Equation 39:

$$L_f = \frac{V_d}{4f_s \Delta i} \quad (39)$$

where: V_d is the dc bus voltage,

Δi is the inductor ripple current

f_s is the inverter switching frequency

The output filter capacitor size is determined by the allowable output ripple voltage, ΔV_o and can be calculated from:

$$C_f = \frac{\Delta i}{8f_s \Delta V_o} \quad (40)$$

L_f can be obtained if the dc input voltage is limited to 750 volt, the switching frequency is limited to 5 KHz, and the maximum inductor ripple current is limited to 20% of the maximum peak-to-peak output current. In order to obtain a sinusoidal load voltage with a small THD, the maximum

ripple voltage is limited to 1% of the maximum peak-to-peak output voltage, after which C_f can be obtained.

4.4 Control algorithms for an inverter output voltage

4.4.1 Inverter and linear model

A model of a single-phase inverter is presented in Figure 4.12, and is made up of an LC filter and a control circuit. Considering the filter, in the model some assumptions have been made, such as the equivalent series resistance (ESR) of the filter capacitor is ignored due to the high switching frequency, and the inductance resistance is taken into consideration.

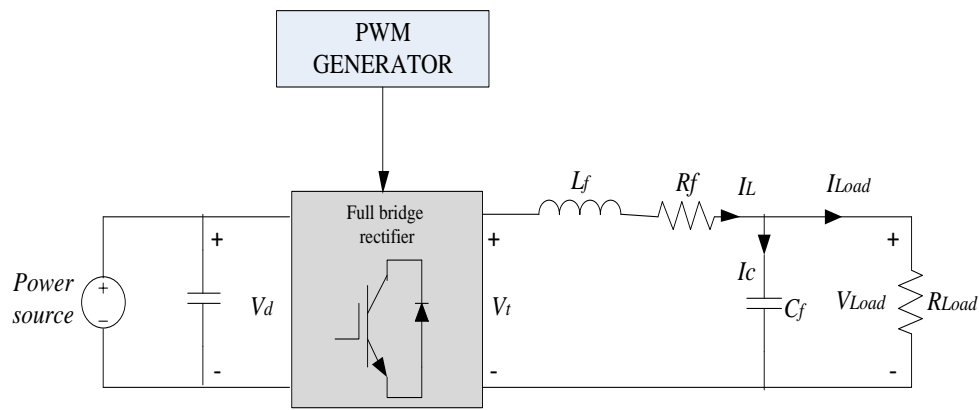


Figure 4.12: A single-phase full- bridge voltage source diagram

The differential equations of the linear model of LC-filter and R-load is derived from the inverter in Figure 4.12 above:

$$V_t = V_l + R_f i_l + V_{load} \quad (41)$$

$$V_t(s) - R_f i_l(s) - V_{load}(s) = L_f i_l(s) \quad (42)$$

$$i_l(s) = \frac{V_t(s) - R_f i_l(s) - V_{load}(s)}{L_f s} \quad (43)$$

$$V_{load}(s) = \frac{1}{C_f s} i_c(s) \quad (44)$$

$$i_{load}(s) = \frac{V_{load}(s)}{R_l} \quad (45)$$

$$i_c(s) = i_l(s) - i_{load}(s) \quad (46)$$

The open-loop of the model is presented in Figure 4.13 below.

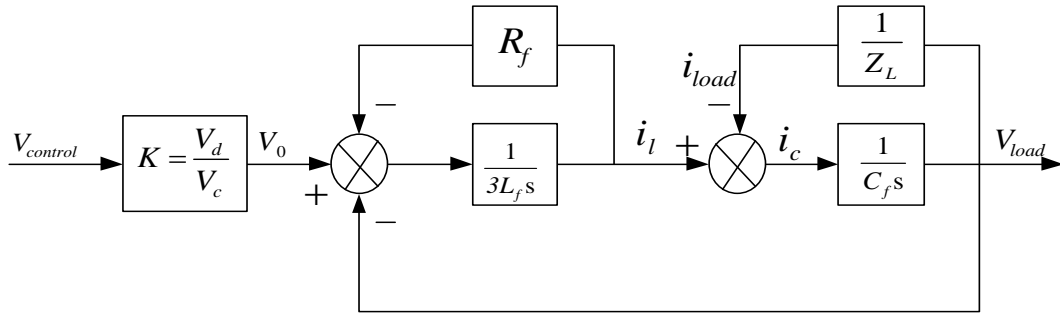


Figure 4.13: Open loop PWM inverter plus output filter and linear load model

K denotes the modulation index of the PWM of the inverter.

V_{dc} denotes the DC power supply of the inverter.

V_c represents the peak voltage of triangular carrier wave.

Using superposition the closed-loop PWM inverter is presented in Figure 4.14 below, in which the current and the voltage are controlled through two loops in the control circuit of PWM. The first loop presents a fast internal current loop of filter capacitor or filter inductor; it reduces the THD of the output voltage. The second loop denotes the lower external voltage loop and provides the regulated output voltage.

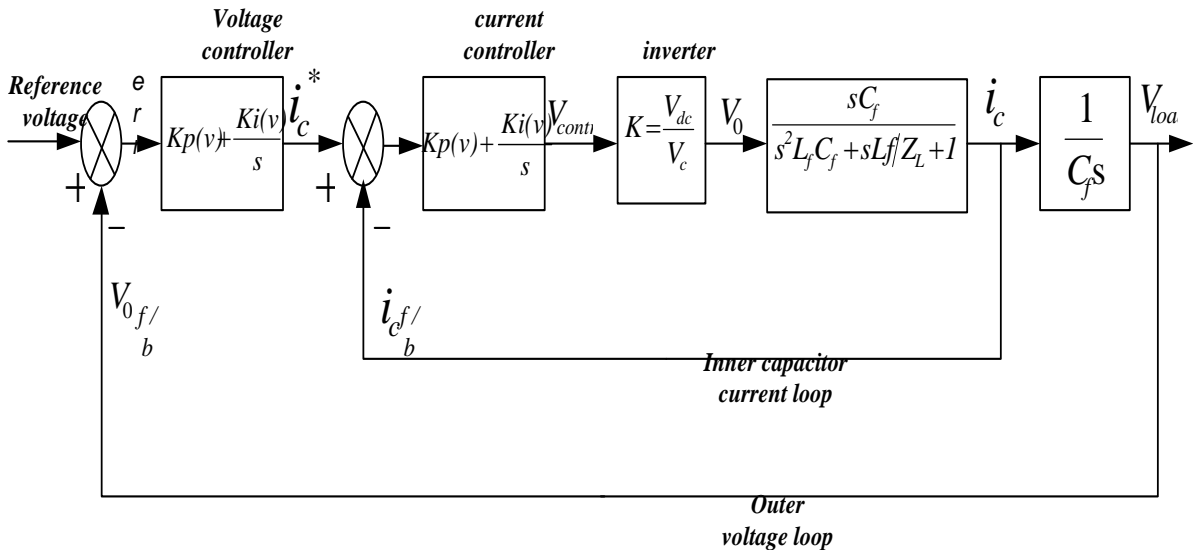


Figure 4.14: Closed- loop PWM inverter current voltage controller

The error voltage signal from the comparison between the output voltage and the desired voltage is fed to the PI controller. The output from the controller becomes the current set point and this is compared to the current measured from the filter capacitor. The error current signal is passed through another PI compensator to form the modulating signal. The modulating signal is compared with a triangular carrier signal to generate the required PWM signal. The PI parameters are obtained through automatic tuning in SIMULINK.

4.4.2 Inverter control using a PI controller

This control method is based on the V_{rms} PI controller to regulate the inverter voltage. The controller used, is a combination of the discrete proportional gain k_p and an integral gain k_i , with fixed sample time. The output signal is the sum of the proportional gain, k_p and the integrator gain, k_i . The total signal and k_i and are limited by upper and lower values. The discrete virtual PLL block has no input signals. It simulates the operation of the actual PLL by using specified grid parameters as seen in Figure 4.16. When the microgrid operates in autonomous mode it is no longer following the grid frequency. The controller ensures voltage stability under load change in the microgrid, or an input voltage change. This controlling method does not require any transformation frame to control the sign from the inverter, as was seen in the droop control method.

The method is as follows:

Figure 4.15 below illustrates a part of the controller. The phase-to-ground V_{rms} value of the operating voltage of each phase of the inverter terminal is calculated. To get the result per unit, the calculated V_{rms} is multiplied by the inverse of the nominal V_{rms} . This result is compared to a reference constant of 1. The error from the previous comparison is passed through the PI controller. The corrected magnitude is multiplied with a three-phase sinusoidal wave and then connected to the PWM block; this has been applied in Section 5.4 below.

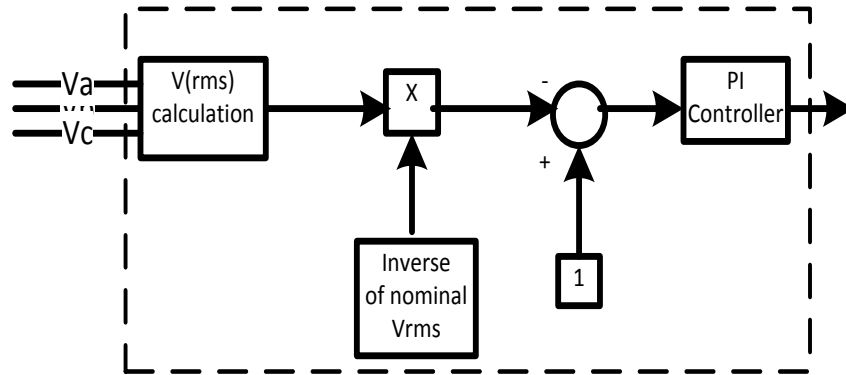


Figure 4.15: V_{rms} + PI controller method

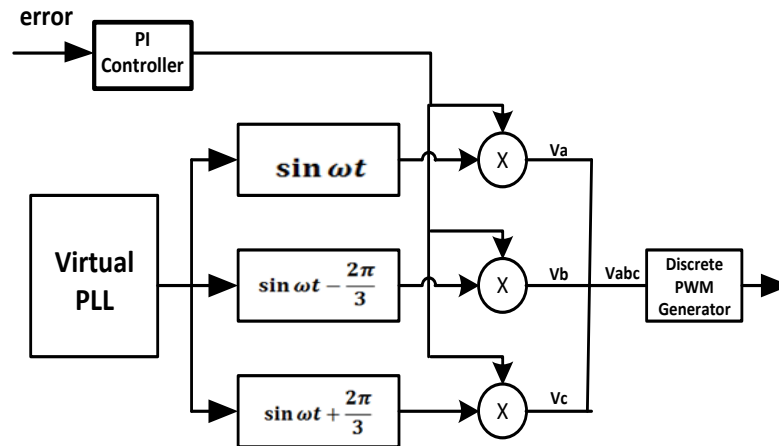


Figure 4.16: Generation of virtual grid voltages

4.4.3 Inverter control using the dq0 transformation + PI controller

The control method for regulating the inverter output voltage relies on the dq0 transformation and the PI controller. The three-phase signal voltage at the inverter terminal is fed to the transformation block $abc \rightarrow dq0$. (for details refer to Section 3.4.1.). This dq0 frame lessens the three-phase AC quantities V_a , V_b , V_c into two DC quantities V_d , V_q and in balanced systems, the 0-component is equal to zero. The DC quantities facilitate easier filtering and it is compared to a constant reference of value 1. The error sign from the comparator is passed through the PI controller block as seen in Figure 4.17 below. Then the controlled signal is converted back to the inverse of the transformation block, $dq0 \rightarrow abc$. The virtual PLL block is connected to both transformation blocks in order to synchronize and maintain the frequency operation at 50 Hz.

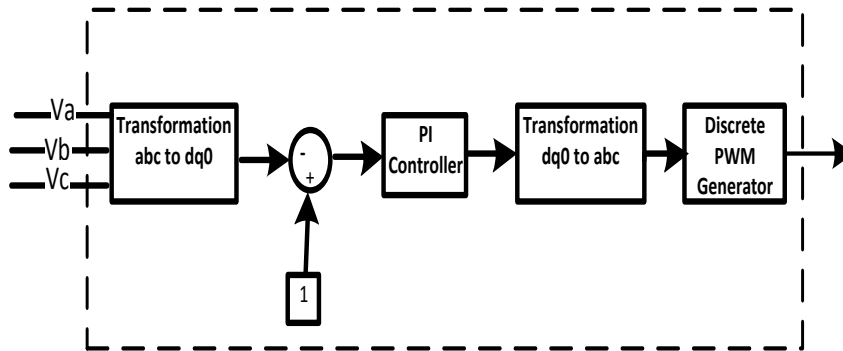


Figure 4.17: dq0 transformation + PI controller

4.4.4 Inverter controls using droop methods

As mentioned above, the control implemented in the microgrid in autonomous mode is different from the grid-connected mode. In autonomous mode, it requires an internal controller since, the voltage and the frequency are not dictated by the grid. This internal control system must be able to accurately regulate the voltage and the frequency of the local loads in order to avoid unstable operation of the microgrid. In general, the technique used is based on the power generator, where the voltage and frequency are determined by the voltage and frequency droop control methods. Figure 4.18 below depicts the control of a microgrid autonomous mode, which is analogous to the control used in conventional power systems. The instantaneous active and reactive power injected by the inverter, are calculated from the measured signals, V_{abc} and I_{abc} , after the filter in the two main blocks. At that stage the voltage is controlled by the reactive power-voltage droop controller and the frequency is regulated by the active power-frequency droop control. The PI controller is used to reduce the error between the measured voltage and the required voltage value, by adjusting the reference voltage with the help of the DQ frame. The output is the required voltage magnitude that is to be applied to the inverter gates (Lasseter & Piagi, 2006).

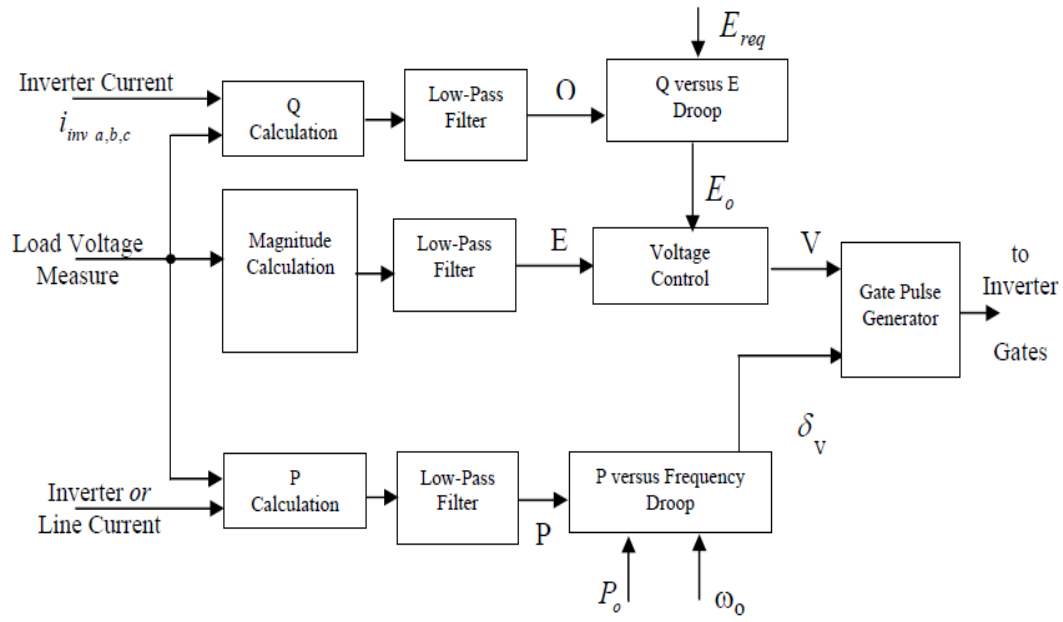


Figure 4.18: Control technique
(Lasseter & Piagi, 2006)

4.4.4.1 Active and reactive power calculations

Figure 4.19 below represents a sub-block of Figure 4.18 above, and shows the computations necessary to find the instantaneous active and reactive powers from the measurable values of the line-to-line voltage and current. Since the power is calculated directly from the available time-domain quantities obtained via the sensing equipment, the additional stage of converting from signals to rotating frame components will not be needed. Also, the quantities are measured without converting the phase-to-phase voltage from phase-to-neutral voltage

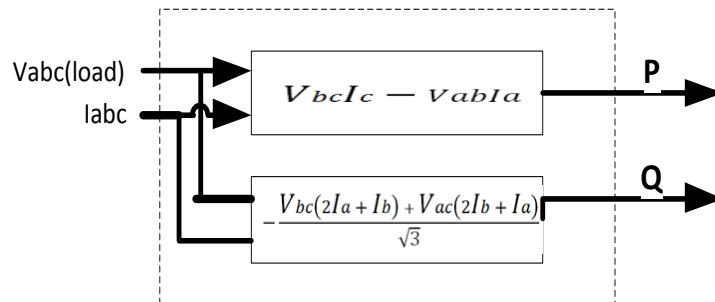


Figure 4.19: P and Q calculation

Equation 47 below determines P from the three-phase voltage and current:

$$P = V_{bc}I_c - V_{ab}I_a \quad (47)$$

Equation 48 below determines Q from the three-phase voltage and current:

$$Q = -\frac{V_{bc}(2I_a + I_b) + V_{ac}(2I_b + I_a)}{\sqrt{3}} \quad (48)$$

4.4.4.2 Voltage control

In order to control the voltage, it is necessary to use the actual voltage magnitude on the load side of the inverter. Thus, the inverter voltage magnitude calculation is submitted to a transformation frame by projecting the rotation phase voltages to a fixed reference frame with two axes which represent the quadrature reference frame.

$$V_{ds}(t) = \frac{V_c(t) - V_b(t)}{\sqrt{3}} \quad (49)$$

$$V_{qs}(t) = \frac{2}{3} \left(V_a(t) - \frac{1}{2}V_b(t) - \frac{1}{2}V_c(t) \right) \quad (50)$$

The components $V_{ds}(t)$ and $V_{qs}(t)$ are then converted from cartesian to polar by a change of coordinates to yield the required magnitude and phase.

$$V = \sqrt{V_q^2 + V_d^2} \quad (51)$$

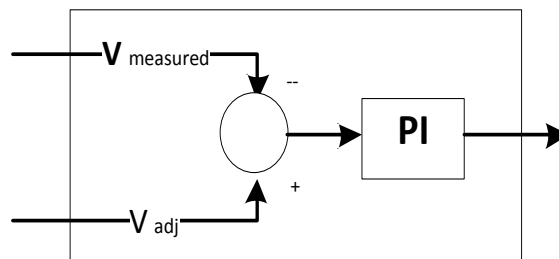


Figure 4.20: Voltage control

Figure 4.20 above shows the essentials of the voltage control, the error between the two inputs, the measured voltage magnitude calculated at the load side, and the adjusted voltage from the

Q-voltage droop. This adjusted voltage passes through the PI controller in order to adjust the voltage to the desired magnitude at the inverter.

4.4.4.3 Reactive power versus voltage droop

The Q-voltage droop method is a fundamental micro-source control system and it is employed to bring about the stable operation of inverter voltages within the microgrid. This method regulates the output voltage at the terminal of power sources. This is done in accordance with the amount of reactive power that is being absorbed or injected. Without this method, and for various technical reasons, the voltage magnitude at the inverter terminals may fluctuate. The adjusted voltage is obtained by taking the difference between the reactive power calculated, modified by mQ and the desired voltage. The output value is determined by the linear characteristic of the droop, based on the input values. Figure 4.21 below represents the block that is used for adjusting a reference voltage value that is directed from outside.

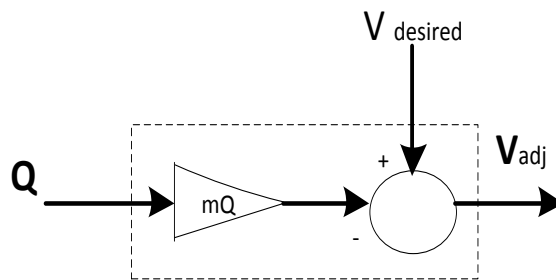


Figure 4.21: Q-voltage droop

The slope of the droop characteristics is given by mQ

This droop method is also suitable for a microgrid in which multiple inverters are operating in parallel, with no communication amongst the inverters. The unit must be connected in such a way that the reactive power versus voltage droop produces a new voltage value that must have a set point. In order to avoid the variation in voltage magnitudes of units with its associated problems, this set point must be the same throughout the entire system.

The unit will not inject or absorb reactive power when the nominal voltage is equal to the requested voltage. However, when the operating voltage is less than the nominal voltage the unit is injecting reactive power. When the operating voltage is higher than the requested voltage the unit will absorb the reactive power. It can also be observed that the regulation of the voltage requires variation in the reactive power supply, since the voltage and the reactive power have a linear relationship (Robert & Paolo, 2006)

4.4.4.4 Real power versus frequency droop

During the autonomous mode the real power versus frequency has the advantage of allowing the output of units to be equal to the load demand. It has the ability to appropriately share real power amount units according to their rated power.

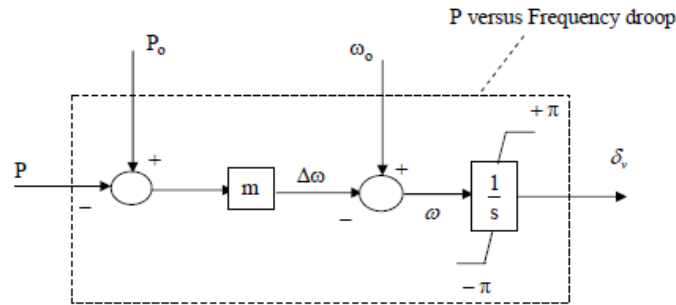


Figure 4.22: Block diagram of the active power droop
(Lasseter & Piagi, 2006)

In Figure 4.22 above it can be seen that the droop control method requires three inputs: these are the nominal frequency operation of the system, the desired power injected and the power measured which result in a modified angle for the inverter. The measured angle of the voltage at the regulator is ignored due to the fact that the measured power injected by the micro-source already contains this information. This output of the block represents the desired angle needed for the voltage at the inverter terminal.

4.5 Energy management system control algorithm

The energy management system (EMS) refers to the method of monitoring and optimizing the operation of the system. In practical applications SCADA/EMS is employed for monitoring and control functions. However the EMS is normally used for controlling energy generation and scheduling a programme for an ensemble of power network applications. EMS can also be used to control the electrical loads in a microgrid. In order to improve the efficiency of the design control, an EMS called logic control switch (LCS) is added to the system grid to further stabilize voltage control. This has been applied in Section 5.7.

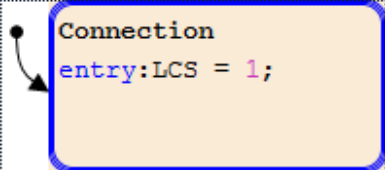
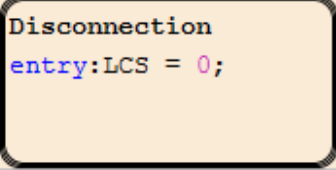
STATES	TRANSITIONS (Condition / Action / Destination State)	
	if	else-if(1)
	[u>0.98&&u<1.8]	[u<0.98]
	\$SELF	Wait
	[u<0.98&&after(0.01,sec)]	[u>0.99]
	Disconnection	Connection
	[u<=0.98]	[x > 0] {x = x + 1;}
	Wait2	\$NEXT
	[u>0.99&&after(0.01,sec)]	[u<=0.97]
	Connection	Disconnection

Figure 4.23: EMS transition state

EMS is implemented in MATLAB by developing an algorithm based on a flow chart as shown in Figure 4.23 above and Figure 4.24 below. This flow chart is developed to maintain further stability by automatically connecting and disconnecting non-sensitive loads. The flow chart transits from state-to-state according to the available input power in order to connect and disconnect the loads as seen in Table 4.5 below.

The EMS controls a breaker switch by connecting and disconnecting non-sensitive heavy load power according to the availability of the input battery voltage. The LCS monitors the system through the V_d component by determining whether or not the non-sensitive load will be connected to the system. When the V_d component from the abc to dq0 transformation and the logic control switch is at normal operation, the phase-to-ground V_{rms} is 230 V and $V_d = 1$. The logic control of the switch is based on the value obtained from V_d component. When V_d is less than 0.98 the switch is **off** and when V_d is greater or equal to 0.99 the switch is **on**.

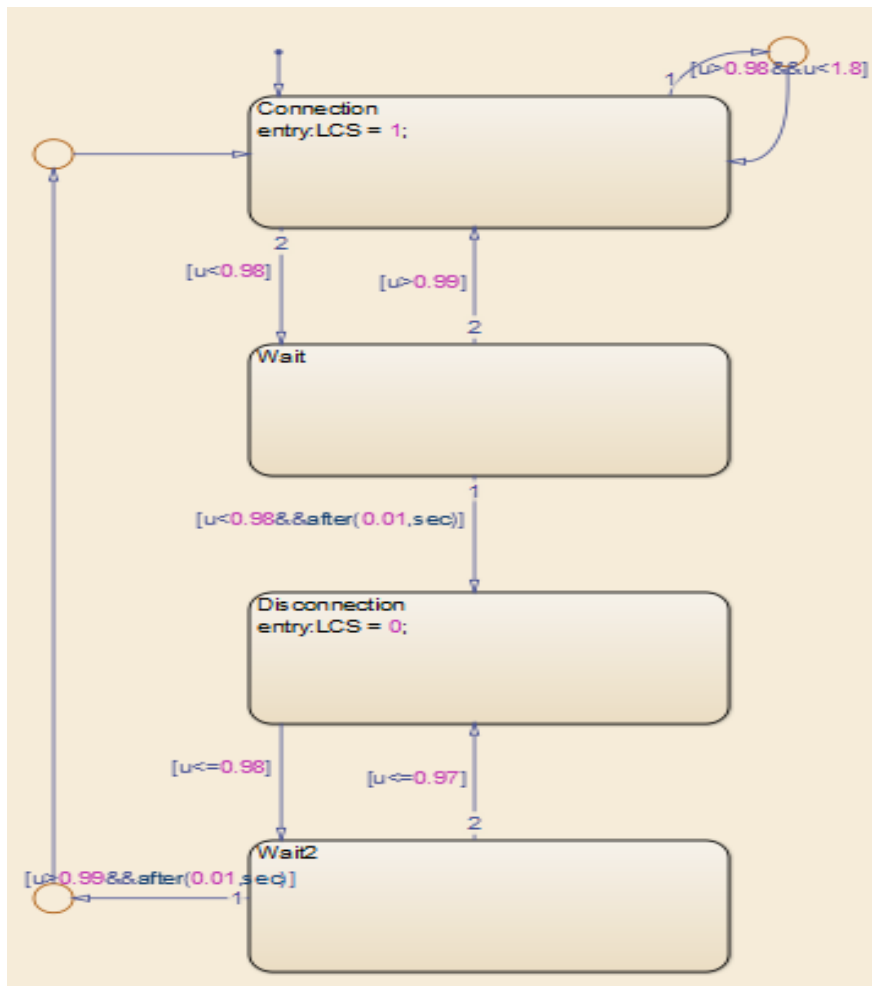


Figure 4.24: EMS flow chart

Table 4.5: State transition matrix

		[u > 0.98 & u < 1.8]	[u < 0.98]	[u < 0.98 & after(0.01, sec)]	[u > 0.99]	[u <= 0.98]	[u > 0.99 & after(0.01, sec)]	[u <= 0.97]
1	Connection entry: LCS = 1;							
		Connection	Wait					
2	Wait							
			Disconnection	Connection				
3	Disconnection entry: LCS = 0;							
						Wait2		
4	Wait2							
							Connection	Disconnection

4.6 Conclusion

The entire system, along with the developed controllers, has been modelled and completed in a MATLAB/SIMULINK environment. The results of these models are discussed in the subsequent chapter.

Chapter 5 : SIMULATION RESULTS AND DISCUSSION

5.1 Introduction

In this chapter, the modelling and simulation results are discussed. The designed autonomous microgrid system is modelled and simulated using SIMULINK software to determine the best controller at the terminal of the inverter.

The remainder of this chapter is organised as follows. In Section 5.2, the simulation results of a PV array system model are discussed. In Section 5.3, the simulation results of inverter output voltage, without any controller, are discussed. In Section 5.4, simulation results of inverter controls, using a PI controller, are discussed. In Section 5.5, simulation results of inverter voltage control using the dq0 transformation + PI controller simulation, are discussed. In Section 5.6, droop control simulations are discussed. In Section 5.7 simulation results of the system using an energy management system algorithm are discussed. A conclusion is drawn in Section 5.8.

5.2 Simulation of PV array model

The entire stand-alone PV system was designed in MATLAB / SIMULINK software environment. The system was built in SIMULINK by using physical electronic components such as resistors , diodes and a current source to represent the equivalent circuit of a solar cell; this is shown in Figure 5.1 and Figure 5.2. A larger number of solar cells was then grouped in series and parallel to form a PV array. The radiation is kept constant at 1000 w/m² in the simulation in this Section 5.2.

A DC-DC boost converter was added to the PV model to step up the output voltage of the PV system from 492 V_{dc} to 750 V_{dc} with a duty cycle equal to 0.34. The input voltage to the boost converter as received from the PV arrays fluctuates. Control of the duty cycle is implemented to keep the output voltage of the boost converter at 750 V_{dc} using Equation 52. The duty cycle varies as the input voltage changes; also it maintains a constant DC-link voltage

$$D = 1 - \frac{V_{in}}{750} \quad (52)$$

The output of the DC-DC boost converter is fed to a three-phase IGBT inverter and set with a modulation index of 0.867.

components. LC filters are connected at the output of the inverter terminal and are connected parallel to the loads. Also, the LC filter is mostly used for voltage control in microgrids operating in stand-alone mode. In this study the load profile was kept constant. An entire autonomous microgrid system is represented in Figure 5.3 below.

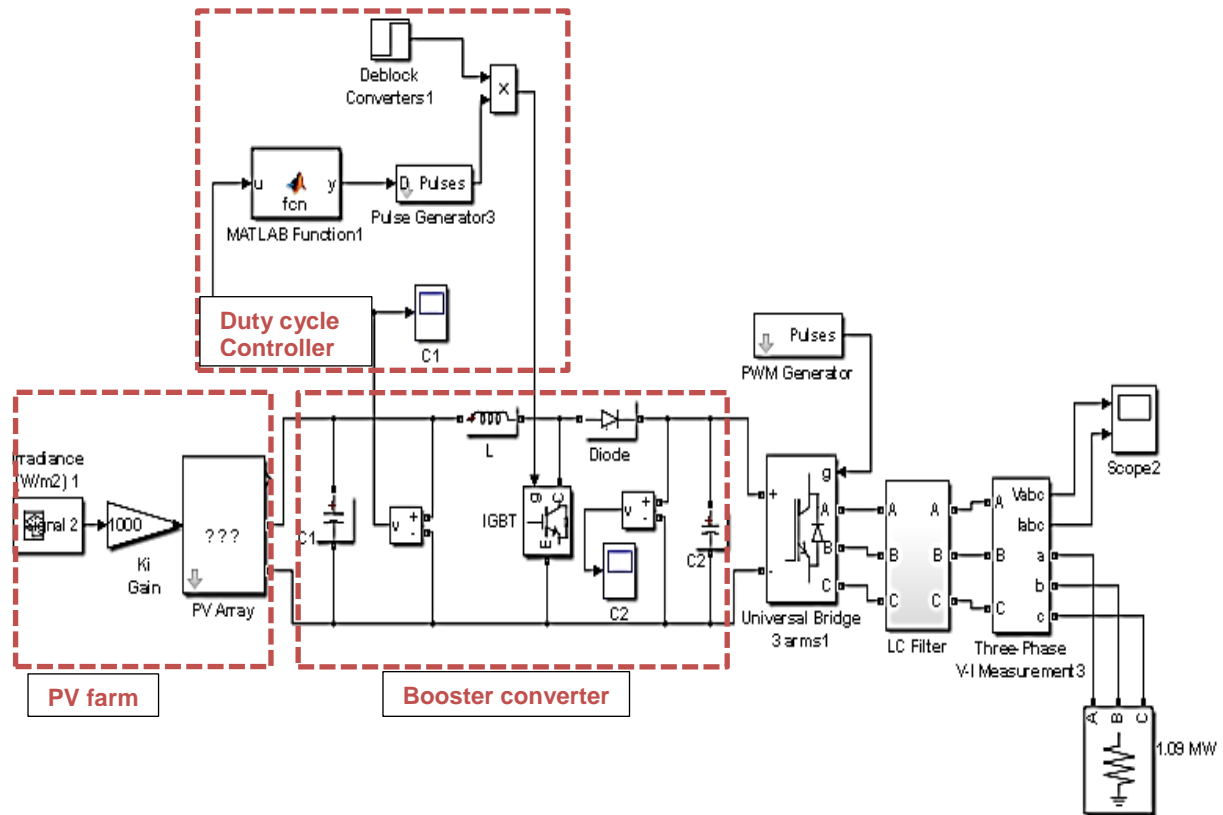


Figure 5.3: Autonomous microgrid system

5.2.1 Simulation results

To confirm whether the model design is correct, one can simulate the model in order to analyse and evaluate its performance. Two PV systems, each with a different power capacity, are considered. The first system consists of a single PV array which has a power capacity of 109.8 kW, a output voltage of 492 V_{dc} and a output current of 222.2 A. The second PV system consists of 10 parallel-connected, identical PV arrays, each identical to the single PV array in the first PV system. This second system has a total power capacity of 1.098 MW, a voltage of 492 V_{dc} , and a total current of 2222.20 A.

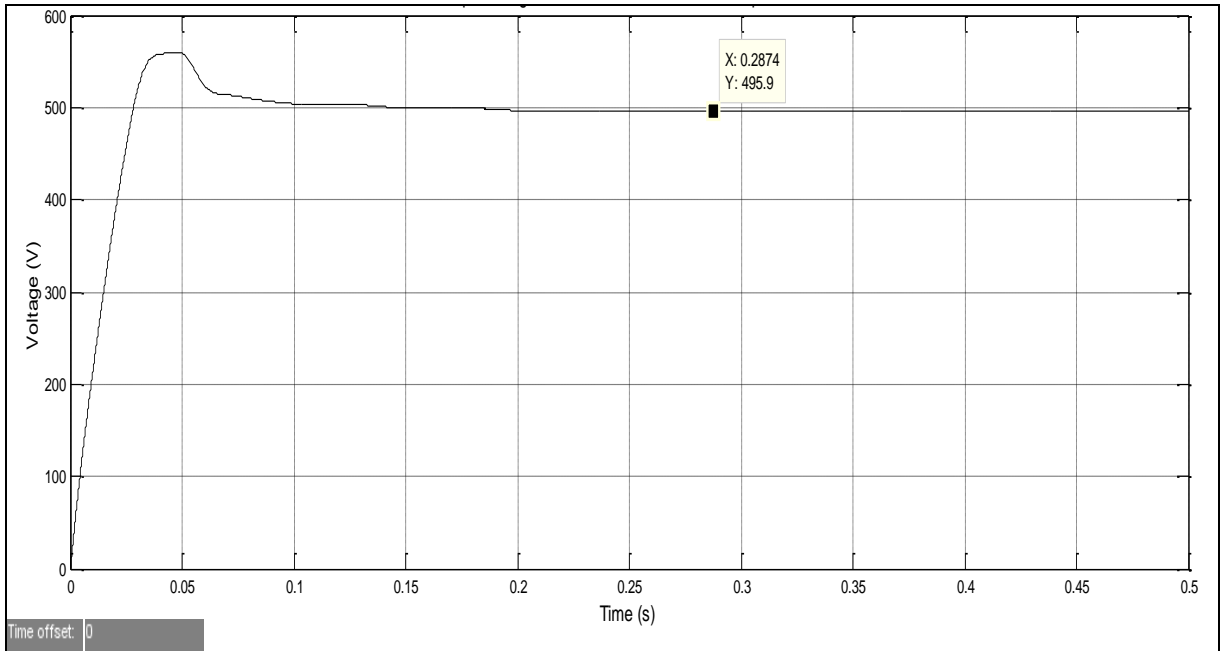


Figure 5.4: The output voltage of the 10-array PV system

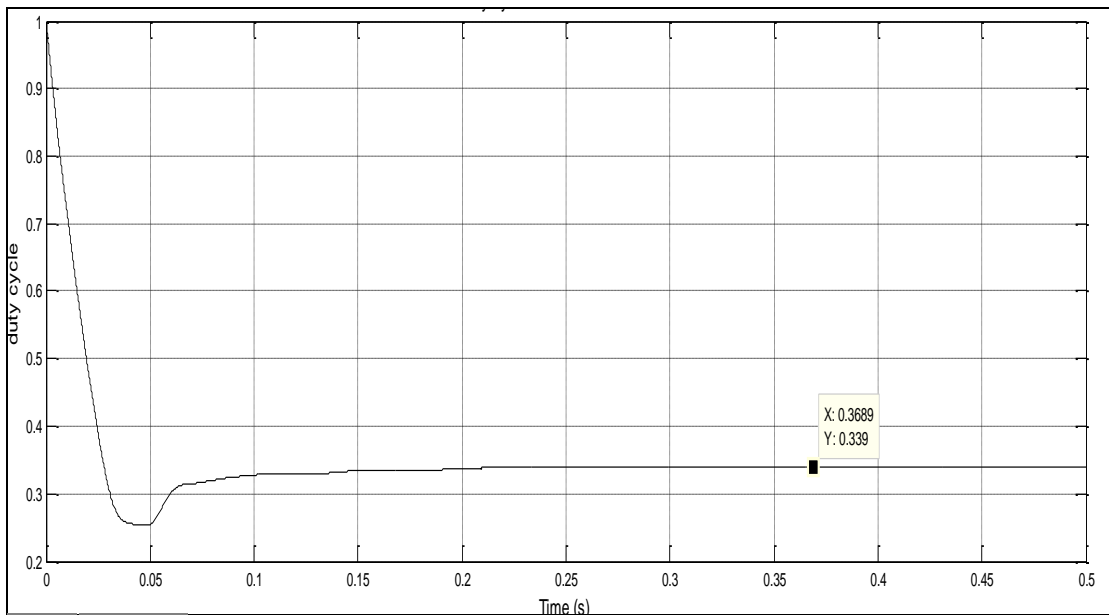


Figure 5.5: The variation of the duty cycle for the second PV system (multi-array)

Figure 5.4 above depicts the output voltage from the second PV system at a constant solar radiation of 1000 W/m^2 ; the value of the output voltage is $495 \text{ V}_{\text{dc}}$ after reaching the steady state after 200 ms. By comparison, the calculated output voltage which is $492 \text{ V}_{\text{dc}}$. The simulation result is almost the same as for the PV system output voltage, calculated in Section 4.2.2 above.

The output voltage from the second PV system (multi-array) shown in Figure 5.4, represents the input to the boost converter. This voltage is stepped up to the required output voltage of $750 \text{ V}_{\text{dc}}$

by a corresponding duty cycle of the DC-DC converter; this cycle is indicated in Figure 5.5 above. The duty cycle varies with the input voltage during the transient state and reaches the steady state at 20 ms with a corresponding duty cycle value of 0.339.

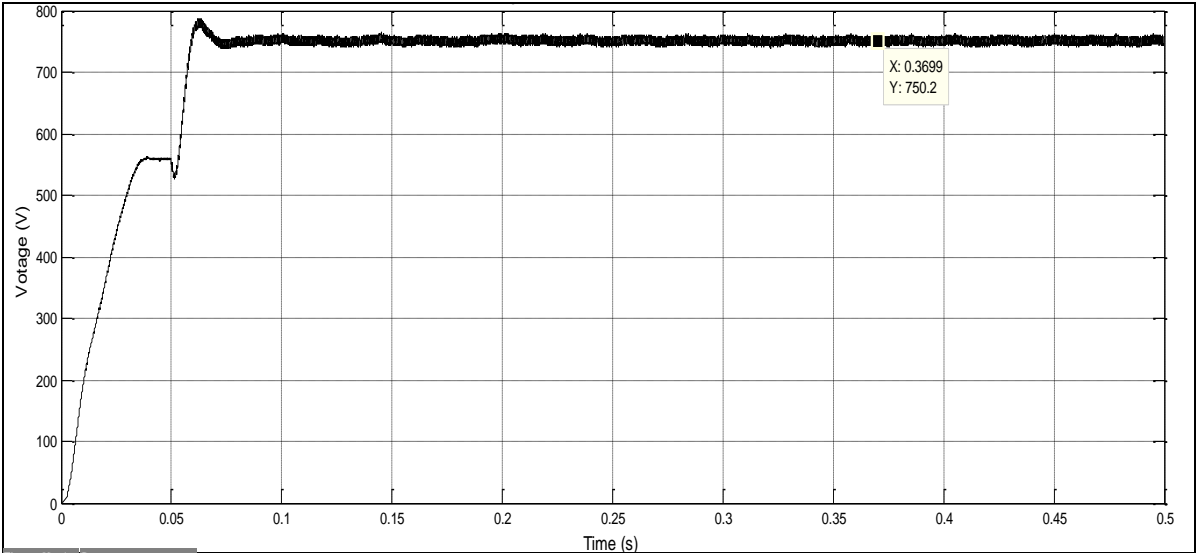


Figure 5.6: Output voltage of boost converter for the second PV system (multi-array)

Figure 5.6 above shows the output voltage of the boost converter as a function of the simulation time. The output voltage increased during the transient state and reached steady state at about 70 ms. Thereafter the output voltage stayed constant at 750 V_{dc} with very small ripples; the design allowed for a ripple with 1% variation from the steady state. The simulation result was the same as the value of the PV system output voltage, as calculated in Section 4.2.2 above. The output voltage corresponded to the expected voltage previously calculated in Section 4.2.3.

Figure 5.7 below represents the output power generated by the second PV system (multi-array), as a function of the simulation time. This power increases during the transient state and reaches a steady state at 150 ms. At the steady state the power produced is 1.098 MW. This result confirms the output power value of the PV farm calculated in Section 4.2.2 above.

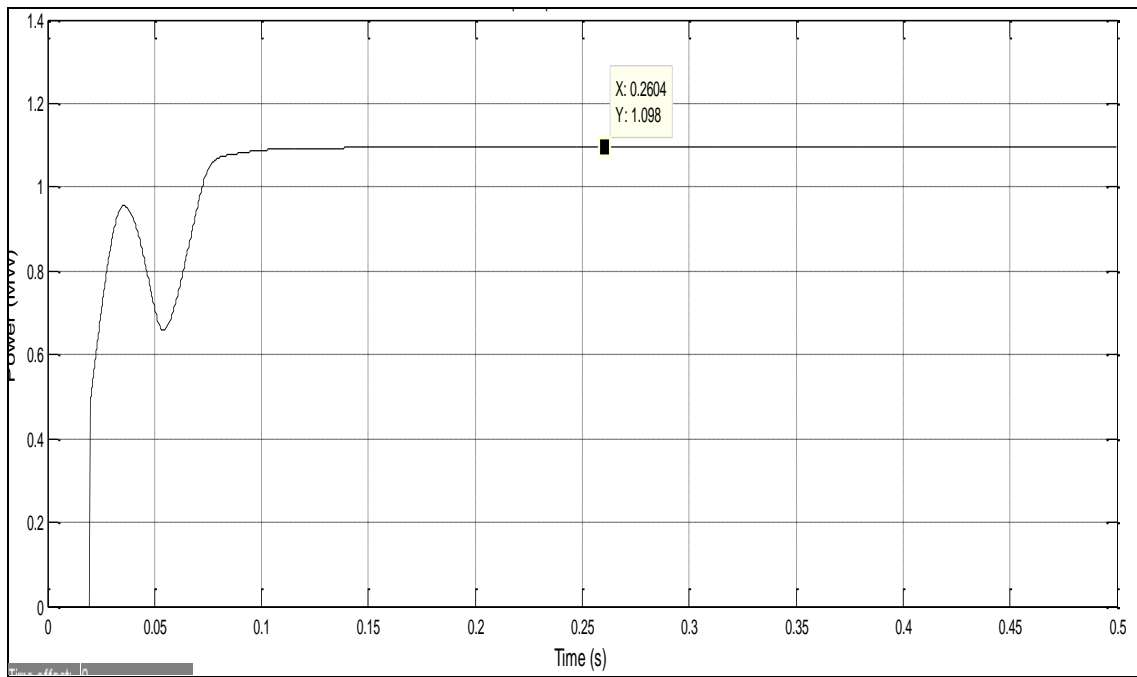


Figure 5.7: Second PV system (multi-array) input power delivery

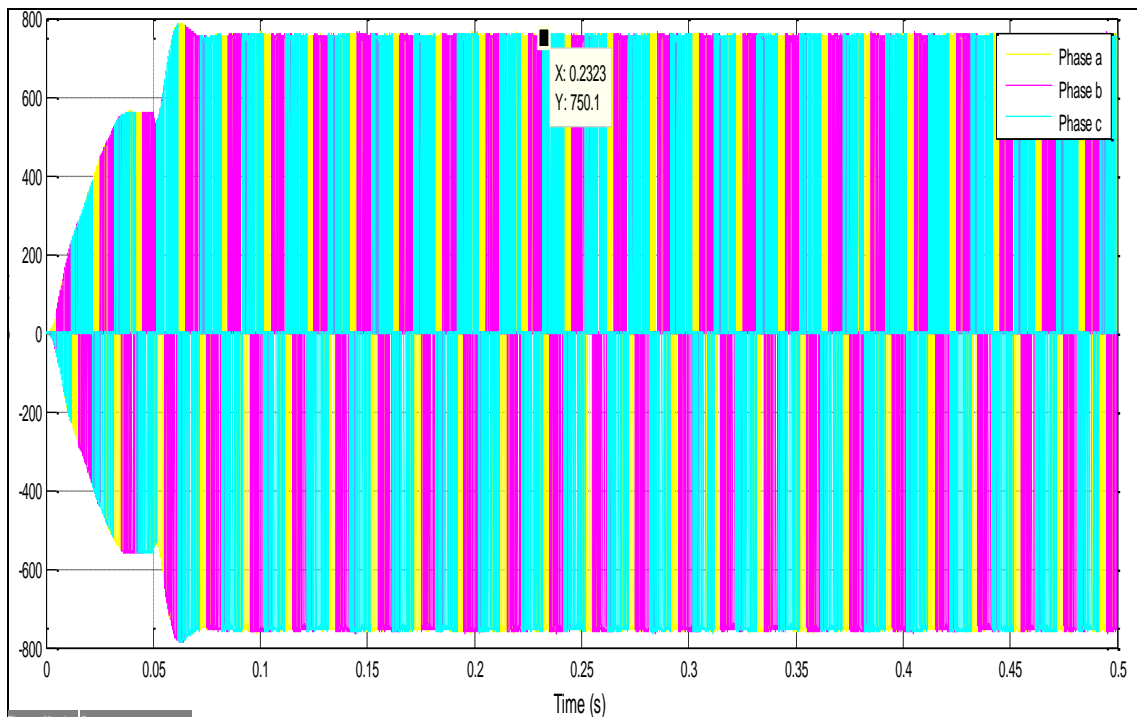


Figure 5.8: The output voltage of second PV system inverter before the filter

The AC side of the design was established by converting the DC to AC using an inverter. The inverter output voltage and current waveform are labelled respectively V_{abc} (V_a is marked as yellow, V_b is marked as pink, and V_c is marked as blue) and are depicted in the Figure 5.8 above.

The output of phase voltages at the inverter terminal in Figure 5.8 above, are measured just before the LC filter and it shows that the output voltage waveforms contained lower- and higher-order harmonic components. This harmonic content is due to the switching effect of the inverter switches. Each phase changes between 0V and +/-750V with the respective phases being out of phase to each other by 120 degrees. Figure 5.9 below presents only Va phase to illustrate the switching transition.

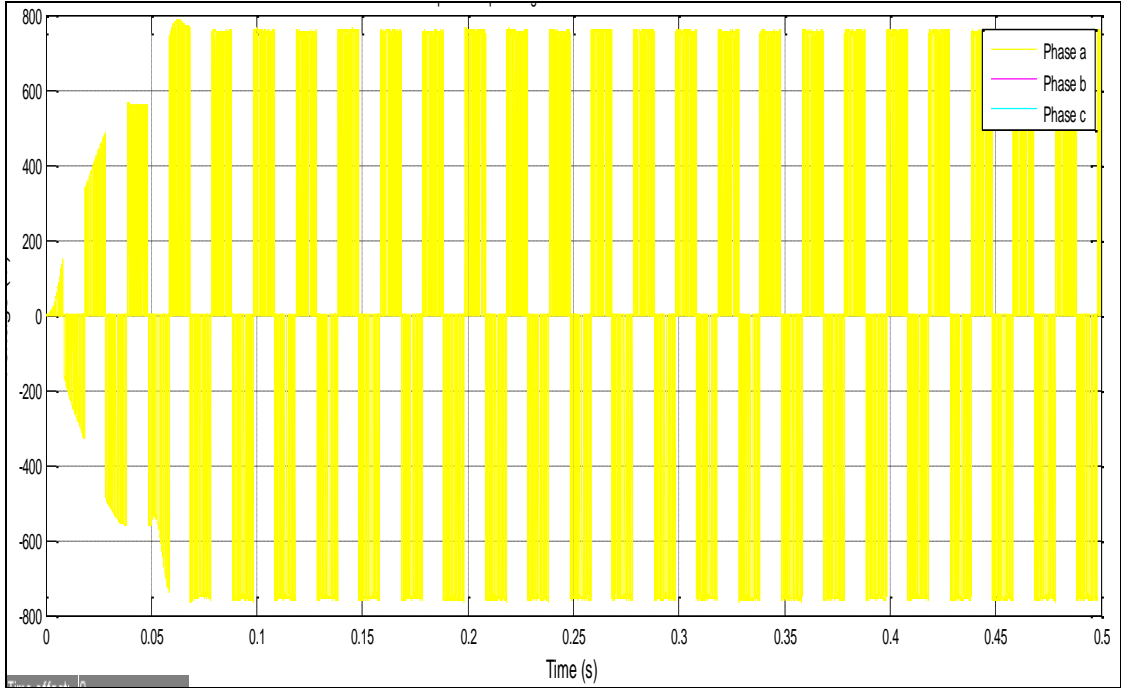


Figure 5.9: Switching of the second PV system voltage phase a

The LC filter at the output of the inverter has reduced and filtered out the presence of the higher-order harmonic components; the waveform remaining contains only the fundamental and the lower-order harmonics. The three-phase output voltage and current waveforms of the inverter terminal after the LC filter, are shown respectively in Figure 5.10 and Figure 5.11 below. These figures confirm the expected value of the output voltage regarding the amplitude modulation index, m_a and the inverter input voltage. Figure 5.10 indicates the line-to-line peak output voltage waveforms V_{ab} value as 563 VAC; the corresponding frequency is 50 Hz, and the line-to-line rms value 398 V. From Figure 5.11, the output current of the three-phase inverter is 2221 A, which is close to the calculated value of 2222. A.

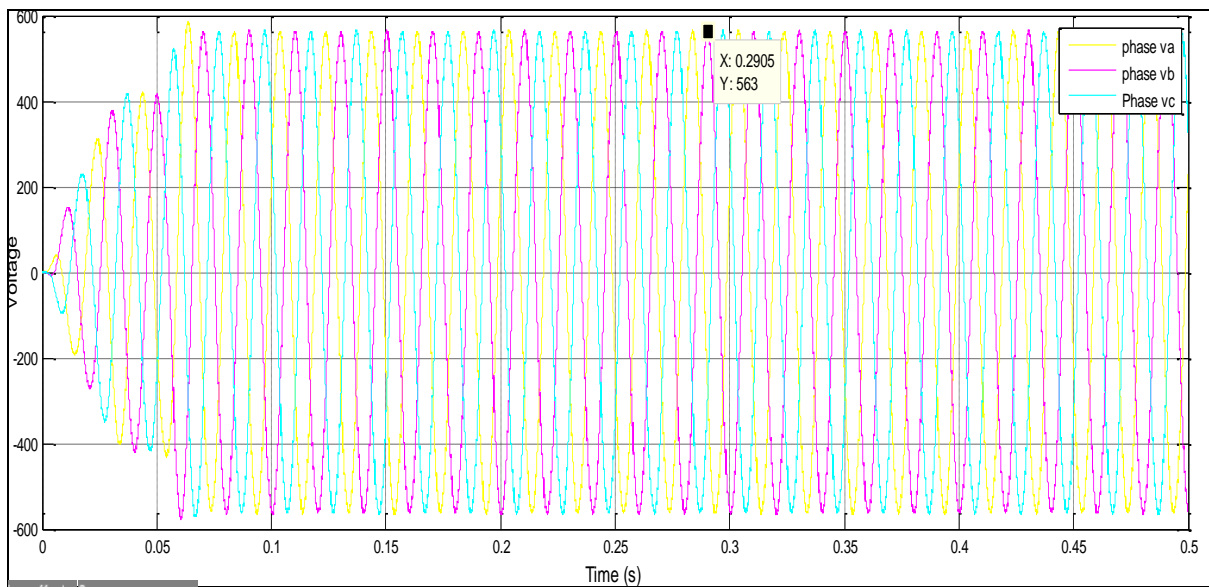


Figure 5.10: Filtered output voltage of three-phase inverter of the second PV system(multi-array)

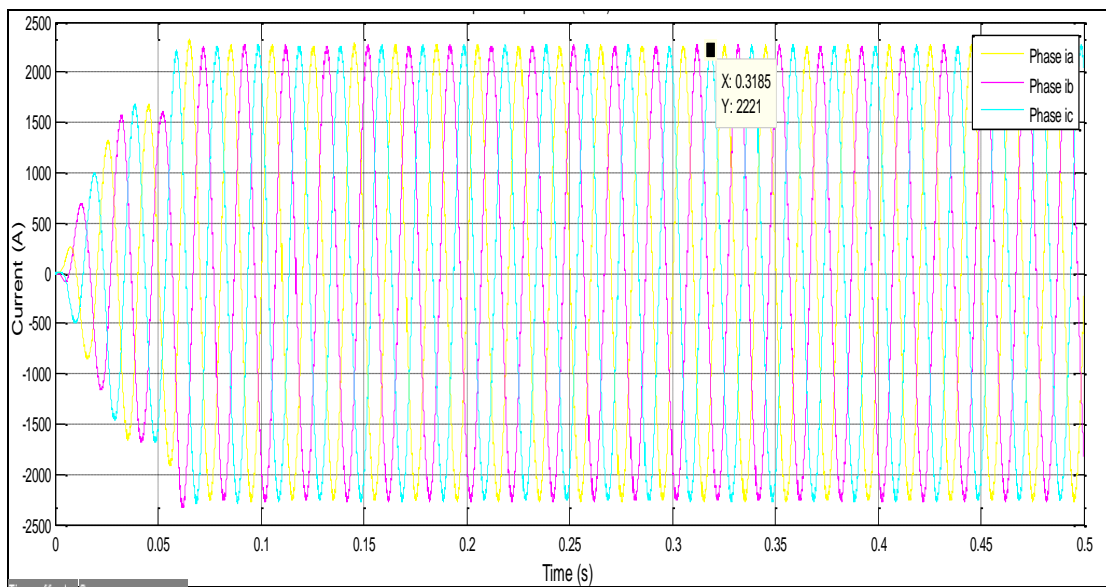


Figure 5.11: The output current after the LC filter of the second PV system(multi-array)

Figure 5.12 below depicts the power consumed by a load which is slightly lower than the input power, due mainly to switching frequency losses upon exiting the inverter, as well as inverter self-consumption which may badly influence. For the load Figure 5.13 below presents the power consumed the line-to-ground output voltage, and the line-to-ground output current.

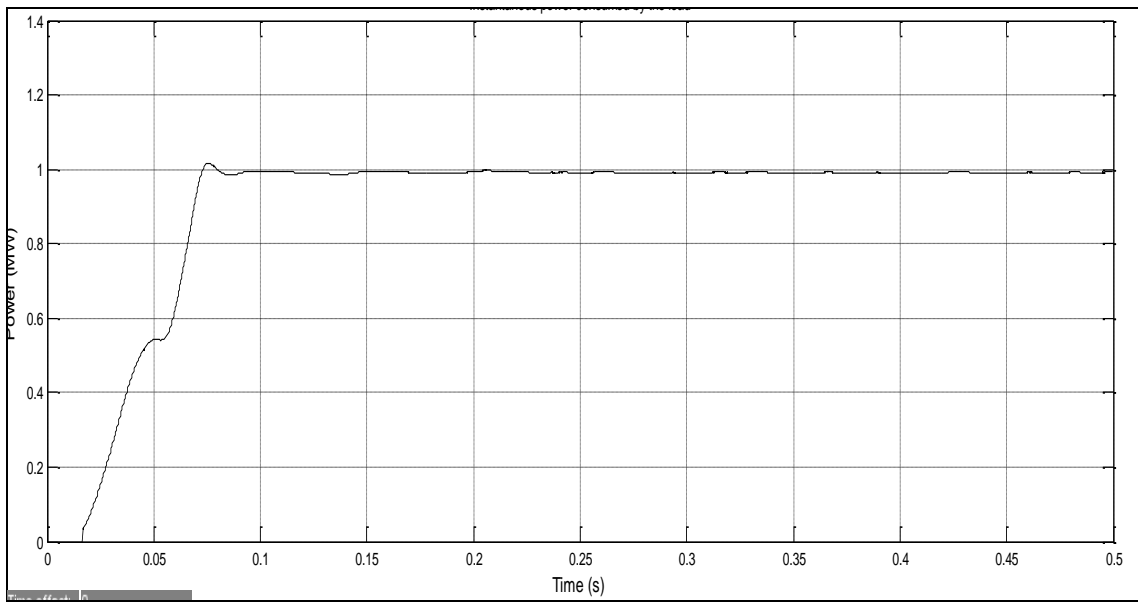


Figure 5.12: Instantaneous power delivered to the load of the second PV system(multi-array)

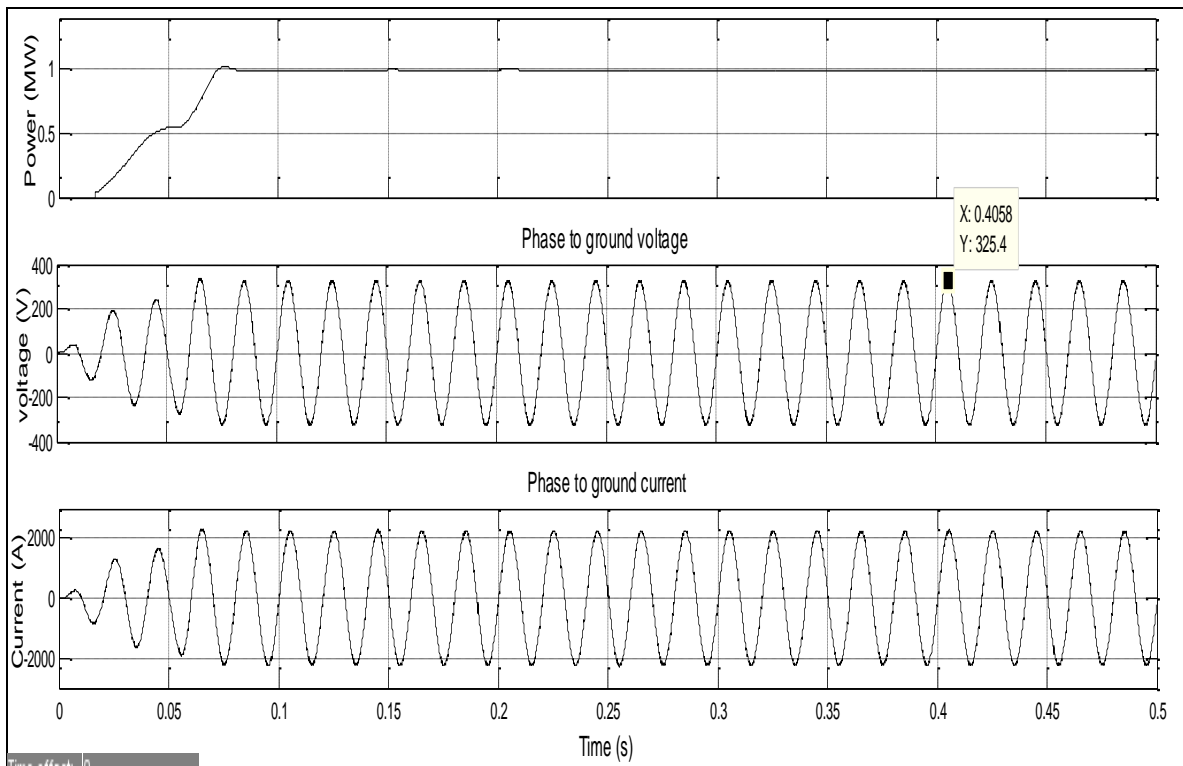


Figure 5.13: For the load: the output power, line-to-ground output voltage, and line-to-ground output current of the second PV system(multi-array)

Due to the unavailability of suitable computer resources, and also to reduce simulation time, the PV system portion of the autonomous microgrid was replaced with batteries; simulations were therefore carried out on models, using batteries instead of a PV system. The microgrid system had a permanent load (sensitive load) and a non-permanent load (non-sensitive load). The non-

sensitive load was connected for a few milliseconds at the start of a simulation, and then disconnected from the system through the entire remainder of the simulation. The size of the load and input power capacity affect the autonomous microgrid system operation; this interaction between load and power is analysed in the following sections.

5.3 Simulation result of the inverter output voltage, without a controller

The model consists of a battery, an inverter, an LC filter and loads (sensitive load power and non-sensitive load power). In this model, the modulation index, m_a is determined so as to achieve the desired operating voltage at the inverter output terminal. The sensitive load power is permanently connected to the microgrid system, while the non-sensitive load power is temporary and not initially connected to the system - see Appendix 1. The non-sensitive load is briefly connected to the microgrid system through the operation of a circuit breaker at time 200 ms, and then disconnected at 700 ms. Figure 5.14 below shows the phase-to-phase V_{rms} to be 398 V before the load was added, and as soon as the non-sensitive load power was connected to the system at 200 ms, the phase-to-phase V_{rms} dropped substantially to 350 V and decreased steadily to 325 V at 700 ms. When the non-sensitive load power was disconnected from the system at time 700 ms, the phase-to-phase V_{rms} increased toward its nominal voltage.

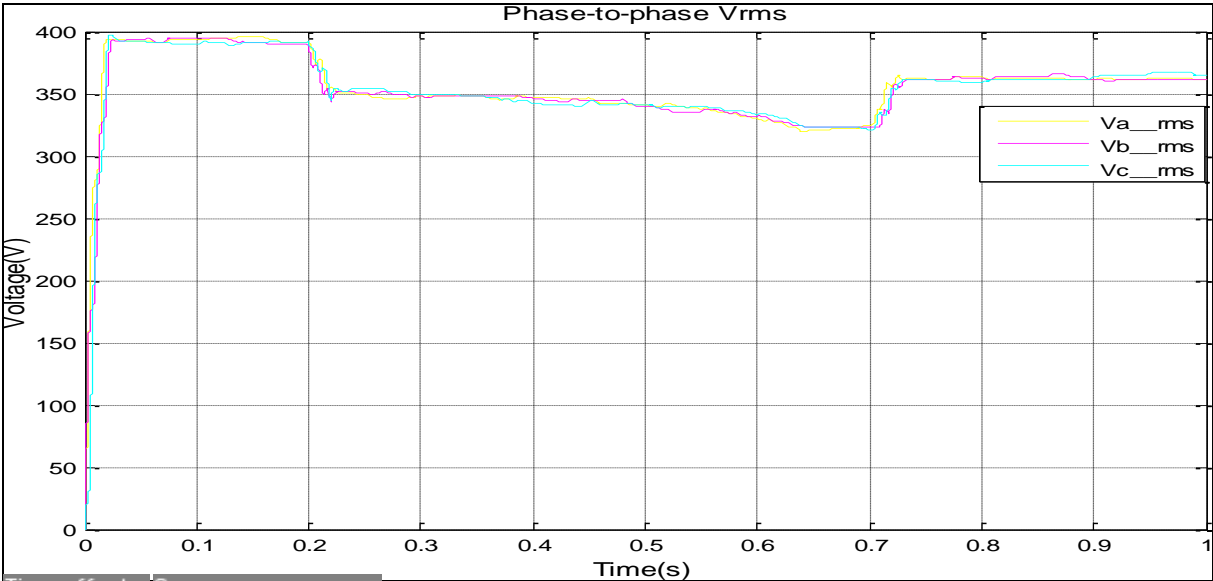


Figure 5.14: V_{abc} (V_{rms}) under load change

The overload is due to excessive loads which induce the voltage sags. When the additional load is removed, the voltage goes back to its nominal peak voltage waveform as seen in Figure 5.15 below. A longer duration of low voltage is called sustained sag. This is observed in the line-to-line peak output voltage waveforms which are 466 V instead of 563 V. In the same period of

time, Figure 5.16 below shows an increase in the current to 600 A. The system cannot handle the change in loads because m_a is kept constant as evidenced by the three-phase voltage waveform.

In order to handle the changes in load power, some controller methods were incorporated into the system to regulate the voltage at the inverter terminal

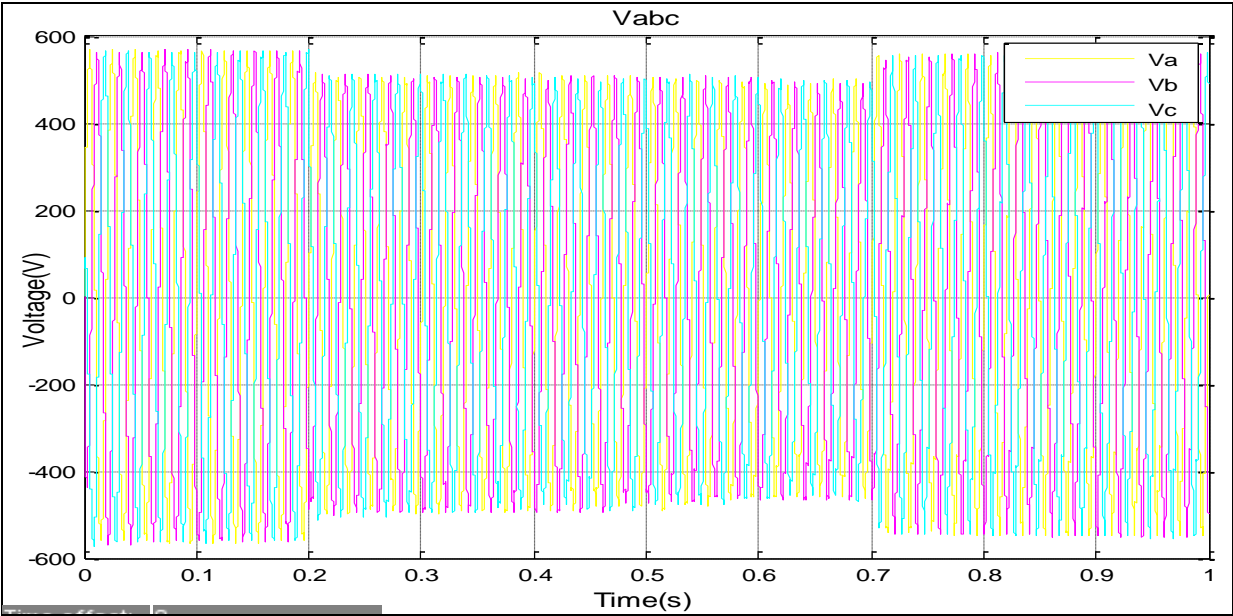


Figure 5.15: V_{abc} under load change

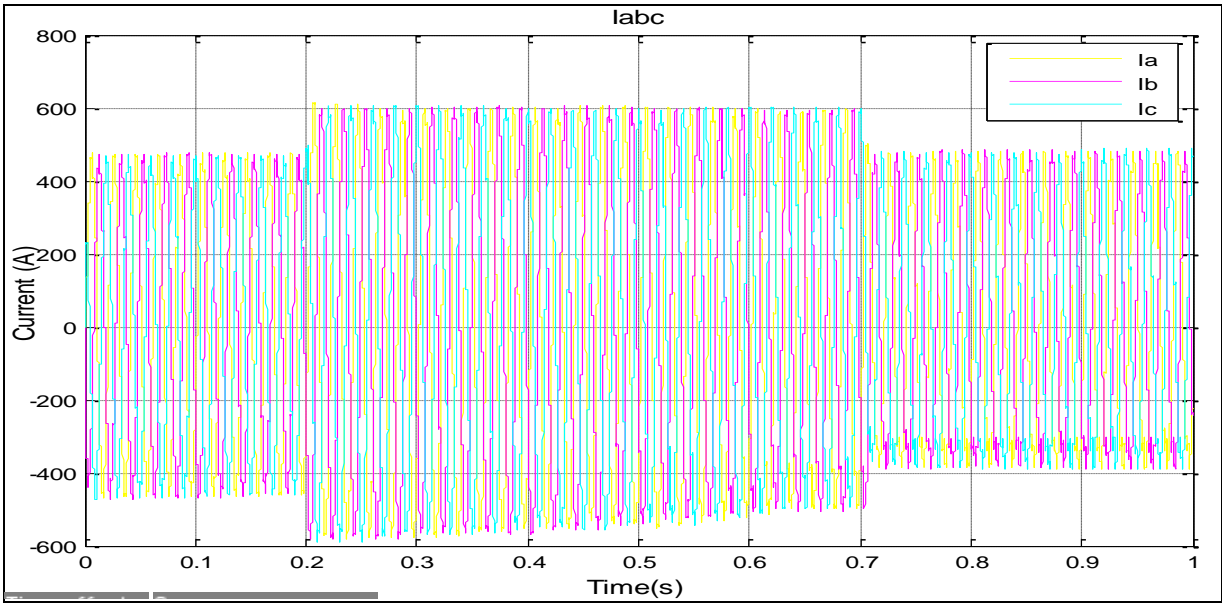


Figure 5.16: I_{abc} under load change

The system parameters used throughout the remainder of the simulation running time, are presented in Table 5.1 below.

Table 5.1: System parameters

Parameter	Value
PWM output switching frequency	5 KHz
Nominal load frequency	50 Hz
Input DC voltage	750 V
RMS load voltage	400V
Full load resistance	100 Ω
Nominal load voltage	400V _{rms}
Filter inductance L	2mH
Filter capacitor C	3uF
Sensitive load power	5 kW
Non-sensitive load power	100 KW
Proportional gain K_p	0.3
Proportional + integral gain K_i	450

5.4 Simulation result of inverter controls using a PI controller

5.4.1 Inverter output voltage control using a PI controller under load power changes

A controller was added to the model as developed in the previous section. The method employed is based on using a PI controller to control the phase-to-ground V_{rms} as the natural reference frame. The same scenario as detailed in Section 5.3, is repeated here.

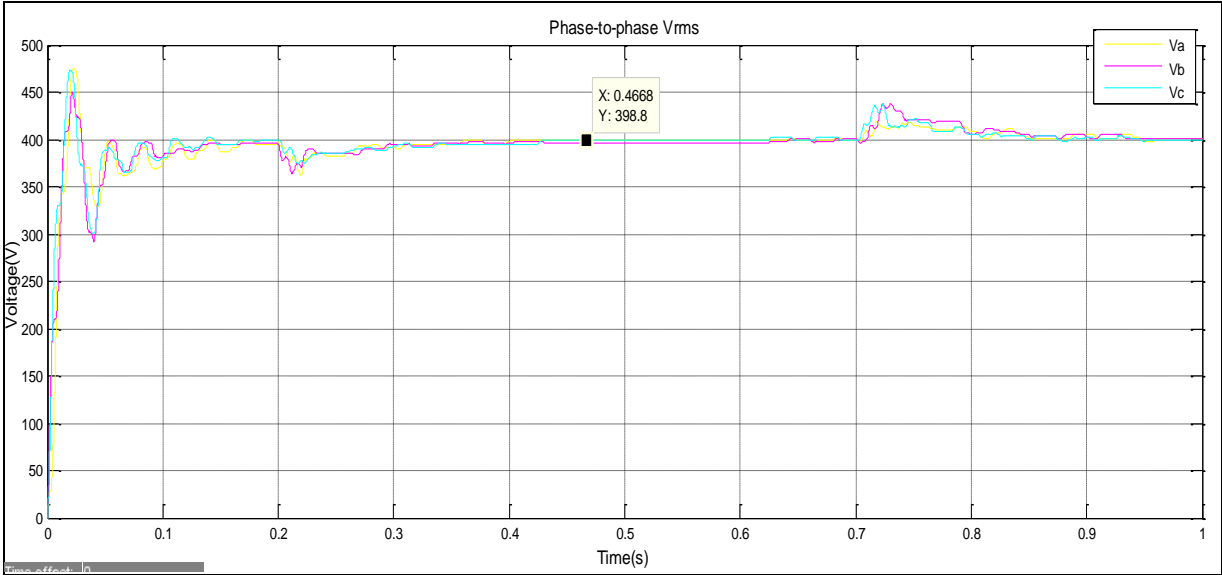


Figure 5.17: Phase-to-phase V_{rms} under load change

The sensitive and non-sensitive load are both operating within the system. The sensitive load power however, is permanently connected to the system, and the non-sensitive load power is temporary load which is not initially connected to the system - see Appendix 2. The non-sensitive load is connected into the system at time 200 ms and removed at 700 ms. Figure 5.17 above indicates that the phase-to-phase V_{rms} reached the steady state value of 398 V at 160 ms, while using the controller. However, when the non-sensitive load power is connected to the system at 200 ms, the phase-to-phase V_{rms} drops briefly to 360 V. The controller designed into the system (PI controller) regulates the nominal V_{rms} to 398.8 V. As soon as, the non-sensitive load is removed, the voltage spiked to 440 V, however, the controller regulated it back to the nominal phase-to-phase V_{rms} of 398 V. The V_{rms} reduces to the nominal voltage due to the controller employer which regulates the output voltage.

Figure 5.18 below shows the effect of the controller employer, which changes the m_a value during overloading, in order to regulate the output voltage at the inverter terminal. In that period the modulation has increased in order to maintain the desired output voltage. When however, m_a goes above the limit of 1 due to the small size of DC link voltage, more harmonics will be generated and the voltage quality will be poor.

In Figure 5.19 below, when the non-sensitive load power is connected into the system at 200 ms, a voltage sag is observed for a few microseconds and it then returns to the normal operating state. At 700 ms the non-sensitive load power is disconnected from the system quickly and a voltage swell is noticed for a few milliseconds. The peak output voltage waveform is maintained at 563 V_{AC} .

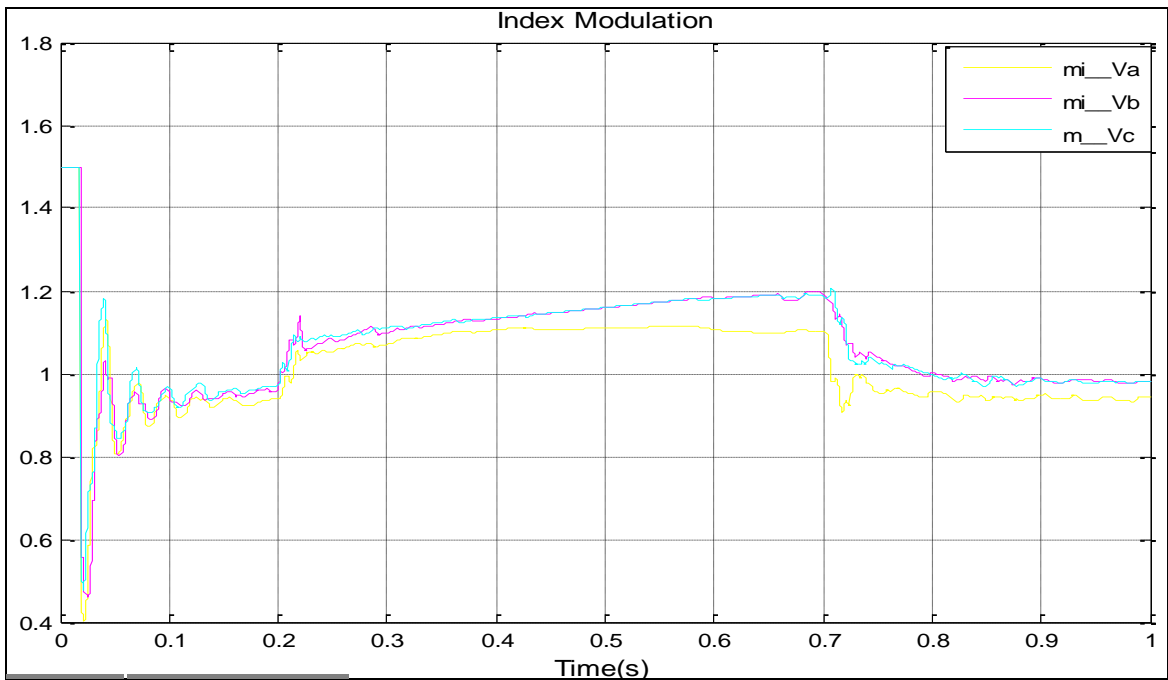


Figure 5.18: Modulation index under load change

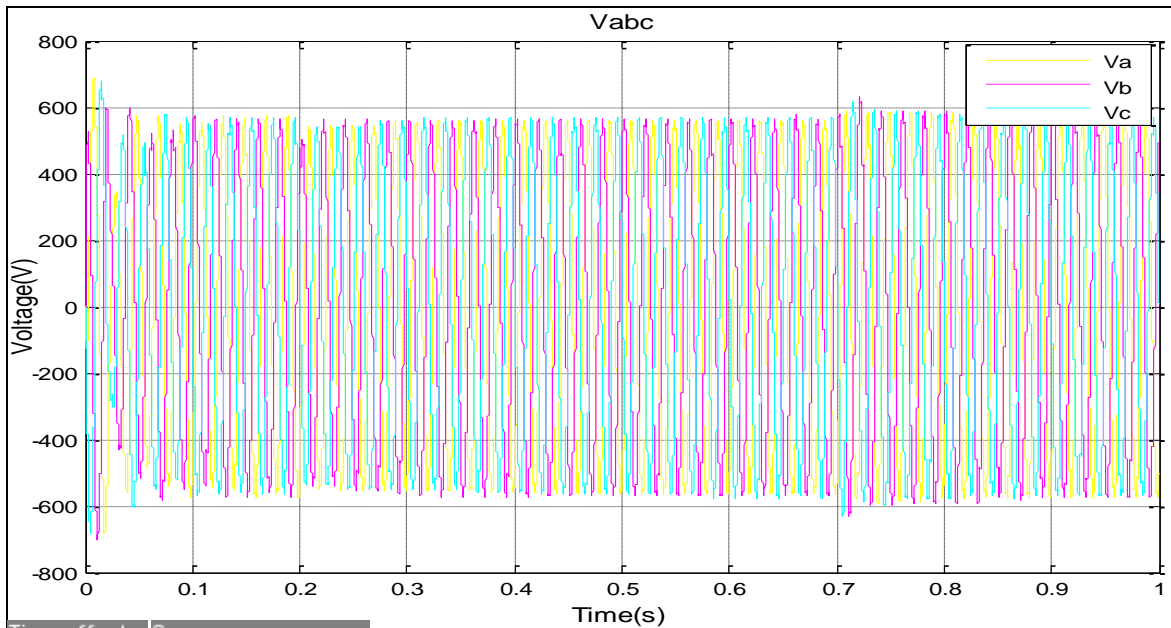


Figure 5.19: Output peak voltage under load change

Figure 5.20 below shows the output current waveform during the time interval from 200 to 700 ms. While the controller maintained the output voltage, the peak output current waveform rose to 690 A. The controller employer handled the change in load power more effectively than compared to a simple inverter without any controller to regulate its output. Following below, an analysis is done of the system with a varying input voltage.

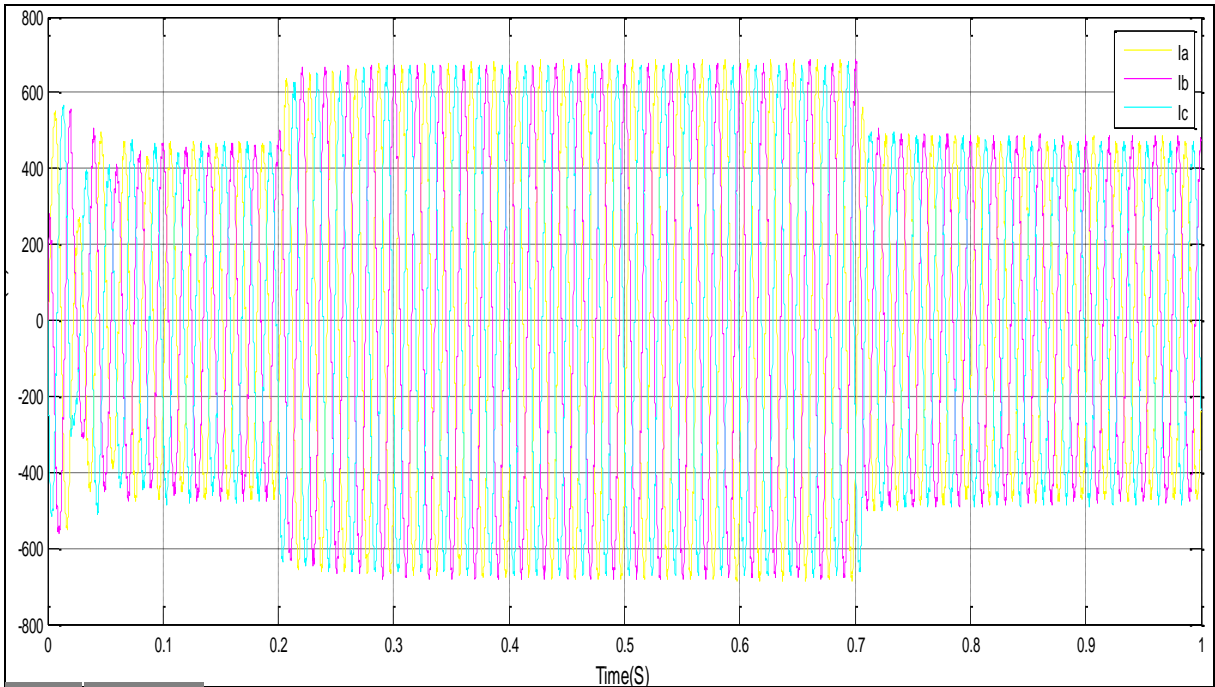


Figure 5.20: Current waveform under load change

5.4.2 Inverter voltage control during an input voltage change, using a PI controller

When the system is suddenly subjected to a change in the input voltage, the controller employer is expected to respond to any such changes. In this case the loads (non-sensitive and sensitive load) are permanently connected to the autonomous microgrid system - see Appendix 3. Figure 5.21 below depicts the intervals in which the input amplitude voltage changes, in order to test the controller of the system. At time intervals 0 to 380 ms, 380 to 630 ms, 630 to 1170 ms, 1170 to 1320 ms, 1320 to 1620 ms and 1620 to 2000 ms the input voltages varied respectively as follows; 750 V, 600 V, 1000 V, 645 V, 980 V and 750 V.

Figure 5.22 below shows the phase-to-phase V_{rms} being controlled to 400 V by the controller employer (PI controller) which stabilised the system during the input voltage change. The action from the controller was observed in time interval from 0 to 380 ms, when the input voltage was 750 V. It reached the steady state at 320+ ms, when the phase-to-phase V_{rms} was at 400 V. The same explanation is valid for the time intervals from 630 to 1170 ms, 1320 to 1620 ms and 1620 to 2000 ms, where the phase-to-phase V_{rms} reached steady state respectively at 1000 ms, 1600 ms and 1940 ms. However, the PI controller presented a slow response and high overshoot in the time interval 380 to 630 ms, when the input voltage is 600 V, and the phase-to-phase V_{rms} dropped to 340 V. The insufficient input voltage amplitude limits controller action due to the small size of DC link voltage; this will result in more harmonics being generated and a poorer voltage

quality. The same explanation applies for the time intervals from 380 to 630 ms and 1170 to 1320 ms.

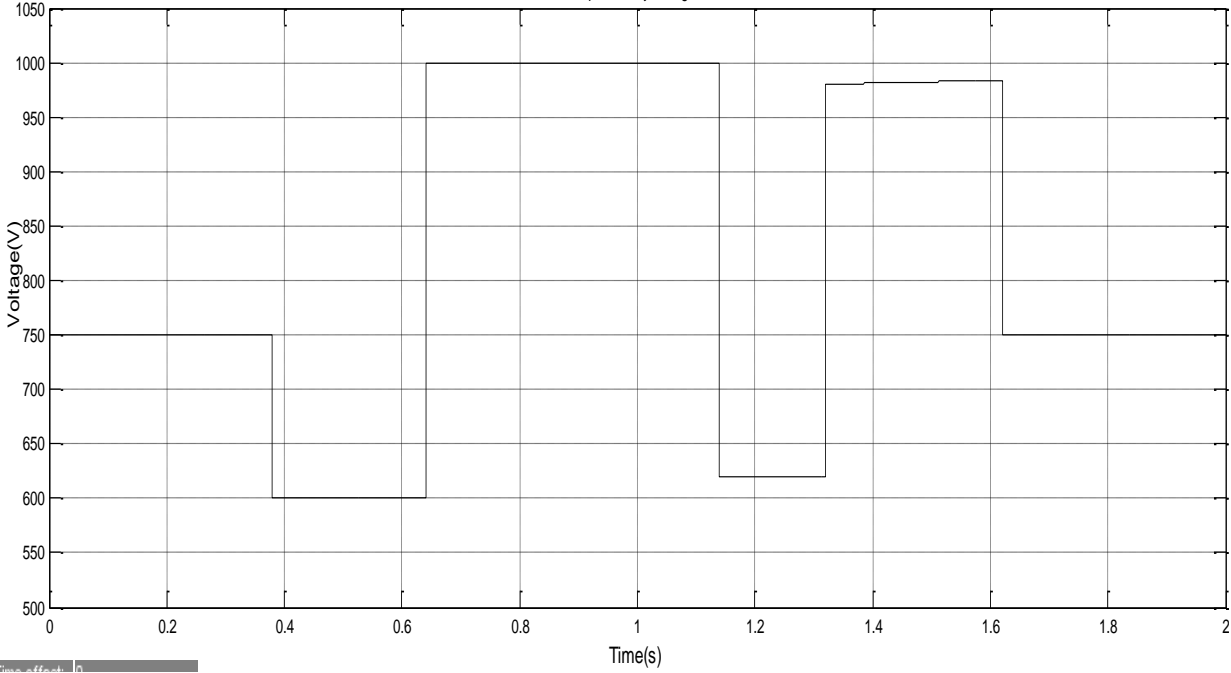


Figure 5.21: Input battery voltage

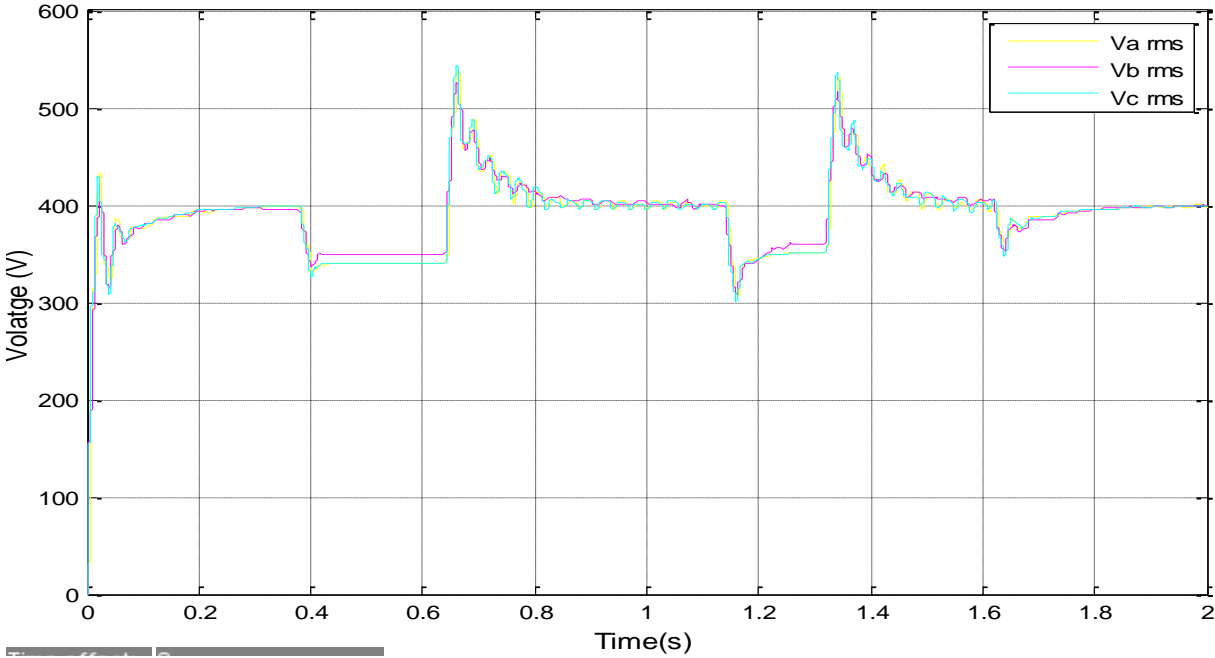


Figure 5.22: Phase-to-phase V_{rms} under input voltage change

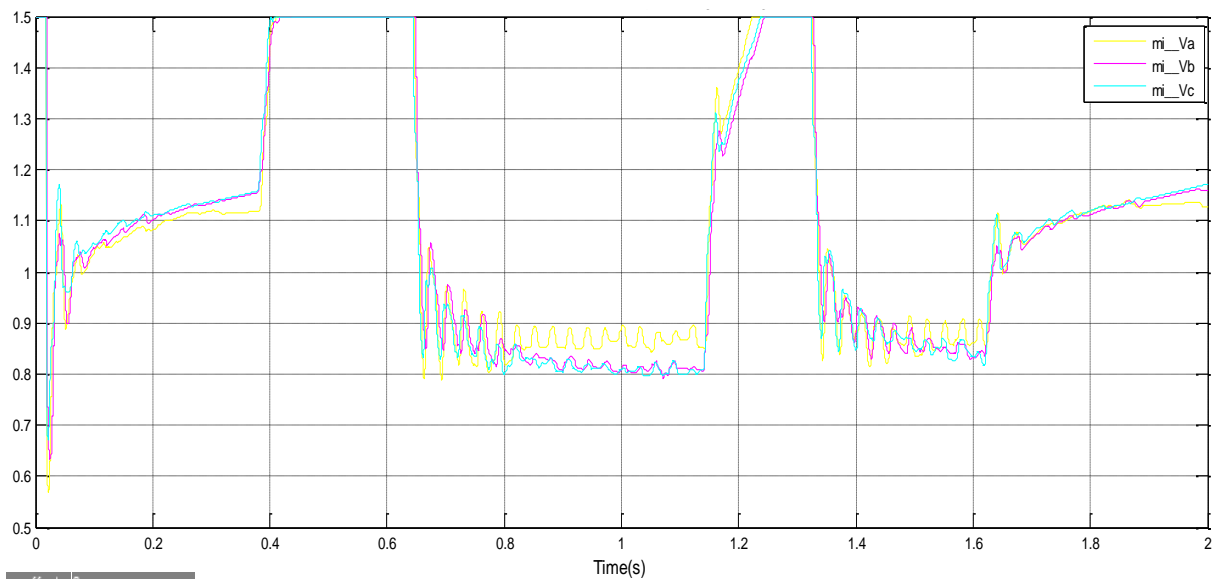


Figure 5.23: Modulation index subjected to input voltage change

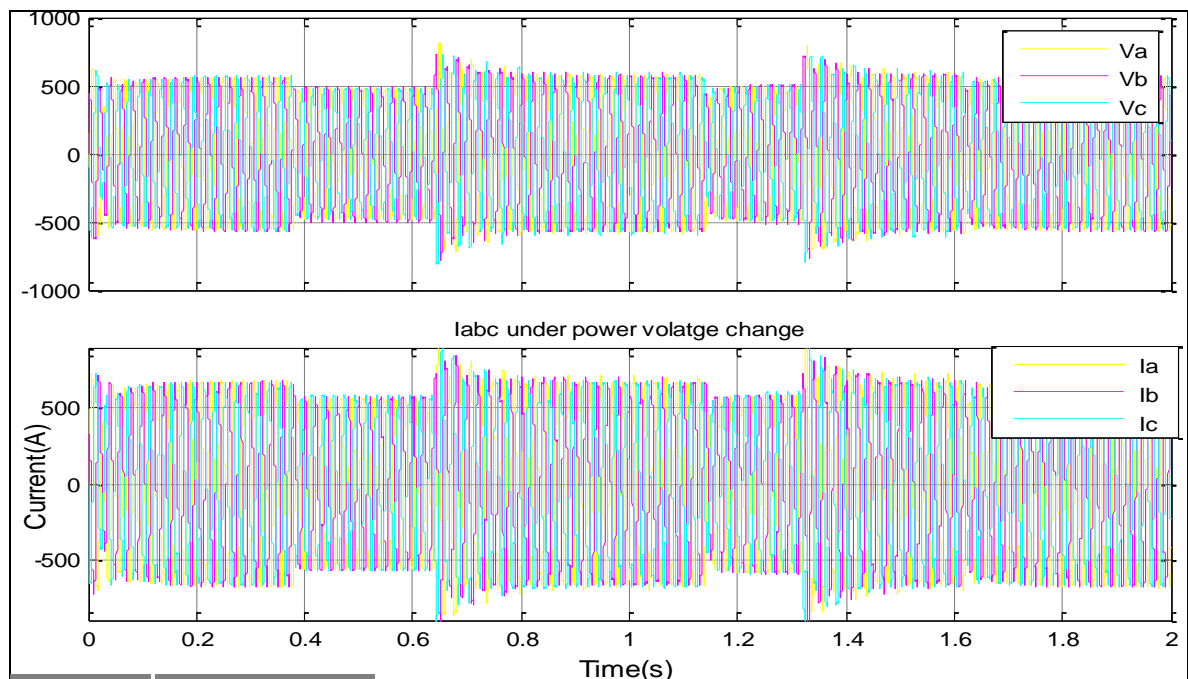


Figure 5.24: Output peak voltage and current under input voltage change

Figure 5.23 above displays the variation in m_a at the PI controller when the input voltage is varied. The modulation index changes to regulate the voltage at the inverter terminal. However, when the amplitude input voltage was at low, the controller reached the saturation value; this occurred at 600 V and 645 V. To further control m_a , the power of the load can be reduced so that the controller will be able to regulate the output voltage. However, the controller can better handle the excess in input voltage, if m_a is proportionally reduced.

In figure 5.24 above, the peak output voltage waveform is controlled to be 563 VAC in the time intervals 0 to 380 ms, 630 to 1170 ms, 1320 to 1620 ms and 1620 to 2000 ms, where the peak output waveforms reached steady state respectively at 200 ms, 1000 ms, 1600 ms and 1940 ms. Furthermore, a similar explanation is applicable for the peak current waveform. The control method presents a large overshoot and a long response time.

In Section 5.5, another control method is used for regulating the voltage at the inverter terminal of the system. It handles the changes in load power according to the input voltage capacity.

5.5 Simulation result of an inverter voltage control using the dq0 transformation + PI controller simulation

This control method is based on the dq0 transformation + PI controller. The dq0 reference frame transforms the three-phase AC quantities V_a , V_b , V_c , into two DC quantities V_d and V_q ; in case of balanced systems, the 0-component is equal to zero. The DC quantities facilitate easier filtering and control.

5.5.1 Inverter control using dq0 transformation + PI controller under constant parameters

Under constant parameters, the input voltage and the power of the loads are kept constant. Moreover, the loads (non-sensitive and sensitive load) are permanently connected to the system. In this section the efficiency of the controller employer under constant parameters is evaluated.

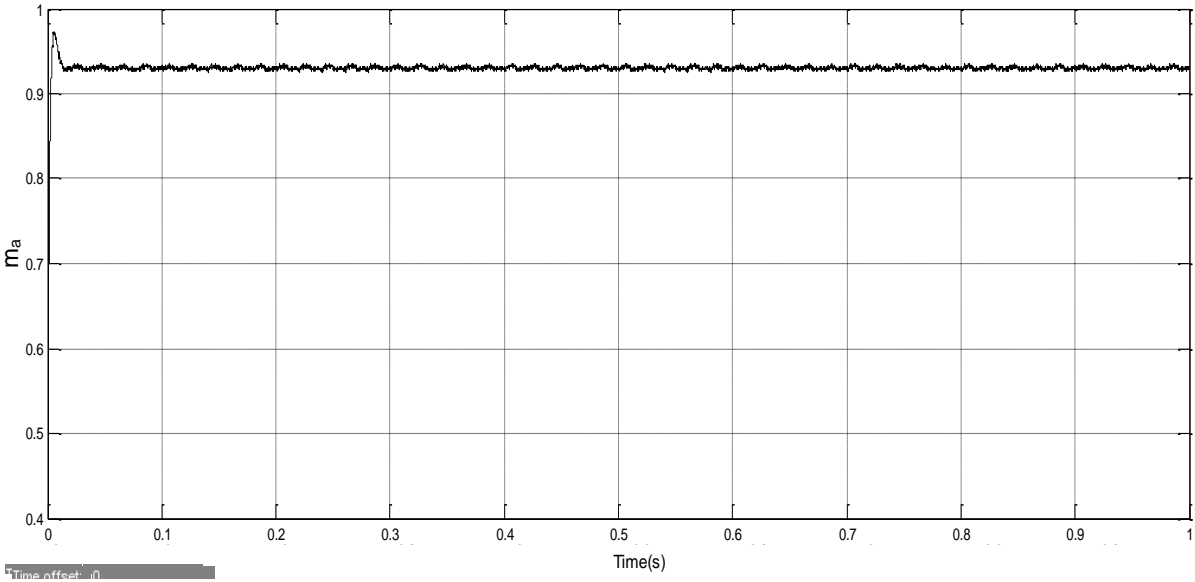


Figure 5.25: Modulation index under constant voltage and loads

Figure 5.25 above indicates a constant modulation index of 0.93 after reaching steady state at 30 ms. The controller automatically calculates the value of m_a to achieve the desired output voltage.

Figure 5.26 below presents a steady phase-to-phase V_{rms} of 400 V and, figure 5.27 below illustrates a line-to-line peak output voltage waveform of 563 V_{AC}. A peak current waveform of 230 A is displayed in Figure 5.28. With constant parameters, the controller functions well and performs as it should.

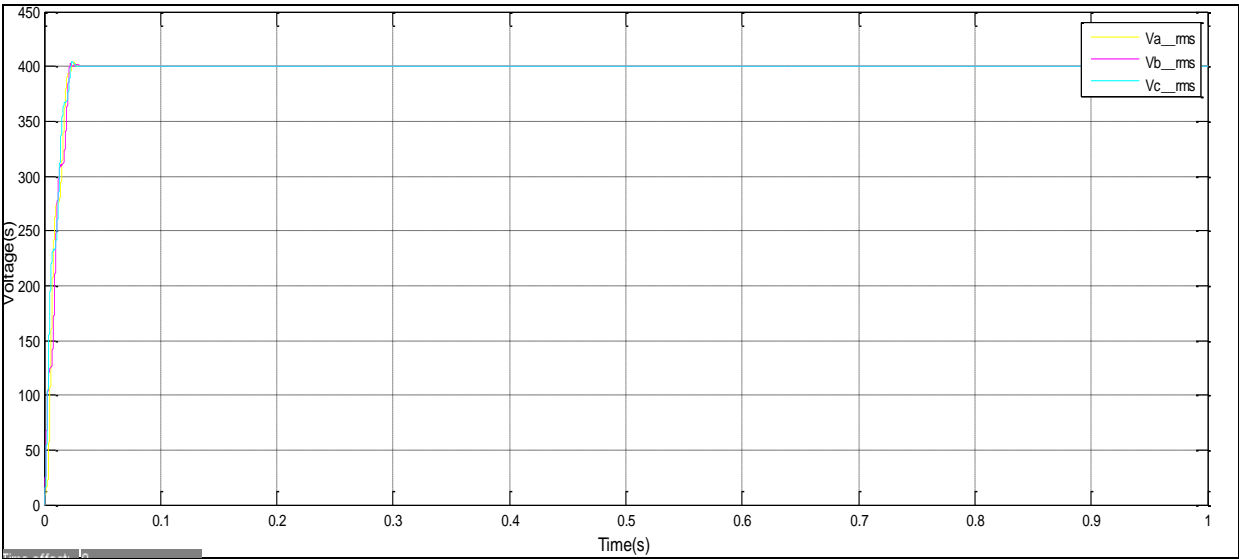


Figure 5.26: Phase-to-phase V_{rms} under constant voltage and loads

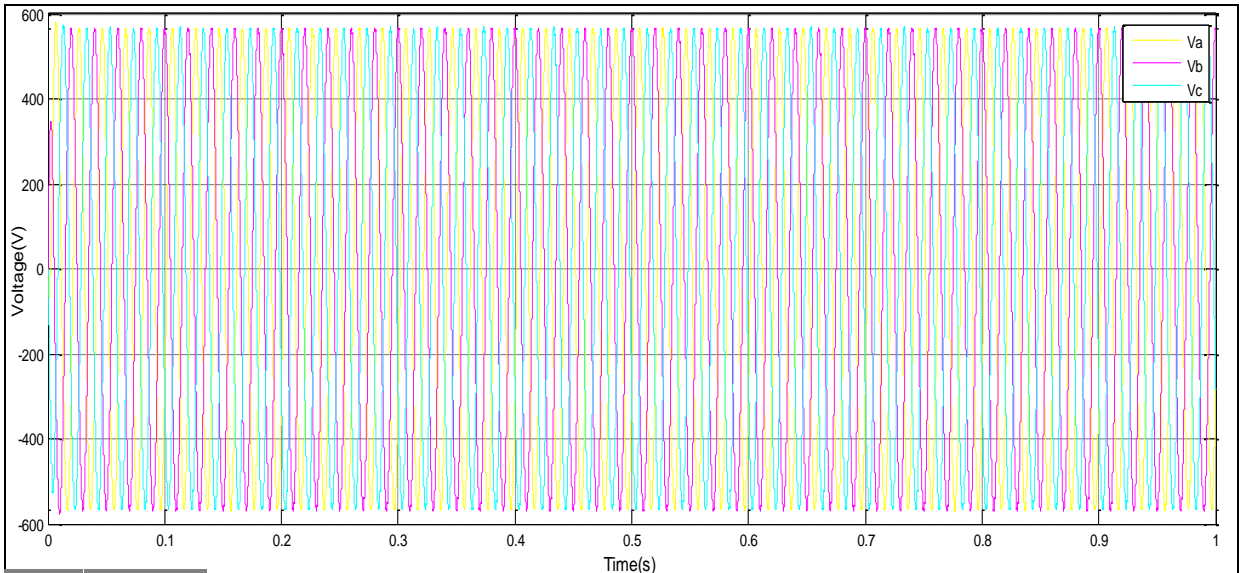


Figure 5.27: Load voltage under constant input voltage and loads

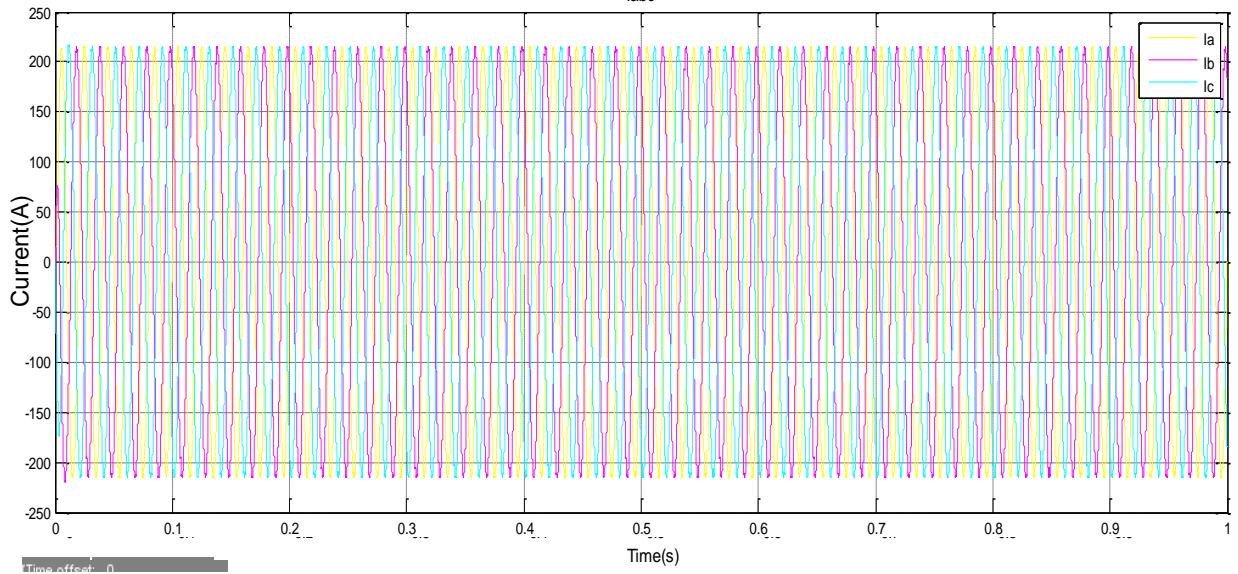


Figure 5.28: Current under constant input voltage and load power

5.5.2 Inverter control using dq0 transformation + PI controller under load power changes

In this section changes in load power, subject to the dq0 transformation + PI controller are analysed in terms of performance. Sensitive load power was connected to the system throughout. Non-sensitive load power was not initially connected to the system, but was temporarily applied during the test run - see Appendix 2. Non-sensitive load was connected to the autonomous microgrid system at time 200 ms and disconnected at 700 ms. The control system is expected to regulate the output voltage, regardless of any change in the input voltage.

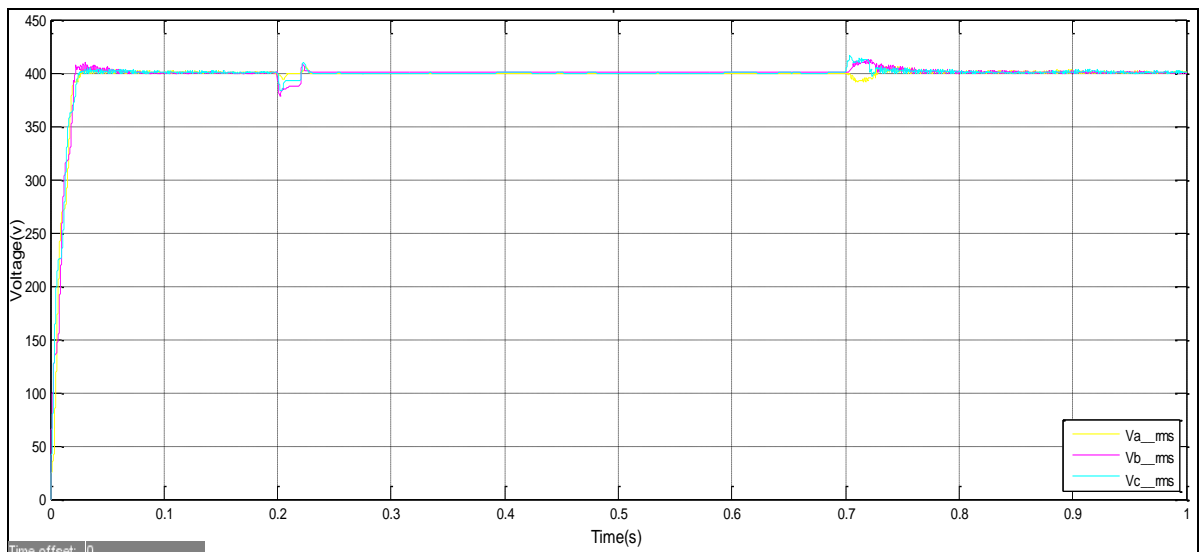


Figure 5.29: Phase-to-phase V_{rms} under load power change

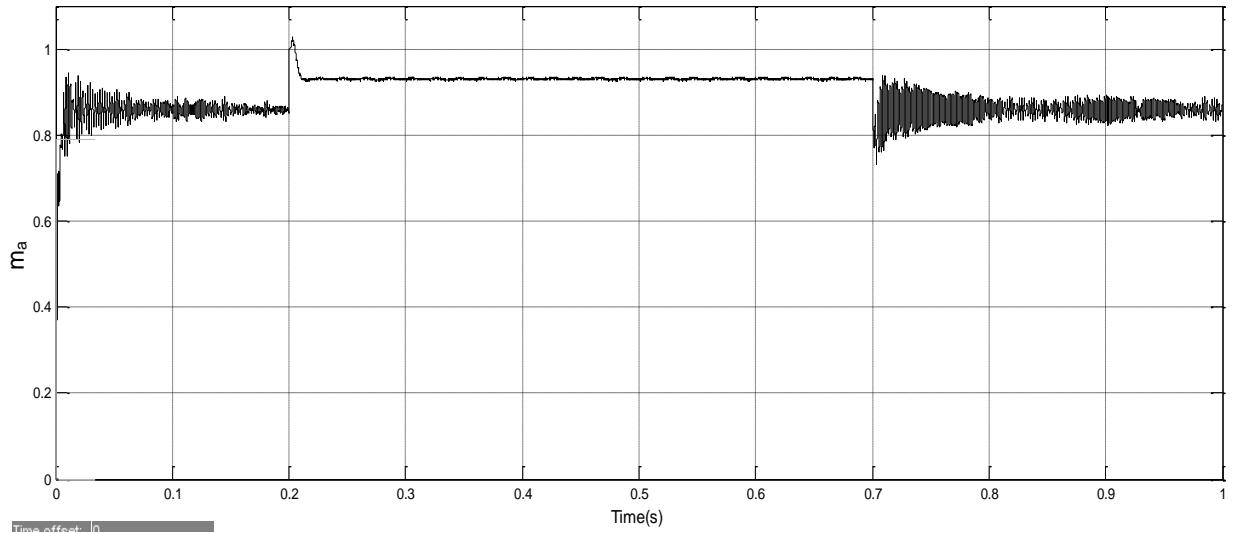


Figure 5.30: Modulation index under load power change

Figure 5.29 above indicates that the phase-to-phase V_{rms} reached the steady state value at 100 ms, when using the controller employer (dq0 transformation + PI controller).

At steady state, the phase-to-phase V_{rms} value is 400 V, but when the non-sensitive load power is connected to the system at 200 ms, the phase-to-phase V_{rms} drops marginally to 370 V and then, at time 230 ms, the controller employer has regulated the system back to its nominal phase-to-phase V_{rms} to 400 V. When the non-sensitive load is disconnected from the system at 700 ms, the phase-to-phase V_{rms} increased suddenly to 430 V. However, the controller had regulated the system back to the nominal phase-to-phase V_{rms} of 400 V, at 800 ms. When compared to Figure 5.17 above, the phase-to-phase V_{rms} voltage was essentially maintained at 400 V. From the results it is clear that the dq0 transformation + PI controller is faster and has a shorter response time when compared to the results for the PI controller as given in Figure 5.29 and Figure 5.17.

Figure 5.30 above presents the variation in m_a when there is a change in the load power; the controller changes the value of m_a so as to achieve the required nominal voltage. When a non-sensitive load was added to the system at 200 ms, the value of m_a increased with a small overshoot, before settling at a stable value at time 230 ms. When the non-sensitive load power was removed, the value of m_a decreased as well. Moreover, the effectiveness and the short response time of the controller are noticed. The data represented in Figure 5.30 above presents a shorter response time and a more stable value of m_a when compared to the data represented by figure 5.23.

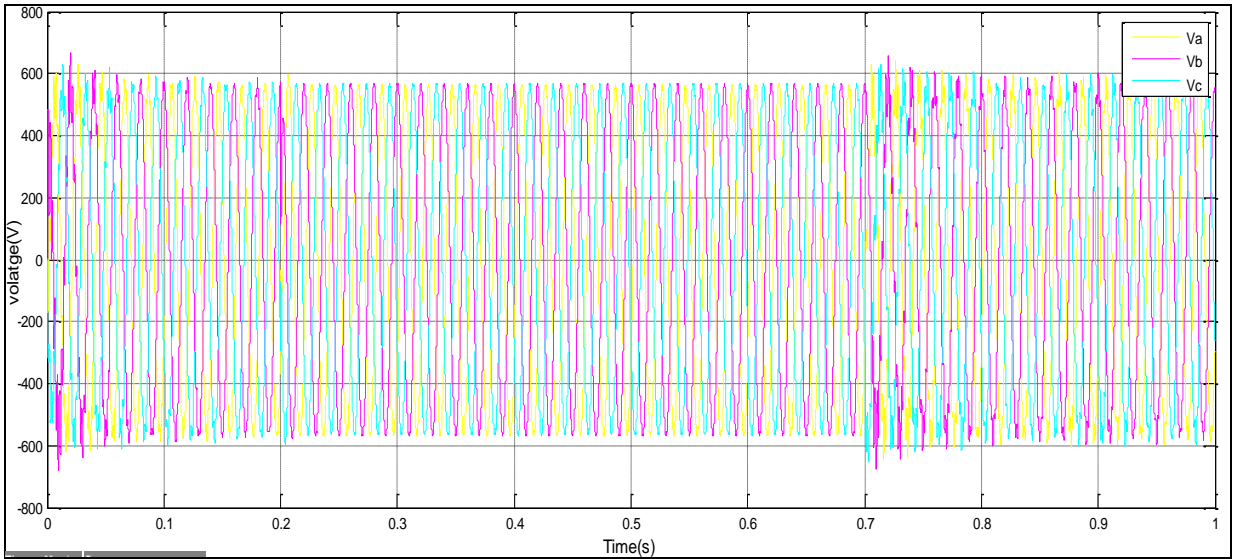


Figure 5.31: Peak voltage under load power change

The line-to-line peak output voltage is perfectly controlled. And the change in load power did not disturb the voltage operation, except for a brief voltage sag and swell which were detected during the transient state, and can be seen in figure 5.31. However, as indicated in figure 5.32 below, the current considerably increased during the time interval from 200 to 700 ms.

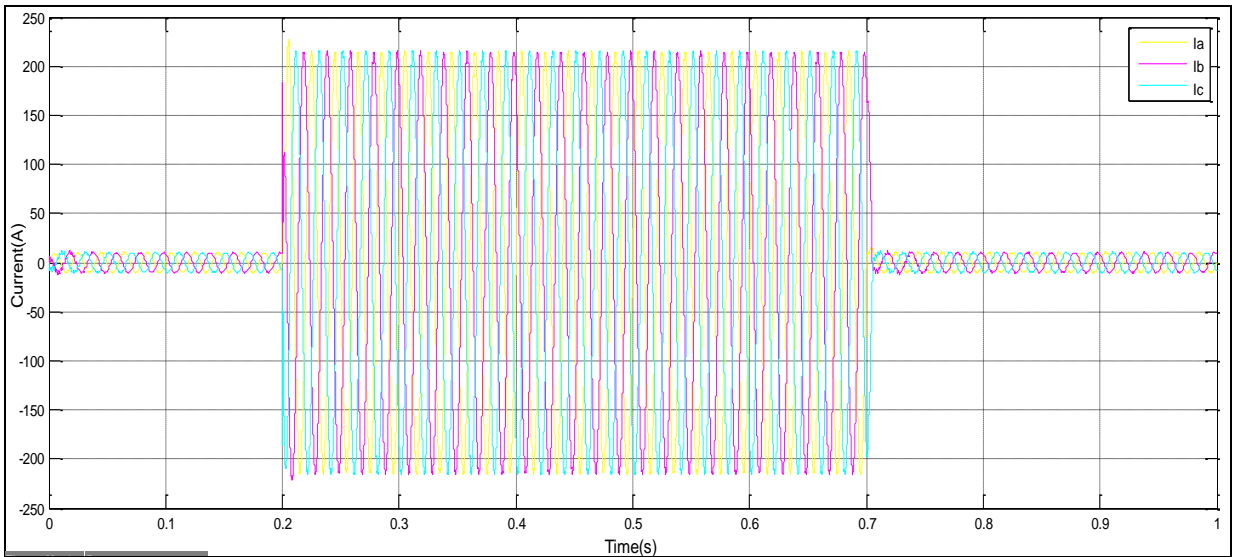


Figure 5.32: Current under load power change

5.5.3 Inverter controls under input voltage battery change

In this section changes in the input voltage, subject to a dq0 transformation + PI controller are analysed in terms of performance.

The controller employer is expected to respond to any changes in the input voltage. Moreover, the loads (non-sensitive and sensitive load) are permanently connected to the system see - Appendix 3. Figure 5.21 describes the intervals in which the input amplitude voltage changes, this is to test the controller of the system. In the time intervals from 0 to 380 ms, 380 to 630 ms, 630 to 1170 ms, 1170 to 1320 ms, 1320 to 1620 ms and 1620 to 2000 ms, the input voltages varied respectively as follows: 750 V, 600 V, 1000 V, 645 V, 980 V and 700 V.

Figure 5.33 below shows the phase-to-phase V_{rms} being controlled at 400 V, by using the controller employer (dq0 transformation + PI controller) to stabilize the system during the change in the input voltage change. The action of the controller is observed at time interval from 0 to 380 ms when the input voltage is 700 V, it reached the steady state at 30 ms and the phase-to-phase V_{rms} is 400 V. A similar explanation applies for the time intervals 630 to 1170 ms, 1320 to 1620 ms, and 1620 to 2000 ms, where the phase-to-phase V_{rms} reached the steady state respectively at 680 ms, 1350 ms and 1640 ms. The input voltage is 600 V during the time interval from 380 to 630 ms, and the phase-to-phase V_{rms} dropped to 340 V due to the insufficient input voltage limiting the controller action. And again, a similar explanation applies to the time intervals from 380 to 630 ms and 1170 to 1320 ms.

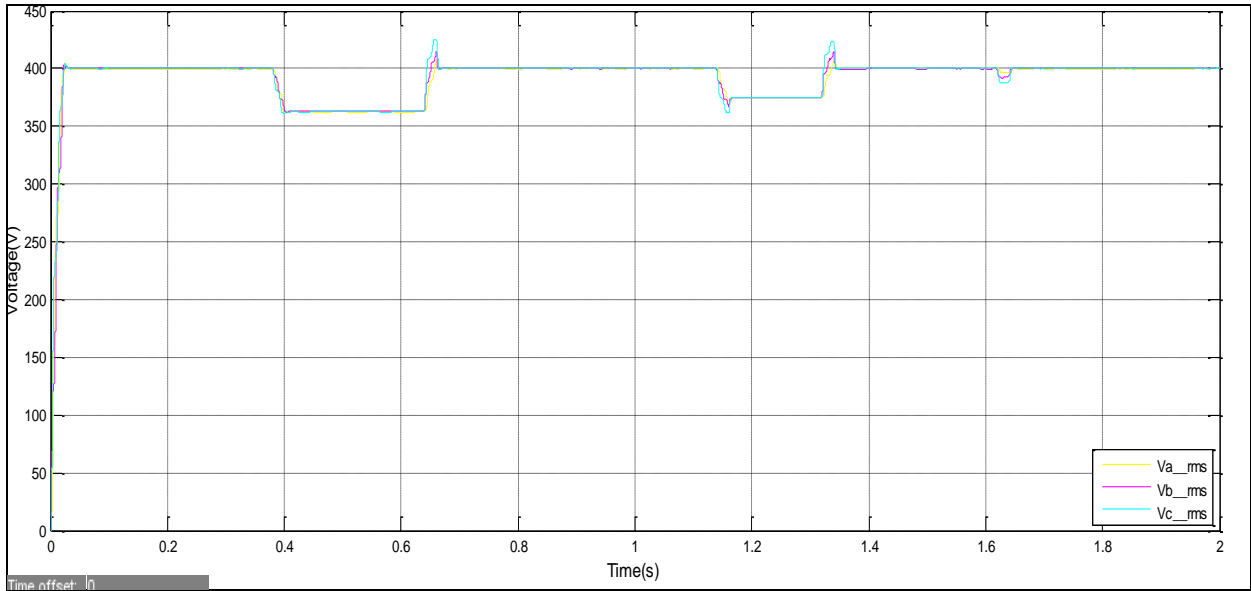


Figure 5.33: V_{rms} under input voltage change

Figure 5.34: Modulation index under an input voltage change

below displays the value of m_a as it is manipulated by the dq0 transformation + PI controller. This value of m_a changes in respect of the changes in the input voltage value, in order to

regulate the inverter terminal. However, when the amplitude of the input voltage was too low, the controller reached the saturation value; this happened at 600 V and 645 V. To further control m_a , the load power can be reduced, to enable the controller to regulate the voltage to the operating point in the case where the input voltage is at 645 V. However, the controller handles well the excess in input voltage by reducing proportionally the m_a . The controller employed, has a fast response time and a short overshoot when compared to the results shown in figure 5.23.

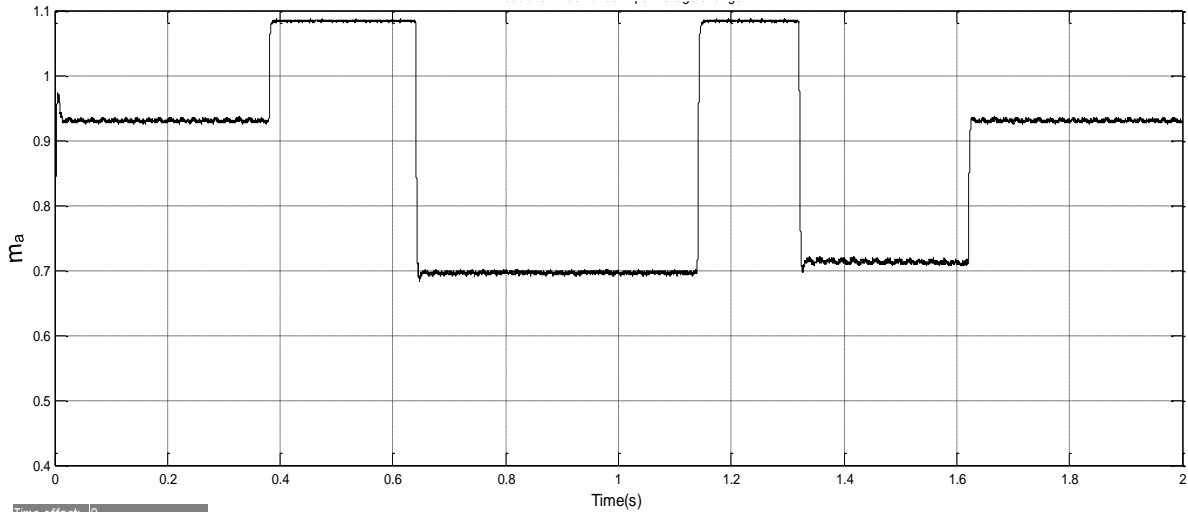


Figure 5.34: Modulation index under an input voltage change

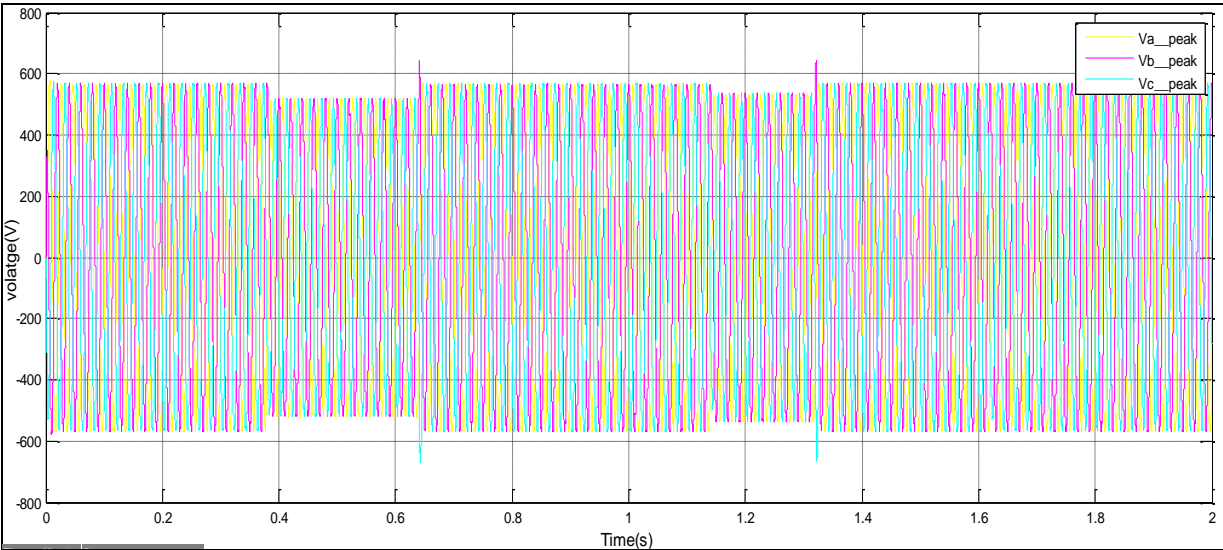


Figure 5.35: Output voltage waveform under an input voltage change

However, there are some limitations at the minimum input voltage required to fully control the output voltage waveform; for the time intervals 380 ms to 630 ms and 1110 ms to 1320 ms, the input voltages are respectively 600 and 625 V_{dc} , which are lower than the required minimum

input voltage. Figure 5.35 above and Figure 5.36 below present respectively the output voltage waveform, and the output current waveform, with voltage sags in the time intervals mentioned in the previous sentence.

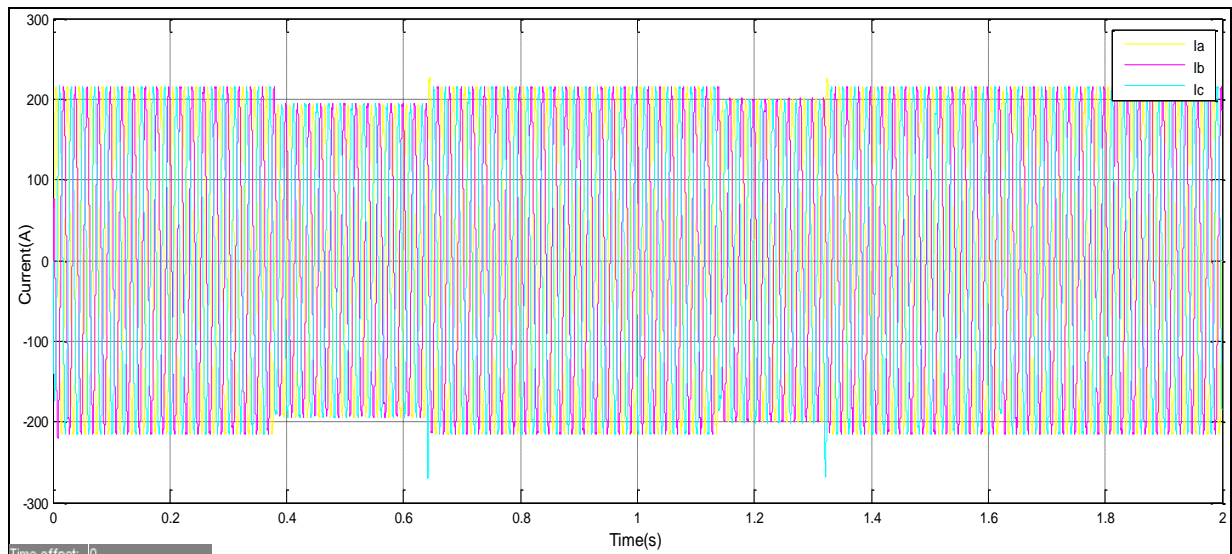


Figure 5.36: Output current waveform under an input voltage change

In Figure 5.33 above it is shown that V_{rms} is controlled to be at 400 V, but it displays a voltage drop in the time intervals previously noted; also, note how much faster the response time of the control method is, when compared to the previous one. This control method (dq0 transformation + the PI controller) presents a faster response time and a low overshoot, when compared to a PI controller on its own.

To handle the changes in load power according to the input voltage available, the next section, presents another method which can be used to regulate the voltage at the inverter terminal of the system.

5.6 Droop control simulation

5.6.1 Inverter control using droop control subject to constant parameters

Under constant parameters, the input voltage of a battery and the load power are kept constant. Moreover, the loads (non-sensitive and sensitive) are permanently connected to the system. This is to evaluate the efficiency of the controller employer under constant parameters. Figure 5.37 presents a constant phase-to-phase V_{rms} value around 400 V.

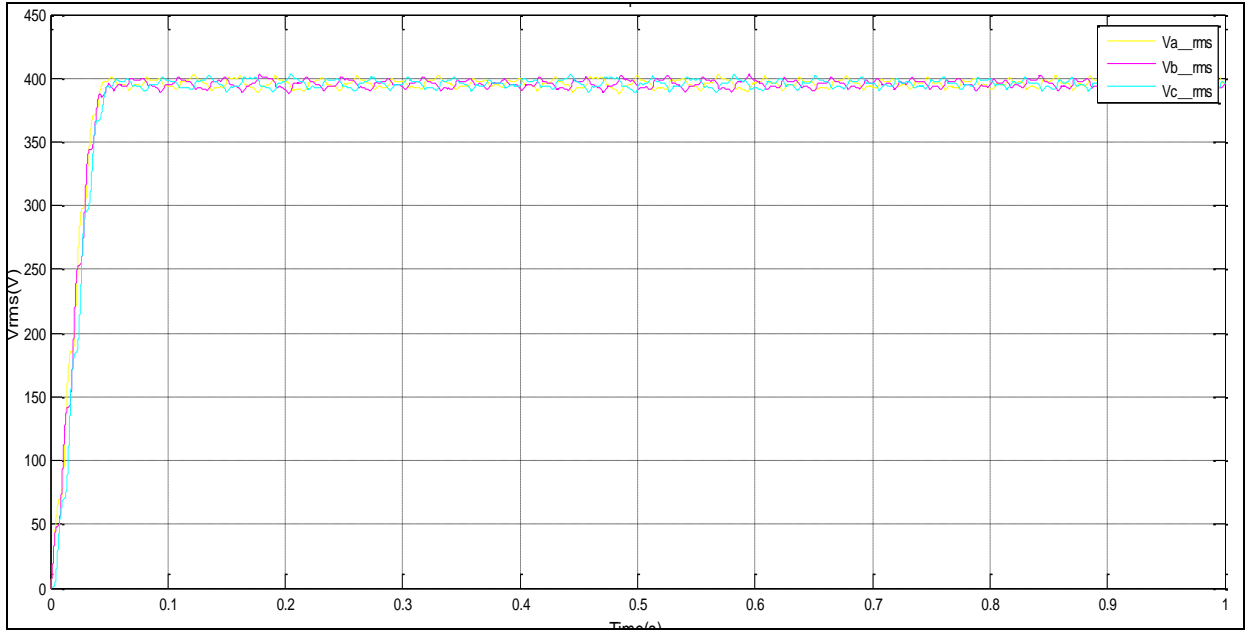


Figure 5.37: Phase-to-phase V_{rms} from droop control

Also, figure 5.38 and figure 5.39 present respectively, the peak output voltage waveform of 563 V AC and peak current waveform 220 A. Subject to constant parameters, the controller operates effectively and delivers the expected results.

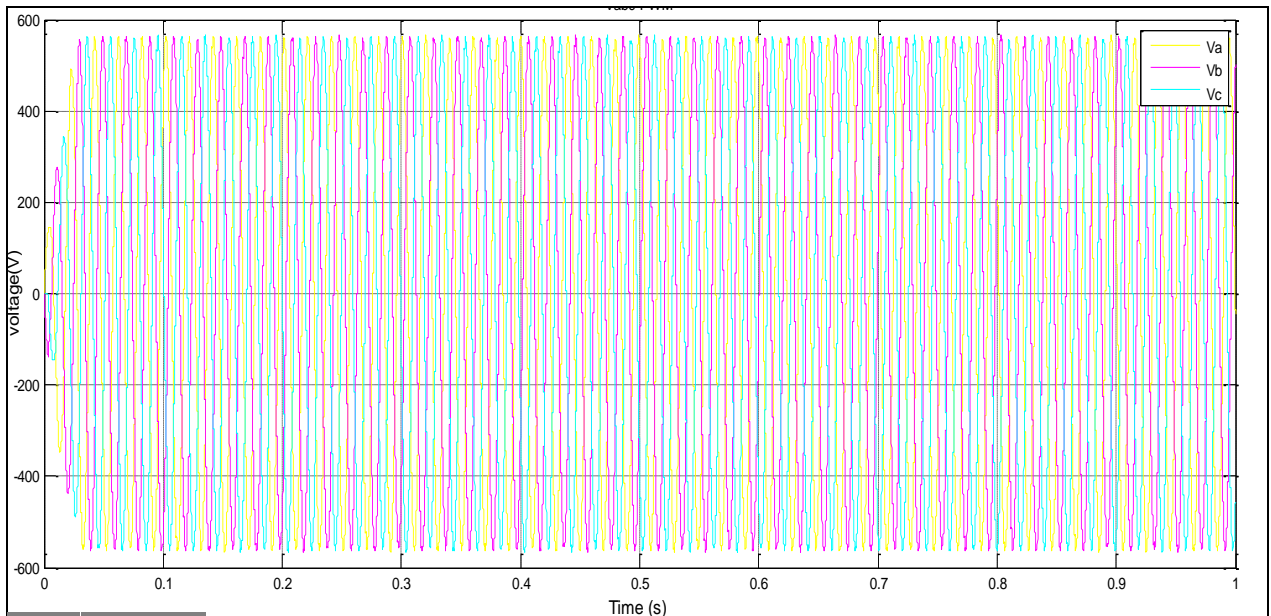


Figure 5.38: line-to-line peak voltage under constant parameters

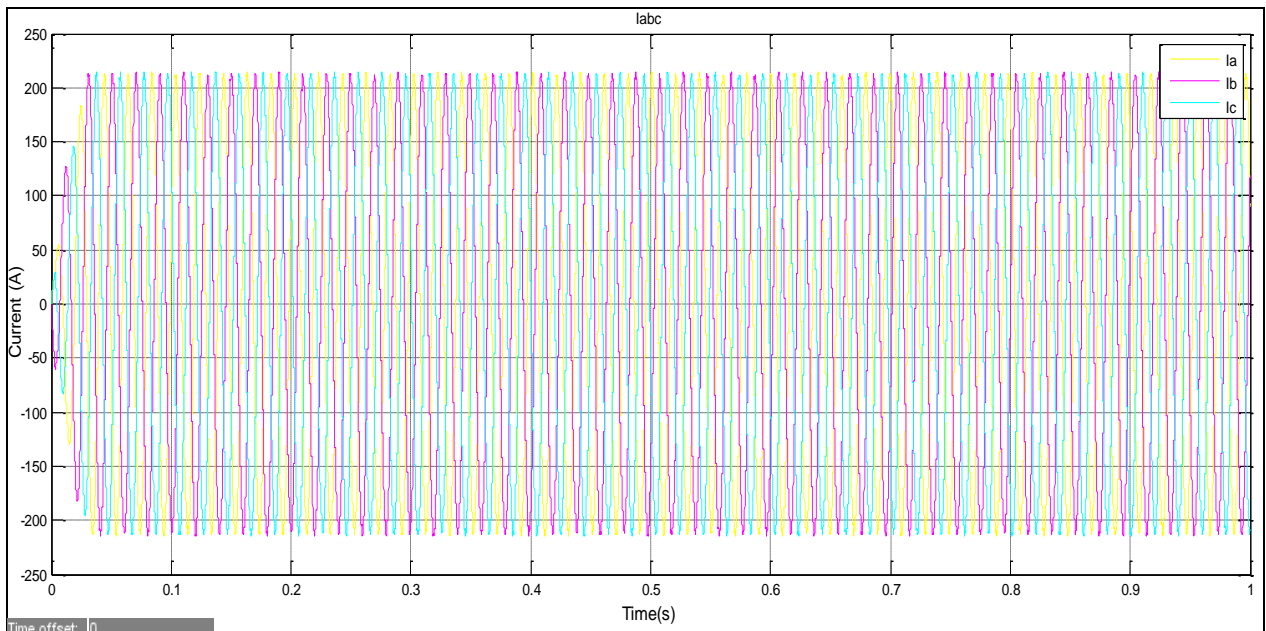


Figure 5.39: Peak current under constant parameters

5.6.2 Inverter control using droop control under load power changes

The changes in load power under droop control performance are analysed in this section. Sensitive load power is permanently connected to the system, and the non-sensitive load power is not permanently connected to the system. Non-sensitive load is initially disconnected from the system and is suddenly then connected at time equal to 200 ms and maintained up until 700 ms whilst the effect of the droop control is observed.

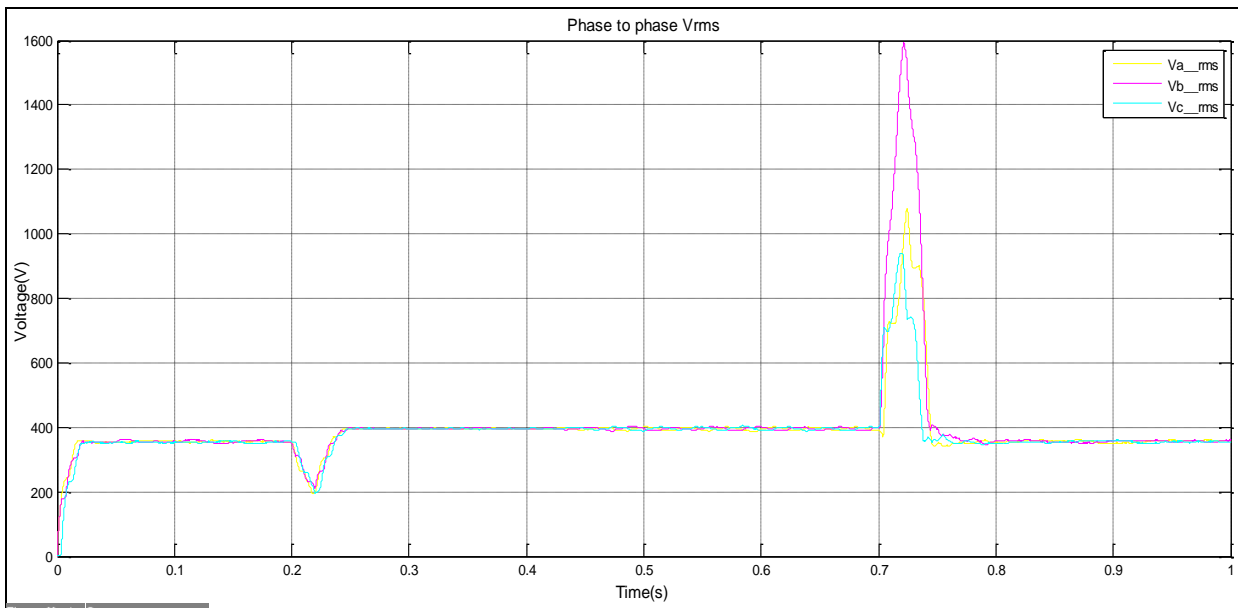


Figure 5.40: V_{rms} under load power change

The employed controller is expected to accommodate any changes in load by regulating the changes in the output voltage to suit. The controller regulates the desired nominal voltage through the V_{rms} .

Figure 5.40 shows that the phase-to-phase V_{rms} reached the steady state value at 20ms, when the droop controller is incorporated); at this steady state, the phase-to-phase V_{rms} value was 385 V. However, when the non-sensitive load power was connected to the system at 200 ms, the phase-to-phase V_{rms} dropped by almost half to 200 V. At time 250 ms, the controller employer adjusts the system to its nominal phase-to-phase V_{rms} to 400 V. As soon as the non-sensitive load is disconnected from the system at 700 ms, the phase-to-phase V_{rms} presents a large overshoot of 1000 V before it falls back to its initial value of 385 V at time 850 ms. Droop control presents a faster response to the change in load power when compared to the results depicted in Figure 5.29, is smoother than Figure 5.39.

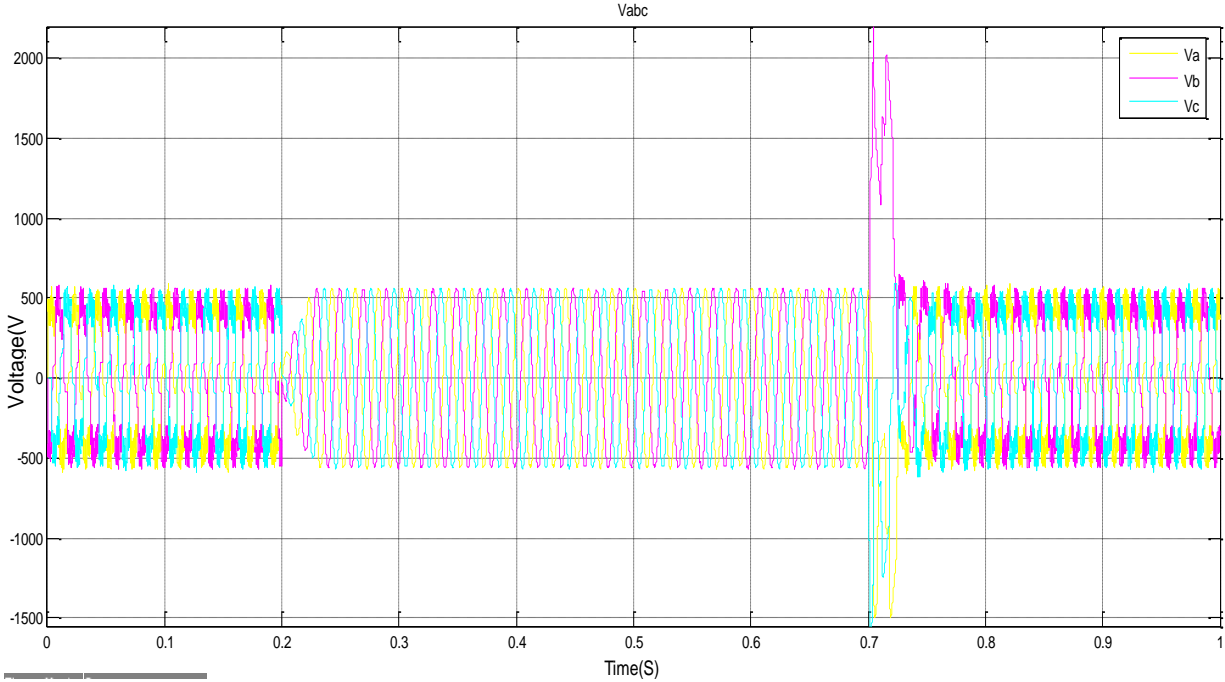


Figure 5.41: line-to-line peak output voltage under load power change

Figure 5.41 illustrates the peak output voltage waveform of the system model when subjected to load power change. The line-to-line peak output voltage is perfectly controlled and the change in load power does not overly influence the voltage operation, except during the transient state where short voltage sags were witnessed at the time the non-sensitive load was connected. When this load was disconnected, a large voltage spike was observed. By contrast disturbances resulting from the connection and disconnection of the non-sensitive load as shown by the graph in Figure 5.31, were mild.

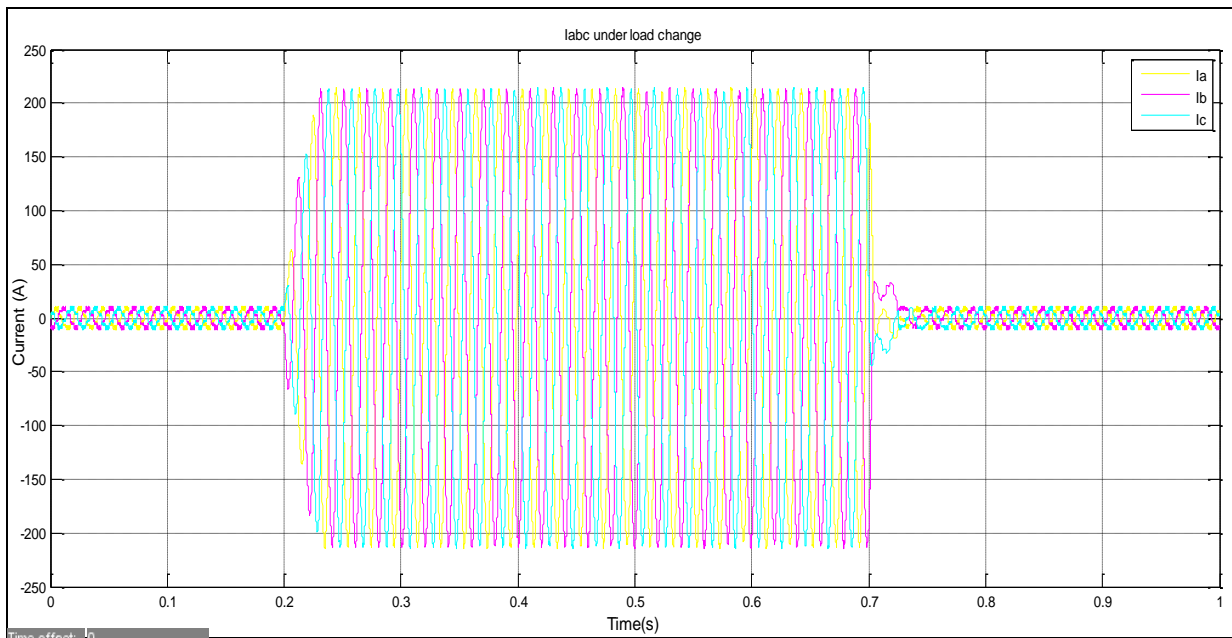


Figure 5.42: Current waveform under load power change

From Figure 5.41 the output waveform is smoother when the second load is added to the system than when it is removed. However, in Figure 5.42 below the current increases dramatically during the time interval 200 to 700 ms, which corresponds time for which the non-sensitive load was connected and the load power was increased. The results have confirmed the effectiveness as well as the short response time of the controller.

5.6.3 Inverter control using droop control when the battery voltage changes

Changes in the input voltage on the performance of a system with droop control in place, are analysed in this section. The employed control is expected to respond to any changes in input voltage. Moreover, the loads (non-sensitive and sensitive) are permanently connected to the system. Figure 5.21 describes the time interval at which the amplitude of the input voltage changes whilst testing the controller of the system. At time intervals from 0 to 380 ms, 380 to 630 ms, 630 to 1170 ms, 1170 to 1320 ms, 1320 to 1620 ms and 1620 to 2000 ms the input voltage varies respectively as follows 750 V, 600 V, 1000 V, 645 V, 980 V and 750 V.

Figure 5.43 below shows the controlled magnitude of the phase-to-phase V_{rms} to be 400 V, but there is slight variation in the V_{rms} values corresponding to the changes in the input voltage. There is limitation on the minimum input voltage that is required in order to enable full control of the output voltage waveform. Figure 5.44 and Figure 5.45 below, respectively present the output voltage waveform with a slight variation in peak output voltage, and the current waveform at time intervals mentioned in the previous paragraph. Figure 5.43 displays voltage drop at time intervals

as previously mentioned. It was also noted that the response of the control method was faster than that of previous one.

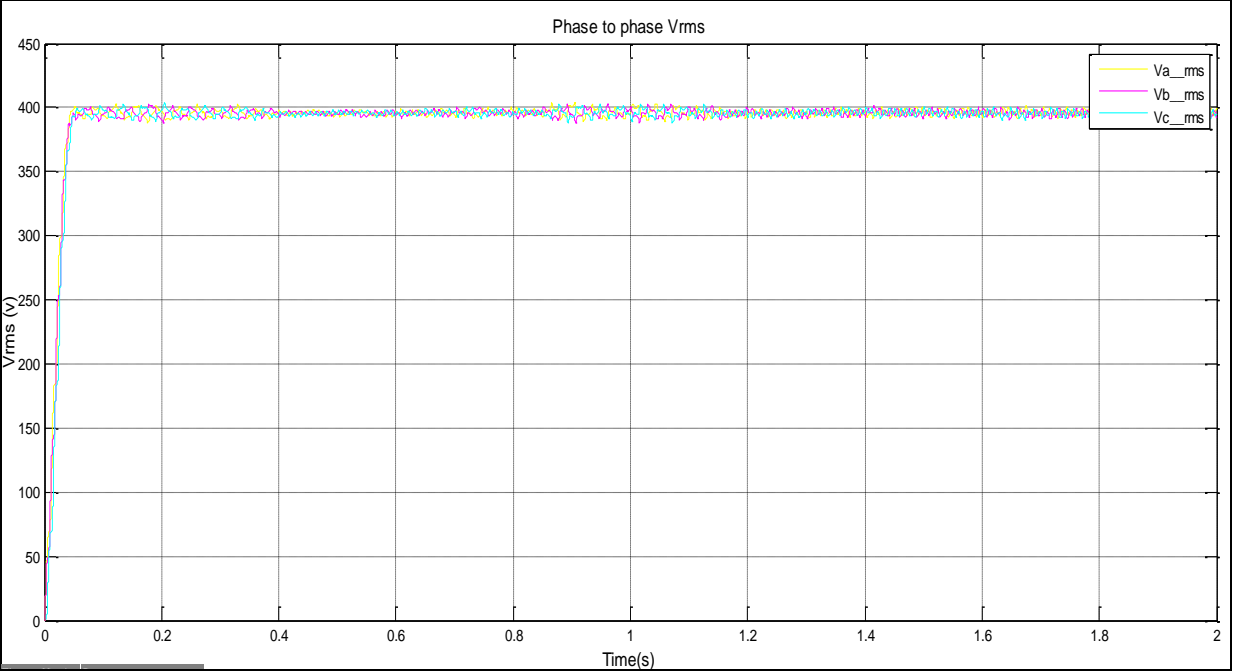


Figure 5.43: V_{rms} under input voltage change

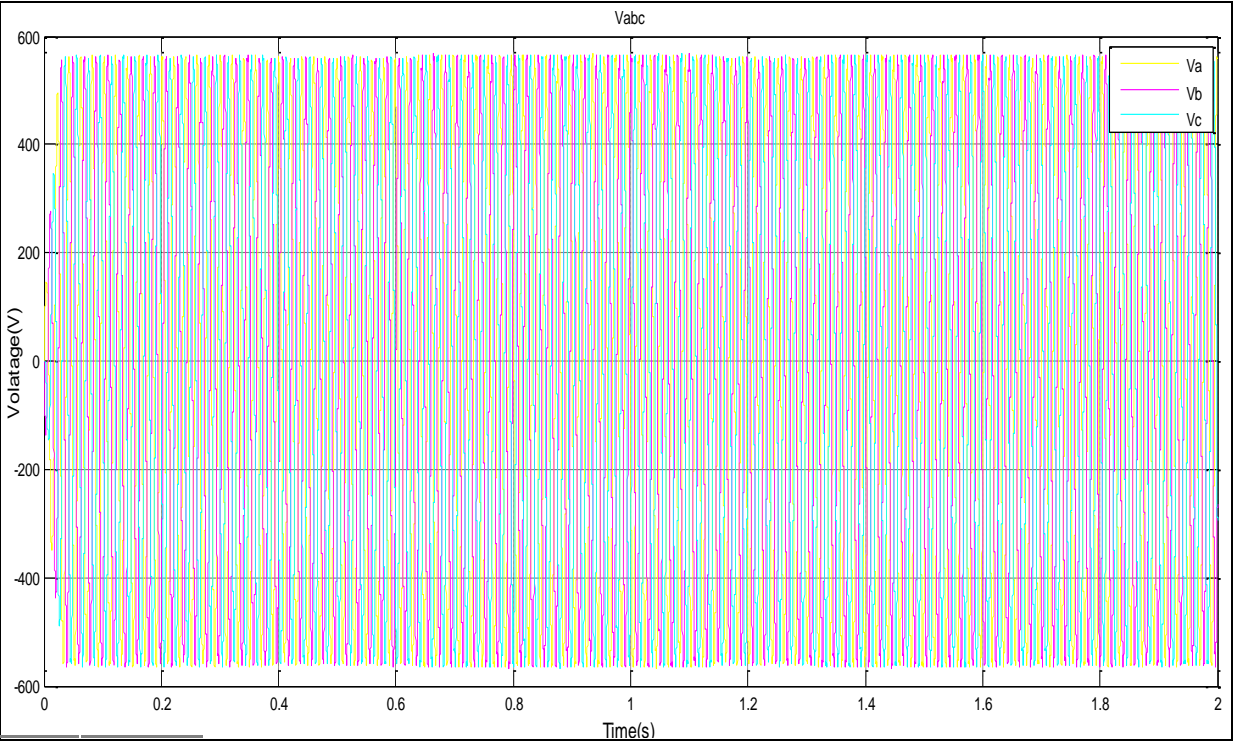


Figure 5.44: Output voltage waveform under droop control

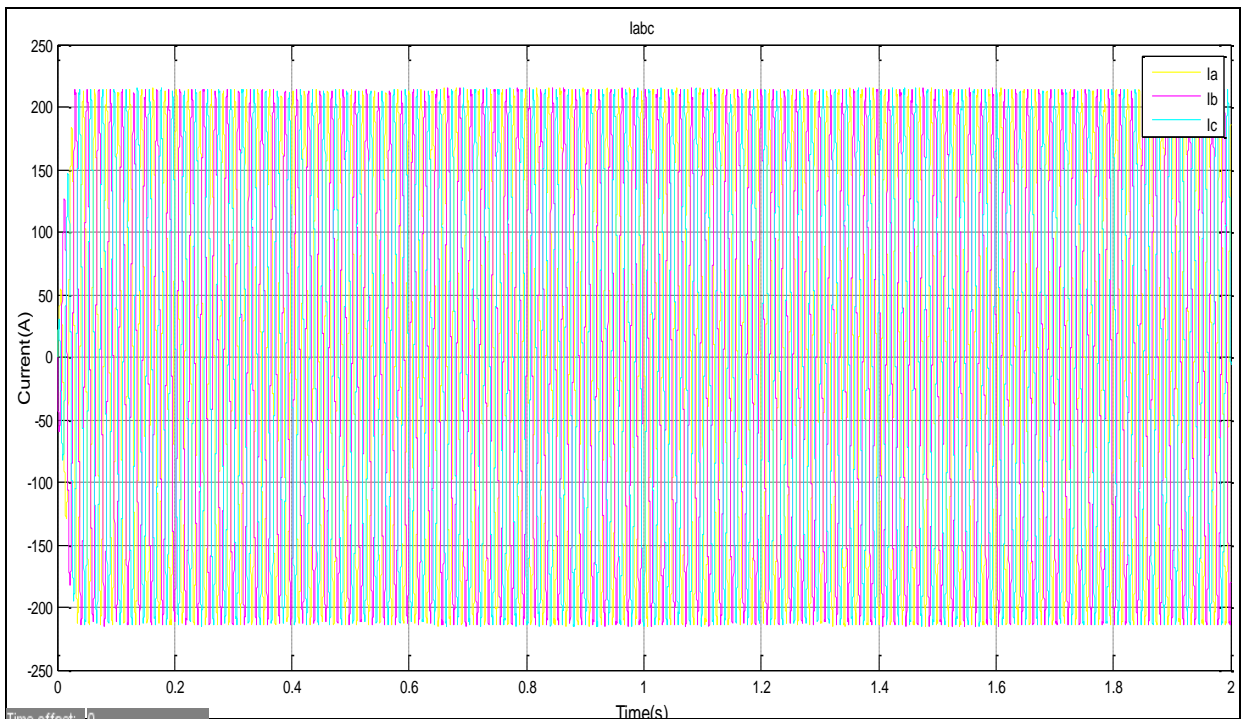


Figure 5.45: Output current waveform under droop control

5.7 Simulation result of the system incorporating the energy management system (EMS) algorithm

The EMS monitors and optimises the operation of a microgrid system; it can be used to improve the results of performances obtained in Sections 5.4, 5.5 and 5.6 above.

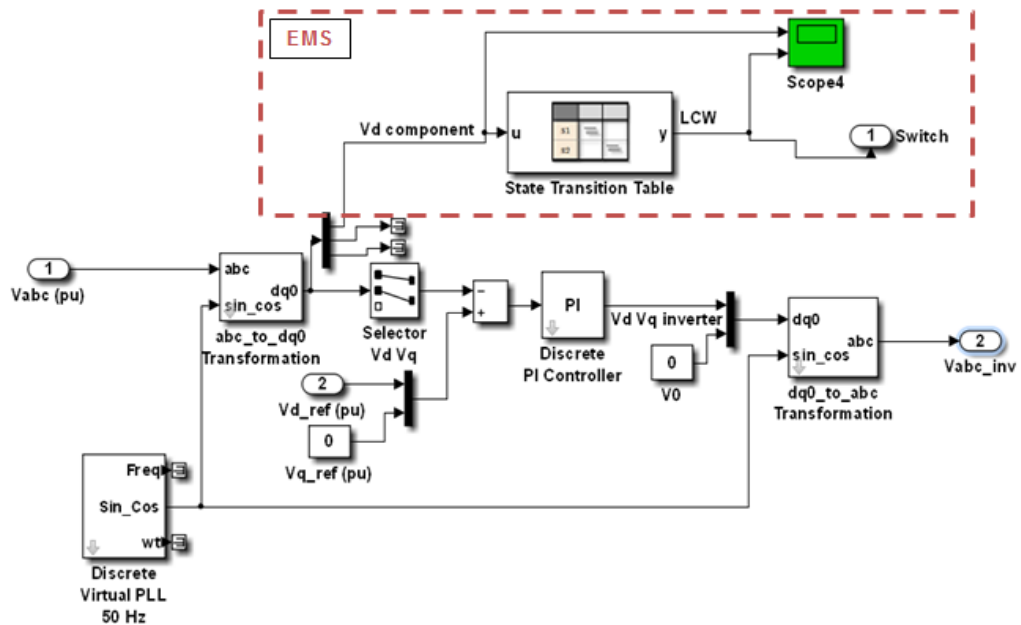


Figure 5.46: EMS integrated with a dq0 transformation + PI controller

In addition an EMS, the system incorporated a dq0 transformation + PI controller; this is shown in figure 5.46 above. Also, the system has the capability that non-sensitive loads can be connected or disconnected, in accordance with the input power capacity - for more details refer to Section 4.5.

5.7.1 Inverter control operating with sensitive load power, but without activating the EMS of the system

Initially the sensitive load power is connected to the system and the non-sensitive load is not connected - see Appendix 4. The operation of the system subject to an input voltage variation from 500 to 668 V, was analysed. The LCS monitors the system through the V_d component of the output voltage, by determining whether or not the non-sensitive load must be connected to the system through the breaker. However, the breaker is omitted and the action of the LCS does not have any effect on the system.

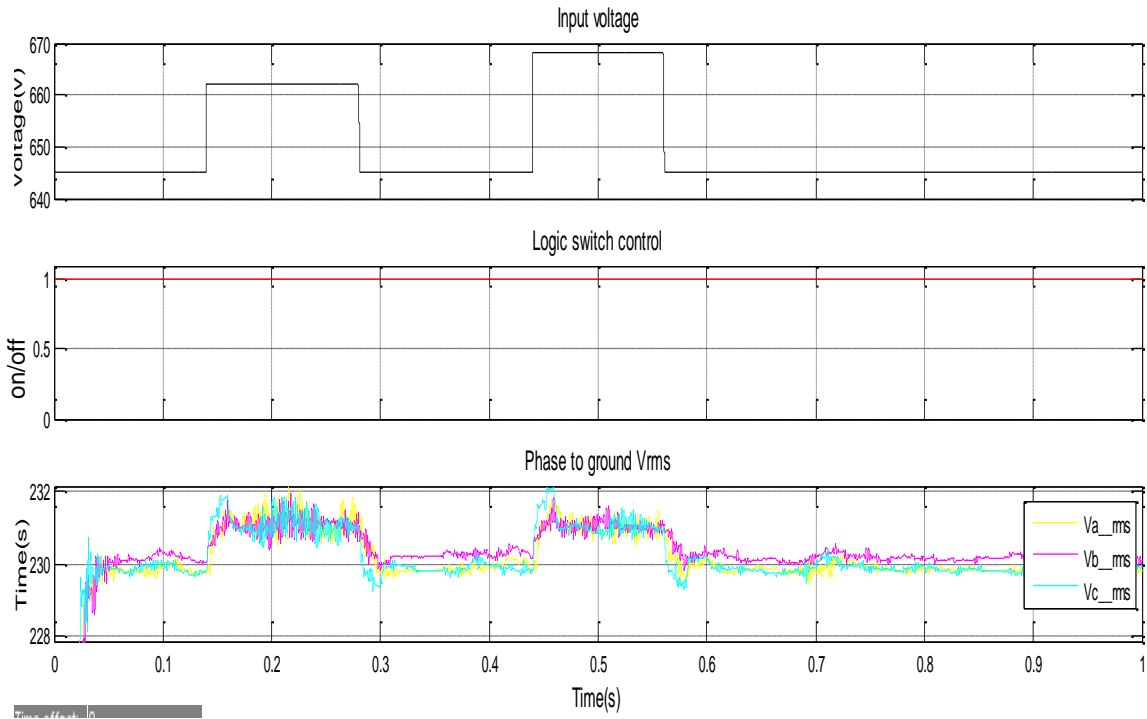


Figure 5.47: input voltage, logic activating switch and phase-to-ground V_{rms} without activating the EMS of the simulated microgrid

Figure 5.47 above shows the input voltage, logic control switch, and phase-to-ground V_{rms} . The intervals in which the input amplitude voltage changes, are 140 to 280 ms and 440 ms to 560 ms; the corresponding input voltages are 661 and 669 V respectively. During the rest of the time intervals, that is from 0 to 140 ms, 280 to 440 ms, 560 to 1000 ms, the input voltage is 645 V. The LCS is **on** throughout the full simulation time. The nominal phase-to-ground V_{rms} is 230 V

throughout the simulation, except in the intervals 140 to 280 ms and 440 ms to 560 ms, which have voltages of 661 and 669 V respectively and the phase-to-ground V_{rms} , is 231 V.

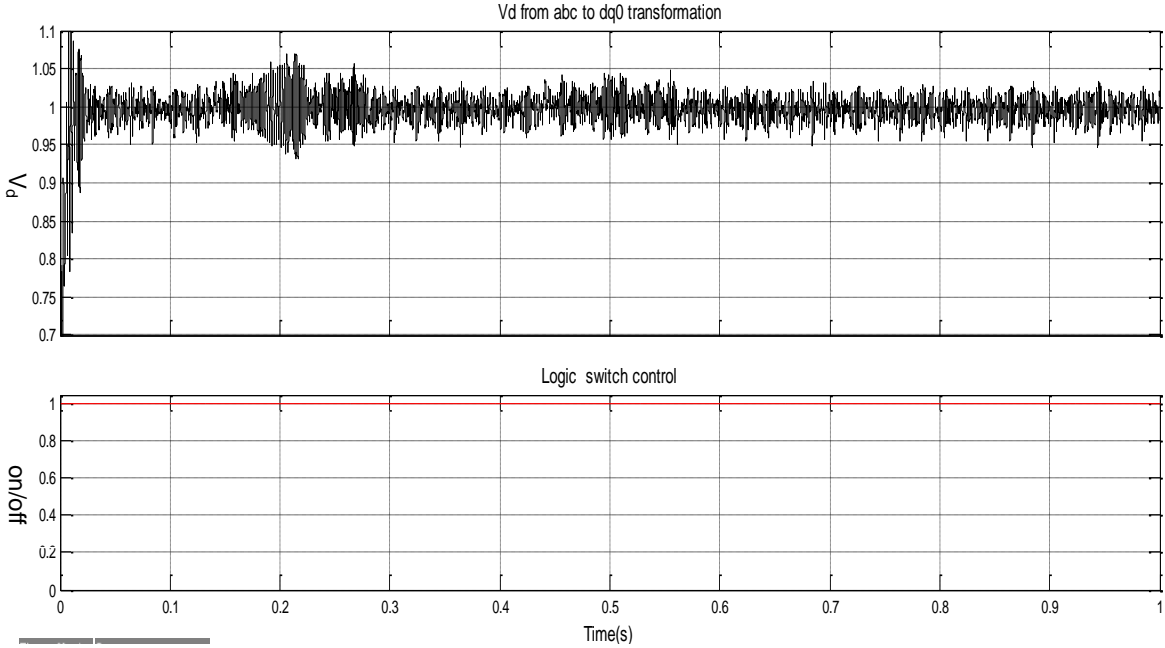


Figure 5.48: The V_d component of the sensitive load without activating the EMS of the simulated microgrid

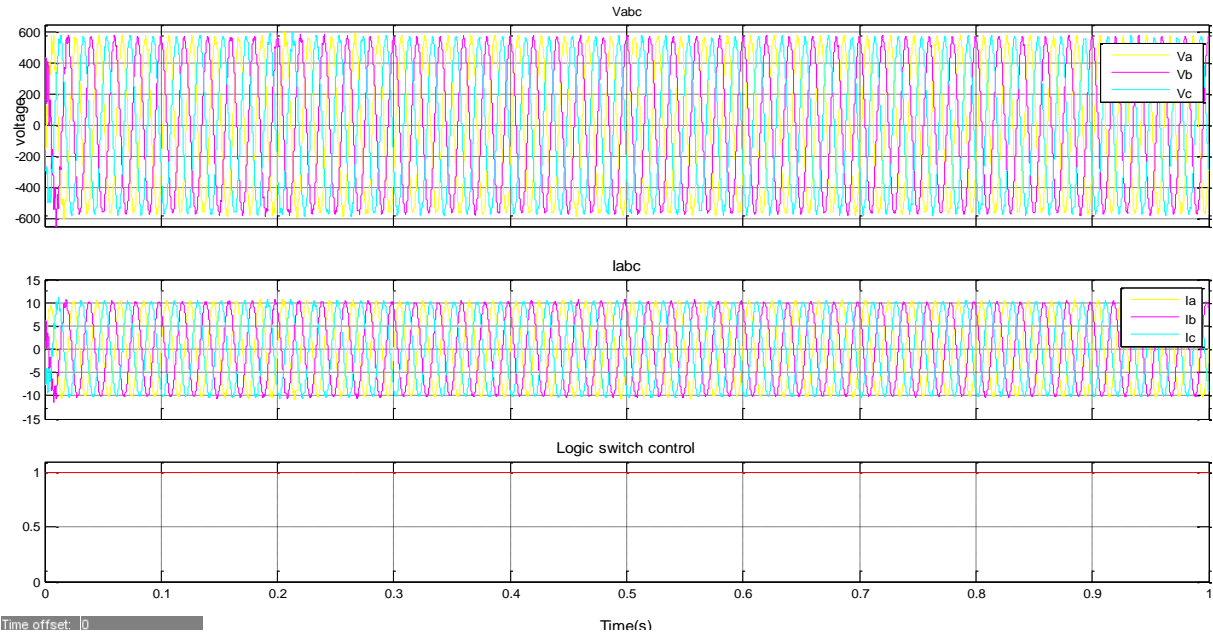


Figure 5.49: Peak output voltage and current waveforms without activating the EMS of the simulated microgrid

In figure 5.48 above, the V_d component from the dq0 transformation fluctuated between 0.98 and 1.01. This explains the stability of the phase-to-phase V_{rms} , as well as the peak output voltage waveform, despite the increases of input voltage to 661 V and 669 V. Figure 5.49 shows stable output peak voltage as 563 VAC, and current waveforms as 12 A.

5.7.2 Inverter control operating with sensitive and non-sensitive loads, but without activating the EMS of the simulated microgrid

Sensitive and non-sensitive load power are both permanently connected to the system and operate together, without an active LCS in the system - see appendix 5. Normally the LCS monitors the system through the V_d component, by determining whether or not the non-sensitive load is connected to the system through the breaker. However, the breaker is omitted and the action of the LCS does not have any effect on the system. Figure 5.50 below shows the input voltage, logic control switch, and phase-to-ground V_{rms} , each as a function of time. The intervals in which the input amplitude voltage changes, are 140 to 280 ms and 430 ms to 570 ms. The corresponding input voltages are 661 and 668 V respectively. During the remainder of the intervals 0 to 140 ms, 280 to 440 ms, 560 to 1000 ms, the input voltage is 645 V.

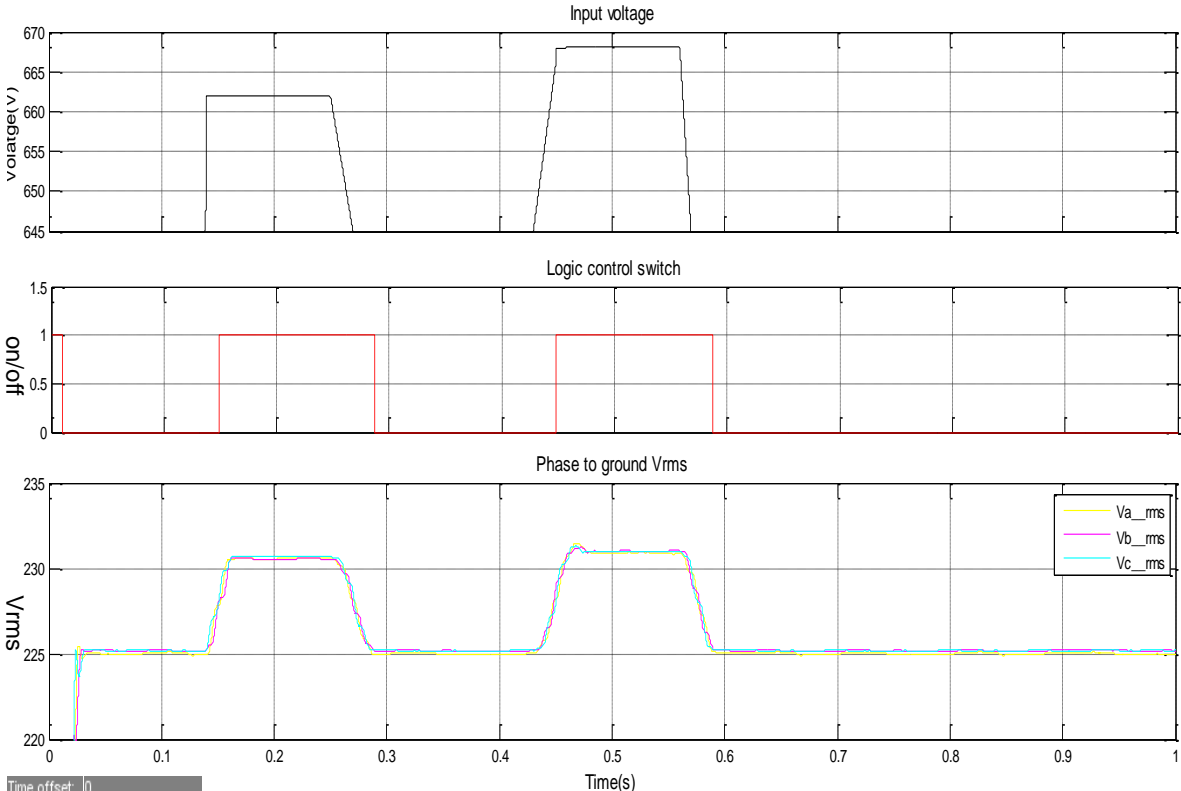


Figure 5.50: input voltage, logic control switch and phase to ground V_{rms} of the total load without active EMS of the simulated microgrid

For the simulation run illustrated by figure 5.50, the changes in the nominal voltage phase-to-ground occur at the intervals 140 to 280 ms and 440 ms to 560 ms when the LCS is switched to the **on** state. The corresponding voltage at the respective time intervals is 231V. For the other intervals, that is when the LCS is **off**, the phase-to-ground V_{rms} drops to 225 V when the voltage is 645 V; compare this to

figure 5.47 where the phase-to-ground is 230V. This difference is due to the low input power capacity that drives the load power and causes instability to the phase-to-phase V_{rms} .

Figure 5.51 below shows that the V_d component of the dq0 transformation is dependent on the input voltage. During the time intervals from 140 to 280 ms and 440 ms to 560 ms, the value of the V_d component varies between 0.99 and 1.01. For the other time intervals from 0 to 140 ms, 280 to 440 ms, 560 to 1000 ms, the V_d component lies within the band 0.96 to 0.98; compare this to figure 5.48 which shows the V_d component fluctuating between 0.98 and 1.01 during the duration of the simulation. The difference in V_d component values is due to the low input power capacity that drives the load power and causes instability of the d component. Figure 5.52 shows the peak output voltage waveform. When the load power is greater than the input voltage, it causes a slight voltage sag of the output voltage.

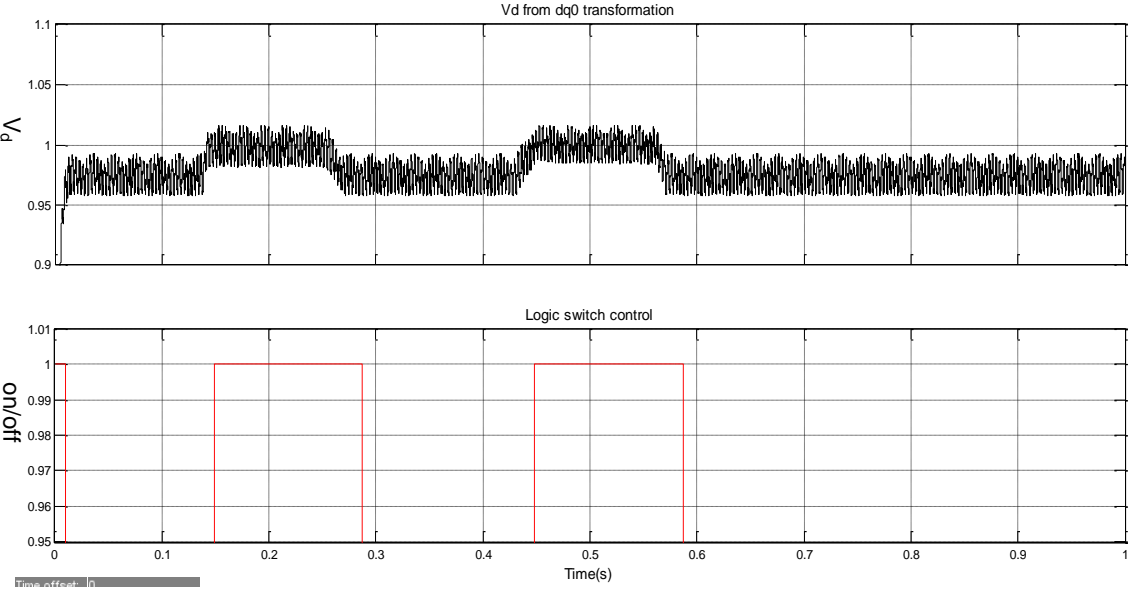


Figure 5.51: The V_d component in the total load without activating the EMS of the simulated microgrid

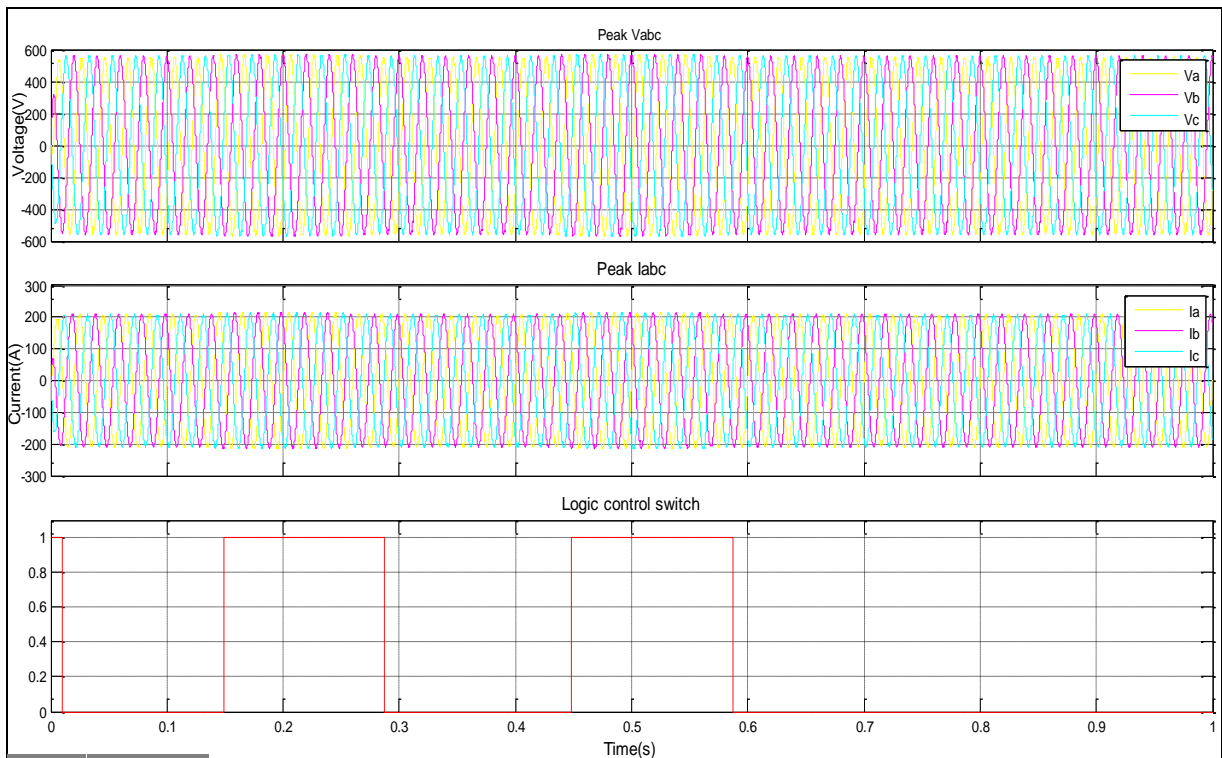


Figure 5.52: Peak output voltage and current of the loads without an active EMS of the simulated microgrid

5.7.3 Inverter control operating with sensitive and non-sensitive loads and the EMS of the system activated

The sensitive and the non-sensitive loads are both available within the system. The sensitive load power is permanently connected to the system, but the non-sensitive load power is initially disconnected from the system - see Appendix 6, however, the connectivity of the non-sensitive load depends on the magnitude of the input voltage. The LCS monitors the system through the V_d component by determining whether or not the non-sensitive load will be connected to the system. This method tends to maintain the phase-to-ground V_{rms} at 230 V, which implies a peak output voltage waveform of 563 V. When, the load power is greater than the input power, the output voltage sags for a few milliseconds. Figure 5.53 above shows the input voltage, Logic control switch and phase to ground V_{rms} . The intervals in which the input amplitude voltage changes, are 140 to 280 ms and 440 ms to 560 ms, the input voltage is respectively a voltage of 662 and 668 V. The rest of the intervals 0 to 140 ms, 280 to 440 ms, 560 to 1000 ms, the input voltage is 646 V.

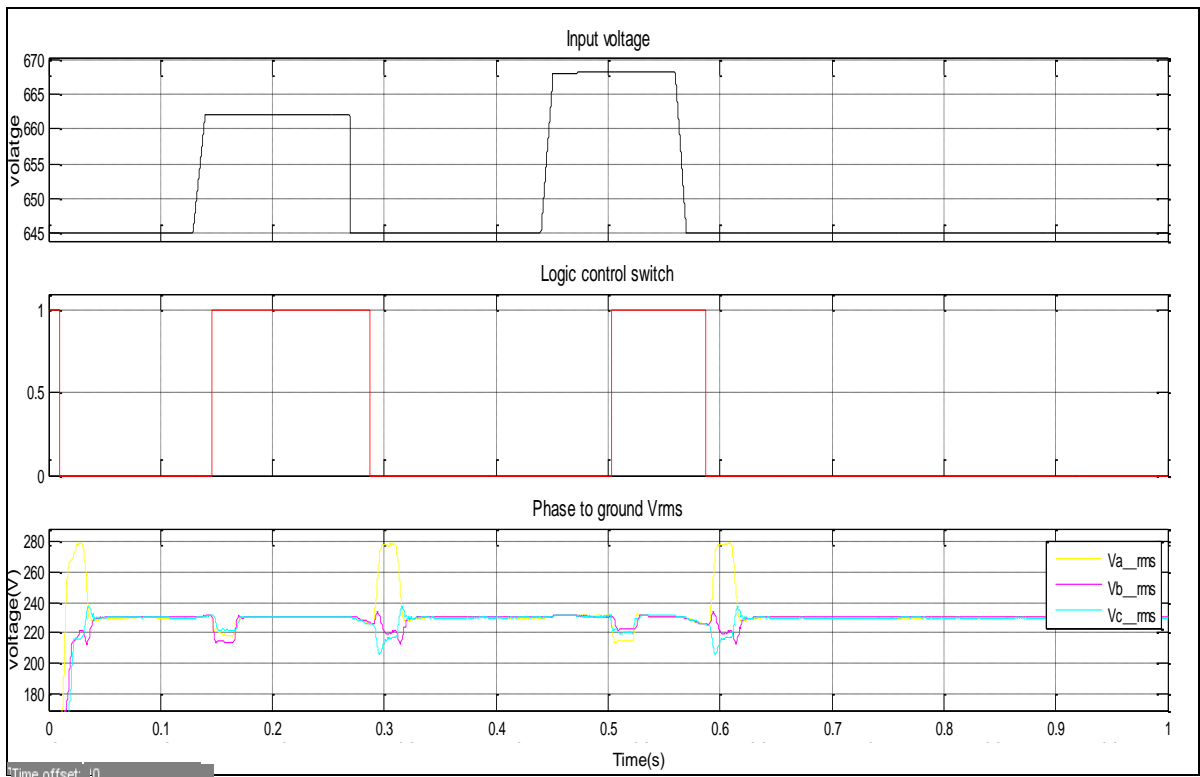


Figure 5.53: Input voltage, logic control switch and phase to ground V_{rms} of the total load with activation of the EMS of the simulated microgrid

The LCS is **on** during the time interval from 130 to 270 ms and 440 ms to 560 ms and it is **off** for the rest of the intervals. The nominal phase-to-ground V_{rms} is maintained at 230 V, the simulation shown on the graph in Figure 5.53 through the simulation except while the LCS changes its state, which occurred at 140 ms, 280 ms, 440 ms and 560 ms. The EMS improved the phase-to-ground V_{rms} value of the system by maintaining it at 230 V, despite the input voltage variation compared to figure 5.50 above where the phase-to-ground V_{rms} dropped considerably. Here, the EMS switches **on** and **off** the non-sensitive load depending on the magnitude of the input power, so that it maintains the V_{rms} value to 230 V except for minor oscillations at the time of LCS switching.

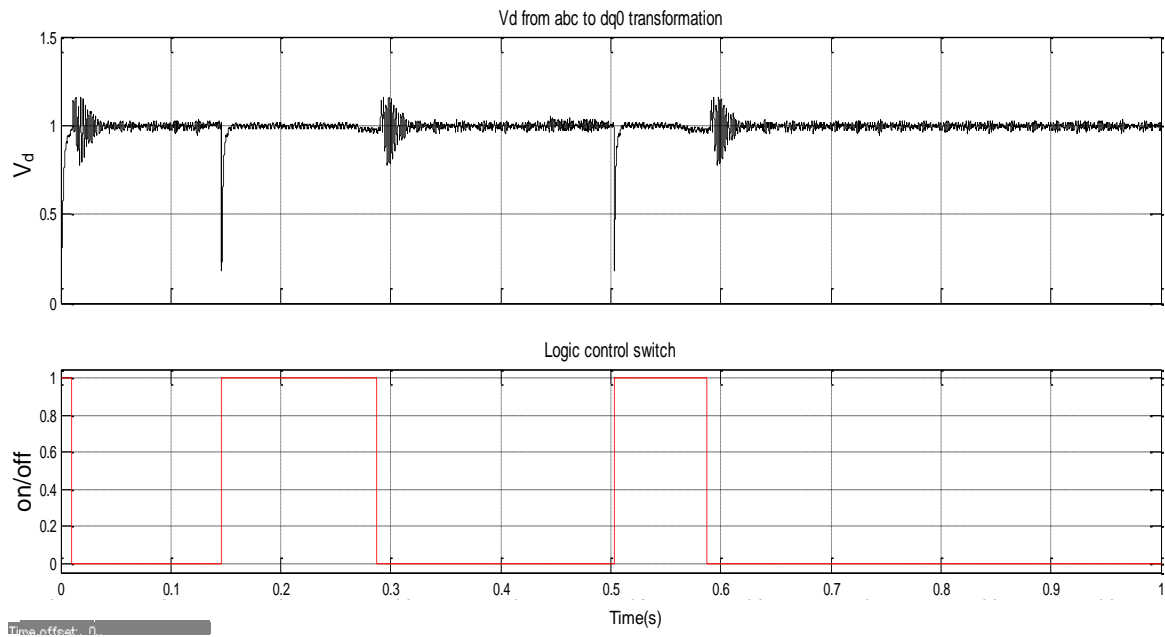


Figure 5.54: The V_d component of the dq0 transformation in the total load with activation of the EMS of the simulated microgrid

Figure 5.54 shows that the V_d component of the dq0 transformation is maintained at a constant value, despite the input voltage variation. The V_d component value of the transformation ranges between 0.99 and 1.01 which is similar to the range depicted in Figure 5.48, but different from that shown in

figure 5.51. In this case, the non-sensitive load is added to the system by the logic control switch, when the input voltage available can handle more loads. When the input voltage cannot handle an additional load, the logic control switch is activated to disconnect the non-sensitive load. Initially, both loads are connected to the system but, the LCS removes the non-sensitive load to keep the phase-to-ground V_{rms} at 230 V for each phase. Just after the non-sensitive load is removed at 10 ms, there is an overshoot during the transient period when the PI controller is applied to change the m_a value to effectively regulate the V_{rms} and the voltage at the inverter terminal. So, in the remaining simulation time the non-sensitive loads are connected during the intervals 140 to 280 ms and and 510 to 560 ms. When, the non-sensitive load is added it causes a short and a quick voltage drop before the PI controller controls it. This explains the stability of the phase-to-ground V_{rms} as well as the peak output voltage waveform, because the EMS plays a bigger role.

Figure 5.55 presents the peak output voltage waveforms of the inverter terminals. Throughout the simulation, the output voltage presents stability except when the logic control switch changes its state.

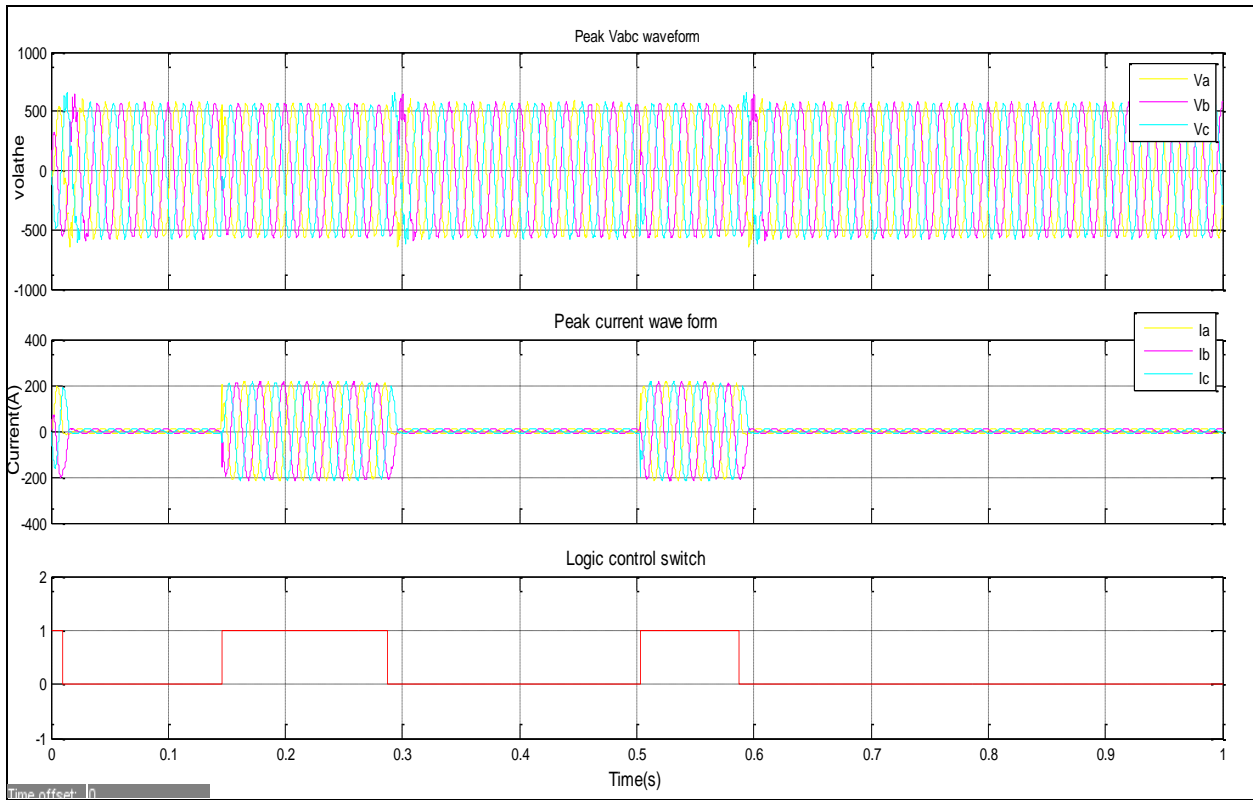


Figure 5.55: Peak output voltage and current in the total load with activation of the EMS of the simulated microgrid

When the LCS is switched the output voltage presents some voltage sags and voltage changes respectively at time 140 ms, 510 ms and at 140 ms and 510 ms. The peak current is very low at the time intervals corresponding to the **off** state of the logic control switch and the peak current is 220 A which corresponds to the **on** state of the logic control switch.

5.8 Conclusion

This chapter reported on the operation of the designed models of a PV farm and microgrid. The results obtained from simulations applied to the models, correlate well with the calculated results from the design. Different inverter controls were compared in order to determine the best controller at the inverter terminal. The simulation results showed that both droop control and the dq0 reference frame + PI controller are much better than a PI controller on its own. These results also compared well with those found in the literature. The results were further improved

with an EMS in order to maintain the output voltage of the microgrid; this was attained by switching **on** and **off** certain loads upon considering the input power.

Chapter 6 : CONCLUSION AND FUTURE WORK

6.1 Conclusion

This research was carried out because microgrid operation is uncertain in terms of resources available, when using distributed generation. In addition, the output voltage of a microgrid depends heavily on weather conditions. Systematic control and stability of the system at the inverter, interfacing between the DG infrastructure and the rest of the microgrid system, was also analysed.

In conclusion, the research work explored the modelling of a practical interface between DG based on photovoltaics and the rest of the microgrid, within the MATLAB/SIMULINK simulation environment. The maximum capacity of the DG system was rated at 1 MW. The work presented, focused on the operation of a microgrid in stand-alone mode. The aim was to maintain the power generated equal to the power required by the loads, since irregularity in the production of the renewable energy and irregularity in consumption lead to frequency and voltage fluctuations. To achieve this aim load balancing was found to be essential for the functionality of the power system, by making sure that no overloading occurs during the operation of the microgrid system.

Additionally, a stable system with different control mechanisms and subject to various loads and resource conditions, was studied.

- The Stateflow logical programming environment, a part of MATLAB, was used to develop an algorithm for load balancing. The environment made it possible to model complex algorithms by combining graphical and tabular representations. This facilitated sequential decision making logic, based on state transition diagrams, flow charts, state transition tables, and truth tables.
- The use of an LCS is one of the ways of continuously monitoring and adjusting the load through breakers, taking account of the power generated by the DG-system. It is a good alternative to load balancing when considering a cluster of villages in a rural area dependent on a microgrid in stand-alone mode.
- In a microgrid serving a cluster of villages, the sum of sensitive and non-sensitive load is 5 kW and 100 kW respectively. Depending on the power, an LCS efficiently balanced the loads; however, when the power was less than the minimum load, overloading occurred.

The dq0 transformation + PI controller presents a better result than PI controller alone. Droop control gives a much better result than the two aforementioned controllers.

6.2 Future work

System load balancing could be improved by taking account of the expected solar radiation from solar forecast estimation information. So that, a storage system can be designed for the entire autonomous microgrid in order to manage power.

In addition, incorporating the results of smart metering from each consumer to collect and process information on patterns in the use of electricity over time. Such information can then be taken account of and incorporated into the distribution control to improve the efficiency of electricity use. Possibly you could find some more benefits of this monitoring process.

REFERENCES

- Abdullah, M.A., Yatim, A.H.M. & Tan, C.W. 2011. A study of maximum power point tracking algorithms for wind energy system. In *2011 IEEE First Conference on Clean Energy and Technology (CET)*. 2011 IEEE First Conference on Clean Energy and Technology (CET). 321–326.
- Ahmad, G.E., Hussein, H.M.S. & El-Ghetany, H.H. 2003. Theoretical analysis and experimental verification of PV modules. *Renewable Energy*, 28(8): 1159–1168.
- Ahmed, K.H., Finney, S.J. & Williams, B.W. 2007. Passive Filter Design for Three-Phase Inverter Interfacing in Distributed Generation. In *Compatibility in Power Electronics, 2007. CPE '07*. Compatibility in Power Electronics, 2007. CPE '07. 1–9.
- Alatise, O.M., Kwa, K.S.K., Olsen, S.H. & O'Neill, A.G. 2009. Improved Analog Performance in Strained-Si MOSFETs Using the Thickness of the Silicon Germanium Strain-Relaxed Buffer as a Design Parameter. *IEEE Transactions on Electron Devices*, 56(12): 3041–3048.
- Alley, R.B., Marotzke, J., Nordhaus, W.D., Overpeck, J.T., Peteet, D.M., Pielke, R.A., Pierrehumbert, R.T., Rhines, P.B., Stocker, T.F., Talley, L.D. & Wallace, J.M. 2003. Abrupt Climate Change. *Science*, 299(5615): 2005–2010.
- Alonso, R., Ibaez, P., Martinez, V., Roman, E. & Sanz, A. 2009. An innovative perturb, observe and check algorithm for partially shaded PV systems. In *13th European Conference on Power Electronics and Applications, 2009. EPE '09*. 13th European Conference on Power Electronics and Applications, 2009. EPE '09. 1–8.
- Anon. 2003. IEEE Standard for Interconnecting Distributed Resources with Electric Power Systems. *IEEE Std 1547-2003*: 1–28.
- Anwar, A. & Pota, H.R. 2011. Loss reduction of power distribution network using optimum size and location of distributed generation. In *Universities Power Engineering Conference (AUPEC), 2011 21st Australasian*. Universities Power Engineering Conference (AUPEC), 2011 21st Australasian. 1–6.
- Applewhite, A. 2002. Africa becomes electric. *IEEE Spectrum*, 39(8): 54–56.
- Asbafkan, A., Mirzaeeian, B., Niroomand, M. & Zarchi, H.A. 2013. Frequency adaptive repetitive control of grid connected inverter for wind turbine applications. In *2013 21st Iranian Conference on Electrical Engineering (ICEE)*. 2013 21st Iranian Conference on Electrical Engineering (ICEE). 1–6.
- Ayob, S.M., Salam, Z., Azli, N.A. & Elbuluk, M.E. 2009. Control of a Single Phase Inverter Using Fuzzy Logic. In *IEEE Industry Applications Society Annual Meeting, 2009. IAS 2009*. IEEE Industry Applications Society Annual Meeting, 2009. IAS 2009. 1–6.
- Azevedo, G.M.S., Bradaschia, F., Cavalcanti, M.C., Neves, F.A.S., Rocabert, J. & Rodriguez, P. 2011. Safe transient operation of microgrids based on master-slave configuration. In *2011 IEEE Energy Conversion Congress and Exposition (ECCE)*. 2011 IEEE Energy Conversion Congress and Exposition (ECCE). 2191–2195.

Azmi, S.A., Adam, G.P., Ahmed, K.H., Finney, S.J. & Williams, B.W. 2013. Grid Interfacing of Multimegawatt Photovoltaic Inverters. *IEEE Transactions on Power Electronics*, 28(6): 2770–2784.

Baran, M.E. & Mahajan, N.R. 2003. DC distribution for industrial systems: opportunities and challenges. *IEEE Transactions on Industry Applications*, 39(6): 1596–1601.

Barklund, E., Pogaku, N., Prodanovic, M., Hernandez-Aramburo, C. & Green, T.C. 2008. Energy Management in Autonomous Microgrid Using Stability-Constrained Droop Control of Inverters. *IEEE Transactions on Power Electronics*, 23(5): 2346–2352.

Basic, D., Ramsden, V.S. & Muttik, P.K. 2001. Harmonic filtering of high-power 12-pulse rectifier loads with a selective hybrid filter system. *IEEE Transactions on Industrial Electronics*, 48(6): 1118–1127.

Bekiarov, S.B. & Emadi, A. 2002. Uninterruptible power supplies: classification, operation, dynamics, and control. In *Seventeenth Annual IEEE Applied Power Electronics Conference and Exposition, 2002. APEC 2002*. Seventeenth Annual IEEE Applied Power Electronics Conference and Exposition, 2002. APEC 2002. 597–604 vol.1.

Bhadoria, V., S., Pal, N., S. & Shrivastava, V. 2014. Review of DG definitions and its impact. *Scribd*. <https://www.scribd.com/doc/217615790/Review-of-DG-definitions-and-its-impact> 29 October 2014.

Bindner, H. & Lundsager, P. 2002. Integration of wind power in the power system. In *IECON 02 [Industrial Electronics Society, IEEE 2002 28th Annual Conference of the]*. IECON 02 [Industrial Electronics Society, IEEE 2002 28th Annual Conference of the]. 3309–3316 vol.4.

Blaabjerg, F., Chen, Z. & Kjaer, S.B. 2004. Power electronics as efficient interface in dispersed power generation systems. *IEEE Transactions on Power Electronics*, 19(5): 1184–1194.

Blaabjerg, F., Teodorescu, R., Liserre, M. & Timbus, A.V. 2006. Overview of Control and Grid Synchronization for Distributed Power Generation Systems. *IEEE Transactions on Industrial Electronics*, 53(5): 1398–1409.

Bose, B.K. 2010. Global Warming: Energy, Environmental Pollution, and the Impact of Power Electronics. *IEEE Industrial Electronics Magazine*, 4(1): 6–17.

Bose, B.K. 2009. Power Electronics and Motor Drives Recent Progress and Perspective. *IEEE Transactions on Industrial Electronics*, 56(2): 581–588.

De Brabandere, K., Bolsens, B., Van den Keybus, J., Woyte, A., Driesen, J. & Belmans, R. 2007. A Voltage and Frequency Droop Control Method for Parallel Inverters. *IEEE Transactions on Power Electronics*, 22(4): 1107–1115.

Brod, D.M. & Novotny, D.W. 1985. Current Control of VSI-PWM Inverters. *IEEE Transactions on Industry Applications*, IA-21(3): 562–570.

Buritica-Arboleda, C.I. & Alvarez-Bel, C. 2011. Decentralized energy: Key to improve the electric supply security. In *2011 IEEE PES Conference on Innovative Smart Grid Technologies (ISGT Latin America)*. 2011 IEEE PES Conference on Innovative Smart Grid Technologies (ISGT Latin America). 1–6.

- Cai, H. & Qian, X. 2008. Uniform modulation principle and ideal operation status of parallel inverters. In *International Conference on Electrical Machines and Systems, 2008. ICEMS 2008*. International Conference on Electrical Machines and Systems, 2008. ICEMS 2008. 1747–1751.
- Carrasco, J.M., Franquelo, L.G., Bialasiewicz, J.T., Galvan, E., Guisado, R.C.P., Prats, M.A.M., Leon, J.I. & Moreno-Alfonso, N. 2006. Power-Electronic Systems for the Grid Integration of Renewable Energy Sources: A Survey. *IEEE Transactions on Industrial Electronics*, 53(4): 1002–1016.
- Chakravorty, M. & Das, D. 2001. Voltage stability analysis of radial distribution networks. *International Journal of Electrical Power & Energy Systems*, 23(2): 129–135.
- Chandorkar, M.C., Divan, D.M. & Adapa, R. 1993. Control of parallel connected inverters in standalone AC supply systems. *IEEE Transactions on Industry Applications*, 29(1): 136–143.
- Chandorkar, M.C., Divan, D.M., Hu, Y. & Banerjee, B. 1994. Novel architectures and control for distributed UPS systems. In *Applied Power Electronics Conference and Exposition, 1994. APEC '94. Conference Proceedings 1994., Ninth Annual*. Applied Power Electronics Conference and Exposition, 1994. APEC '94. Conference Proceedings 1994., Ninth Annual. 683–689 vol.2.
- Chan, W.L., So, A.T.P. & Lai, L.L. 2000. Harmonics load signature recognition by wavelets transforms. In *International Conference on Electric Utility Deregulation and Restructuring and Power Technologies, 2000. Proceedings. DRPT 2000*. International Conference on Electric Utility Deregulation and Restructuring and Power Technologies, 2000. Proceedings. DRPT 2000. 666–671.
- Chel, A., Tiwari, G.N. & Chandra, A. 2009. Simplified method of sizing and life cycle cost assessment of building integrated photovoltaic system. *Energy and Buildings*, 41(11): 1172–1180.
- Chen, C.-L., Wang, Y., Lai, J.-S., Lee, Y.-S. & Martin, D. 2010. Design of Parallel Inverters for Smooth Mode Transfer Microgrid Applications. *IEEE Transactions on Power Electronics*, 25(1): 6–15.
- Cheng, P.-T., Chen, C.-A., Lee, T.-L. & Kuo, S.-Y. 2009. A Cooperative Imbalance Compensation Method for Distributed-Generation Interface Converters. *IEEE Transactions on Industry Applications*, 45(2): 805–815.
- Chen, H.F. & Klemm, H. 2011. Environmental Barrier Coatings for Silicon Nitride. *Key Engineering Materials*, 484: 139–144.
- Chen, J.-F. & Chu, C.-L. 1995. Combination voltage-controlled and current-controlled PWM inverters for UPS parallel operation. *IEEE Transactions on Power Electronics*, 10(5): 547–558.
- Chen, Y.-K., Wu, T.-F., Wu, Y.-E. & Ku, C.-P. 2001. A current-sharing control strategy for paralleled multi-inverter systems using microprocessor-based robust control. In *TENCON 2001. Proceedings of IEEE Region 10 International Conference on Electrical and Electronic Technology*. TENCON 2001. Proceedings of IEEE Region 10 International Conference on Electrical and Electronic Technology. 647–653 vol.2.
- Chen, Z. & Blaabjerg, F. 2006. Wind Energy: The World's Fastest Growing Energy Source. *IEEE Power Electronics Society Newsletter*, 18(3): 15–19.

Chiang, S.J., Lin, C.-H. & Yen, C.Y. 2004. Current limitation control technique for parallel operation of UPS inverters. In *Power Electronics Specialists Conference, 2004. PESC 04. 2004 IEEE 35th Annual*. Power Electronics Specialists Conference, 2004. PESC 04. 2004 IEEE 35th Annual. 1922–1926 Vol.3.

Chiang, S.J., Yen, C.Y. & Chang, K.T. 2001. A multimodule parallelable series-connected PWM voltage regulator. *IEEE Transactions on Industrial Electronics*, 48(3): 506–516.

Chowdhury, S., Chowdhury, S.P. & Crossley, P. 2009. *Microgrids and Active Distribution Networks*. Stevenage: The Institution of Engineering and Technology.

Chowdhury, S., Chowdhury, S.P., Taylor, G.A. & Song, Y.-H. 2008. Mathematical modelling and performance evaluation of a stand-alone polycrystalline PV plant with MPPT facility. In *2008 IEEE Power and Energy Society General Meeting - Conversion and Delivery of Electrical Energy in the 21st Century*. 2008 IEEE Power and Energy Society General Meeting - Conversion and Delivery of Electrical Energy in the 21st Century. 1–7.

Colet-Subirachs, A., Ruiz-Alvarez, A., Gomis-Bellmunt, O., Alvarez-Cuevas-Figuerola, F. & Sudria-Andreu, A. 2012. Centralized and Distributed Active and Reactive Power Control of a Utility Connected Microgrid Using IEC61850. *IEEE Systems Journal*, 6(1): 58–67.

Cortes, P., Kazmierkowski, M.P., Kennel, R.M., Quevedo, D.E. & Rodriguez, J. 2008. Predictive Control in Power Electronics and Drives. *IEEE Transactions on Industrial Electronics*, 55(12): 4312–4324.

De, D. & Ramanarayanan, V. 2010. Decentralized Parallel Operation of Inverters Sharing Unbalanced and Nonlinear Loads. *IEEE Transactions on Power Electronics*, 25(12): 3015–3025.

Delghavi, M.B. & Yazdani, A. 2012. A Unified Control Strategy for Electronically Interfaced Distributed Energy Resources. *IEEE Transactions on Power Delivery*, 27(2): 803–812.

Descampe, A., Devaux, F.-O., Rouvroy, G., Legat, J., Quisquater, J.-J. & Macq, B. 2006. A Flexible Hardware JPEG 2000 Decoder for Digital Cinema. *IEEE Transactions on Circuits and Systems for Video Technology*, 16(11): 1397–1410.

Dimeas, A.L. & Hatziargyriou, N.D. 2005. Operation of a Multiagent System for Microgrid Control. *IEEE Transactions on Power Systems*, 20(3): 1447–1455.

Dolman, K. & Peters, B. 2003. The signification of micro-turbines as CHP (combined heat power system). In *Modern Techniques and Technologies, 2003. MTT 2003. Proceedings of the 9th International Scientific and Practical Conference of Students, Post-graduates and Young Scientists*. Modern Techniques and Technologies, 2003. MTT 2003. Proceedings of the 9th International Scientific and Practical Conference of Students, Post-graduates and Young Scientists. 20–22.

Dou, C., Jin, S.-J., Jiang, G.-T. & Bo, Z.-Q. 2009. Multi-Agent Based Control Framework for Microgrids. In *Power and Energy Engineering Conference, 2009. APPEEC 2009. Asia-Pacific*. Power and Energy Engineering Conference, 2009. APPEEC 2009. Asia-Pacific. 1–4.

El-Habrouk, M., Darwish, M.K. & Mehta, P. 2000. Active power filters: a review. *Electric Power Applications, IEE Proceedings -*, 147(5): 403–413.

El-Hefnawi, S.H. 1997. Digital firing and digital control of a photovoltaic inverter. *Renewable Energy*, 12(3): 315–320.

El Khateb, A., Rahim, N.A., Selvaraj, J. & Uddin, M.N. 2013. Maximum power point tracking of single-ended primary-inductor converter employing a novel optimisation technique for proportional-integral-derivative controller. *IET Power Electronics*, 6(6): 1111–1121.

Eltawil, M.A. & Zhao, Z. 2010. Grid-connected photovoltaic power systems: Technical and potential problems—A review. *Renewable and Sustainable Energy Reviews*, 14(1): 112–129.

Engery. 2014. Estimating Appliance and Home Electronic Energy Use. *Energy.gov*. <http://energy.gov/energysaver/articles/estimating-appliance-and-home-electronic-energy-use> 26 October 2014.

Erdinc, O. & Uzunoglu, M. 2012. Optimum design of hybrid renewable energy systems: Overview of different approaches. *Renewable and Sustainable Energy Reviews*, 16(3): 1412–1425.

Farret, F.A. & Simões, M.G. 2006. *Integration of Alternative Sources of Energy*. 1 edition. Piscataway : Hoboken, N.J: Wiley-IEEE Press.

Femia, N., Petrone, G., Spagnuolo, G. & Vitelli, M. 2009. A Technique for Improving P MPPT Performances of Double-Stage Grid-Connected Photovoltaic Systems. *IEEE Transactions on Industrial Electronics*, 56(11): 4473–4482.

Femia, N., Petrone, G., Spagnuolo, G. & Vitelli, M. 2005. Optimization of perturb and observe maximum power point tracking method. *IEEE Transactions on Power Electronics*, 20(4): 963–973.

Firouz, A. 2010. Lecture #3 Centralized Electric Power Systems. <http://fgamedia.org/faculty/rdcormia/ENGR40/lesson03/Lecture-3.pdf> 12 December 2013.

Da Fonseca, A.L.A., Lambert, J.A., Monteiro, R.V.A., de Vasconcellos, A.B. & Carvalho, B.C. 2014. Behavioral and statistical analysis of total harmonic distortion input frequency converter of a triggering an industrial fan: A case study. In *2014 IEEE 16th International Conference on Harmonics and Quality of Power (ICHQP)*. 2014 IEEE 16th International Conference on Harmonics and Quality of Power (ICHQP). 152–156.

Georgakis, D., Papathanassiou, S., Hatziaargyriou, N., Engler, A. & Hardt, C. 2004. Operation of a prototype microgrid system based on micro-sources quipped with fast-acting power electronics interfaces. In *Power Electronics Specialists Conference, 2004. PESC 04. 2004 IEEE 35th Annual*. Power Electronics Specialists Conference, 2004. PESC 04. 2004 IEEE 35th Annual. 2521–2526 Vol.4.

Ghani, Z.A., Hannan, M.A., Mohamed, A. & Subiyanto. 2011. Three-phase photovoltaic grid-connected inverter using dSPACE DS1104 platform. In *2011 IEEE Ninth International Conference on Power Electronics and Drive Systems (PEDS)*. 2011 IEEE Ninth International Conference on Power Electronics and Drive Systems (PEDS). 447–451.

Ghosh, R. & Narayanan, G. 2007. A Simple Analog Controller for Single-Phase Half-Bridge Rectifier. *IEEE Transactions on Power Electronics*, 22(1): 186–198.

Gong, R.-X., Shu, P.-F., Xie, L.-L. & Wei, J.-Q. 2011. A Novel and Practical Multi-Loop Control Strategy for Photovoltaic Inverters Based on DSP. In *Power and Energy Engineering Conference (APPEEC), 2011 Asia-Pacific*. Power and Energy Engineering Conference (APPEEC), 2011 Asia-Pacific. 1–5.

- Grover, H.K. & Pretorius, M.W. 2007. The technology assessment of demand side bidding within the South African context. In *AFRICON 2007*. AFRICON 2007. 1–8.
- Guerrero, J.M., Garcia De Vicuna, L., Matas, J., Castilla, M. & Miret, J. 2004. A wireless controller to enhance dynamic performance of parallel inverters in distributed generation systems. *IEEE Transactions on Power Electronics*, 19(5): 1205–1213.
- Guerrero, J.M., Garcia De Vicuna, L., Matas, J., Castilla, M. & Miret, J. 2005. Output Impedance Design of Parallel-Connected UPS Inverters With Wireless Load-Sharing Control. *IEEE Transactions on Industrial Electronics*, 52(4): 1126–1135.
- Guerrero, J.M., Hang, L. & Uceda, J. 2008. Control of Distributed Uninterruptible Power Supply Systems. *IEEE Transactions on Industrial Electronics*, 55(8): 2845–2859.
- Guerrero, J.M., Matas, J., Vicuna, L.G. de, Castilla, M. & Miret, J. 2007. Decentralized Control for Parallel Operation of Distributed Generation Inverters Using Resistive Output Impedance. *IEEE Transactions on Industrial Electronics*, 54(2): 994–1004.
- Guerrero, J.M., Vasquez, J.C., Matas, J., Castilla, M. & de Vicuna, L.G. 2009. Control Strategy for Flexible Microgrid Based on Parallel Line-Interactive UPS Systems. *IEEE Transactions on Industrial Electronics*, 56(3): 726–736.
- Guerrero, J.M., Vasquez, J.C., Matas, J., de Vicuña, L.G. & Castilla, M. 2011. Hierarchical Control of Droop-Controlled AC and DC Microgrids #x2014;A General Approach Toward Standardization. *IEEE Transactions on Industrial Electronics*, 58(1): 158–172.
- Gu, W., Wu, Z. & Yuan, X. 2010. Microgrid economic optimal operation of the combined heat and power system with renewable energy. In *2010 IEEE Power and Energy Society General Meeting*. 2010 IEEE Power and Energy Society General Meeting. 1–6.
- Habetler, T.G. 1993. A space vector-based rectifier regulator for AC/DC/AC converters. *IEEE Transactions on Power Electronics*, 8(1): 30–36.
- Hanaoka, H., Nagai, M. & Yanagisawa, M. 2003. Development of a novel parallel redundant UPS. In *Telecommunications Energy Conference, 2003. INTEL'03. The 25th International*. Telecommunications Energy Conference, 2003. INTEL'03. The 25th International. 493–498.
- Hannan, M.A., Abd Ghani, Z. & Mohamed, A. 2011. An Enhanced Inverter Controller for PV Applications Using the dSPACE Platform. *International Journal of Photoenergy*, 2010: e457562.
- Harley, C.D.G. & Paine, R.T. 2009. Contingencies and compounded rare perturbations dictate sudden distributional shifts during periods of gradual climate change. *Proceedings of the National Academy of Sciences*, 106(27): 11172–11176.
- Hatziaargyriou, N.D., Dimeas, A., Tsikalakis, A.G., Lopes, J.A.P., Karniotakis, G. & Oyarzabal, J. 2005. Management of microgrids in market environment. In *2005 International Conference on Future Power Systems*. 2005 International Conference on Future Power Systems. 7 pp.–7.
- Holmes, D.G. & Martin, D.A. 1996. Implementation of a direct digital predictive current controller for single and three phase voltage source inverters. In *Conference Record of the 1996 IEEE Industry Applications Conference, 1996. Thirty-First IAS Annual Meeting, IAS '96.* , Conference Record of the 1996 IEEE Industry Applications Conference, 1996. Thirty-First IAS Annual Meeting, IAS '96. 906–913 vol.2.

- Holtz, J. & Werner, K.-H. 1990. Multi-inverter UPS system with redundant load sharing control. *IEEE Transactions on Industrial Electronics*, 37(6): 506–513.
- Hwang, J.G., Lehn, P.W. & Winkelkemper, M. 2010. A Generalized Class of Stationary Frame-Current Controllers for Grid-Connected AC #x2013;DC Converters. *IEEE Transactions on Power Delivery*, 25(4): 2742–2751.
- IEP. 2013. Draft-2012-Integrated-Energy-Planning-Report-an-Executive-Summary.pdf.
- Ilić, M. & Zaborszky, J. 2000. *Dynamics and Control of Large Electric Power Systems*. Wiley.
- Isle, D., Vaziri, M., Zarghami, M. & Vadhva, S. 2014. Review of Concepts to Increase Distributed Generation into the Distribution Network. In *2014 Sixth Annual IEEE Green Technologies Conference (GreenTech)*. 2014 Sixth Annual IEEE Green Technologies Conference (GreenTech). 118–125.
- Itoh, Y. & Kawauchi, S. 1991. Easy digital control of three-phase PWM convertor. In *Telecommunications Energy Conference, 1991. INTEL'91., 13th International Telecommunications Energy Conference, 1991. INTEL'91., 13th International*. 727–734.
- Ito, Y. & Iyama, O. 1997. Parallel redundant operation of UPS with robust current minor loop. In *Power Conversion Conference - Nagaoka 1997., Proceedings of the. Power Conversion Conference - Nagaoka 1997., Proceedings of the*. 489–494 vol.1.
- Iwahashi, M. & Kiya, H. 2009. Finite word length error analysis based on basic formula of rounding operation. In *International Symposium on Intelligent Signal Processing and Communications Systems, 2008. ISPACS 2008. International Symposium on Intelligent Signal Processing and Communications Systems, 2008. ISPACS 2008*. 1–4.
- Iyer, S.V., Belur, M.N. & Chandorkar, M.C. 2011. Analysis and Mitigation of Voltage Offsets in Multi-inverter Microgrids. *IEEE Transactions on Energy Conversion*, 26(1): 354–363.
- Jamian, J.J., Mustafa, M.W., Mokhlis, H. & Bahamdin, M.A. 2011. Conceptual data management and communication for smart distribution system. In *2011 IEEE First Conference on Clean Energy and Technology (CET)*. 2011 IEEE First Conference on Clean Energy and Technology (CET). 364–368.
- Jiang, J., Zhang, B.H., Hao, Z.G., Yuan, Y.Y., Bo, Z.Q. & Klimek, A. 2010. Study on factors affecting the harmonics of large-scale rectification device in power grid. In *Universities Power Engineering Conference (UPEC), 2010 45th International*. Universities Power Engineering Conference (UPEC), 2010 45th International. 1–5.
- Jiang, Q., Xue, M. & Geng, G. 2013. Energy Management of Microgrid in Grid-Connected and Stand-Alone Modes. *IEEE Transactions on Power Systems*, 28(3): 3380–3389.
- Ji, J., Zeng, G., Liu, H., Luo, L. & Zhang, J. 2012. Research on selection method of Passive Power Filter topologies. In *Power Electronics and Motion Control Conference (IPEMC), 2012 7th International*. Power Electronics and Motion Control Conference (IPEMC), 2012 7th International. 2844–2848.
- Jung, J.-H. & Ahmed, S. 2010. Model construction of single crystalline photovoltaic panels for real-time simulation. In *2010 IEEE Energy Conversion Congress and Exposition (ECCE)*. 2010 IEEE Energy Conversion Congress and Exposition (ECCE). 342–349.

Justo, J.J., Mwasilu, F., Lee, J. & Jung, J.-W. 2013. AC-microgrids versus DC-microgrids with distributed energy resources: A review. *Renewable and Sustainable Energy Reviews*, 24: 387–405.

Kamel, R.M., Chaouachi, A. & Nagasaka, K. 2011. Enhancement of micro-grid performance during islanding mode using storage batteries and new fuzzy logic pitch angle controller. *Energy Conversion and Management*, 52(5): 2204–2216.

Kandlawala, M.F. & Nguyen, T.T. 2009. An optimized fuzzy logic-based control of static VAR compensator in a power system with wind generation. In *Transmission Distribution Conference Exposition: Asia and Pacific, 2009*. Transmission Distribution Conference Exposition: Asia and Pacific, 2009. 1–4.

Kanellos, F.D. & Hatziargyriou, N.D. 2009. Control of variable speed wind turbines equipped with synchronous or doubly fed induction generators supplying islanded power systems. *IET Renewable Power Generation*, 3(1): 96–108.

Karimi-Ghartemani, M., Mokhtari, H., Iravani, M.R. & Sedighy, M. 2004. A signal Processing system for extraction of harmonics and reactive current of single-phase systems. *IEEE Transactions on Power Delivery*, 19(3): 979–986.

Katiraei, F. & Iravani, M.R. 2006. Power Management Strategies for a Microgrid With Multiple Distributed Generation Units. *IEEE Transactions on Power Systems*, 21(4): 1821–1831.

Katiraei, F., Iravani, M.R. & Lehn, P.W. 2005. Micro-grid autonomous operation during and subsequent to islanding process. *IEEE Transactions on Power Delivery*, 20(1): 248–257.

Katiraei, F., Iravani, R., Hatziargyriou, N. & Dimeas, A. 2008. Microgrids management. *IEEE Power and Energy Magazine*, 6(3): 54–65.

Kawamura, A., Haneyoshi, T. & Hoft, R.G. 1988. Deadbeat controlled PWM inverter with parameter estimation using only voltage sensor. *IEEE Transactions on Power Electronics*, 3(2): 118–125.

Kawamura, A. & Yokoyama, T. 1990. Comparison of five different approaches for real time digital feedback control of PWM inverters. In , *Conference Record of the 1990 IEEE Industry Applications Society Annual Meeting, 1990*. , Conference Record of the 1990 IEEE Industry Applications Society Annual Meeting, 1990. 1005–1011 vol.2.

Kazmierkowski, M.P. & Malesani, L. 1998. Current control techniques for three-phase voltage-source PWM converters: a survey. *IEEE Transactions on Industrial Electronics*, 45(5): 691–703.

Khan, M.S. & Iravani, M.R. 2007. Supervisory Hybrid Control of a Micro Grid System. In *Electrical Power Conference, 2007. EPC 2007. IEEE Canada*. Electrical Power Conference, 2007. EPC 2007. IEEE Canada. 20–24.

Kim, H. & Sul, S.-K. 2005. Compensation voltage control in dynamic voltage restorers by use of feed forward and state feedback scheme. *IEEE Transactions on Power Electronics*, 20(5): 1169–1177.

Kim, H., Yu, T. & Choi, S. 2008. Indirect Current Control Algorithm for Utility Interactive Inverters in Distributed Generation Systems. *IEEE Transactions on Power Electronics*, 23(3): 1342–1347.

- Kim, J., Guerrero, J.M., Rodriguez, P., Teodorescu, R. & Nam, K. 2011. Mode Adaptive Droop Control With Virtual Output Impedances for an Inverter-Based Flexible AC Microgrid. *IEEE Transactions on Power Electronics*, 26(3): 689–701.
- Kim, K.-H. & Youn, M.-J. 2001. A simple and robust digital current control technique of a PM synchronous motor using time delay control approach. *IEEE Transactions on Power Electronics*, 16(1): 72–82.
- Kjaer, S.B., Pedersen, J.K. & Blaabjerg, F. 2005. A review of single-phase grid-connected inverters for photovoltaic modules. *IEEE Transactions on Industry Applications*, 41(5): 1292–1306.
- Kocybik, P.F. & Bateson, K.N. 1995. Digital control of a ZVS full-bridge DC-DC converter. In *Applied Power Electronics Conference and Exposition, 1995. APEC '95. Conference Proceedings 1995., Tenth Annual*. Applied Power Electronics Conference and Exposition, 1995. APEC '95. Conference Proceedings 1995., Tenth Annual. 687–693 vol.2.
- Kolmakov, N.M. & Bakhovtsev, I.A. 2013. Analysis of output characteristics of three-phase voltage source inverter with new hysteresis control algorithms. In *2013 14th International Conference of Young Specialists on Micro/Nanotechnologies and Electron Devices (EDM)*. 2013 14th International Conference of Young Specialists on Micro/Nanotechnologies and Electron Devices (EDM). 293–297.
- Kulatunga, N.A., Navaratne, S., Dole, J., Liyanagedera, C. & Martin, T. 2012. Hardware development for Smart Meter based innovations. In *2012 IEEE Innovative Smart Grid Technologies - Asia (ISGT Asia)*. 2012 IEEE Innovative Smart Grid Technologies - Asia (ISGT Asia). 1–5.
- Laaksonen, H.J. 2010. Protection Principles for Future Microgrids. *IEEE Transactions on Power Electronics*, 25(12): 2910–2918.
- Lago, J. & Heldwein, M.L. 2011. Operation and Control-Oriented Modeling of a Power Converter for Current Balancing and Stability Improvement of DC Active Distribution Networks. *IEEE Transactions on Power Electronics*, 26(3): 877–885.
- Lasseter, B. 2001. Microgrids [distributed power generation]. In *IEEE Power Engineering Society Winter Meeting, 2001*. IEEE Power Engineering Society Winter Meeting, 2001. 146–149 vol.1.
- Lasseter, R.H. 2011. Smart Distribution: Coupled Microgrids. *Proceedings of the IEEE*, 99(6): 1074–1082.
- Lasseter, R.H. & Paigi, P. 2004. Microgrid: a conceptual solution. In *Power Electronics Specialists Conference, 2004. PESC 04. 2004 IEEE 35th Annual*. Power Electronics Specialists Conference, 2004. PESC 04. 2004 IEEE 35th Annual. 4285–4290 Vol.6.
- Lasseter, R. & Piagi, P. 2006. Control and Design of Microgrid Components.
- Leelajindakraierk, E.J.S.C.M. & Chompoo-Inwai, C.-C. 2012. Optimal technique for total harmonic distortion detection and estimation for smart meter. In *IPEC, 2012 Conference on Power Energy*. IPEC, 2012 Conference on Power Energy. 369–373.
- Li, H. & Chen, Z. 2008. Overview of different wind generator systems and their comparisons. *IET Renewable Power Generation*, 2(2): 123–138.

- Li, H.-X. & Gatland, H.B. 1995. A new methodology for designing a fuzzy logic controller. *IEEE Transactions on Systems, Man and Cybernetics*, 25(3): 505–512.
- Lin, B.-R. & Yang, T.-Y. 2004. Single-phase half-bridge rectifier with power factor correction. *Electric Power Applications, IEE Proceedings -*, 151(4): 443–450.
- Liserre, M., Teodorescu, R. & Blaabjerg, F. 2006. Stability of photovoltaic and wind turbine grid-connected inverters for a large set of grid impedance values. *IEEE Transactions on Power Electronics*, 21(1): 263–272.
- Little, B.P. 2005. Hysteresis Control of Parallel-Connected Hybrid Inverters. : 164.
- Liu, F., Zha, X., Zhou, Y. & Duan, S. 2009. Design and research on parameter of LCL filter in three-phase grid-connected inverter. In *Power Electronics and Motion Control Conference, 2009. IPEMC '09. IEEE 6th International. Power Electronics and Motion Control Conference, 2009. IPEMC '09. IEEE 6th International.* 2174–2177.
- Li, Y., Vilathgamuwa, D.M. & Loh, P.C. 2004. Design, analysis, and real-time testing of a controller for multibus microgrid system. *IEEE Transactions on Power Electronics*, 19(5): 1195–1204.
- Loh, P.C., Vilathgamuwa, D.M., Lai, Y.S., Chua, G.T. & Li, Y. 2005. Pulse-width modulation of Z-source inverters. *IEEE Transactions on Power Electronics*, 20(6): 1346–1355.
- Loh, P.C., Vilathgamuwa, D.M., Lai, Y.S., Chua, G.T. & Li, Y. 2004. Pulse-width modulation of Z-source inverters. In *Conference Record of the 2004 IEEE Industry Applications Conference, 2004. 39th IAS Annual Meeting.* Conference Record of the 2004 IEEE Industry Applications Conference, 2004. 39th IAS Annual Meeting. -155.
- Luan, S.-W., Teng, J.-H., Chan, S.-Y. & Hwang, L.-C. 2009. Development of a smart power meter for AMI based on ZigBee communication. In *International Conference on Power Electronics and Drive Systems, 2009. PEDS 2009.* International Conference on Power Electronics and Drive Systems, 2009. PEDS 2009. 661–665.
- Lu, D., Li, W., Xu, G. & Zhou, M. 2012. Fuzzy logic control approach to the energy management of Parallel Hybrid Electric Vehicles. In *2012 International Conference on Information and Automation (ICIA).* 2012 International Conference on Information and Automation (ICIA). 592–596.
- Madureira, A., Moreira, C. & Lopes, J.P. 2005. Secondary load-frequency control for microgrids in islanded operation. In *Proc. International Conference on Renewable Energy and Power Quality ICREPQ '05, Spain.* http://www.researchgate.net/publication/228363954_Secondary_load-frequency_control_for_MicroGrids_in_islanded_operation/file/e0b49525f8a01a429a.pdf 25 October 2014.
- Maheswaran, D., Kailas, K.K.J., Rangaraj, V. & Kumar, W.A. 2012. Energy efficiency in electrical systems. In *2012 IEEE International Conference on Power Electronics, Drives and Energy Systems (PEDES).* 2012 IEEE International Conference on Power Electronics, Drives and Energy Systems (PEDES). 1–6.
- Maji, P., Patra, S.K. & Mahapatra, K.K. 2012. Design of Fuzzy Logic Controller based on TMS320C6713 DSP. In *2012 12th International Conference on Intelligent Systems Design and*

Applications (ISDA). 2012 12th International Conference on Intelligent Systems Design and Applications (ISDA). 635–639.

Majumder, R., Chaudhuri, B., Ghosh, A., Majumder, R., Ledwich, G. & Zare, F. 2010. Improvement of Stability and Load Sharing in an Autonomous Microgrid Using Supplementary Droop Control Loop. *IEEE Transactions on Power Systems*, 25(2): 796–808.

Martin, J. 2009. Distributed vs. centralized electricity generation: are we witnessing a change of paradigm. *An introduction to distributed generation*. Paris: HEC:< www.vernimmen.net/ftp/An_introduction_to_distributed_generation.pdf. pdf. http://www.vernimmen.net/ftp/An_introduction_to_distributed_generation.pdf 25 October 2014.

Martins, A.P., Carvalho, A.S. & Araujo, A.S. 1995. Design and implementation of a current controller for the parallel operation of standard UPSs. In , *Proceedings of the 1995 IEEE IECON 21st International Conference on Industrial Electronics, Control, and Instrumentation, 1995*. , Proceedings of the 1995 IEEE IECON 21st International Conference on Industrial Electronics, Control, and Instrumentation, 1995. 584–589 vol.1.

Martin, T.W. & Ang, S.S. 1995. Digital control for switching converters. In , *Proceedings of the IEEE International Symposium on Industrial Electronics, 1995. ISIE '95*. , Proceedings of the IEEE International Symposium on Industrial Electronics, 1995. ISIE '95. 480–484 vol.2.

Mattavelli, P. 2002. A modified dead-beat control for UPS using disturbance observers. In *Power Electronics Specialists Conference, 2002. pesc 02. 2002 IEEE 33rd Annual*. Power Electronics Specialists Conference, 2002. pesc 02. 2002 IEEE 33rd Annual. 1618–1623.

McConnach, J.S. 2006. Proposed Standards for the Quantification of GHG Emission Credits in the Electricity Sector. In *2006 IEEE EIC Climate Change Technology*. 2006 IEEE EIC Climate Change Technology. 1–3.

Md Kafiul Islam, T.A. 2011. Analysis of Maximum Possible Utilization of Solar Radiation on a Solar Photovoltaic Cell with a Proposed Model. , 1: 66–69.

Meiqin, M., Chang, L. & Ming, D. 2008. Integration and intelligent control of micro-grids with multi-energy generations: A review. In *IEEE International Conference on Sustainable Energy Technologies, 2008. ICSET 2008*. IEEE International Conference on Sustainable Energy Technologies, 2008. ICSET 2008. 777–780.

Meiqin, M., Wei, D. & Chang, L. 2011. Multi-agent based simulation for Microgrid energy management. In *2011 IEEE 8th International Conference on Power Electronics and ECCE Asia (ICPE ECCE)*. 2011 IEEE 8th International Conference on Power Electronics and ECCE Asia (ICPE ECCE). 1219–1223.

Mekhilef, S. & Rahim, N.A. 2002. Xilinx FPGA based three-phase PWM inverter and its application for utility connected PV system. In *TENCON '02. Proceedings. 2002 IEEE Region 10 Conference on Computers, Communications, Control and Power Engineering*. TENCON '02. Proceedings. 2002 IEEE Region 10 Conference on Computers, Communications, Control and Power Engineering. 2079–2082 vol.3.

Mihalache, L. 2003. Paralleling control technique with no intercommunication signals for resonant controller-based inverters. In *Industry Applications Conference, 2003. 38th IAS Annual Meeting. Conference Record of the*. Industry Applications Conference, 2003. 38th IAS Annual Meeting. Conference Record of the. 1882–1889 vol.3.

- Ming, W.-L. & Zhong, Q.-C. 2014. Single-phase half-bridge rectifiers with extended voltage ranges and reduced voltage ripples. In *2014 IEEE 5th International Symposium on Power Electronics for Distributed Generation Systems (PEDG)*. 2014 IEEE 5th International Symposium on Power Electronics for Distributed Generation Systems (PEDG). 1–6.
- MN Ambia, M.K.I. 2010. An analysis & design on micro generation of a domestic solar-wind hybrid energy system for rural & remote areas-perspective Bangladesh. : V2–107.
- Mohamed, Y.A.-R. & El-Saadany, E.F. 2008. Adaptive Discrete-Time Grid-Voltage Sensorless Interfacing Scheme for Grid-Connected DG-Inverters Based on Neural-Network Identification and Deadbeat Current Regulation. *IEEE Transactions on Power Electronics*, 23(1): 308–321.
- Mohan, N. 2012. *Power electronics: a first course*. Wiley. <http://www.nhmnc.info/wp-content/uploads/fbpdfs2014/Power-Electronics-A-First-Course-by-Ned-Mohan-First-Course.pdf> 25 October 2014.
- Mohan, N., Undeland, T.M. & Robbins, W.P. 2002. *Power Electronics: Converters, Applications, and Design*. 3 edition. Hoboken, NJ: Wiley.
- Moreira, C.L., Resende, F.O. & Peas Lopes, J.A. 2007. Using Low Voltage MicroGrids for Service Restoration. *IEEE Transactions on Power Systems*, 22(1): 395–403.
- Munoz, J.A., Espinoza, J.R., Baier, C.R., Moran, L.A., Espinosa, E.E., Melin, P.E. & Sbarbaro, D.G. 2012. Design of a Discrete-Time Linear Control Strategy for a Multicell UPQC. *IEEE Transactions on Industrial Electronics*, 59(10): 3797–3807.
- Nagaraj, R. 2012. Renewable energy based small hybrid power system for desalination applications in remote locations. In *2012 IEEE 5th India International Conference on Power Electronics (IICPE)*. 2012 IEEE 5th India International Conference on Power Electronics (IICPE). 1–5.
- Nassif, A., Xu, W. & Freitas, W. 2010. An investigation on the selection of filter topologies for passive filter applications. In *2010 IEEE Power and Energy Society General Meeting*. 2010 IEEE Power and Energy Society General Meeting. 1–1.
- Nousiainen, L. & Suntio, T. 2012. DC-link voltage control of a single-phase photovoltaic inverter. In *6th IET International Conference on Power Electronics, Machines and Drives (PEMD 2012)*. 6th IET International Conference on Power Electronics, Machines and Drives (PEMD 2012). 1–6.
- Nussbaumer, T., Heldwein, M.L., Gong, G., Round, S.D. & Kolar, J.W. 2008. Comparison of Prediction Techniques to Compensate Time Delays Caused by Digital Control of a Three-Phase Buck-Type PWM Rectifier System. *IEEE Transactions on Industrial Electronics*, 55(2): 791–799.
- Odavic, M., Zanchetta, P. & Sumner, M. 2006. A Genetic Algorithm Design Method for A Current Controller Employing ‘Two Ahead’ Prediction. In *IEEE International Conference on Industrial Technology, 2006. ICIT 2006*. IEEE International Conference on Industrial Technology, 2006. ICIT 2006. 812–817.
- Oshikata, T., Matsuo, H. & Kurokawa, F. 2003. Digitally controlled three-phase power factor correction circuit with partially resonant circuit. In *Telecommunications Energy Conference, 2003. INTEL EC '03. The 25th International*. Telecommunications Energy Conference, 2003. INTEL EC '03. The 25th International. 290–295.

Parida, B., Iniyar, S. & Goic, R. 2011. A review of solar photovoltaic technologies. *Renewable and sustainable energy reviews*, 15(3): 1625–1636.

Peas Lopes, J.A., Moreira, C.L. & Madureira, A.G. 2006. Defining control strategies for MicroGrids islanded operation. *IEEE Transactions on Power Systems*, 21(2): 916–924.

Percec, V., Bae, J.-Y., Zhao, M. & Hill, D.H. 1995. Aryl Mesylates in Metal-Catalyzed Homocoupling and Cross-Coupling Reactions. 3. A Simple and General Method for the Synthesis of 2,2'-Diaroyl-4,4'-dihydroxybiphenyls. *The Journal of Organic Chemistry*, 60(4): 1066–1069.

Pereira, O.S., Reis, T.M., de Araujo, R.G.B. & Gongalves, F.F. 2006. Renewable Energy as a Tool to Assure Continuity of Low Emissions in the Brazilian Electric Power Sector. In *2006 IEEE EIC Climate Change Technology*. 2006 IEEE EIC Climate Change Technology. 1–8.

Piacentini, R. 2012. Modernizing power grids with distributed intelligence and smart grid-ready instrumentation. In *Innovative Smart Grid Technologies (ISGT), 2012 IEEE PES*. Innovative Smart Grid Technologies (ISGT), 2012 IEEE PES. 1–6.

Piagi, P. & Lasseter, R.H. 2006. Autonomous control of microgrids. In *IEEE Power Engineering Society General Meeting, 2006*. IEEE Power Engineering Society General Meeting, 2006. 8 pp.–

Ponnaluri, S., Linhofer, G.O., Steinke, J.K. & Steimer, P.K. 2005. Comparison of single and two stage topologies for interface of BESS or fuel cell system using the ABB standard power electronics building blocks. In *2005 European Conference on Power Electronics and Applications*. 2005 European Conference on Power Electronics and Applications. 9 pp.–P.9.

Prodic, A. & Maksimovic, D. 2000. Digital PWM controller and current estimator for a low-power switching converter. In *The 7th Workshop on Computers in Power Electronics, 2000. COMPEL 2000*. The 7th Workshop on Computers in Power Electronics, 2000. COMPEL 2000. 123–128.

Query, D.S. & Tescher, G. 1990. Advantages of microprocessors versus discrete digital electronics in appliance controls. *IEEE Transactions on Industry Applications*, 26(6): 1131–1138.

Quinn, C.A., Mohan, N. & Mehta, H. 1993. A four-wire, current-controlled converter provides harmonic neutralization in three-phase, four-wire systems. In *Applied Power Electronics Conference and Exposition, 1993. APEC '93. Conference Proceedings 1993., Eighth Annual*. Applied Power Electronics Conference and Exposition, 1993. APEC '93. Conference Proceedings 1993., Eighth Annual. 841–846.

Rahim, N.A., Selvaraj, J. & Krismadinata, C. 2010. Five-level inverter with dual reference modulation technique for grid-connected PV system. *Renewable Energy*, 35(3): 712–720.

Abu-Rub, H., Iqbal, A. & Guzinski, J. 2012. *High Performance Control of AC Drives with Matlab / Simulink Models*. John Wiley & Sons.

Saiful Islam, A.W. 2006. Cost effective second generation AC-modules: Development and testing aspects. *Energy*, (12): 1897–1920.

Salam, Z., Soon, T.L. & Ramli, M.Z. 2006. Hardware Implementation of the High Frequency Link Inverter Using the dSPACE DS1104 Digital Signal Processing Board. In *Power and Energy Conference, 2006. PECon '06. IEEE International*. Power and Energy Conference, 2006. PECon '06. IEEE International. 348–352.

- Salomonsson, D., Soder, L. & Sannino, A. 2009. Protection of Low-Voltage DC Microgrids. *IEEE Transactions on Power Delivery*, 24(3): 1045–1053.
- Sanchis, P., Ursaea, A., Gubia, E. & Marroyo, L. 2005. Boost DC-AC inverter: a new control strategy. *IEEE Transactions on Power Electronics*, 20(2): 343–353.
- Sao, C.K. & Lehn, P.W. 2008. Control and Power Management of Converter Fed Microgrids. *IEEE Transactions on Power Systems*, 23(3): 1088–1098.
- Sao, C.K. & Lehn, P.W. 2006. Intentional islanded operation of converter fed microgrids. In *IEEE Power Engineering Society General Meeting, 2006*. IEEE Power Engineering Society General Meeting, 2006. 6 pp.—.
- Selvaraj, J. & Rahim, N.A. 2009. Multilevel Inverter For Grid-Connected PV System Employing Digital PI Controller. *IEEE Transactions on Industrial Electronics*, 56(1): 149–158.
- Sera, D., Kerekes, T., Lungeanu, M., Nakhost, P., Teodorescu, R., Andersen, G.K. & Liserre, M. 2005. Low-cost digital implementation of proportional-resonant current controllers for PV inverter applications using delta operator. In *31st Annual Conference of IEEE Industrial Electronics Society, 2005. IECON 2005*. 31st Annual Conference of IEEE Industrial Electronics Society, 2005. IECON 2005. 6 pp.—.
- Serban, E. & Serban, H. 2010. A Control Strategy for a Distributed Power Generation Microgrid Application With Voltage- and Current-Controlled Source Converter. *IEEE Transactions on Power Electronics*, 25(12): 2981–2992.
- Serban, I. & Marinescu, C. 2011. Frequency control issues in microgrids with renewable energy sources. In *2011 7th International Symposium on Advanced Topics in Electrical Engineering (ATEE)*. 2011 7th International Symposium on Advanced Topics in Electrical Engineering (ATEE). 1–6.
- Shah, J., Wollenberg, B.F. & Mohan, N. 2011. Decentralized power flow control for a smart micro-grid. In *2011 IEEE Power and Energy Society General Meeting*. 2011 IEEE Power and Energy Society General Meeting. 1–6.
- Shan, H., Kang, Y., Kong, X., Liu, Z., Yu, M., Li, H., Luo, F. & Liu, L. 2008. The research on the digital controlled effect of performance on the PWM inverter. In *Telecommunications Energy Conference, 2008. INTEL EC 2008. IEEE 30th International*. Telecommunications Energy Conference, 2008. INTEL EC 2008. IEEE 30th International. 1–6.
- Shan, H., Zhang, Y., Kang, Y., Kong, X., Wang, H. & Li, H. 2009. The research for the stability of SPWM inverter affected by digital control. In *Telecommunications Energy Conference, 2009. INTEL EC 2009. 31st International*. Telecommunications Energy Conference, 2009. INTEL EC 2009. 31st International. 1–4.
- Shen, G., Zhu, X., Zhang, J. & Xu, D. 2010. A New Feedback Method for PR Current Control of LCL-Filter-Based Grid-Connected Inverter. *IEEE Transactions on Industrial Electronics*, 57(6): 2033–2041.
- Shiple, A.M. & Elliott, R.N. 2006. Ripe for the Picking: Have We Exhausted the Low-Hanging Fruit in the Industrial Sector? In American Council for an Energy-Efficient Economy. <https://www.greenbiz.com/sites/default/files/document/CustomO16C45F69267.pdf> 25 October 2014.

Silva, M., Morais, H. & Vale, Z. 2012. An integrated approach for distributed energy resource short-term scheduling in smart grids considering realistic power system simulation. *Energy Conversion and Management*, 64: 273–288.

Singh, A., Bapat, J. & Das, D. 2013. Two tier communication architecture for smart meter. In *2013 Fifth International Conference on Communication Systems and Networks (COMSNETS)*. 2013 Fifth International Conference on Communication Systems and Networks (COMSNETS). 1–2.

Sofla, M.A. & King, R. 2012. Control method for multi-microgrid systems in smart grid environment #x2014;Stability, optimization and smart demand participation. In *Innovative Smart Grid Technologies (ISGT), 2012 IEEE PES*. Innovative Smart Grid Technologies (ISGT), 2012 IEEE PES. 1–5.

Sporn, P. 1946. Centralized power generation. *Electrical Engineering*, 65(3): 105–107.

Srisawang, A. 2010. A study of EMI and switching loss reductions of unipolar and improved limited unipolar switching circuits. In *2010 International Conference on Electrical Engineering/Electronics Computer Telecommunications and Information Technology (ECTI-CON)*. 2010 International Conference on Electrical Engineering/Electronics Computer Telecommunications and Information Technology (ECTI-CON). 1211–1215.

Steimer, P.K. 2010. Enabled by high power electronics - Energy efficiency, renewables and smart grids. In *Power Electronics Conference (IPEC), 2010 International*. Power Electronics Conference (IPEC), 2010 International. 11–15.

Subiyanto, S., Ghani, Z.A., Mohamed, A. & Hannan, M.A. 2013. Prototype development of an intelligent power conditioning unit for PV generation system. In *2013 IEEE International Conference on Industrial Technology (ICIT)*. 2013 IEEE International Conference on Industrial Technology (ICIT). 758–763.

Sun, X., Lee, Y.-S. & Xu, D. 2003. Modeling, analysis, and implementation of parallel multi-inverter systems with instantaneous average-current-sharing scheme. *IEEE Transactions on Power Electronics*, 18(3): 844–856.

Svensson, J. & Lindgren, M. 1999. Influence of nonlinearities on the frequency response of a grid-connected vector-controlled VSC. *IEEE Transactions on Industrial Electronics*, 46(2): 319–324.

Tan, C.W., Green, T.C. & Hernandez-Aramburo, C.A. 2007. A current-mode controlled maximum power point tracking converter for building integrated photovoltaics. In *2007 European Conference on Power Electronics and Applications*. 2007 European Conference on Power Electronics and Applications. 1–10.

Tan, C.W., Green, T.C. & Hernandez-Aramburo, C.A. 2008. Analysis of perturb and observe maximum power point tracking algorithm for photovoltaic applications. In *Power and Energy Conference, 2008. PECon 2008. IEEE 2nd International*. Power and Energy Conference, 2008. PECon 2008. IEEE 2nd International. 237–242.

Tarak Salmi, M.B. 2012. MATLAB/Simulink Based Modelling of Solar Photovoltaic Cell. , 2.

Teodorescu, R., Blaabjerg, F., Liserre, M. & Loh, P.C. 2006. Proportional-resonant controllers and filters for grid-connected voltage-source converters. *Electric Power Applications, IEE Proceedings*, 153(5): 750–762.

- Teodorescu, R., Liserre, M. & Rodríguez, P. 2011. *Grid Converters for Photovoltaic and Wind Power Systems*. 1 edition. Piscataway, N.J.: Chichester, West Sussex; Hoboken, N.J.: Wiley.
- Timbus, A., Liserre, M., Teodorescu, R., Rodríguez, P. & Blaabjerg, F. 2009. Evaluation of Current Controllers for Distributed Power Generation Systems. *IEEE Transactions on Power Electronics*, 24(3): 654–664.
- Timbus, A.V., Teodorescu, R., Blaabjerg, F., Liserre, M. & Rodríguez, P. 2006. Linear and Nonlinear Control of Distributed Power Generation Systems. In *Conference Record of the 2006 IEEE Industry Applications Conference, 2006. 41st IAS Annual Meeting*. Conference Record of the 2006 IEEE Industry Applications Conference, 2006. 41st IAS Annual Meeting. 1015–1023.
- Trujillo Rodriguez, C., Velasco de la Fuente, D., Garcera, G., Figueres, E. & Guacaneme Moreno, J.A. 2013. Reconfigurable Control Scheme for a PV Microinverter Working in Both Grid-Connected and Island Modes. *IEEE Transactions on Industrial Electronics*, 60(4): 1582–1595.
- Tsai-Fu Wu, Y.-K.C. 2000. 3C strategy for inverters in parallel operation achieving an equal current distribution. *Industrial Electronics, IEEE Transactions on*, (2): 273 – 281.
- Tsourapas, V., Stefanopoulou, A. & Sun, J. 2005. Dynamics, optimization and control of a fuel cell based combined heat power (CHP) system for shipboard applications. In *American Control Conference, 2005. Proceedings of the 2005*. American Control Conference, 2005. Proceedings of the 2005. 1993–1998 vol. 3.
- Tunyasirirut, S., Srilad, S. & Suksri, T. 2008. Comparison power quality of the voltage source inverter type SVPWM and SPWM technique for induction motor drive. In *SICE Annual Conference, 2008*. SICE Annual Conference, 2008. 241–246.
- Twining, E. & Holmes, D.G. 2003. Grid current regulation of a three-phase voltage source inverter with an LCL input filter. *IEEE Transactions on Power Electronics*, 18(3): 888–895.
- Ustun, T.S., Ozansoy, C. & Zayegh, A. 2011. Recent developments in microgrids and example cases around the world—A review. *Renewable and Sustainable Energy Reviews*, 15(8): 4030–4041.
- Vandoorn, T.L., Vasquez, J.C., De Kooning, J., Guerrero, J.M. & Vandevelde, L. 2013. Microgrids: Hierarchical Control and an Overview of the Control and Reserve Management Strategies. *IEEE Industrial Electronics Magazine*, 7(4): 42–55.
- Vargas-Serrano, A., Saez, D., Reyes, L., Severino, B., Palma-Behnke, R. & Cárdenas-Dobson, R. 2012. Design and experimental validation of a dual mode VSI control system for a micro-grid with multiple generators. In *IECON 2012 - 38th Annual Conference on IEEE Industrial Electronics Society*. IECON 2012 - 38th Annual Conference on IEEE Industrial Electronics Society. 5631–5636.
- Wang, X., Guerrero, J.M., Blaabjerg, F. & Chen, Z. 2012. A Review of Power Electronics Based Microgrids. *Journal of Power Electronics*, 12(1): 181–192.
- Wei, Q., Liang, X., Liu, C. & Nie, T. 2012. Research on the combined control method for parallel inverters control of micro-grid. In *2012 7th International Forum on Strategic Technology (IFOST)*. 2012 7th International Forum on Strategic Technology (IFOST). 1–5.

- Wong, M.C., Lam, C.-S. & Dai, N.-Y. 2008. Comparison of structure topologies for hybrid filters. In *Universities Power Engineering Conference, 2008. UPEC 2008. 43rd International. Universities Power Engineering Conference, 2008. UPEC 2008. 43rd International.* 1–5.
- Wu, B.F. & Lin, C.-F. 2006. Memory-efficient architecture for JPEG 2000 coprocessor with large tile image. *IEEE Transactions on Circuits and Systems II: Express Briefs*, 53(4): 304–308.
- B. Wu, R.C. 2007. IMPLEMENTATION OF MAXIMUM POWER POINT TRACKING ALGORITHM FOR RESIDENTIAL PHOTOVOLTAIC SYSTEMS. : 1–6.
- Xuezhi, H. & HongXia, W. 2009. The Research Based on TMS320F2812 Full-Digital Inverter. In *International Workshop on Intelligent Systems and Applications, 2009. ISA 2009. International Workshop on Intelligent Systems and Applications, 2009. ISA 2009.* 1–4.
- Yang, S.M., Lin, F.-C. & Chen, M.-C. 2003. Control of a two-phase linear stepping motor with three-phase voltage source inverter. In *Electric Machines and Drives Conference, 2003. IEMDC'03. IEEE International. Electric Machines and Drives Conference, 2003. IEMDC'03. IEEE International.* 1720–1725 vol.3.
- Yao, W., Chen, M., Chen, J. & Qian, Z. 2007. An Improved Multiple-loop Controller for Parallel Operation of Single-phase Inverters with No Control Interconnections. In *IEEE Power Electronics Specialists Conference, 2007. PESC 2007. IEEE Power Electronics Specialists Conference, 2007. PESC 2007.* 448–452.
- Yao, W., Lu, Z., Long, H. & Li, B. 2013. Research on grid-connected interleaved inverter with L filter. In *Future Energy Electronics Conference (IFEEC), 2013 1st International. Future Energy Electronics Conference (IFEEC), 2013 1st International.* 87–92.
- You-jie, M., Ming, Q., Xue-Song, Z. & Hai-Tao, Z. 2010. The Research of Cascaded Five-level Variable Frequency and Variable Speed System Based on DSP and IPM. In *Power and Energy Engineering Conference (APPEEC), 2010 Asia-Pacific. Power and Energy Engineering Conference (APPEEC), 2010 Asia-Pacific.* 1–4.
- Yubing, D., Yulei, G., Qingmin, L. & Hui, W. 2008. Modelling and simulation of the microsources within a microgrid. In *International Conference on Electrical Machines and Systems, 2008. ICEMS 2008. International Conference on Electrical Machines and Systems, 2008. ICEMS 2008.* 2667–2671.
- Yunusov, T., Holderbaum, W. & Potter, B. 2011. Sub-agent elements for control methods in multi-agent energy management system. In *Telecommunications Energy Conference (INTEL), 2011 IEEE 33rd International. Telecommunications Energy Conference (INTEL), 2011 IEEE 33rd International.* 1–7.
- Yu, Z., Mohammed, A. & Panahi, I. 1997. A review of three PWM techniques. In *American Control Conference, 1997. Proceedings of the 1997. American Control Conference, 1997. Proceedings of the 1997.* 257–261 vol.1.
- Zha, F. & Chen, L. 2011. Research on shunt APF's control system based on DSP and #x03BC;C/OS-II. In *2011 6th IEEE Conference on Industrial Electronics and Applications (ICIEA). 2011 6th IEEE Conference on Industrial Electronics and Applications (ICIEA).* 884–888.
- Zhang, W., Zhang, Y., Wang, R. & Pan, X. 2010. A model-based DSP control platform for rapid prototype of SVPWM. In *2010 IEEE 10th International Conference on Signal Processing (ICSP). 2010 IEEE 10th International Conference on Signal Processing (ICSP).* 2523–2526.

Zhang, X., Zhu, H., Li, F., Liu, F., Liu, C. & Li, B. 2013. An LCL-LC power filter for grid-tied inverter. In *TENCON 2013 - 2013 IEEE Region 10 Conference (31194)*. TENCON 2013 - 2013 IEEE Region 10 Conference (31194). 1–4.

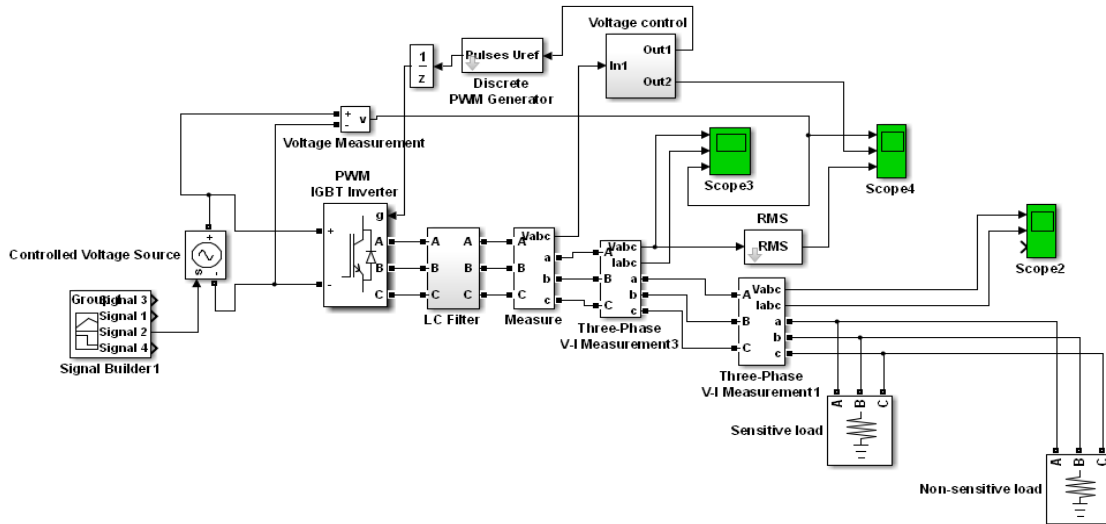
Zhang, Z., Huang, X., Jiang, J. & Wu, B. 2010. A load-sharing control scheme for a microgrid with a fixed frequency inverter. *Electric Power Systems Research*, 80(3): 311–317.

Zhao, B., Zhang, X. & Chen, J. 2012. Integrated Microgrid Laboratory System. *IEEE Transactions on Power Systems*, 27(4): 2175–2185.

Zhaoguang, H., Jinghong, Z., Xiandong, T., Quan, W., Xu, M. & Baoguo, S. 2010. A low-carbon electricity model: Integrated Resource Strategic Planning and its application. In *2010 IEEE Power and Energy Society General Meeting*. 2010 IEEE Power and Energy Society General Meeting. 1–7.

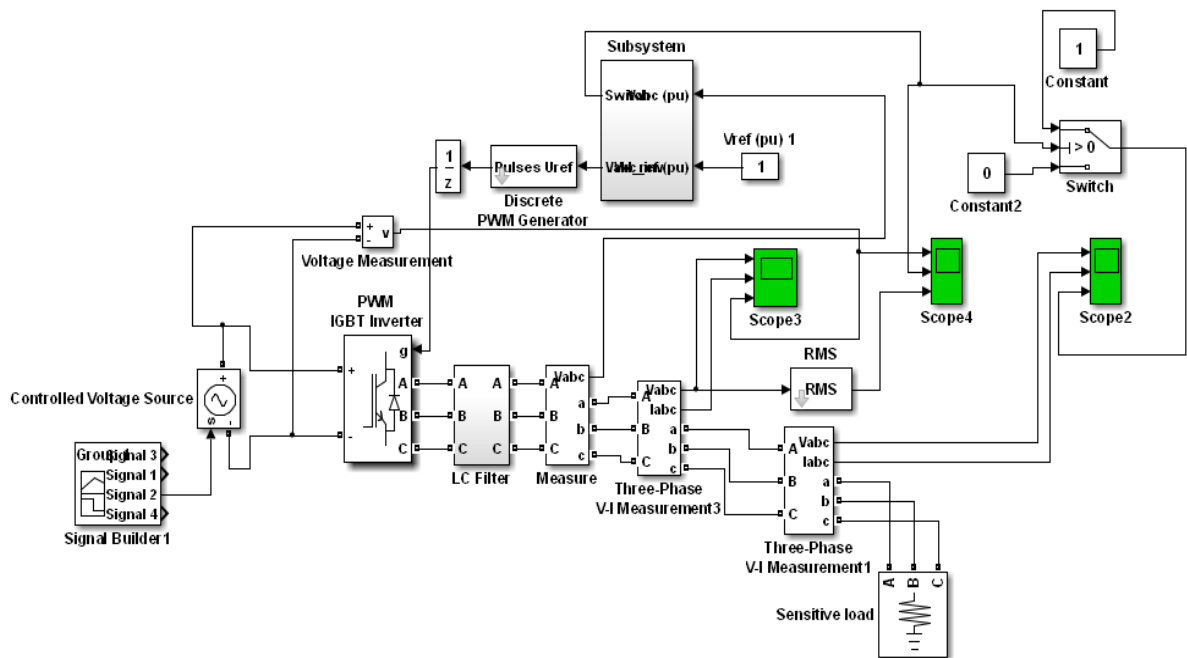
Appendix 3 Inverter control using under input voltage changes

The sensitive and non-sensitive load power is permanently connected to the system, and the non-sensitive load power is not permanently connected to the system.



Appendix 4 Inverter control operating with sensitive load power without activating the EMS to the system

The sensitive load power is permanently connected to the system, and the non-sensitive load power is not connected to the system and the EMS is not activated.



The sensitive load power is permanently connected to the system, and the non-sensitive load power is permanently disconnected to the system.